8-2017

# Characterization and Evaluation of Ground Glass Fiber as a Cementitious Component in Portland Cement and Geopolymer Concrete Mixtures

Hassan Rashidian Dezfouli
*Clemson University*, hrashid@g.clemson.edu

# CHARACTERIZATION AND EVALUATION OF GROUND GLASS FIBER AS A CEMENTITIOUS COMPONENT IN PORTLAND CEMENT AND GEOPOLYMER CONCRETE MIXTURES

---

A Dissertation
Presented to
the Graduate School of
Clemson University

---

In Partial Fulfillment
of the Requirements for the Degree
Doctor of Philosophy
Civil Engineering

---

by
Hassan Rashidian Dezfouli
August 2017

---

Accepted by:
Dr. Prasad Rangaraju, Committee Chair
Dr. Amir Poursaee
Dr. Brad Putman
Dr. Brandon Ross

# ABSTRACT

A large amount of glass fiber is commercially produced for use in various applications. However, this process generates millions of tons of waste glass fiber annually around the world. This material has an amorphous structure that is rich in silica, alumina and calcium oxides, and if milled into a fine powder, it could potentially be used a supplementary cementitious material (SCM) in portland cement mixtures; or as a source material for production of geopolymer. So, the first objective of this research work, is to evaluate the utilization of ground glass fiber (GGF) as a SCM in portland cement mixtures, and the second objective is to study the mechanical and durability properties of GGF-based geopolymers.

To fulfill the first objective, concrete and mortar mixtures containing different dosage of GGF (i.e. 10, 20 and 30% by mass) were prepared. Fresh and hardened properties of these mixtures were tested and compared with two control mixtures, including: (i) a mixture made from 100% portland cement, and (ii) a mixture having 75% portland cement and 25% class F fly ash (by mass). It was observed that utilization of GGF up to 30% (as a cement replacement) did not influence the mechanical properties of the concrete and mortar mixtures significantly compared to control mixtures; however, the use of GGF as SCM resulted in a remarkable improvement in the durability of the mixtures. It was also seen that the utilization of GGF at the 30% replacement level, successfully mitigated the ASR-related expansion of mortar and concrete mixtures containing the crushed glass aggregate.

For the second objective, the possibility of producing geopolymer from GGF was investigated. To activate GGF, different dosage and combinations of sodium hydroxide solution (NaOH) and sodium silicate solution were used, and specimens were cured at 60$^{o}$C for 24 h. Fresh and hardened properties of geopolymer mixtures made from GGF as the precursor, were studied and compared to glass-powder (GLP) and fly ash-based geopolymer mixtures. The effect

of change in the $Na_2O$-to-binder ratio (alkali content of the activator solution) and the $SiO_2/Na_2O$ (silica content of the solution) ratio on the workability of and compressive strength of the mortar mixtures was monitored and compared to the GLP and fly ash-based geopolymers. It was seen that the strength gain in GGF-based geopolymers does not depend on the presence of sodium silicate in the activator solution; and a high compressive strength (as high as 80 MPa) can be achieved in three days, only by using sodium hydroxide solution alone.

Furthermore, to better understand parameters affecting the activation of GGF-based geopolymers, effect of temperature (from ambient to 110$^o$C) and duration of heat-curing on the compressive strength and micro-structure of GGF-based geopolymers was studied. The temperature of heat curing was seen to affect the early-age (i.e. 3 to 7 days) compressive strength of the GGF-based samples but had no significant effect on the later-age (i.e. 28 to 56 days) strength. Finally, it was concluded that GGF has a good potential to be used as a precursor to produce high strength geopolymers even at ambient temperature (23$^o$C).

Based on the results obtained from the compressive strength experiments, mixtures with the highest compressive strength were selected from each precursor to be used for the durability experiments. Durability aspects of GGF-based geopolymer such as resistance against sodium sulfate solution and magnesium sulfate solution, alkali silica reaction, drying shrinkage and corrosion of steel rebar were investigated and were compared to fly ash and GLP-based geopolymer, and an ordinary portland cement mixture (OPC). Based on this investigation it was found that GGF and fly ash-based geopolymers showed superior performance against ASR-related deterioration in comparison to GLP-based geopolymer and the OPC mixture. It was also observed that despite the fluctuation in properties at early ages, immersion in the sodium sulfate ($Na_2SO_4$) solution and magnesium sulfate ($MgSO_4$) solution did not lead to a significant mass or strength loss of GGF-based geopolymer at the later ages.

In conclusion, it can be stated that a high compressive strength GGF-based geopolymers could be produced by using an activator solution that is comprised of only NaOH. Durability experiments conducted on GGF-based geopolymer mixtures showed good performance in resisting ASR and sulfate solution exposure. Based on preliminary results it was observed that drying shrinkage of GGF and fly ash-based geopolymer was similar to the OPC mixture while the drying shrinkage of GLP-based geopolymer was significantly higher. Findings from basic experiments conducted in this study showed that factors such as: (i) the low amount of CH in the structure, (ii) low porosity, and (iii) the durable structure of the geopolymer gel in the GGF-based geopolymers, which remains stable under the aggressive conditions such as, exposure to sulfate solutions, are responsible for the superior durability performance of GGF-based geopolymer.

**DEDICATION**

*To Sepideh Yazdekhasti,*

*My lovely wife, who stood by my side in good and bad days.*

*Also, my parapets who supported me in every state of my life.*

## ACKNOWLEDGMENTS

I would like to thank and acknowledge my advisor Dr. Prasad Rangaraju, for his continues support, valuable feedbacks, mentorship, and guidance. I learned a lot from him, about many aspects of a scientific work, from planning and conducting a research work to interpreting results and writing.

Furthermore, I express my thanks to committee members of this dissertation, Dr. Amir Poursaee, Dr. Brad Putman, and Dr. Brandon Ross, for serving on my committee and for their guidance and patience throughout my research.

Also, I thank my friends, Zhengqi Li (Jason), Kaveh Afshinnia, Hatiham Zaidan, Trent Dellinger, and Hamidreza Sarraf for their great helps during this work. Whose, I had the opportunity to spend time and learn from them.

Last but not the least, I would like to thank my lovely wife and family for their unconditional love and support.

TABLE OF CONTENTS

Page

TITLE PAGE ..... i

ABSTRACT ..... ii

DEDICATION ..... v

ACKNOWLEDGMENTS ..... vi

LIST OF TABLES ..... xiv

LIST OF FIGURES ..... xviii

1 INTRODUCTION ..... 1

1.1 Glass fiber ..... 2

1.2 Production of glass fiber and waste stream ..... 3

1.3 Ground Glass Fiber (GGF) ..... 5

1.4 Potential Advantages of using GGF ..... 6

1.4.1 Chemical properties ..... 6

1.4.2 Physical properties ..... 8

1.5 Problem statement and Research significance ..... 8

1.6 Organization of the dissertation ..... 10

2 LITERATURE REVIEW ..... 15

2.1 Utilization of GGF as a SCM ..... 15

2.1.1 Properties of concrete mixtures with GGF as a SCM ..... 15

2.1.2 Durability aspects of concrete mixture having GGF as a SCM ..... 19

2.2 Geopolymer concrete ..... 20

2.2.1 Activation and formation process of geopolymers ..... 20

2.2.2 Different source material ..... 25

2.2.3 2.2.2 Role of aluminum content ..... 34

Table of Contents (Continued) Page

2.2.4 Role of calcium ..... 39
2.2.5 Effect of alkali solution on mechanical properties ..... 42
2.2.6 Effect of curing time and temperature on mechanical properties ..... 44
2.2.7 Durability properties of geopolymer ..... 47

3 EXPERIMENTAL WORK ..... 62

3.1 Material ..... 62
3.1.1 Portland cement ..... 62
3.1.2 Ground Glass Fiber ..... 62
3.1.3 Fly ash ..... 63
3.1.4 Glass-Powder ..... 63
3.1.5 Fine aggregate (siliceous sand) ..... 65
3.1.6 Coarse aggregate ..... 66
3.1.7 Crushed aggregate for ASR studies ..... 66
3.1.8 Chemicals ..... 66
3.2 Mixture proportion and curing ..... 67
3.2.1 Mixture proportion for utilization of GGF as a SCM ..... 67
3.2.2 Utilization of GGF in geopolymer production ..... 68
3.3 Test procedure ..... 71
3.3.1 Basic properties ..... 71
3.3.2 Tests for utilization of GGF as a SCM ..... 74
3.3.3 Tests for geopolymer ..... 81

4 PROPERTIES AND PERFORMANCE OF GROUND GLASS FIBER AS A POZZOLAN IN PORTLAND CEMENT CONCRETE RESULTS ON UTILIZATION OF GGF AS A SCM ..... 88

4.1 Introduction ..... 88
4.2 Materials, Mixture Proportions and Test Methods ..... 89
4.3 Results and Discussion ..... 94
4.4 Conclusion ..... 102
References ..... 102

5 ROLE OF GROUND GLASS FIBER AS A SCM IN IMPROVING SELECTED PROPERTIES OF PORTLAND CEMENT CONCRETE ..... 104

5.1 Introduction: ..... 104
5.2 EXPERIMENTAL PROGRAM ..... 106

Table of Contents (Continued) Page

5.2.1 Materials: ..... 106
5.2.2 Cement ..... 106
5.2.3 Ground Glass Fiber ..... 106
5.2.4 Fly Ash ..... 107
5.2.5 Fine Aggregate (Siliceous Sand) ..... 107
5.2.6 Coarse Aggregate: ..... 107
5.2.7 Crushed reactive aggregates: ..... 108
5.3 Mixture Properties ..... 108
5.4 Experimental Test Methods ..... 109
5.4.1 Mechanical Properties: ..... 109
5.4.2 Pozzolanic Activity ..... 109
5.4.3 Resistance Against Alkali-Silica Reaction ..... 110
5.4.4 Sulfate Attack Resistance ..... 110
5.4.5 Rapid Chloride Penetration Test ..... 110
5.5 RESULTS AND DISCUSSION ..... 111
5.5.1 Mechanical Properties: ..... 111
5.5.2 Pozzolanic Reactivity ..... 113
5.5.3 Alkali-Silica Reaction: ..... 115
5.5.4 Sulfate Attack: ..... 117
5.5.5 Chloride Permeability ..... 121
5.6 CONCLUSION ..... 122
References ..... 124

6 EFFICIENCY OF GROUND GLASS FIBER AS A CEMENTITIOUS MATERIAL, IN MITIGATION OF ALKALI-SILICA REACTION OF GLASS AGGREGATES IN MORTARS AND CONCRETE ..... 127

6.1 Introduction ..... 127
6.1.1 Background: ..... 128
6.1.2 Significance of this research ..... 131
6.2 Experimental Procedure ..... 132
6.2.1 Materials: ..... 132
6.2.2 Cement: ..... 132
6.2.3 Test procedure: ..... 133
6.2.4 Mixture proportion ..... 137
6.3 Results and discussion ..... 140

Table of Contents (Continued) Page

6.3.1 Flow test: 140
6.3.2 Pozzolanic reactivity 141
6.3.3 ASR Mitigation Performance 143
6.4 Conclusion 154
Reference 156

7 COMPARISON OF STRENGTH AND DURABILITY CHARACTERISTICS OF A GEOPOLYMER PRODUCED FROM FLY ASH, GROUND GLASS FIBER AND GLASS POWDER 161

7.1 Introduction 161
7.2 EXPERIMENTAL PROCEDURE 163
7.2.1 Materials 163
7.2.2 Mixture Proportions 165
7.2.3 Flow test and compressive strength 167
7.2.4 Dissolution of paste in HCl acid solution 167
7.2.5 Extent of dissolution 168
7.2.6 Alkali-silica reactivity of aggregates in geopolymers 168
7.3 RESULTS AND DISCUSSION 169
7.3.1 Flow test 169
7.3.2 Compressive strength 171
7.3.3 Alkali-silica reaction 178
7.4 Conclusion 182
Reference 184

8 INFLUENCE OF SELECTED PARAMETERS ON PERFORMANCE OF GEOPOLYMER PRODUCED FROM GROUND GLASS FIBER 191

8.1 Introduction: 191
8.2 Materials 196
8.2.1 Ground Glass Fiber (GGF): 196
8.2.2 Fly ash: 196
8.2.3 Activator solutions: 196
8.2.4 Fine aggregate (siliceous sand): 197
8.3 Experimental program. 197
8.3.1 Mixture proportions: 197
8.3.2 Mixing procedure and compressive strength test 199

Table of Contents (Continued) Page

8.3.3 Extent of dissolution of precursors ..... 200
8.3.4 Dissolution of Geopolymer Paste in HCl Acid ..... 200
8.3.5 Solubility of geopolymer paste in water: ..... 200
8.3.6 SEM, XRD-EDX and TGA ..... 201
8.3.7 Quantification of Unreacted Precursor Using Image Analysis ..... 202
8.4 Results and discussion ..... 202
8.4.1 Effect of precursor type on the compressive strength (GGF versus fly ash) ..... 203
8.4.2 Effect of activator solutions ..... 208
8.4.3 Effect temperature and duration of heat curing ..... 217
8.5 Conclusion ..... 222

9 A COMPARATIVE STUDY ON THE DURABILITY OF GEOPOLYMERS PRODUCED WITH GROUND GLASS FIBER, FLY ASH, AND GLASS-POWDER IN SODIUM SULFATE SOLUTION ..... 236

9.1 Introduction: ..... 236
9.1.1 Background ..... 237
9.1.2 Significance of the research ..... 240
9.2 Materials: ..... 241
9.2.1 Preparation and selection of mixture designs: ..... 244
9.2.2 Test procedure: ..... 247
9.3 Results and Discussion ..... 249
9.3.1 Change in the weight ..... 249
9.3.2 Change in the compressive strength ..... 251
9.3.3 Leaching of the alkalis from geopolymers into the soak solution ..... 253
9.3.4 Dissolution of geopolymers in sodium sulfate-solution: ..... 256
9.3.5 Mercury Intrusion Porosimetry (MIP) ..... 258
9.3.6 X-Ray Diffraction (XRD) ..... 261
9.3.7 SEM analyses ..... 267
9.3.8 EDX and TGA analysis: ..... 269
9.4 Conclusion: ..... 271

10 STUDY ON THE EFFECT OF SELECTED PARAMETERS ON THE ALKALI SILICA REACTION OF AGGREGATE IN GROUND GLASS FIBER AND FLY ASH-BASED GEOPOLYMER MORTARS ..... 282

10.1 Introduction: ..... 282
10.2 Materials ..... 285

10.2.1 Ground Glass Fiber (GGF): ..... 285
10.2.2 Fly ash: ..... 286
10.2.3 Cement ..... 286
10.2.4 Activator solutions: ..... 287
10.2.5 Fine aggregates (siliceous sand): ..... 287
10.2.6 Crushed aggregate for ASR studies ..... 287
10.3 Experimental program. ..... 288
10.3.1 Preparation and selection of mixture designs: ..... 288
10.3.2 Alkali-silica reactivity of aggregates in geopolymers ..... 289
10.3.3 Dynamic modulus of elasticity ..... 291
10.3.4 Dissolution of paste in HCl acid solution ..... 291
10.3.5 Dissolution of geopolymer paste in the alkali solution: ..... 292
10.3.6 Leachate of crushed aggregate in 1N NaOH solution: ..... 292
10.4 Results and discussion ..... 292
10.4.1 Effect of the paste type ..... 293
10.4.2 Effect of curing condition ..... 299
10.4.3 Effect of aggregate type ..... 304
10.5 Conclusion ..... 310

11 OTHER DURABILITY STUDIES (RESISTANCE AGAINST MAGNESIUM SULFATE SOLUTION, DRYING SHRINKAGE, AND CORROSION OF REBAR): 319

11.1 Resistance against magnesium sulfate solution: ..... 319
11.1.1 Change in mass and compressive strength ..... 319
11.1.2 Change in the pH of the soak solution: ..... 320
11.1.3 Dissolution of the GGF-0-10 geopolymer paste in $MgSO_4$ solution ..... 321
11.1.4 XRD pattern and expansion of GGF-0-10 geopolymer soaked in $MgSO_4$ solution 322
11.1.5 SEM images and EDX analyses: ..... 323
11.2 Drying shrinkage ..... 325
11.3 Corrosion studies: ..... 326
11.3.1 Rapid chloride permeability: ..... 327
11.3.2 Chloride penetration test ..... 328
11.3.3 Electrochemical test ..... 329

12 CONCLUSION AND RECOMMENDATIONS ..... 332

12.1 Utilization of GGF as an SCM ..... 332

Table of Contents (Continued) Page

12.2 Utilization of GGF in geopolymer concrete ..... 334
12.3 Recommendations for future works ..... 336
12.3.1 Using GGF as a SCM: ..... 336
12.3.2 Use in geopolymer mixtures: ..... 337

# LIST OF TABLES

Table Page

Table 1-1. Different types of glass fibers..... 2

Table 1-2. Chemical composition (W%) of different types of glass fiber..... 3

Table 2-1. Chemical composition of the material used in other literatures and this study. ... 19

Table 2-2. The chemical shift of $AlQn$ ..... 23

Table 2-3. Solubility results of si and al from kaolinite, albite and fly ash in NaOH and KOH. ..... 32

Table 2-4. Effect of concentration of na and silica content on the compressive strength of fly ash-based geopolymer ..... 44

Table 2-5. Effect of curing temperature and time of curing on the compressive strength of geopolymer samples ..... 46

Table 2-6. Effect of curing temperature on the compressive strength ..... 46

Table 2-7. Results of mercury intrusion porosimetry of geopolymer and opc pastes (57).... 50

Table 3-1. Chemical composition of the cementitious material ..... 64

Table 3-2. Basic properties of the cementitous materials ..... 64

Table 3-3.chemical composition of crushed aggregates ..... 66

Table 3-4. Chemical composition ration in sodium silicate solution. ..... 67

Table 3-5. Mix ID and mixture composition of the binder portion of concrete and mortar having GGF or Fly ash as a cement replacement ..... 68

Table 3-6. Details of the mixtures proportion..... 70

Table 4-1. Basic properties of the cementitous materials ..... 90

Table 4-2. Chemical composition of the cementitous materials..... 90

Table 4-3. Mixture ID and their binder composition ..... 91
Table 4-4. Flow results of fresh mortar mixtures ..... 94
Table 4-5. Compressive strength and Strength Activity Index of mortar cubes for 7 and 28 days..... 95
Table 5-1. Chemical Composition and Physical Properties of the Cementitious Materials 107
Table 5-2. Mixture ID and Composition of the Binder Portion of Concrete and Mortar .... 108
Table 5-3. Compressive Strength and Strength Activity Index of Mortar Cubes for 7 and 28 Days.....113
Table 6-1. Chemical composition of cementitious material ..... 133
Table 6-2. Mix ID and composition of the of the mixtures ..... 139
Table 6-3. Average sodium and potassium content in the paste portion of AMBT samples 154
Table 7-1. Basic properties of the precursors ..... 164
Table 7-2. Chemical composition of the precursors ..... 164
Table 7-3. Mixture proportions..... 166
Table 7-4.Compressive strength of geopolymer cubes (MPa)..... 173
Table 7-5. Residue percent of GGF-0-10 and GGF-1-10 paste after dissolution in HCl solution ..... 173
Table 7-6. Extent of the Dissolution of GGF, Fly ash and GLP in a High Alkali Media (5N NaOH Solution, for 2 h) ..... 175
Table 8-1. Chemical composition of the precursors ..... 196
Table 8-2. Mixture proportion of the geopolymer pastes (to produce mortars, fine aggregate was added to fill 55% of the volume of the mixtures)..... 198
Table 8-3. Compressive strength of the GGF and fly ash-based geopolymer mortar cubes (MPa)..... 203

Table 8-4. Extent of dissolution of GGF and Fly ash in a High Alkali Media (5N NaOH solution, for 2 h) ..... 206

Table 8-5. Results of dissolution in HCl solution for GGF-0-10 and GGF-1-10 pastes .....211

Table 8-6. Final setting time of GGF-based geopolymer paste (minutes)..... 216

Table 8-7. Results of HCl dissolution test for the GGF-0-10 paste cured at different temperatures ..... 220

Table 9-1. Chemical composition of precursor source materials ..... 241

Table 9-2. Physical properties of precursor source materials ..... 242

Table 9-3. Mix ID and the proportion of geopolymers..... 245

Table 9-4. Mix proportion for per cubic meter of geopolymer mixtures..... 246

Table 9-5. Specimen type used for each of the test. ..... 249

Table 9-6. Change in the weight of geopolymer mortar specimens due to soaking in the 5% sodium sulfate solution (possitive values show weightn and negative values show weight loss) ..... 250

Table 9-7. Change in the compressive strength of geopolymer mortar samples due to the sulfate attack..... 252

Table 9-8. Change in the sodium and potassium content of the geopolymer samples due to sulfate attack..... 254

Table 9-9. Concentration of ions leached from each geopolymer sample into the sodium sulfate solution (dissolution test)..... 257

Table 9-10. Sulfur content of geopolymers by EDX. (*The elements considered for the EDX analysis are: Si, Al, Ca, Na, K, Fe, and S)..... 270

Table 11-1. Effect of 5% $MgSO_4$ solution on the compressive strength and weight of GGF-0-10 specimens ..... 320

Table 11-2. Ions concentration in $MgSO_4$ solution (ppm) ..... 322

Table 11-3. Sulfur content of geopolymers by EDX. (*The elements considered for the EDX analysis are: Si, Al, Ca, Na, K, Fe, and S)..... 324

Table 11-4. Mixture design of the paste portion of mortar mixtures and their compressive strength (required amount of sand was used to fill 55% of the volume of each mixture)... 327

Table 11-5. RCPT test results at 7 and 28 days ..... 328

LIST OF FIGURES

Figure Page

Figure 1-1. A bundle of glass fibers..... 2

Figure 1-2. Furnace for glass melting..... 4

Figure 1-3. Fiberglass forming process ..... 4

Figure 1-4. Production of glass fiber ..... 5

Figure 1-5. View of Ground Glass Fiber (GGF) ..... 6

Figure 2-1. Simplified geopolymerisation process..... 21

Figure 2-2. Chemical shift of the $Si(nAl)$ structural unit ..... 23

Figure 2-3. The MAS-NMR result of the (a) 27Al and (b) 29Si..... 24

Figure 2-4. The geopolymer structure presented by Davidovits ..... 24

Figure 2-5. The geopolymer structure model presented by Barbosa 2000 ..... 25

Figure 2-6. Effect of NaOH concentration on (a) flexural strength (b) and compress strength ..... 27

Figure 2-7. Development of compressive strength of geopolymer made from slag, class C, and class F fly ash ..... 30

Figure 2-8. The isothermal conduction calorimetric results a) when test performed on fresh samples at 27oC b) when test performed at 60°C on the samples cured at 27oC for 48h. .... 30

Figure 2-9 Microstructure of mortar samples containing 5% metakaolin activated with a) 5M NaOH solution b) 8M NaOH solution and c) 10M NaoH solution ..... 32

Figure 2-10. Effect of Si/Al ratio on the structure of geopolymer ..... 34

Figure 2-11. Compressive strength and young's modules of the geopolymer samples with varying Si/Al ratio..... 36

Figure 2-12. Effect of $SiO2/Al2O3$ on the compressive strength and setting time. ..... 37

Figure 2-13. Influence of calcium content on the compressive strength of fly ash-based geopolymer ..... 39

Figure 2-14. Coexistence of two zones of geopolymer binder (a) and C-S-H (b) for 20% slag (left picture-a) and 60% slag replacement (right picture b) ..... 41

Figure 2-15. Results of 7-days compressive strength of two geopolymer sample containing various Ca salts. ..... 42

Figure 2-16. Effect of curing temperature (a) and time of the curing (b) on the 7-day compressive strength of geopolymer samples ..... 45

Figure 2-17. Expansion of geopolymer and OPC samples due to ASR ..... 49

Figure 2-18. Change in the compressive strength of OPC and geopolymer samples (BFAGC) due to the sulfate attack ..... 52

Figure 2-19. Residual compressive strength of geopolymer samples immersed in the $MgSO4$ solution. Mix design with 5%, 6.5% and 8% Na2O content are named as GP1, GP2 and GP3 respectively ..... 53

Figure 3-1. Appearance of GGF. a) normal view, and b) SEM image ..... 63

Figure 3-2. Appearance of GLP. a) normal view, and b) SEM image ..... 64

Figure 3-3. Particle size distribution of Cement, fly ash and GGF ..... 65

Figure 3-4. XRD pattern of a) GGF, b) Fly ash, c) Glass-powder and d) Cement. ..... 65

Figure 3-5. View of the Blaine apparatus ..... 73

Figure 3-6. A view of tensile strength test a) under load in universal testing machine b) after the test ..... 79

Figure 3-7. View of sample in compressometer cage to measure the MOE ..... 80

Figure 3-8. View of the RCPT set-up ..... 81

Figure 3-9. GGF-based geopolymer mortar cubes in a 5% sodium sulfate solution ..... 84
Figure 3-10. Dissolution of geopolymer powder sample in sulfate-rich solutions. a) The bottles containing crushed paste and the sulfate solution; b) filtered solution, c) filtered solids. ..... 85
Figure 4-1. XRD results of GGF (left) and fly ash (right) ..... 90
Figure 4-2. Expansion curve of the mortar bras (AMBT) ..... 97
Figure 4-3. Visual appurtenance of mortar bars after 28 days ..... 98
Figure 4-4. SEM observation on polished mortar bars a) CTRL-1 b) CTRL-2 and C) GGF-30 mixtures. ..... 98
Figure 4-5. Expansion curves of concrete bars (MCPT) ..... 99
Figure 5-1. Compressive strength (top) and splitting tensile strength (bottom) of concrete samples [1 MPa is equal to 145 psi]. ..... 112
Figure 5-2. Effect of GGF dosage on the TGA result [where CH is calcium hydroxide content of the sample and CHo is the calcium hydroxide content of the CTRL-1 (100% Cement)] ..... 114
Figure 5-3. Expansion of the mortar bar versus time ..... 116
Figure 5-4. Expansion results of mortar bars subjected to 5% sodium sulfate solution. ..... 119
FIGURE 5-5. TGA and DTGA results of mortar samples immersed in 5% sodium-sulfate solution for 200 days: (a) CTRL-1 (b) CTRL-2 (c) GGF-30 ..... 120
Figure 5-6. Result of rapid chloride penetration on concrete samples ..... 122
Figure 6-1. Flow test results of control mixture and mixtures containing 20% SCM ..... 140
Figure 6-2. Particle shape of GGF (a) and glass-powder (b) ..... 141
Figure 6-3. Strength activity index of mortar cubes containing GGF, GLP and meta-kaolin at 28 days ..... 142

Figure 6-4. Normalized Calcium hydroxide content of paste samples containing 20% GGF, GLP and meta-kaolin. (CH is the calcium hydroxide content of the samples, and, CH0 is the calcium hydroxide content of the control sample) ..... 143
Figure 6-5. Expansion behavior of mortar bars (ASTM C1567)..... 144
Figure 6-6. Expansion behavior of miniature concert prisms (AASHTO-TP110)..... 146
Figure 6-7. Formation of ASR gel within glass aggregate in the control samples without SCMs ..... 148
Figure 6-8. SEM image from GLP-30 mortar bar section..... 150
Figure 6-9. SEM images from mortar bar section a) MK-10 and b) GGF-30..... 151
Figure 7-1. XRD pattern of the cementitious materials: GGF (top left), Fly ash (top right), Glass-powder (bottom left) and Cement (bottom right) ..... 165
Figure 7-2. Flow results of geopolymer mortars ..... 171
Figure 7-3. Change in the compressive strength of geopolymers mortar at 28 days due to the change in Na content and $SiO_2/Na_2O$ ..... 174
Figure 7-4. XRD pattern of fly ash particles and F-1-10 paste ..... 175
Figure 7-5. General appearance of GGF-0-10 (a), F-1-10 (b) and GLP-1-10 (c)..... 176
Figure 7-6. Microstructure of a) GGF-0-10 and b) F-1-10 Paste ..... 177
Figure 7-7. Formation of ASR gel in the paste matrix of GLP-1-10 Paste ..... 178
Figure 7-8. Expansion due to ASR ..... 179
Figure 7-9. a) Severely cracked mortar bars after 7 days of exposure to ASR accelerating condition, and b) SEM picture of GLP-1-10 sample after 3 days of exposure to ASR accelerating condition..... 180
Figure 7-10. TGA and DTGA curve of 7-days old paste samples. a) F-1-10 paste, and b) G-0-10 paste. ..... 181

Figure 7-11. SEM of GGF-0-10, a) Uncracked aggregate, and b) paste matrix. SEM of F-1-10, c) Uncracked aggregate, and d) Paste Matrix ..... 182
Figure 8-1. Raw GGF, (a). Normal appearance, (b). SEM image ..... 197
Figure 8-2. XRD pattern of precursors, (a). GGF, and (b). Fly ash ..... 197
Figure 8-3. SEM images of cracked surface of geopolymer samples. a). GGF-based specimen, b). Fly ash-based specimen ..... 205
Figure 8-4. XRD pattern of the raw fly ash and F-1-10 geopolymer paste ..... 207
Figure 8-5. Effect of sodium content of the activator solution on the compressive strength of the GGF and fly ash-based geopolymer mortar mixtures. ..... 209
Figure 8-6. Effect of silica content of the activator solution on the compressive strength of GGF and fly ash-based geopolymers ..... 210
Figure 8-7. Image analysis results: a) performed on GGF-0-10, and b) Performed on GGF-1-10 pastes. (The unreacted GGF ratio is defined as: area of the unreacted particles" divided by the total area of the pate and unreacted particles) ..... 212
Figure 8-8. Effect of $Na_2O$-to-binder ratio on the compressive strength of GGF-based geopolymer samples (after 28 days) ..... 214
Figure 8-9. Image analysis results: a) performed on GGF-0-5, and b) Performed on GGF-0-20 pastes. (The unreacted GGF ratio is defined as: area of the unreacted particles" divided by the total area of the pate and unreacted particles) ..... 215
Figure 8-10. Dissolution of Si and Al from GGF-based geopolymer paste into deionized water ..... 217
Figure 8-11. Effect of curing temperature on the compressive strength of GGF-0-10 mortar cubes ..... 218
Figure 8-12. SEM image of geopolymer paste samples: a). cured at 60°C, b). cured at 110°C

..... 219

Figure 8-13. Comparison of XRD patterns of GGF-0-10 paste cured at 23°C and 110°C .. 221

Figure 8-14. Effect of heat-curing duration on the compressive strength of GGF-0-10 mortar cubes ..... 222

Figure 9-1. XRD pattern of the precursors. (a). GGF, (b). Fly ash, (c). GLP. (Q: Quartz, M: Mullite and H: Hematite) ..... 243

Figure 9-2. Visual appearance of geopolymer cubes after being soaked in the 5% sodium sulfate solution for 120 days, a) F-1-10 and, b) GGF-0-10. ..... 250

Figure 9-3. a) Formation of a white deposit on the surface of GLP-1-10 sample. b) EDX results of the white deposit ..... 251

Figure 9-4. Change in pH of the solution versus time. (Five grams of crushed paste was introduced to 100 ml of 5% sodium sulfate solution) ..... 255

Figure 9-5. Formation of an ASR-like gel in the structure of the GLP-1-10 sample ..... 258

Figure 9-6. MIP test results. a) Pore size vs volume intruded for non-exposed samples, b) change in the porosity of exposed samples by time. ..... 259

Figure 9-7. Hollow fly ash particles in F-1-10 sample ..... 260

Figure 9-8. XRD pattern of the unexposed and exposed fly ash-based geopolymer samples. (Q: Quartz, M: Mullite, H: Hematite, C: Calcite, N: Natrite, F: Feldspar) ..... 263

Figure 9-9. XRD pattern of the unexposed and exposed GGF-based geopolymer samples. (Q: Quartz, C: Calcite, T: Tobermorite, N: Natrite) ..... 265

Figure 9-10. XRD pattern of the unexposed and exposed GLP-based geopolymer samples. (Q: Quartz, C: Calcite,) ..... 266

Figure 9-11. SEM images of the geopolymer specimen exposed to the 5% sodium sulfate solution ..... 268

Figure 9-12. Paste portion of geopolymer samples after 120-day exposure to a 5% sodium sulfate solution. (a). GGF-0-10, (b). F-1-10, and (c). GLP-1-10..... 269

Figure 9-13. TGA and DTGA results of unexposed geopolymer pastes. (a). GGF-0-10, and (b). GLP-1-10. ..... 271

Figure 11-1. Change in pH of sulfate solution versus time. (Five grams of crushed GGF-0-10 paste was introduced to 100 ml of 5% of each sulfate solution) ..... 321

Figure 11-2. XRD pattern of GGF-0-10 paste after exposure to 5% $MgSO_4$ solution for 28 days..... 323

Figure 11-3. Expansion of GGF-0-10 mortar bars in different aqueous media .....323

Figure 11-4. View of GGF-0-10 sample after 240 days of exposure to 5% $MgSO_4$ solution. a) Middle part of the crossed section, and b) edge of the crossed section. .....324

Figure 11-5. Shrinkage of mortar bars versus time .....326

Figure 11-6. Depth of chloride penetration for each mixture versus time .....329

Figure 11-7. View of the exposure condition.....330

Figure 11-8. View of steel bars in the exposed specimens after nine month.....330

# CHAPTER ONE

# INTRODUCTION

Ordinary Portland cement concrete is by far the most widely used material in construction of infrastructure. However, the cement production process is associated with a large amount of $CO_2$ emission. Approximately one ton of $CO_2$ is emitted due to production of every ton of cement (1). In an effort to develop a low $CO_2$ footprint construction material and to use a large volume of waste or industrial byproducts without having to dispose them off in landfills, utilization of large volumes of supplementary cementitious materials (SCM) in concrete mixtures has gained a lot of attention in recent years (2). SCMs are being used to improve the properties of both the fresh and hardened concrete mixtures. Materials such as fly ash, slag and silica fume are some of the very well-known examples of SCMs.

While use of SCMs to reduce portland cement consumption in concrete is now widely practiced in the industry, another approach that is gaining traction in limited circumstances is the use of "geopolymer" concrete. Geopolymer binders contain Al-Si network, which form due to the reaction between a source material for alumino-siliceous compounds, such as various supplementary cementitious materials (SCMs) (for ex: fly ash, slag, meta-kaolin, ground glass and others) and alkali activators such as sodium hydroxide (NaOH) and sodium silicate solutions. Due to the superior durability properties of geopolymer concretes in comparison to the conventional portland cement concretes, this material has a good potential to be used as an alternative construction material.

Considering the chemical composition of the glass fiber, which contains silica, alumina and calcium as its main components; the utilization of waste glass fiber as an SCM or as a source material for geopolymer concrete can be considered. This study, therefore investigates the utilization of waste glass fiber as an SCM in portland cement concrete and as a source material

for the geopolymer concrete.

## 1.1 Glass fiber

Glass fibers a material made of several extremely fine fibers of glass (Figure 1-1) bundled together with an adhesive coating to form a strand. This material is the key component in the production of fiber-glass-based composites such as Fiber-Feinforced Plastic (FRP), also known as Glass-Reinforced Plastic (GRP) and has several applications in different fields, including aerospace, construction, pipes, tanks, electronics, etc.

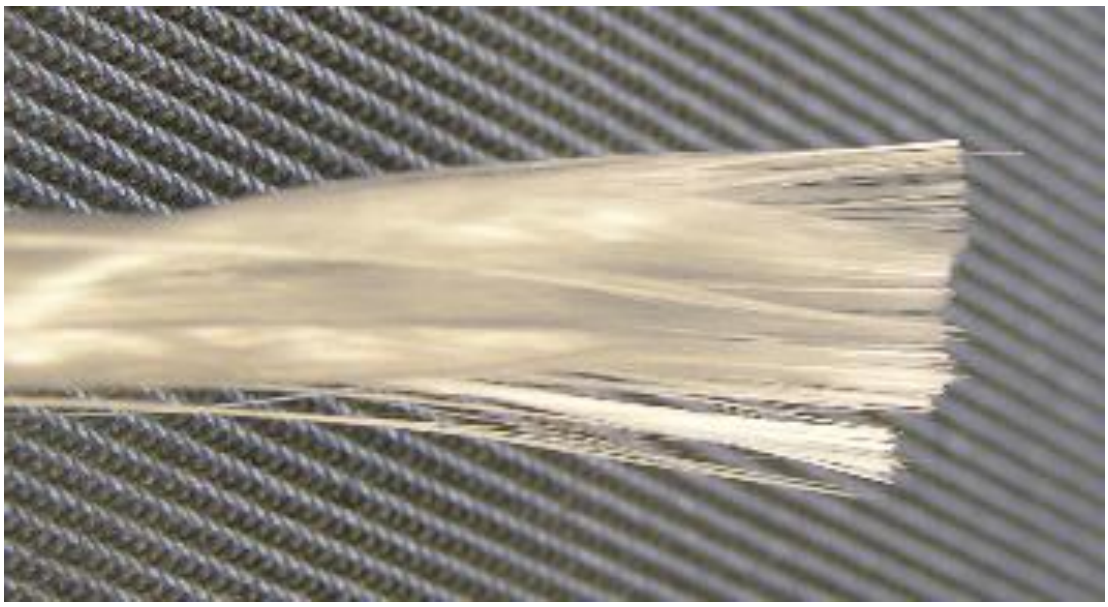

Figure 1-1. A Bundle of glass fibers

Depending on the final use of the products, several types of glass fiber are being produced. Table 1-1 shows the main types of glass fiber that are used in different applications. Among these types, over 90% of all the glass fibers are E-glass fiber, which is a general purpose glass fiber. The difference between each type of glass fiber is mostly related to their chemical composition and the sizing process. Table 1-2 and Table 1-3, show the chemical composition, and selected Physical and mechanical properties of commercial glass fibers (1).

Table 1-1. Different types of glass fibers (1)

| Letter designation | Property or characteristic |
|---|---|
| E, electrical | Low electrical conductivity |
| S, strength | High strength |
| C, chemical | High chemical durability |
| M, modulus | High stiffness |
| A, alkali | High alkali or soda lime glass |
| D, dielectric | Low dielectric constant |

Table 1-2. Chemical composition (w%) of different types of glass fiber (modified from 1)

| Fiber | $SiO_2$ | $B_2O_3$ | $Al_2O_3$ | $CaO$ | $MgO$ | $TiO_2$ | $Na_2O$ | $K_2O$ | $Fe_2O_3$ |
|---|---|---|---|---|---|---|---|---|---|
| Boron-containing E-glass | 52-56 | 4-6 | 12-15 | 21-23 | 0.4-4 | 0.2-0.5 | 0-1 | Trace | 0.2-0.4 |
| Boron-free E-glass | 60.1 | - | 13.2 | 22.1 | 3.1 | 0.5 | 0.6 | 0.2 | 0.4 |
| ECR-glass | 58.2 | - | 11.6 | 21.7 | 2.0 | 2.5 | 1.0 | 0.2 | 0.1 |
| D-glass | 55.7 | 26.5 | 13.7 | 2.8 | 1.0 | - | 0.1 | 0.1 | - |
| S-, R-glass | 60-65 | | - | 23-25 | 0-9 | 6-11 | 0-0.1 | - | 0-0.1 |

## 1.2 Production of glass fiber and waste stream

The schematic view of glass fiber production is presented in Figures 1-2 and 1-3. The production process starts with the selection and blending of the required amount of raw materials such as silica sand, limestone, and soda ash and other ingredients like calcined alumina, borax, feldspar (3). These material are heated to over 1300 degrees Celsius (Figure 1-2, furnace) to melt and form a homogenized liquid which is free of all gaseous inclusions. The molten glass then goes through the refiner section and forehearth section, in which the material is cooled to reach the desirable viscosity. The glass liquid then flows through a bushing made of platinum-rhodium alloy which has a large number of small holes (400 to 8000) through which the glass fiber is drawn. The glass fiber is cooled rapidly to avoid any crystallization. Finally, a sizing is applied on the surface of the fiber, by using a cylindrical applicator which rotates continuously thorough a sizing bath. The applicator, maintains a thin film of the sizing and applies it to the surface of the glass filaments as they contact the applicator (1). Considering the production process of glass fibers, waste glass

fiber may be produced during each of the three production stages - 1) melting and extrusion of the melt glass (chemical impurity), 2) sizing and handling (physical damage) and 3) weaving the final product (left over)

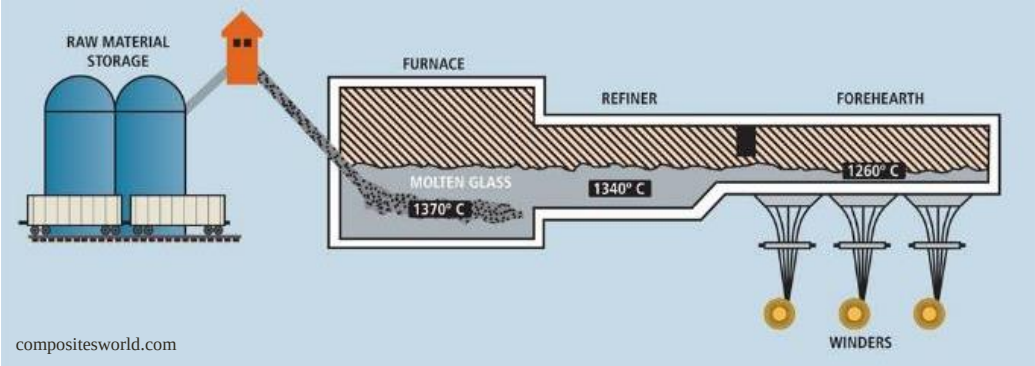


Figure 1-2. Furnace for glass melting

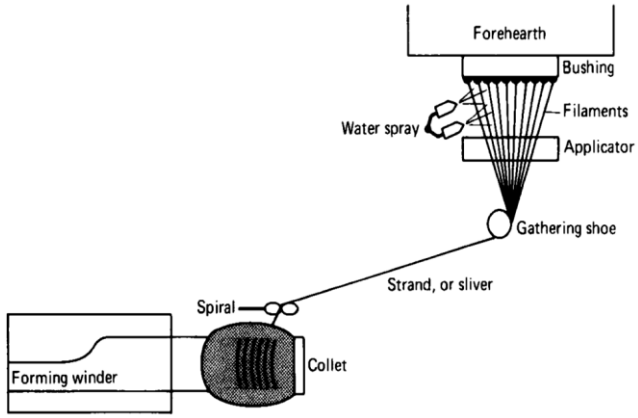


Figure 1-3. Fiberglass forming process (1)

In 2011, a total amount of 4.88 million metric-tons of glass fiber was produced worldwide, of which 1 million tons was produced in the North America (4, 5). According to a report by the Department of Energy in 2005, the total amount of waste glass fiber in United States that ends up in landfills was about 250,000 tons per year, which can be reclaimed for beneficial uses. This amount can be further increased to 500,000 tons/year if the waste streams from the users of glass fibers is also considered (6). Therefore, using this material as a construction material can save thousands of tons of this material from ending up in landfills. Although, number

of studies have been performed on recycling potential of waste GRP and other glass fiber product in concrete, very few studies have focused on utilizing glass fiber waste as a cementitious material in portland cement and geopolymer concretes. Figure 1-4 shows the final form of the glass-fiber product.


Figure 1-4. Production of glass fiber

## 1.3 Ground Glass Fiber (GGF)

Ground Glass Fiber (GGF) is a fine powder material that is produced by milling the off-spec glass fiber using a mill machine (Figure 1-5). As a result, this material possesses the same chemical composition as the original material but failed to achieve the required physical properties of the final products. This powder is rich in silica, alumina and calcium and has a good potential for use as a SCM in portland cement based concrete. In this study, the utilization of GGF as a pozzolan for cement replacement and also a source material for geopolymer production is investigated.

Figure 1-5. View of Ground Glass Fiber (GGF)

## 1.4 Potential Advantages of using GGF

Considering the large volumes of waste produced during the manufacturing process of glass fiber, finding a sustainable solution for recycling of this material is very important. Considering the physical properties of GGF and its silica-rich chemical composition, GGF is a good candidate for further study to investigate it ability to meet the requirements of ASTM C618, for being considered as a pozzolanic material. In addition, unlike the other pozzolanic material such as fly ash, silica fume and slag, GGF is an engineered material which has been produced in a controlled environment. This results in a uniform chemical composition of the material which eases the usage of this material as a SCM in concrete or a source material in geopolymer without concerns for variability in material properties.

### *1.4.1 Chemical properties*

Utilizing different types of glass powder in concrete is not a novel solution for recycling waste glass. However, due to the high amount of alkali present in glass powder (typically from recycling the soda-lime glass from container glass) susceptibility to Alkali-Silica Reaction (ASR)

has been always a big concern in usage of glass powder in concrete. On the other hand, GGF has a very low sodium content which could reduce the risk of ASR of the aggregate in the concrete mixtures. In addition, GGF has a relatively high amount of alumina. Presence of alumina in the concrete paste is known to reduce the risk of ASR by either absorbing the alkali or lowering in the silica dissolution rate from the reactive aggregate (7, 8).

Like the other glass based products, GGF has a high silica content (around 50%). Presence of reactive silica is essential for any supplementary cementitious material (SCM) to cause the pozzolanic reaction. The manufacturing procedure of the glass fiber leads to the formation of an amorphous structure in this material. Therefore, the silica portion of the GGF can promote the pozzolanic reaction by reacting with the calcium hydroxide of the cement hydration.

GGF also can be used as source material in geopolymer. Geopolymer is a cement-free concrete which is produced by the activation of the silica and alumina rich material. Considering the high amount silica, (around 50%) and alumina (10-11%) GGF can be used in producing geopolymer material. In addition to this, GGF has a high level of calcium oxide (20%) which is known to accelerate the geopolymer strength gain (9, 10).

Finally, the major benefit of GGF is its uniform and constant chemical composition. Glass fiber is an engineered material that is used in many of the technical applications. Therefore, unlike the other common SCMs like fly ash, slag, and silica-fume its chemical composition does not vary significantly from one batch to another. This characteristic is particularly beneficial in usage of GGF in geopolymer production as the amount of each component plays an important role in the geopolymer properties. As a result of this constant chemical composition, mixture design of the geopolymer can be done with higher level of certainty in compare to conventional fly ash based geopolymer.

### *1.4.2 Physical properties*

In addition to its chemical properties, the physical properties of GGF such as its high specific surface area (fineness) make it a suitable choice for utilization of this material as an SCM for concrete or as a source material for geopolymer production. Also, due to the hardness of this material, the small particles of GGF can potentially act as micro aggregates in the geopolymer paste and enhance the mechanical properties of the final product.

In addition, due to the production process of glass fiber as the thin yarn, the GGF had a small particles sizes with the smooth and shiny surfaces. The small particle size of GGF (average size of 4 $\mu$m) increases the rate of the chemical reaction and also refines the pore structure of the paste. Finally, materials has a specific gravity of 2.6 which is in the range of other conventional SCMs and can be used in concrete mixture by the weight replacement.

## 1.5 Problem statement and Research significance

Every year a huge amount of cement is being produced worldwide. According to the U.S. Geological Survey, Mineral Commodity Summaries, the world total production of cement in 2014, has reached 4.1 billion tons (11). This process is responsible for a considerable amount of $CO_2$ releases and in 2004 represented a 3.8% of the global $CO_2$ emission (12). Utilization of the supplementary cementitious materials (SCMs) like fly ash, slag, metakaolin etc. is one of the accepted ways in reducing the total cement usage. In addition, usage of the SCMs in the concrete improves the durability properties of the final product.

In past years, utilizing of the conventional SCMs (i.e. fly ash, slag, silica fume, metakaolin etc.) has been the subject of a large number of studies. In addition, in recent years the pozzolanic properties of the different waste glass products have been researched by a number of researchers. However few studies have been conducted on the employing waste glass fiber as a construction material. This study, therefore, presents a comprehensive research on evaluating the

fresh and hardened properties of concrete and mortar mixtures with more emphasis on its ability in mitigation of deleterious alkali-silica reaction.

In addition to employing SCMs, one of the other methods that is being explored to reduce the cement consumption is the utilization of the portland cement-free construction materials. Geopolymer is a portland cement free construction material that is getting more popular recently. Considering its unique durability properties, geopolymer can be a good choice in replacing portland cement concrete in an aggressive environment. As of now, several studies have been conducted on manufacturing of geopolymer by activation of the silica and alumina rich waste materials. However, very few studies have been found to be performed on the activation of the GGF (two published paper on the activation of VCAS).

Preliminary results, have confirmed the pozzolanic properties of the GGF when used as the cement replacement in concrete. Furthermore, the material was successfully activated, and a geopolymer mixture with a compressive strength of more than 10,000 psi was produced. Therefore, considering the possibility of usage of this material in the field of construction an effort is made to investigate the characteristic of the construction materials made with GGF.

Present study has three main objectives:

(1) To perform a comprehensive investigation on the properties of portland cement concrete made with GGF as the cement replacement material.

(2) To develop and investigate the properties of a GGF-based geopolymer (GGF as its source material)

(3) Based on the work accomplished in objectives 1 and 2, to develop a guideline for application of GGF as a pozzolanic material or as a source material for use with portland cement concrete and geopolymer concrete, respectively.

## 1.6 Organization of the dissertation

This dissertation includes twelve chapters. The first and second chapters are the introduction and the literature review, respectively. Chapter three contains the experimental work which was conducted in this study. The materials used, the test procedures employed and the mixtures' proportion developed are presented in this chapter. Chapters four trough ten consist of seven research papers, that have been either published, in-press, under review, or to be submitted that focus on investigations conducted on different aspects of utilization of GGF as either SCM or as a source material in the production of geopolymer. Chapter eleven presents the results from ongoing studies, and chapter twelve presents the conclusions and recommendations.

Chapter 1: This chapter presents an introduction on the current study. The production process of glass fiber and the waste stream associated with it are explained in this chapter. Furthermore, the purpose of the research, the problem statement, and the significance of the research are presented in this chapter.

Chapter 2: This chapter contains a literature review on the past studies that are related to the current work. Considering two different objectives of this study, the first part of this chapter presents the results of the earlier work, in which, products of waste glass fiber have been used in concrete mixtures. In the second part, a comprehensive review is made on the mechanical and durability properties of geopolymer mortar and concrete mixtures.

Chapter 3: In this chapter, the experimental program, materials that were used in this research, and some basic characteristics of GGF, fly ash, cement, GLP, and other materials are evaluated and presented.

Chapter 4. This chapter discusses the basic characteristics of the GGF containing mixtures. The pozzolanic reactivity of GGF, and the resistance of mortar and concrete mixtures, having different levels of GGF, against ASR was investigated. Results were compared to a control

mixture which had no cement replaced (CTRL-1) and another concrete mixture congaing 25% class F fly ash as the cement replacement material (CTRL-2).

Chapter 5. In this chapter, mechanical and durability properties of mortar and concrete mixtures having 10, 20, and 30% GGF as the cement replacement were investigated. Mechanical properties such as compressive strength, tensile splitting strength, and modulus of elasticity of concrete samples were evaluated. In addition, durability properties of these mixtures against ASR, sulfate attack and chloride ion penetration were evaluated. Both mechanical and durability properties of GGF containing mixtures were compared with the results obtained from CTRL-1 and CTRL-2 mixture.

Chapter 6. In this chapter, the utilization of GGF as a source material for the geopolymer production is presnted. Fresh and hardened properties of the GGF-based geopolymer made with different dosages of alkali activators were evaluated and compared with a fly ash-based and GLP-based geopolymer. The mixtures with the highest compressive strength from each of the source materials were selected, and their durability resistance against alkali silica reaction was evaluated.

Chapter 7. In this chapter, effectiveness of GGF in the mitigation of ASR in mortar and concrete mixtures containing glass aggregates was studied. For comparison purposes, results were compared with mixture made with different dosages of GLP and meta-kaolin.

Chapter 8. Effect of using different alkali content and different combinations of alkali activator solutions on the compressive strength and micro-structure of GGF-based geopolymer mixtures were investigated and compared with fly ash-based geopolymer mixtures. Furthermore, effect of temperature (from ambient to 110$^{o}$C) and duration of heat-curing on the compressive strength and micro-structure of GGF-based geopolymers were studied.

Chapter 9. This chapter, resistance of selected geopolymer mortar mixtures against the sodium sulfate solution was evaluated. The mixture with the highest compressive strength from

each of the source materials was selected tested, and change in the compressive strength, mass, microstructure, leaching behaviors, etc. were monitored up to 120 days.

Chapter 10. This chapter discusses the parameters affecting the ASR deterioration in GGF and fly ash-based geopolymer mixtures. For this purpose, fly ash and GGF-based geopolymer mortar bars were produced, and the expansion results were compared to a portland cement mixture. Moreover, the effect two different ASR-accelerating curing conditions on the expansion behavior of geopolymers were studied. In this study, three sets of aggregate, each showing different level of reactivity, and having various Si and Ca contents were used.

Chapter 11. In this chapter, preliminary results of ongoing experiments on the durability properties of GGF-based geopolymer are presented. These experiments include, the resistance against magnesium sulfate solution, drying shrinkage, and corrosion of steel rebar.

Chapter 12. This chapter summarizes the conclusions of this work. Also, some recommendations for future works are presented in this chapter.

# References:


1. Henry, S. D., Moosbrugger, C., Anton, G. J., Sanders, B. R., Hrivnak, N., Terman, C., ... & Scott Jr, W. W. (2001). ASM handbook (Vol. 21). Materials Park, OH, USA: ASM international.
2. Li, C., Sun, H., & Li, L. (2010). A review: The comparison between alkali-activated slag (Si+ Ca) and metakaolin (Si+ Al) cements. Cement and Concrete Research, 40(9), 1341-1349.
3. Masuelli, M. A. (Ed.). (2013). Fiber Reinforced Polymers: The Technology Applied for Concrete Repair. InTech.
4. R. A. Cubeta, "Utilizing Recycled Fiberglass for Affordable, Green Composite Technology," in COMPOSITES 2013, Orlando, 2013.
5. http://www.tecnologiademateriais.com.br/mt/2012/cobertura_paineis/congresso_pr/apresentacoes/Jushi.pdf.
6. Hemmings, R. Process for Converting Waste Glass Fiber into Value-dded Products. DOE Report No. DE-FG36-03GO13015. Albacem, LLC, Peoria, Ill., 2005
7. Chappex, T. and Scrivener, K.L., 2012. The influence of aluminium on the dissolution of amorphous silica and its relation to alkali silica reaction. Cement and Concrete Research, 42(12), pp.1645-1649.
8. Hong, S.Y. and Glasser, F.P., 2002. Alkali sorption by CSH and CASH gels: Part II. Role of alumina. Cement and Concrete Research, 32(7), pp.1101-1111.
9. Yip, C.K., Lukey, G.C. and Van Deventer, J.S.J., 2005. The coexistence of geopolymeric gel and calcium silicate hydrate at the early stage of alkaline activation. Cement and Concrete Research, 35(9), pp.1688-1697.
10. Puligilla, S. and Mondal, P., 2013. Role of slag in microstructural development and hardening of fly ash-slag geopolymer. Cement and Concrete Research,43, pp.70-80.

11. U.S. Geological Survey, 2015, Mineral commodity summaries 2015: U.S. Geological Survey, 196 p, http://minerals.usgs.gov/minerals/pubs/mcs/2015/mcs2015.pdf
12. National Ready Mixed Concrete Association, 2008. Concrete CO2 Fact Sheet. NRMCA Publication, (2PCO2), p.13.

# CHAPTER 2

# LITERATURE REVIEW

This section, presents findings from past studies related to the utilization of waste glass fiber as a SCM, and also reviews some of the published studies in the geopolymer area relevant to the consideration of GGF as a source material. Considering the aim of present study, this section has two main parts. First, the utilization of glass powder as a SCM are presented (section 2.1), and secondly, some of the published literatures related to the production of geopolymer are reviewed in sections 2.2 and 2.3.

## 2.1 Utilization of GGF as a SCM

Utilization of GGF as a SCM is a relatively new idea. Unlike the conventional SCMs like fly ash, slag, metakaolin and silica fume, which are known to be used for several decades, the first usage of this material as pozzolan was patented in 2004 by Hemmings et al. In this patent, they named the milled glass fiber as VCAS Pozzolan (for Vitreous Calcium-Alumino-Silicate). (1).

### *2.1.1 Properties of concrete mixtures with GGF as a SCM*

Considering the great potential of GGF – if used as a SCM - in saving the energy that is associated with production of portland cement, a comprehensive study on this subject was done by the Department Of Energy (DOE) and reported in 2005. In this study, VCAS was produced by shredding and milling the waste glass powder into a very small particle size (i.e. 3 and 8 microns). Using the milled product, several properties of fresh and hardened mixtures containing VCAS pozzolan were evaluated and compared with a control mixture with plain cement. In addition, the amount of energy that can be saved by replacing cement with this material was also estimated (2).

It was found that VCAS improved the workability of the fresh mortar and a mixture

containing 20% VCAS showed a flow equal to 131% of the flow of the control mixture. The strength activity index results also revealed a clear pozzolanic effect of this material as the mortar containing 20% of 3 microns VCAS pozzolan achieved 123% and 149% strength of the control sample. The durably properties of the mix with 20% VCAS were tested against sulfate attack and ASR damage. The sulfate attack results showed that while the control sample (made with white cement) completely disintegrated after 290 days, the mix with 20% VCAS showed a very small amount of expansion after 405 days. The ASR tests results also showed an excellent performance of the mixture with 20% VCAS over the control sample. It was also reported that when the mixtures were tested using the ASTM C441 method, a significant difference was seen in the 14-day expansion (0.0045% for a mix with 20% VCAS and 0.337% for the control mix).

The energy saving potential associated with the replacement of cement with VCAS was also calculated in this report. According to this study, 250,000 tons of waste glass fiber is produced each year in 2005. It was estimated that if 200,000 tons of this material can be used as a cement replacement in 2010, a 946,340 million BTU of energy can be saved each year.

Properties of concrete containing VCAS Pozzolan were studied by Hossain et al. (3). The results were compared with a control mix (with 100% cement), and mixtures with silica fume. It was observed that while mixtures with silica fume lowered the slump, the VCAS containing mixtures increased the slump amount. It was also observed that both VCAS and silica fume improved the short-term and long-term compressive strength. However, both pozzolans caused higher free and plastic shrinkage (higher shrinkage of silica fume mixtures with an equal dosage with VCAS) of the mortars in compare to the control mix. In addition, a clear improvement was seen in the case of chloride permeability test when VCAS was used as the cement replacement at 15% dosage level (3).

A comprehensive study on the pozzolanic properties of VCAS was performed by

Neithalath et al. (4). According to this study, it was found that while VCAS (with almost 24% Ca) does not have any cementitious properties, it does show a significant pozzolanic effect. It was also found that, mixtures with 6, 9 and 15% VCAS as cement replacement showed a strength activity index of higher than 100% for all the 14, 28 and 56-days tests. In addition, it was reported that addition of VCAS (as cement a replacement) is very beneficial in reducing the $Ca(OH)_2$ level, after 7 days (4).

In another study, Kamali and Gharemaninezhad (5) investigated the hydration and microstructure of cement pastes modified with glass powders (fiber-glass and waste glass). In this study, the hydration characteristics of the glass-powder modified pastes were evaluated using a set of experiments such as setting time, chemical shrinkage, degree of hydration, heat of hydration, and $Ca(OH)_2$ of the paste. It was found that addition of fiber-glass powder as cement replacement, improves the early hydration of the cement and also shows the pozzolanic activity in later ages (i.e. 91 days). Furthermore, it was observed that the addition of fiber-glass reduces the porosity of the paste and increases the specific surface area of the pores by refining the paste structure (5).

Pozzolanic/hydraulic reactivity of VCAS was investigated by Tashima et al. (6). In this study, TGA, pH and electrical conductivity studies were performed on paste systems with different levels of VCAS/calcium hydroxide and VCAS/Portland cement. For the first case (VCAS/calcium hydroxide system) the TGA results showed a significant pozzolanic reactivity of VCAS as the amount of $Ca(OH)_2$ in the system was decreased significantly by the increase in the amount of VCAS in the paste. It was observed that after 90 days, up to 92% of $Ca(OH)_2$ had been fixed in a system with VCAS:$Ca(OH)_2$ of 2:1. However, the results of pH and electrical conductivity measurements indicated that the pozzolanic reaction rate of VCAS is slow, even when tested in a high temperature (60°C) (6).

On the other hand, it was reported that unlike the first system, no significant pozzolanic activity was seen in the paste system made of VCAS/portland cement. The TGA results of this system showed that after 28 days test only 5-18% of $Ca(OH)_2$ had been fixed in the system. Therefore, they suggested that in the case of VCAS, the hydraulic activity is the main mechanism in yielding the cementing products. It should be noted that this suggestion is in contrast with the results presented by (5) and (6), as they relate the higher amount of $Ca(OH)_2$ in the early ages to the further hydration of cement that results in higher production of $Ca(OH)_2$.

While for most of the presented studies the term of "VCAS" has been used for the powder form of fiber glass, the term "E-glass" particles was used in a study by Chen et al. (7). In this study, utilization of E-glass particles as cement or aggregate replacement was studied. It was seen that the replacement of E-glass as cementitious material, by 40% of mass, showed a clear sign of pozzolanic reactivity by showing 117%, 127% and 143% strength activity index. Furthermore, it was observed that the addition of E-glass as a cement replacement improved the ASR, sulfate attack and chloride penetration resistance of the samples. The improvement in the compressive strength and the durability properties were related to the refinement the paste structure (7).

In this study, it was reported that the E-glass with particles size smaller than 75 microns can be used as a cement replacement. For the particles size larger than this size not much pozzolanic reactivity was observed due to the reduction in the specific surface area. However, the particles with a larger size can be used as the aggregate replacement due to their hard nature.

While the powder form of glass fiber is known by many names such as "VCAS", "Glass-Powder", "E-glass" and GGF (in this study) the main chemical composition of all the materials are almost same. The chemical composition of the above-mentioned materials are presented in Table 2-1. As it can be seen, all of the materials have an almost same chemical composition,

however, there is a slight difference between the chemical composition of them and the chemical composition of GGF that is used in this study.

Table 2-1. Chemical composition of the material used in other literatures and this study.

| Study | $SiO_2$ | $Al_2O_3$ | $Fe_2O_3$ | CaO | MgO | $Na_2O$ | $K_2O$ |
|---|---|---|---|---|---|---|---|
| Report by DOE (2) | 50-55 | 15-20 | <1 | 20-25 | <1 | <1 | <0.2 |
| Hossein et al. (2008) (3) | 50-55 | 15-20 | <1 | 20-25 | <1 | <1 | <0.2 |
| Neithalath et al. (2009) (4) | 54.2 | 17.8 | 1 | 24.2 | 0.8 | 0.75 | 0.2 |
| Kamali et al. (2016) (5) | 57.5 | 12.7 | 0.06 | 22.7 | 3.6 | 0.62 | 0.06 |
| Tashima et al. (2016) (6) | 57.9 | 12.92 | 0.47 | 23.51 | 2.88 | 0.74 | 0.13 |
| Chen et al. (2006) (7) | 54 | 15 | 0 | 17 | 4.5 | 0.8 ($Na_2O$+$K_2O$) | |
| Present study | 47.72 | 10.36 | 0.34 | 19.62 | 2.27 | 0.67 | 0.1 |

In conclusion, following points can be considered from the literature review of this section:

1) While a number of studies have been performed on the cementitious properties of waste glass fiber in powdered from, very few studies have been conducted on the durability properties of mixtures containing this material.
2) Most of the studies indicated that addition of glass fiber powder leads to a higher degree of hydration of the cement as more water is available for the hydration of cement particles at early ages.
3) Addition glass fiber shows clear pozzolanic reactivity by reducing $Ca(OH)_2$ level, especially at later ages, i.e. 91 days.
4) Addition of glass fiber improved the durability properties of mixtures in many cases. However, they caused more drying and plastic shrinkage in compare to control samples.

### *2.1.2 Durability aspects of concrete mixture having GGF as a SCM*

The reviewed literature revealed that among the few studies conducted on the properties of GGF containing concrete mixtures, most of them have focused on its hydration process; and very few

information is available on their durability aspects. The published results on the durability aspects (2, 3, 7) showed that, addition of glass fiber improved most of durability properties of mixtures significantly. However, during to the limited amount of information in this area, present study will focus more on the durability aspects of the GGF containing concrete mixtures.

## 2.2 Geopolymer concrete

### *2.2.1 Activation and formation process of geopolymers*

The term of "geopolymer" was introduced by Davidovits (8). Geopolymer is a cement-free material which is produced by the alkali activation of alumino-siliceous rich materials. Studies on geopolymer have shown comparable mechanical properties and superior durability properties compared to the conventional portland cement concrete. In addition to these, perhaps the most significant advantage of using this material is its potential in reducing the $CO_2$ emission associated with the portland cement production (9).

The principal binding reaction in geopolymers is significantly different from the hydration process observed in portland cement. This process includes the activation of a silica-alumina rich material such as fly ash, slag, metakaolin etc. with a high pH alkali solution like sodium hydroxide (NaOH) or combination of sodium hydroxide and sodium silicate ($NaO_2.nSiO_2$). Although several studies have been published on the activation mechanism of the geopolymer, perhaps the most useful one has been presented by Duxson et al. (10) as can be seen in Figure 2-1.

As it is it can be seen in Figure 2-1 (10), this process starts with the dissolution of alumina and silica in the activator solution. When the speciation equilibrium stage is reached, the gelation process takes place. Considering the rapid dissolution rate of the source material in a high pH activator, a supersaturated solution is soon reached, and alumina-silica oligomers start to form a gel. This gel goes through the process of reorganization and polymerization and forms the

hard network of geopolymer. It should be noted that gelation, reorganization, polymerization and hardening may not occur at the explained linear order form and may occur simultaneously.

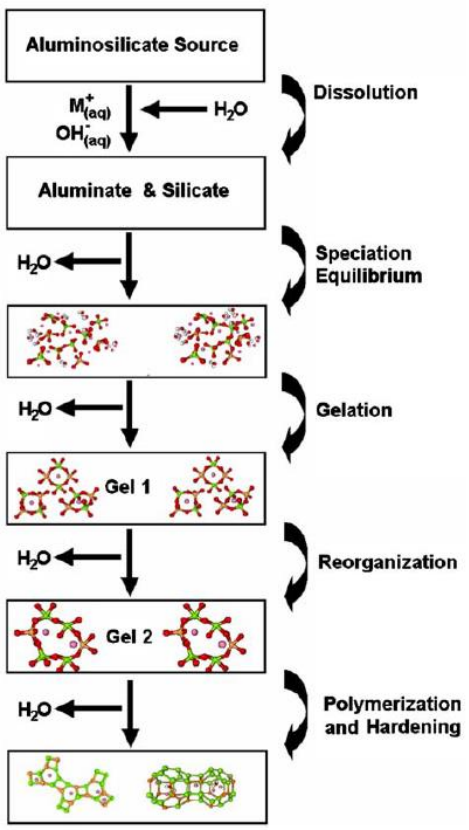


Figure 2-1. Simplified geopolymerisation process (10)

The microstructure of the geopolymer is different with microstructure of the hardened portland cement. Unlike the Portland cement based concrete, the strength of the geopolymer structure is not mainly provided by the calcium-silicate hydrate gel but is based on the silica-alumina network. The formation of this network depends mainly on the Si-to-Al ratio. According to Davidovits (11), the empirical formula for the geopolymer network can be written as $M_n\{-(SiO_2)_z - AlO_2\}_n.wH_2O$. In this formula, "M" is an alkali cation such as sodium, potassium or calcium, "z" is the ratio of $(SiO_2)$ to $(AlO_2)$, and "n" is degree of polycondensation which can vary from 1 up to 32. Depending on Si to Al ratio three types of three dimension

networks can be formed as below.

| | | |
|---|---|---|
| Poly(sialate) | $M_n(-Si-O-Al-O-)_n$ | Si/Al = 1 |
| Poly(sialate-siloxo) | $M_n(-Si-O-Al-O-Si-O)_n$ | Si/Al = 2 |
| Poly(sialate-desiloxo) | $M_n(-Si-O-Al-O-Si-O-Si-O)_n$ | Si/Al = 3 |

For the other cases with the higher Si to Al ratio (Si/Al >>3), the resulted polymeric structure forms a structure of poly silicate chains, sheets, or networks which are cross linked with a sialate link (11).

Several studies have been performed on geopolymers in order to specify their structure. In these studies, different characterization techniques such as X-ray diffraction (XRD) spectroscopy, high resolution transmission electron microscope (TEM), Fourier transformation infrared (FTI) and solid state nuclear magnetic resonance (NMR) have been employed to get specific information on the structure of the geopolymers (12, 13). However, among all the performed techniques, the NMR is generally known to provide the most useful results and have been used by several authors (8, 13, 14, 15).

Davidovits reported the results of performing magic-angle spinning MAS-NMR in studying the structure model of a metakaolin-based geopolymer (8, 16). He started with introducing the different structural units that could be formed with either alumina or silica. Considering the Loewenstein aluminum avoidance principal, by which no Al-O-Al-O unit could be formed, he defined five possible structural units for alumina in the form of $AlQ_n(nSi)$ with n=0, 1, 2, 3 and 4. In addition, it was considered that silica-alumina structure can form all possible structure units as $SiQ_4(4Al)$, $SiQ_4(3Al)$, $SiQ_4(2Al)$ and $SiQ_4(1Al)$. The chemical shift of the each of the $AlQ_n$ structural units with $^{27}$Al from $[Al(H_2O)_6]^{3+}$ is presented in Table 2-2. In addition, the range of chemical shift of the $Si(nAl)$ structural units with $^{29}$Si are presented in Figure 2-2.

Table 2-2. The chemical shift of $AlQ_n$ (modified from reference 8)

| Unit formula | $AlQ_0$ | $AlQ_1(1Si)$ | $AlQ_2(2Si)$ | $AlQ_3(3Si)$ | $AlQ_4(4Si)$ |
|---|---|---|---|---|---|
| Chemical shift (ppm) | 79.5 | 74.3 | 69.5 | 64.2 | 55 |

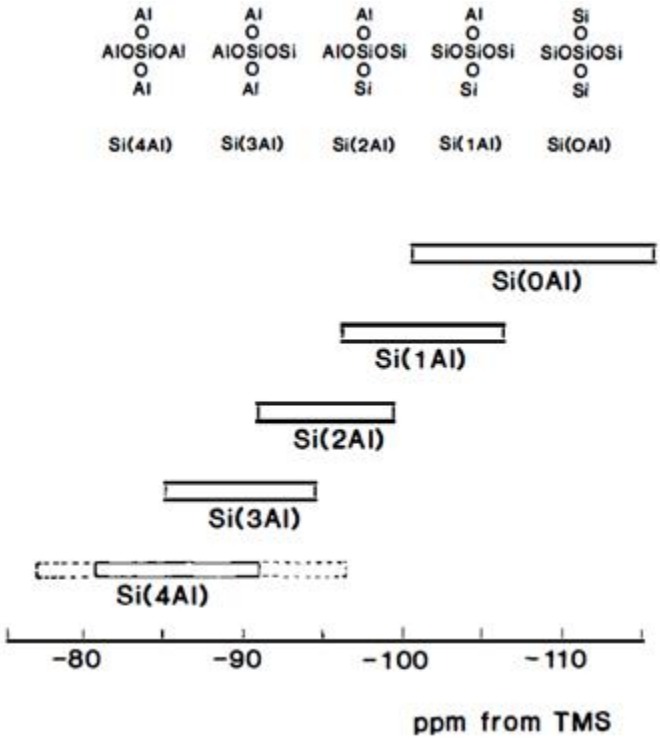


Figure 2-2. Chemical shift of the $Si(nAl)$ structural unit (17)

The MAS-NMR result of the $^{27}$Al performed on a metakaolin-based geopolymer is presented in Figure 2-3a. As it can be seen the major peak is located at the 55ppm which is equal to the chemical shift of $AlQ_4(4Si)$ presented in Table 2-2. As a result, and in the absence of any other major peaks, it was suggested all the $AlQ_n(nSi)$ units have the $AlQ_4(4Si)$ formation. Existence of other small peaks were related to the presence of some un-reacted metakaolin with other structural units. On the other hand, as presented in Figure 2-3b, the MAS-NMR test of $^{29}$Si did not show a single unique peak and covered a vast range of chemical shift. According to Davidovits (8), the MAS-NMR suggests a model as presented in Figure 2-4.

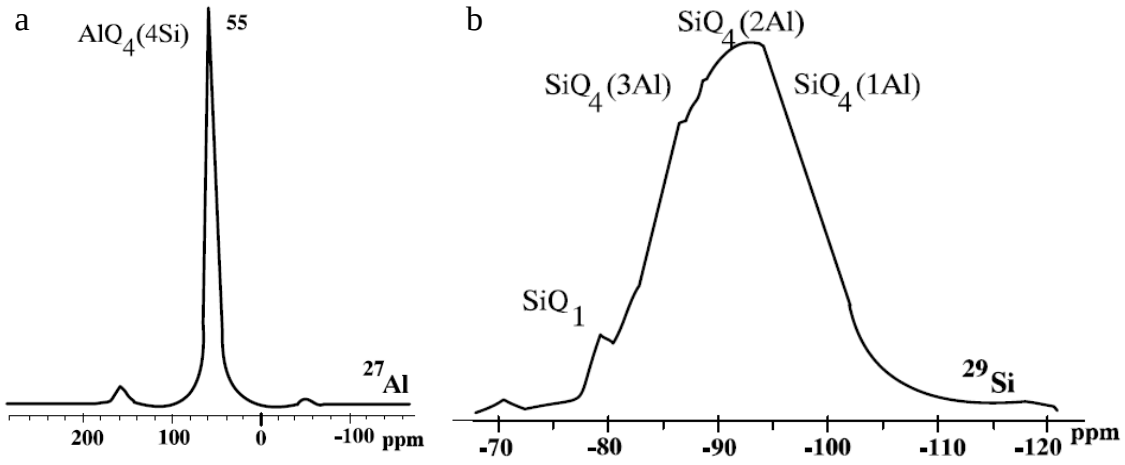


Figure 2-3. The MAS-NMR result of the (a) $^{27}Al$ and (b) $^{29}Si$ (16)

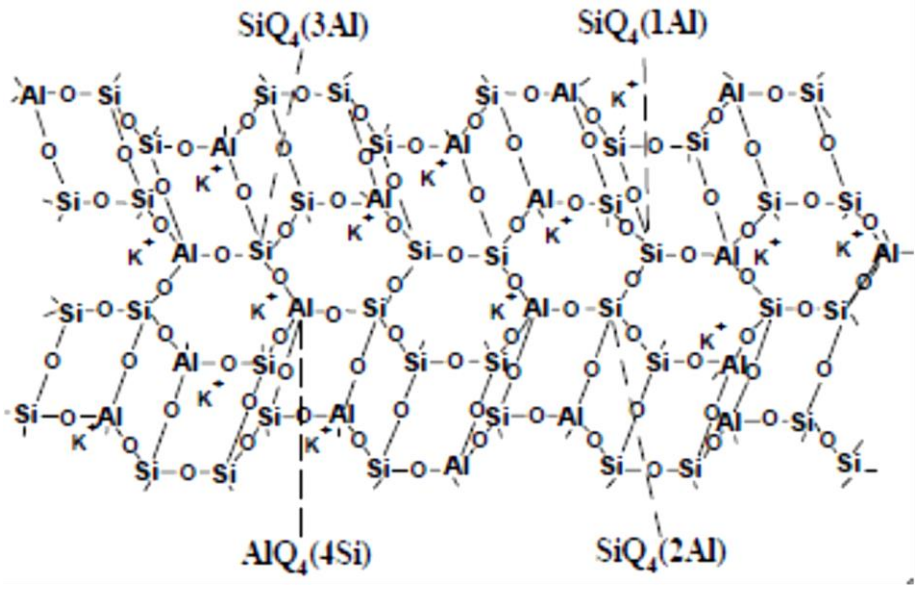


Figure 2-4. The geopolymer structure presented by Davidovits (8)

Barbosa et al. (13) studied the activation process of Metakaolin using a sodium silicate activator. In order to define the structure of the cured geopolymer, they performed several techniques, including FTIR, XRD and MAS NMR on the cured material. The results of these techniques showed an amorphous structure of the final material with the aluminum being mainly formed in its tetrahedral structure. In addition, it was observed that silicon occurred in a variety of different forms with the predominant formation of $Q_4(3Al)$ units in a glassy three-dimensional

structure. Furthermore, the MAS NMR result suggested the presence of sodium ions in an aqueous form. Based on the test's results, Barbosa et al. (13) presented below model for the structure of a geopolymer with a Si:Al ratio of 2:1 (Figure 2-5).

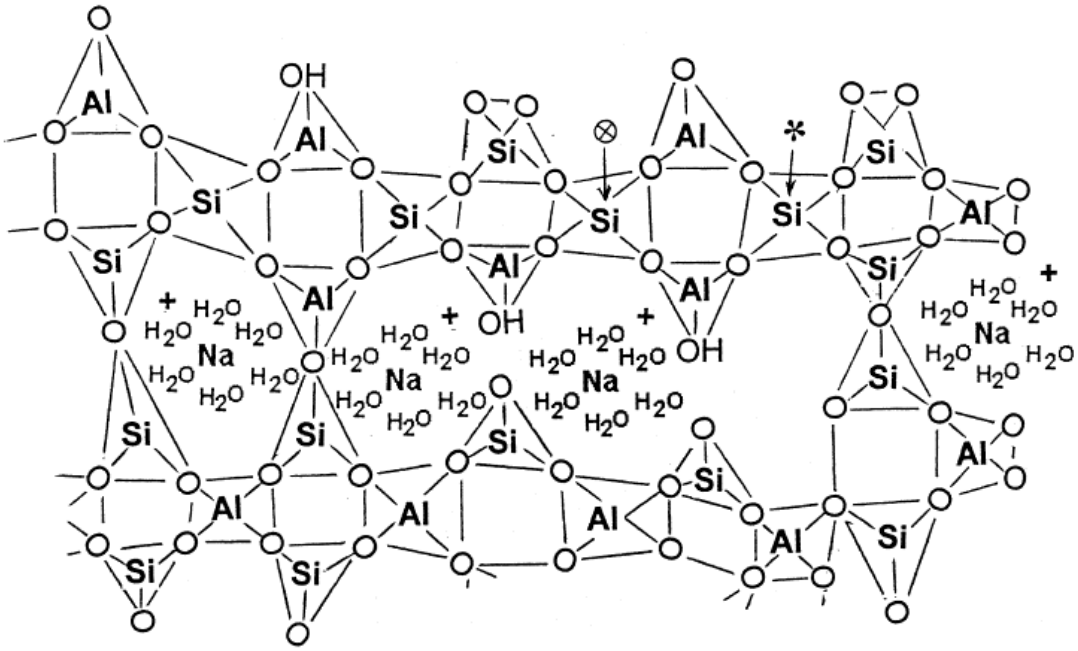


Figure 2-5. The geopolymer structure model presented by Barbosa 2000 (13).

### *2.2.2 Different source material*

Literatures show a large number of by-products and waste materials that have been used in producing geopolymer mortars and concrete. Among which, fly ash, meta-kaolin, slag and their combinations were the most widely studied materials. In addition, other source materials such as Waste Paper Sludge Ash (18), kaolinite and albite (19), Palm oil Fuel Ash (20), waste glass powder (21), VCAS (22) and blend of fly ash and anhydrous borax (23) was studied by other authors.

As it can be seen, although several studies have been conducted on producing geopolymer from a variety of waste materials, no research has been done on the activation of ground glass fiber. This study investigates the possibility of using GGF as a source material in

manufacturing of geopolymer. In addition, the activation process of two other source materials, i.e. class F fly ash and ground bottle glass in a powder form, is investigated and the results were compared to the GGF based geopolymer.

Palomo et al. (24), studied the activation of a class F fly ash with 4 different type of alkali activators. The geopolymer mixtures were reported to show a good workability even with a low liquid/binder ratio (i.e. 0.25 and 0.3). It was also seen that parameters like curing time and temperature, molarity of activators, Si-to-Al ratio is of the parameters that affect the final compressive strength of the materials.

Van Jaarsveld et al. (25), studied the activation of six different types of fly ash. It was observed that parameters like surface charge of the particles and their calcium content affect the initial setting behavior of the geopolymer mixtures. In addition, parameters such as water to fly ash ratio, calcium content of the fly ashes, crystallinity and degree of amorphous nature of the sample, dissolution rate of Al and Si as well as Al and Si content are of the parameters that affect the setting behavior of the geopolymer mixtures. It was also seen that while parameters such as particles size, and Na and K ions from the fly ash can change the geopolymer properties, their affect didn't seem to be as significant as Ca content and the water to fly ash ratio.

Xu and Van Deventer (26) studied the geopolymerisation behavior of 16 natural Al–Si minerals. The result showed almost all the source materials had a higher extent of dissolution in NaOH than in KOH. Moreover, source materials with the framework structure showed a higher extent of dissolution than other structures for both Si and Al while those with chain structure had the second extent of dissolution. At the end, it was concluded that factors like the percent of CaO, $K_2O$ and the molar ratio of Si/Al in the original mineral as well as type of activator and extent of dissolution had significant correlation with compressive strength. It was also observed that while for some of the tested minerals the compressive strength of the those with a higher extent of

dissolution were higher than the average amount, few of the minerals with a lower extent of dissolution did not follow this trend.

Wang et al. (27) studied the activation process and mechanical properties of metakaolin-based geopolymer. Metakaolin was activated using a combination of NaOH and sodium silicate with the 4.15:1 ratio and different mixes were cast with the concentration of the NaOH increasing from 4 to 12 mol/L. The samples then were tested for their compressive strength, flexural strength (Figure 2-6) and apparent density. As it can be seen in this figure, increase in the NaOH concentration of the activator has a significant effect on all the tested parameters.

According to (27), the geopolymerisation mechanism of metakaolin can be expressed as follows: process starts with the dissolution of surface layer of metakaolin particles by NaOH solution. Upon the dissolution, polymerisation of alumino-silicate units occur in the presence of available Si-O-Si chain (monomers, dimers and oligomers) that have been released in the system from the sodium silicate. Finally, dissolved metakaolin particles are connected together through the reaction products. Since the dissolution of metakaolin depends on the concentration of the solution, an activator solution with higher NaOH concentration can produce stronger connections between the particles. As a result of higher connection, higher compressive strength and higher flexural strength were achieved in solution with higher concentration (Figure 2-6).

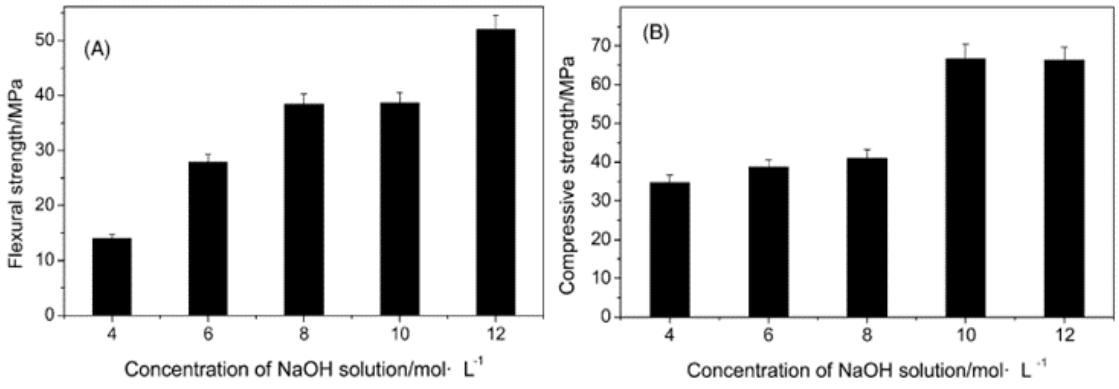


Figure 2-6. Effect of NaOH concentration on (a) flexural strength (b) and compress strength (27)

Granizo et al. (28), studied the alkali activation of metakaolin, and a mixtures of metakaolin and $Ca(OH)_2$ with a 1:1 ratio, using 5 and 12M NaOH solution. It was seen that in the absence of $Ca(OH)_2$, the 5M NaOH solution was not enough to activate the metakaolin, and the material stayed in a plastic state rather than producing a hard network. However, when the concentration of the activator was increased to 12M, a hard network was formed, and material showed a compressive strength gain.

Presence of $Ca(OH)_2$ was seen to have a significant effect on the hardening of the mixture. In the presence of $Ca(OH)_2$, the material could be activated using the 5M NaOH solution. It was suggested that in the presence of $Ca(OH)_2$, C-S-H gel can be formed readily in a low alkali environment; however, the production of alkali material (geopolymer), requires an activator with a higher alkali concentration. In addition, it was seen that the Al:Na ratio of the geopolymer material was close to 1 in both cases of with and without $Ca(OH)_2$. Based on this ratio, they concluded that for the studied materials, the structure of the network had no $OH^-$ group, and the charge of $AlO_4$ tetrahedra is balanced by the Na.

It should be noted that in this study, extraction of C-S-H gel was done using a combination of methanol and salicylic acid. The attack of this combination is known to dissolve the calcium-silicate product while the network of the geopolymer and the unreacted metakaolin remains unchanged.

Oh et al. (29), studied the synthesis of geopolymer using different source materials, namely, slag, class C and Class F fly sh. Their studies showed that while the major products in the slag-based geopolymer were hydrotalcite ($Mg_6Al_{12}CO_3(OH)_{16}.4H_2O$) and C-S-H; presence of some amount of hydrotalcite and very little amount of C-S-H gel were observed in the fly ash based geopolymers activated by NaOH solution. In addition, the XRD results of slag-based geopolymer indicated the presence calcium hydroxide $Ca(OH)_2$ in the geopolymer paste;

however, no $Ca(OH)_2$ peak was observed in any of the fly ash-based geopolymers. Based on their findings, Oh et al. (29) concluded that 1) when NaOH solution was used as the activator, the main crystalline phases were C-S-H(I) and hydrotalcite, for slag-based geopolymer, and hydroxycancrinite for the fly ash-based geopolymer. 2) Despite a large amount of available Ca in the class C fly ash, unlike the slag-based geopolymer, the final product didn't show the presence of any $Ca(OH)_2$.

The development of compressive strength of the slag, class C and class F fly ash is presented in then Figure 2-7. In this figure "FAF" and "FAC" stands for class F and class C fly ash respectively. Also, the sign "N" and "NW" indicates the use of NaOH and combination of NaOH and water glass as the activator.

The reaction kinetics of slag and fly ash-based geopolymer as well as geopolymer made from their combinations was done by Kumar et al. (30). In their study, the isothermal conduction calorimetry was used. The isothermal conduction calorimetry test was performed on both ambient temperature (27°C) and elevated temperature (48h at 27°C following by 60°C). The results of the tests are presented in Figure 2-8. As it can be seen in Figure (a), for the sample kept in 27°C, only one pick is observed. This peak is small for the case of raw fly ash (RAF) but gets bigger and bigger as the replacement level is increased. According to (30), this peak is related to the formation of C-S-H gel and the smaller amount that is seen in the case of RAF is due to the lower glassy content of fly ash as well as deficiency of calcium ions in the RAF mixture.

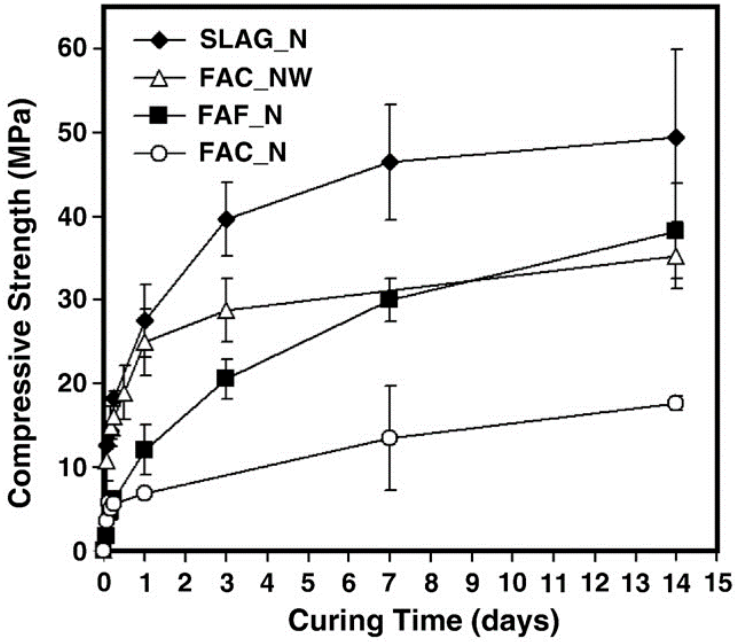


Figure 2-7. Development of compressive strength of geopolymer made from slag, class C, and class F fly ash (29)

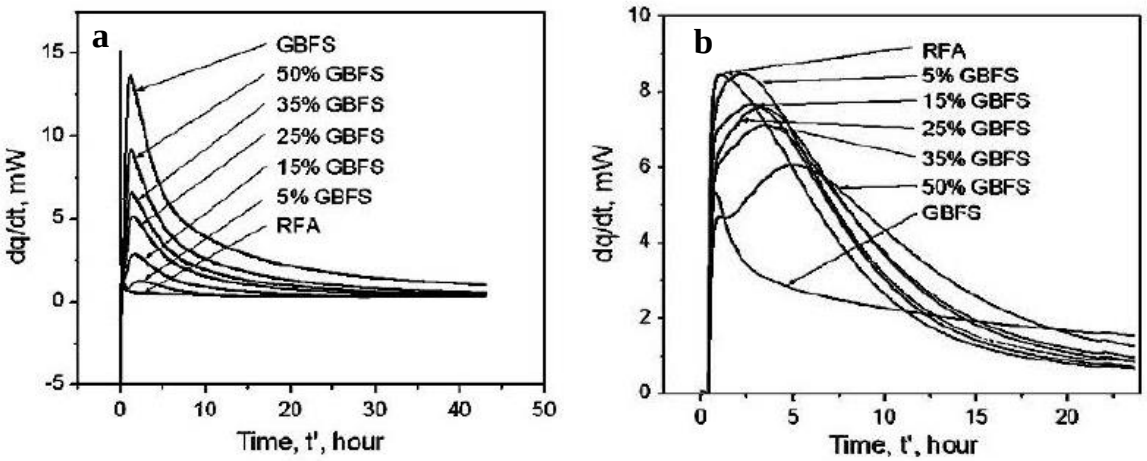


Figure 2-8. The isothermal conduction calorimetric results a) when test performed on fresh samples at 27°C b) when test performed at 60°C on the samples cured at 27°C for 48h (30).

On the other hand, as it can be seen in Figure (b), the mixtures with the combinations of fly ash and slag showed two peaks. The first peak, was suggested to be due to the geopolymerisation of slag, while the second peak was related to the geopolymerisation of the fly ash, and fly ash and slag mixtures. Although not presented here, they study also showed that in

the case of combining slag and fly ash, the actual calorimetry results were higher than calculated results. This suggests an interaction exists between slag and fly ash when they are combined together and activated.

In addition to fly ash, slag and metakaolin, other materials were also subjected to geopolymer studies. Anuar et al. (18), studied the activation of Waste Paper Sludge Ash (WPSA). In their study, the activation process was done with 8M and 14M NaOH solution at the ambient temperature. It was reported that the material could reach 13 and 18 MPa after 28 days when 8M and 14M NaOH was used respectively. In another study, Bhutta et al. (20) studied the activation of palm oil fuel ash. In their study, a combination of NaOH solution and sodium silicate solution which provide the solution-to-binder ratio of 0.4 was used as the alkali activator. The curing process were performed at 28°C for 28 days, and the material achieved the compressive strength 28 MPa.

Geopolymerisation of waste glass-powder was studied by Pascual et al. (21). In addition, effect of replacing glass-powder with metakaolin up to 8% percent was investigated. It was seen that while substitution up to 3% reduced the compressive strength of the samples; further substitution (after 5%) improved the mechanical properties as well as microstructure of the samples. In their study, a 5M NaOH solution was used as the activator. It was seen that in the absence of metakaolin, the activation cause formation of carbonated products, which reduced the compressive strength of the material. Carbonation attack, in absence of metakaolin, was attributed to the excess amount of unbonded alkalis, which were available in the mixture. In addition, it was observed that the carbonation attack was increased with addition in the concentration of the alkali solution from 5M to 10M (Figure 2-9). The blackish parts that are seen in these pictures are the results of carbonation attack.

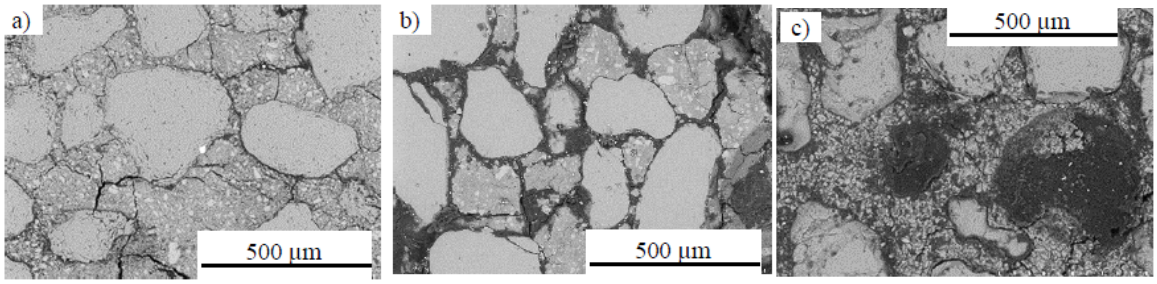


Figure 2-9 Microstructure of mortar samples containing 5% metakaolin activated with a) 5M NaOH solution b) 8M NaOH solution and c) 10M NaoH solution (21).

The effect of amorphicity, and solubility in high alkali solutions, of source materials on the compressive strength of the geopolymer were studied by Xu and Van Deventer (19). They studied activation process of three industrial materials, i.e. fly ash, kaolinite and albite, and their combination. They used techniques such as XRD and leaching in a high alkali environment to evaluate the amorphicity of the source materials. It was seen that more amorphous source material (i.e. fly ash and albite) showed a higher compressive strength when activated with the alkali activators. In addition, it was observed that the combination of source materials with higher rate of leaching (i.e. fly ash and albite in Table 2-3) resulted in a higher compressive strength. Furthermore, they noticed that the unreacted albite particles play a reinforcing role in the structure of the geopolymer, as they block the micro-cracks and hinder the formation of deeper cracks.

Table 2-3. Solubility results of Si and Al from kaolinite, albite and fly ash in NaOH and KOH (5g of material was dissolved in 10 ml of alkali solution). (19)

| Sample | Al (ppm) in NaOH | Si (ppm) in NaOH | Al (ppm) in KOH | Si (ppm) in KOH |
|---|---|---|---|---|
| Kaolinite | 550 | 1052 | 511 | 836 |
| Albite | 1345 | 2876 | 874 | 2013 |
| Fly ash | 1238 | 2197 | 567 | 1032 |

Very few studies have been performed on alkali activation of ground glass fiber powder. To the best knowledge of the author, as of now, there are only two published papers on the alkali activation of VCAS. Tahima et al. (22), studied the alkali activation of VCAS using NaOH and

KOH solutions with varying concentration as the activators. After three days of curing at 65ºC and 95% relative humidity, it was found that the samples that made with NaOH resulted in a higher compressive strength (77 MPa-11.2 ksi- after 3 days). The higher compressive strength in this case, was attributed to the lower total porosity in samples with NaOH as well as the higher dissolution of VCAS in the NaOH activator. In another study, Tashima et al. (31) studied the alkali activation of VCAS in room temperature (20ºC). It was reported that since activation of VCAS with NaOH solution does not produce a hard material at room temperature, the use of waterglass (i.e. sodium silicate) is necessary. It was seen that the compressive strength of the samples that were cured at room temperature was increased significantly with time. The compressive strength at 28, 91 and 360 days were 38.6 MPa, 78.5 MPa and 89.5 MPa (5.6 ksi, 11.4 ksi and 13 ksi) respectively. In addition, it was found that the amount of larger sized pores decreased significantly at 360 days compared to 28 days.

In conclusion, following points can be considered from the literature review of this section:

1) Parameters like curing time and temperature, molarity of activators, Si-to-Al ratio, K and CaO content affect the final compressive strength of the geopolymer.
2) Generally, materials with the higher rate of dissolution in highly alkaline media, lead to the formation of the geopolymer samples with higher compressive strength.
3) The studies on the relation of Al and Na in the geopolymer structure suggested that all the remaining charge of $AlO_4^-$ components (i.e. not balanced by the silica) are balanced with the Na at almost 1:1 ratio as observed in the reaction product of geopolymer.
4) Presence of Ca was seen to significantly affect the setting behavior of the geopolymer mixtures. The reviewed studies showed confirmation of the formation of C-S-H gel in the samples made of class C fly ash, metakaolin, and slag based-geopolymers.

5) In the presence of a Ca source (i.e. slag) in a geopolymer mixture, the main mechanism responsible for hardening of material is the formation of C-S-H gel at low temperatures, and geopolymerisation at high temperatures.

6) In the case of geopolymer made from glass-powder, carbonation can cause a lot of damage, especially in the samples with the high amount of alkali content.

### *2.2.3 2.2.2 Role of aluminum content*

In order to form the geopolymer structure, pretense of Si and Al is necessary. While role of Si as the main element in formation of back bone of geopolymer structure is pretty clear, in this section, literatures that are related to the role of Al content in geopolymer mixtures will be reviewed. In most of the cases, the Al content of the mixture has been expressed as a ratio, proportional to the Si content (i.e. Si:Al of 1:1 or Si:Al of 2, etc.).

According to Davidovits 1999, the atomic ratio of Si:Al in geopolymer structure determines its properties. While the low ratio of Si:Al (1, 2, 3) lead to a formation of a 3-D rigid network, the higher ratio (>15) lead to a formation of geopolymer with more polymeric characteristic. Figure 2-10, shows the structures of geopolymers with different Si:Al ratio (modified from 11).

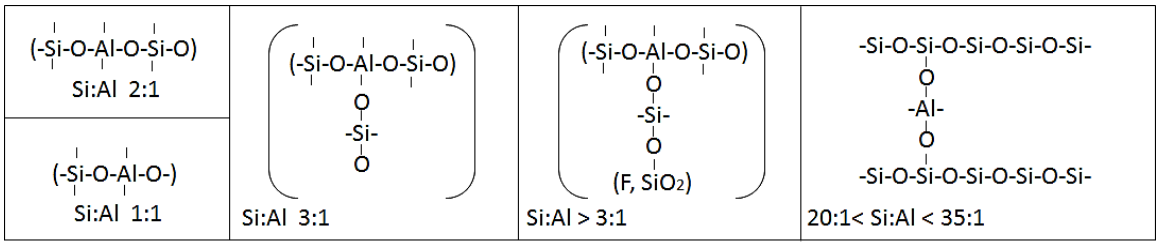


Figure 2-10. Effect of Si/Al ratio on the structure of geopolymer (modified from reference 11)

Effect of aluminum release rate affects the strength gain and structure of the geopolymer. Hajimohammadi, et al. (32), studied the effect of Al release rate from the source materials on the compressive strength gain and micro structure of the system. In thus study, two mixtures with

fixed Si/Al ratio of 1.5 were designed, 1) with lower Al release rates using amorphous alumina and 2) a sample with a higher Al release rate having sodium aluminate. It was seen that while after three weeks, both samples showed an almost same compressive strength, the samples with higher Al release rate showed a faster strength gain in the early ages. It was concluded that the early strength gain in the sample with higher release rate is related to the availability of Al that can participate in the formation of the geopolymer gel. However, the excessive amount of Al, can hamper dissolution if Si, which delays the strength gain. On the other hand, sample with the lower release rate of Al needs more time in order to rich a gel with enough amount of available Al. Finally, it was concluded that the sample with higher rate of release of Al forms a more homogenous structure in compare to the mixture with lower release rate.

Effect of Si-to-Al ratio (Atomic ratio) on the compressive strength and module of elasticity of geopolymer pastes were studied by Duxson et al. (12). In this study geopolymer samples were synthesized by the activation of metakaolin by sodium silicate solutions with varying Si content in a manner that total Si/Al ratio of the mixture were ranging from 1.15 to 2.15 (5 mixtures). It was seen that the increase in Si/Al ratio up to 1.90 increased the resulted in a significant increase in compressive strength and module of elasticity, while a further increase up to 2.15 reduced these parameters (Figure 2-11).

The SEM observation of samples showed a large amount of inter connected porous in the samples with the Si/Al ratio smaller than 1.65 and a dense and homogeneous structure for the Si/Al ratio of 1.90. However, unlike the sample with Si/Al ratio of 1.90, samples with Si/Al ratio of 2.15 showed a few amounts of voids and cracks in their structure. In this study, the lower compressive strength of the sample with Si/Al ratio of 2.15 was related to the effect of unreacted source material (Metakaolin), which was considered as a defect in the structure of the sample. Based on the NMR results of this study, it was observed that the amount of unreacted Metakaolin

increased with the increase in Si/Al ratio.

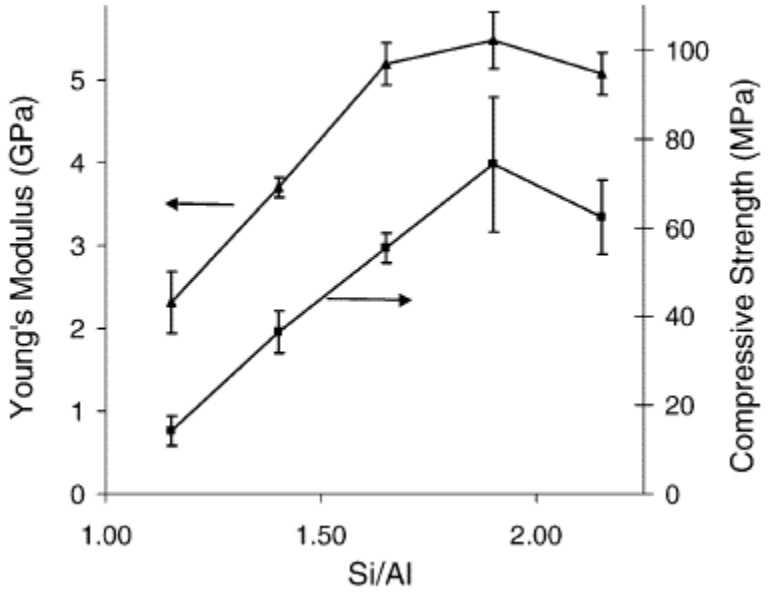


Figure 2-11. Compressive strength and young's modules of the geopolymer samples with varying Si/Al ratio (12)

Rolle of alumina content in setting time and compressive strength of metakaolin-based geopolymer concrete was investigated by De Silva et al. (33). In this study, geopolymer samples with a different ratio of $SiO_2/Al_2O_3$ were produced by addition of sodium silicate activator having different Si content. It was observed that Al content affects the setting time significantly, and samples with higher Al content showed lower setting time. However, the increase in the Al content resulted in a uniform increase in the compressive strength as the highest strength occurred when $SiO_2/Al_2O_3$ was in the range of 3.4 to 3.8 (Figure 2-12). The further increase in Al content resulted in lower compressive strength. It should be noted that these results are in agreement with previously reviewed study (12), at which highest compressive strength would occurred at the Si/Al ratio of 1.9.

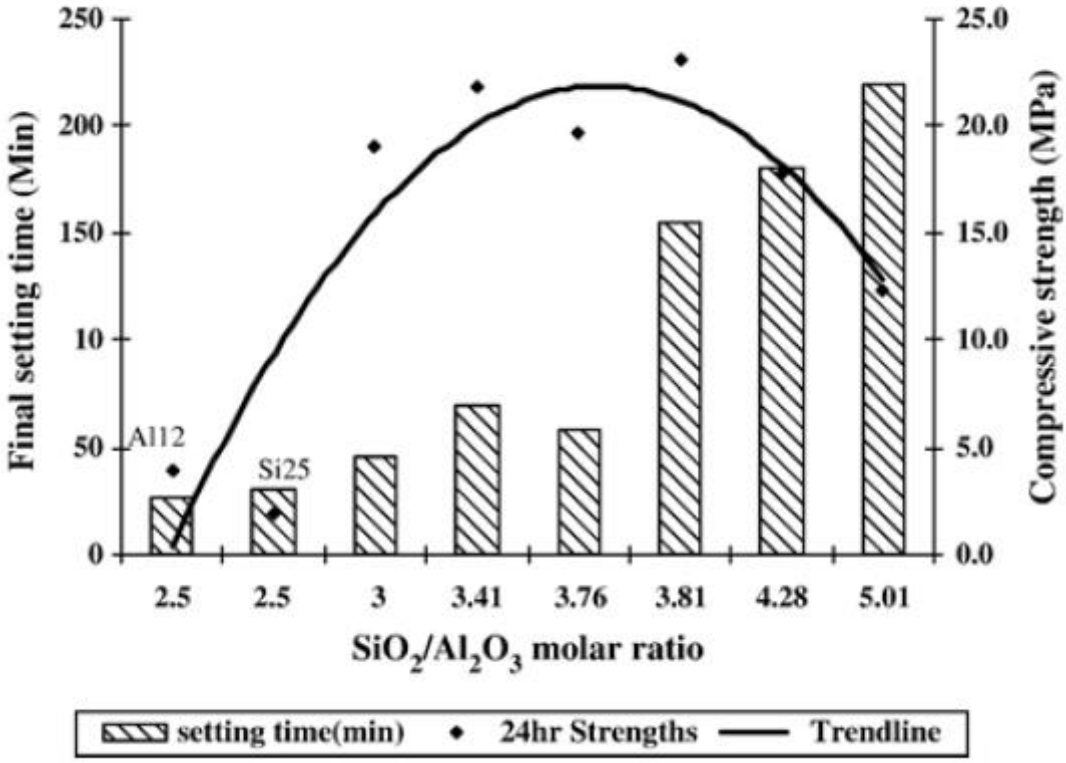


Figure 2-12. Effect of $SiO_2/Al_2O_3$ on the compressive strength and setting time. (33)

In this study, the lower setting time of the mixtures with a lower $SiO_2/Al_2O_3$ ratio (higher Al content), was related to the tendency of Al components of metakaolin to dissolve more easily than Si components. In addition, since the condensation rate of between silicate spices is slower than that of silicate and aluminate spices, setting time is delayed in the samples with a higher $SiO_2/Al_2O_3$ ratio. In this study, the lower compressive strength of samples with a low or high $SiO_2/Al_2O_3$ ratio were respectively related to the poor microstructure with low strength Na-Al-Si grains (low $SiO_2/Al_2O_3$) , and lack of rigid 3D networks in the micro structure (high $SiO_2/Al_2O_3$).

The effect of the increase in Al content by mass replacement of source material with $Al_2O_3$ was studied by Kouamo et al (34). In this study, metakaolin and volcanic ash-based geopolymer with various amounts of $Al_2O_3$ (i.e. 0, 10, 20, 30 and 40% by mass replacement of

solid part) were synthesized. The results showed that the addition in $Al_2O_3$ level up to 20% replacement caused an increase in the compressive strength of the metakaolin-based geopolymer and further replacement levels resulted in a lower compressive strength. However, for the case of volcanic ash-based geopolymer, the increase in the replacement level (up to 40% replacement by mass of solid) led to the increase in compressive strength. In this study, the reduction of compressive strength of metakaolin-based geopolymer with the more $Al_2O_3$ content (i.e. 30% and 40%) was related to the possible formation of octahedral Al at the very high Al content. In addition, the different behavior of metakaolin and volcanic-ash based geopolymer in the case of addition of $Al_2O_3$ level was related to the variation in the chemical composition of the starting materials. In this study, the molar ratio of $SiO_2/Al_2O_3$ of volcanic ash and metakaolin were 4.55 and 1.42 respectively.

In conclusion, following points can be considered as the summary of this section:

1) In geopolymer structure, Al components act as the bridges which connect the silica chains. In the presence of the sufficient amount of Al, this leads to a formation of a rigid 3-D network.
2) Due to its higher solubility (in compare to Si), presence of Al reduce the setting time. However, at the very high levels, it can hamper the dissolution of Si from the source materials which affects the later compressive strength.
3) According to the reviewed literatures, there is an optimum range for the Al to achieve the highest compressive strength. This range was reported to be in the range of 3.4 to 3.8 for $SiO_2/Al_2O_3$ and around 1.9 for Si/Al.
4) Low or high Al content reduces the compressive strength of the geopolymer samples. While low Al content leads to the lack in formation of rigid 3-D network, very high alumina content can affect the compressive strength by 1) reduce the reaction rate (increment in the amount of unreacted particles) and 2) possible formation of octahedral Al which cannot be merged in the

geopolymer structure.

### *2.2.4 Role of calcium*

Presence of Ca components in the geopolymer mixtures are known to affect the setting time and other properties of the hardened geopolymer. However, despite of large number of studies, the exact mechanism(s) by which calcium is bonded within the geopolymer structure is still unclear. In this section, some of the literatures that have studied the effect of Ca content on the properties of geopolymer mixtures will be reviewed.

Buchwald et al. (35) studied the effect of boosting calcium content of flay ash and metakaolin-based geopolymer. It was observed that increasing the Ca content (by replacement of source materials with $Ca(OH)_2$) showed an increase in the compressive strength of the flash based samples. As shown in Figure 2-13, for the case fly ash-based geopolymer the increase in the compressive strength was seen up to 30% replacement level. However, for the case of metakaolin-based geopolymer, while addition of Ca content improved the compressive at the lower levels, further addition of Ca content after 10-15% of mass replacement, reduced the compressive strength.

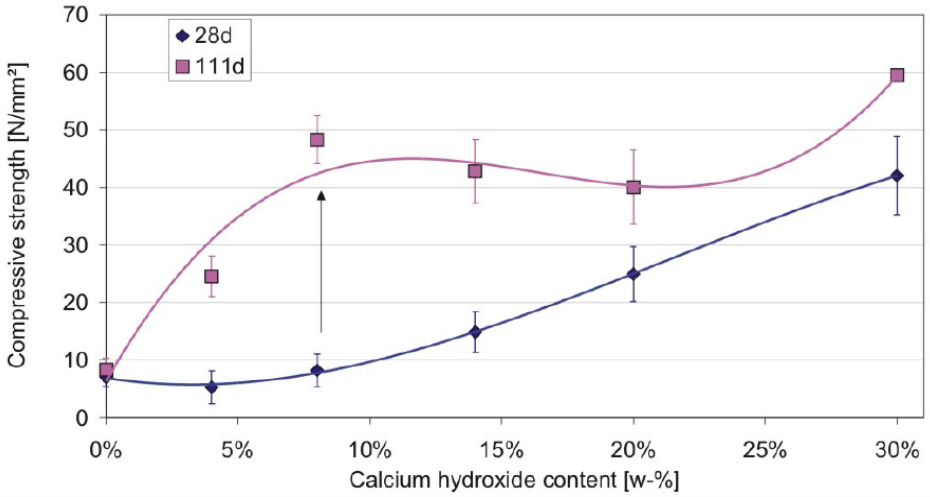


Figure 2-13. Influence of calcium content on the compressive strength of fly ash-based geopolymer (35)

In this study, the increase in the compressive strength with addition in Ca content was attributed to the denser structure (SEM observation) of the geopolymer that produced with the higher Ca content. It was also seen that in the samples with a high amount of Ca content both C-S-H phase and geopolymer phase coexist. Furthermore, the XRD results of the samples with a high amount of Ca content indicated the charge balancing roll of Ca in the structure of the geopolymer.

Jaarsveld et al. (25), studied the activation process of six types of fly ash with different properties (including various Ca content). It was seen that while factors such as specific surface area, glass content of the fly, alkali metal content, solubility of Al and Si from source materials, etc. affect the compressive strength of geopolymer samples, however, that the calcium content of fly ash seems to play a greater role in improving the compressive strength. This study suggests that the formation of calcium-compound such as calcium silicates, calcium aluminate hydrates, and calcium–silico–aluminates are formed during the geopolymerisation which can reduce the setting time of the mixture.

In a paper published by Yip et al. (36), the effect of addition of Ca in the term of slag on the geopolymerisation behavior of a metakaolin-based geopolymer was studied.in this study, metakaolin was replaced by slag from 20 to 100% by the mass. The compressive strength results showed that replacement level of 20% resulted in a higher compressive strength, from 37.7 MPa to 46.2 MPa for 0% and 20% slag replacement respectively, after 240 days. However, higher replacement levels reduced the compressive strength significantly, 13.5 MPa and 9.2 MPa after 240 days for 40% and 60% replacement level respectively. The rise in the compressive strength at 20% was related to the formation of Ca rich component such as C-S-H gel which was detected in the SEM observation (Figure 2-14). It was suggested that formation of C-S-H gel within the geopolymer binder act as a micro-aggregate and lead to more dense and homogenous structure.

However, when the replacement level were increased to higher numbers, the formation of two phases (C-S-H and geopolymer) was seen to cause more cracks in the interfacial of two zones Figure 2-14 which reduced the compressive strength significantly. It is also very important to note that, based on the EDX results which were performed on each zone (i.e. C-S-H or geopolymer zone), it was suggested that addition of Ca only lead to the formation of C-S-H gel and will not participate in the structure of the geopolymer zone.

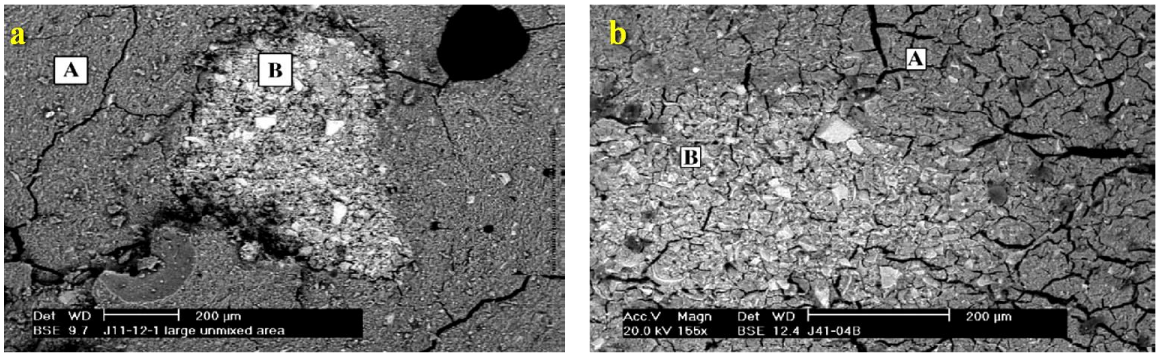


Figure 2-14. Coexistence of two zones of geopolymer binder (A) and C-S-H (B) for 20% slag (left picture-a) and 60% slag replacement (right picture b) (36)

In a study conducted by Lee et al. (37), studied the effect of various calcium containing salts on the setting and early compressive strength of the geopolymer samples. They results showed that presence of calcium containing salts accelerated the setting behavior and also improved the compressive strength of the geopolymer samples for all the tested Ca continuing salts. In this study the effect of in faster setting time and higher compressive strength (7 days) were related to the formation of nucleation sites due to the formation of calcium hydroxide which act as a nucleation site, and trigger the formation of silicate polymers. The effect of addition of calcium salts on the 7-days compressive strength of two geopolymer systems with a different fly ash/metakaolin ratio are presented in Figure 2-15.

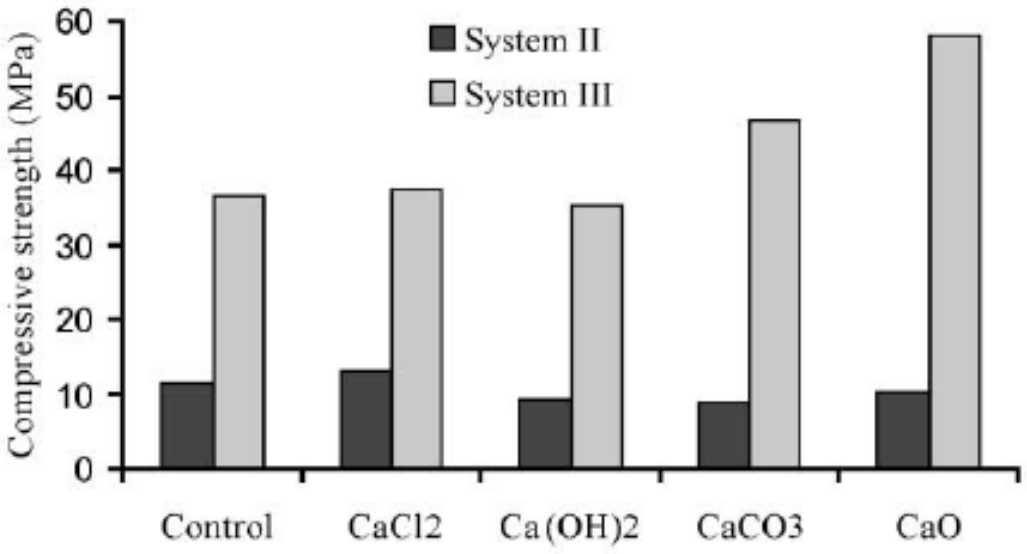


Figure 2-15. Results of 7-days compressive strength of two geopolymer sample containing various Ca salts. (37)

In conclusion, it can be said that there is a general agreement on the effect of Ca in reducing the setting time and increasing the compressive strength. However, as of now, the exact mechanism by which Ca plays it role is not understood. While numbers of mechanisms have been suggested by several workers in this area, none of them has been generally accepted or rejected, and the research in this area is still ongoing. Some of the purposed mechanisms are:

1) Formation of C-S-H gel which can act as micro aggregate and dense the structure of the paste (36, 38).
2) Effect of calcium compound in creating a nucleation site for the precipitation of the geopolymer compound (37, 39).
3) Charge balancing capacity of Ca in the alumino-silicate structure (35, 40).

### *2.2.5 Effect of alkali solution on mechanical properties*

Composition of alkali solution is known to greatly affect the properties of geopolymer. Alkali solution such as NaOH solution, KOH solution, combination of NaOH and sodium silicate, and combination KOH and potassium silicate are the mostly used and studied activators. Palomo et al.

(24), studied the activation process of a class F fly ash using four different type of alkali solutions. Four types of activators, including, 12M NaOH, 18M KOH, combinations of NaOH (pellets) and sodium silicate with the total ratio of $SiO_2/Na_2O$=1.23 and KOH (pellets) and potassium silicate with the total ratio of $SiO_2/K_2O$ =0.63 were used. The results showed that the combination of NaOH and sodium silicate ended in higher compressive strength for all varying curing methods.

Xu and Van Deventer (26) studied the geopolymerisation behavior of 16 natural Al–Si minerals. The result showed almost all the source materials had a higher extent of dissolution in NaOH than in KOH. It has been suggested that the ion size difference between $Na^+$ and $K^+$ is a determining factor in the kinetics of the reactions (10). In addition, in some other studies like (22, 24, 41), it was observed that activation of same source material with NaOH solution, resulted in a higher compressive strength than the case when KOH solution was used. Nevertheless, most studies have used sodium based alkali activators, however, in some studies like (42), better performance of KOH in terms of higher compressive strength has been reported.

In the case of using sodium based alkali activators, it has been reported that using a combination of NaOH and sodium-silicate with higher silica content as the activator will result in higher compressive strength in compare to the NaOH or a combination of NaOH and $Na_2SiO_3$ with lower $SiO_2/Na_2O$ ratio (24, 43, 44). In addition, the higher concentration of the alkali activators has been reported to result in the higher compressive strength of the geopolymer. Table 2-4 form (43), shows the effect of concentration of the alkali activator as well as its silica content on the compressive strength. As it can be seen, for the equal concentration, increase in the silica content of the activator raises the compressive strength of the geopolymer samples. It should be however noted that increasing in the silica content (high silica content) of the activator can mess with the Si-to-Al ratio of the total mixture and reduce the compressive strength as was seen in

(45). Finally, it should be noted that addition of soluble silica in the activator solution generally improves the mechanical behavior, as it increases the amount of readily available silicate oligomers in the mixtures. According to (26), the $Al(OH)_4^-$ dose not readily combine with the short-length silica chain, as a result presence of more long-chain silicate oligomers can fasten the formation of geopolymer structure.

Table 2-4. Effect of concentration of Na and Silica content on the compressive strength of fly ash-based geopolymer (43)

| Mixture | Concentration of NaOH liquid in molarity (M) | Sodium silicate/NaOH liquids ratio by mass | 7-day compressive strength after curing at 60 °C for 24 h, MPa |
|---|---|---|---|
| A-1 | 8M | 0.4 | 17.3 |
| A-2 | 8M | 2.5 | 56.8 |
| A-3 | 14M | 0.4 | 47.9 |
| A-4 | 14M | 2.5 | 67.6 |

### *2.2.6 Effect of curing time and temperature on mechanical properties*

Time and temperature of curing, play an important role in the properties of hardened geopolymer. Hardjito et al. (43), investigated the effect of these factors on the compressive strength of a fly ash based geopolymer concrete. In their study, the effect of different temperature of curing was also examined on the development in compressive strength of geopolymer concrete. Samples were cured for 24 h at the temperatures of 30, 45, 60, 75 and 90°C. Their findings suggest that the higher temperatures result in higher compressive strength, especially up to 75°C.

Also, their study showed that curing duration played an important role. For instance, when curing time was varied from 0 to 96 h at a constant curing temperature of 60°C, the seven-day compressive strength was increased with the increase in the curing time. However, the increase in the compressive strength was not significant beyond 48 h. The effect of curing

temperature and time of curing on the 7-days compressive strength of geopolymer samples are presented in Figure 2-16.

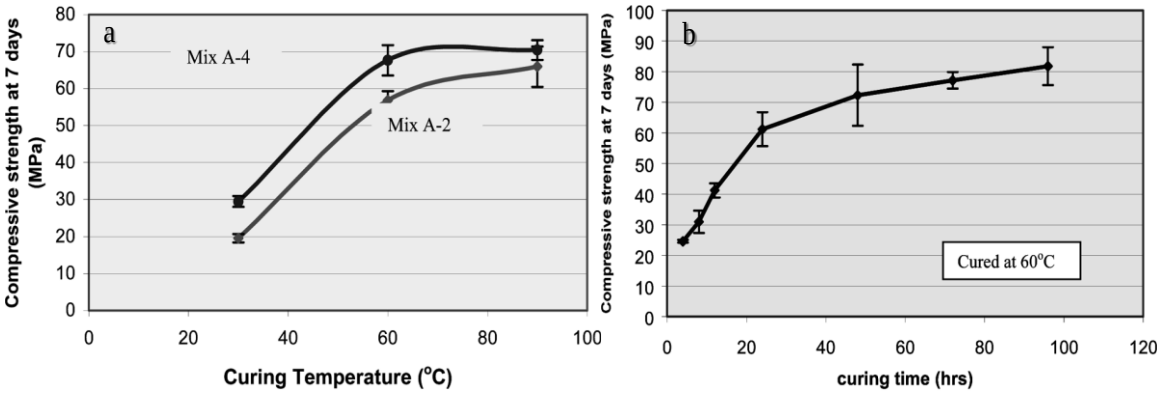


Figure 2-16. Effect of curing temperature (a) and time of the curing (b) on the 7-day compressive strength of geopolymer samples (43).

Palomo et al. (24) studied the effect of these parameters on activation of class F flay ash. Selected times of curing were 2, 5 and 24 hours at the 65 and 85°C. Four types of activators, including, 12M NaOH, 18M KOH, combination of NaOH (pellets) and sodium silicate with the total ratio of $SiO_2/Na_2O$ =1.23 and KOH (pellets) and potassium silicate with the total ratio of $SiO_2/K_2O$ =0.63 were used. The results showed that the curing temperature is a reaction accelerator in fly ash-based geopolymers, and significantly affected the mechanical strength. As presented in Table 2-5, it was also observed that the higher curing temperature and longer curing time were proved to result in higher compressive strength.

Muñiz-Villarreal et al. (46) studied the effect of temperature on the geopolymerisation process of a metakaolin-based geopolymer. In this study, geopolymer samples were cured at six different temperatures, ranging from 30°C to 90°C. The compressive strength, total amount of porosity, and total heat evaluation of each sample is presented in Table 2-6. As it can be seen both lower and higher temperature results in a lower compressive strength in compare to the 60°C cured samples.

Table 2-5. Effect of curing temperature and time of curing on the compressive strength of geopolymer samples (24)

| Activator | Curing temperature (°C) | Activator/fly ash ratio 0.25 (time of curing) | | | Activator/fly ash ratio of 0.30 (time of curing) | | |
|---|---|---|---|---|---|---|---|
| | | 2 h | 5 h | 24 h | 2 h | 5 h | 24 h |
| Solution 1 | 65 | 0.0 | 0.0 | 21.2 | 0.0 | 1.8 | 17.3 |
| | 85 | 9.3 | 22.0 | 34.6 | 9.2 | 9.6 | 23.4 |
| Solution 2 | 65 | 0.0 | 0.0 | 8.7 | 0.0 | 0.0 | 3.9 |
| | 85 | 1.4 | 9.4 | 23.3 | 2.6 | 16.4 | 27.3 |
| Solution 3 | 65 | 4.3 | 31.7 | 52.7 | 0.0 | 30.0 | 62.6 |
| | 85 | 39.8 | 48.2 | 54.5 | 31.6 | 57.4 | 68.7 |
| Solution 4 | 65 | 0.0 | 9.5 | 38.7 | 0.0 | 10.2 | 39.0 |
| | 85 | 7.7 | 34.3 | 63.0 | 16.0 | 31.6 | 35.9 |

Table 2-6. Effect of curing temperature on the compressive strength (24)

| Reference | | Property | | |
|---|---|---|---|---|
| Step1 | Step 2 | Porosity ($ccg^{-1}$) | Total heat evolution ($Jg^{-1}$) | Compressive strength (MPa) |
| 2 h, 40 °C | 30 °C | 0.2251 ± 0.001 | 497.07 | 7.032 ± 1.009 |
| 2 h,40 °C | 40 °C | 0.2244 ± 0.005 | 1267.79 | 8.553 ± 1.326 |
| 2 h,40 °C | 50 °C | 0.2038 ± 0.013 | 1414.58 | 11.771 ± 0.096 |
| 2 h,40 °C | 60 °C | 0.1651 ± 0.020 | 1796.50 | 17.867 ± 1.009 |
| 2 h,40 °C | 75 °C | 0.1710 ± 0.008 | 1480.82 | 13.771 ± 1.326 |
| 2 h,40 °C | 90 °C | 0.1821 ± 0.002 | 1149.59 | 13.130 ± 0.496 |

According to this study, the lower compressive strength of low, and high temperature cured samples can be attributed to the following factors:

1) As presented in Table 2-6, lower and higher curing temperature resulted in higher total porosity in compare to the 60°C curing temperature. For the case of lower temperatures, this was related to low reaction rate of metakaolin; while for the higher temperatures, it happens because of the higher rate of water evaporation.
2) In higher temperatures, a fast reaction occurs on the surface of metakaolin particles; which hamper the further dissolution of Si and Al compound in the activator solution. However, for lower temperatures, not enough amount of metakaolin will dissolve in the solution.

3) As presented in Table 2-6, maximum heat evaluation was seen in the case of 60°C curing temperature. This indicates that samples that were cured in this temperature, have reached a more stable structure which leads to a higher compressive strength.

While some studies like (46-49) showed there is an optimum temperature range for the highest compressive strength; some of the other researchers have reported the higher compressive strength of geopolymer mixtures that were cured in higher temperature (i.e. up to 90 and 120°C) (50-52). However, other researchers have reported that extremely high temperature (i.e. higher than 400°C) will reduce the compressive strength of the geopolymers (53, 54). According to the reviewed literatures and preliminary test results, In present research, the curing temperature of 60°C was selected.

### *2.2.7 Durability properties of geopolymer*

#### *2.2.7.1 Alkali silica reaction*

Several studies have been published on the durability characteristics of geopolymers. Considering the high level of alkali in these mixtures, the risk of alkali silica reaction (ASR) of aggregates in geopolymer concrete has always been a big concern. The impact of ASR on geopolymer concrete prisms made with activation of class F fly ash was studied by Kupwade-Patil & Allouche (55). In this study, two types of class F fly ash and a class C fly ash were used as the source materials for the geopolymer. The expansion results of these samples were compared to an OPC mortar mixture after subjecting them to the ASTM C 1260 accelerated condition for 90 days. The findings indicated that the fly ash activated geopolymer concrete showed a significantly better performance compared to a Portland cement concrete (OPC sample showed an almost six times greater expansion). In addition, the SEM studies confirmed the formation of ASR gel in the OPC and class C fly ash-based samples; however, no ASR gel were seen in the samples made with class F fly ash. The lower expansion of geopolymer samples was attributed to the lower amount

of calcium (especially in the class F fly ash-based geopolymer) as well as the further reaction of unreacted fly ash particles in the subjected condition.

Puertas et al. (56) investigated the resistance of alkali-activated slag mortar bars against ASR in an accelerated condition (80°C and 1N NaOH solution). In their study, a combination of NaOH and sodium silicate solution with the total amount of $Na_2O$ equal to 4% of the slag mass and a $SiO_2/Na_2O$ ratio of 1.08 were used to activate the slag. The expansion results up to 120 days showed that the activated slag mortar bars were more resistant against the ASR than Portland cement mortar bars.

Pouhet and Cyr (57) studied the ASR behavior of a meta-kaolin based geopolymer. In this study, the expansion results of six different aggregate with none to high theoretical ASR reactivity were tested at the 95% RH and 60°C environment. The expansion results of all the tested aggregates showed a better performance of geopolymer samples (Figure 2-17). In addition, the effect of ASR on the dynamic modulus of elasticity was measured at the age 21 and 90 days after exposure. The results showed that in most of the cases, the dynamic modulus of elasticity of the geopolymer samples increased while that of OPC samples decreased for all the cases (expect in the case of the none-reactive sand).

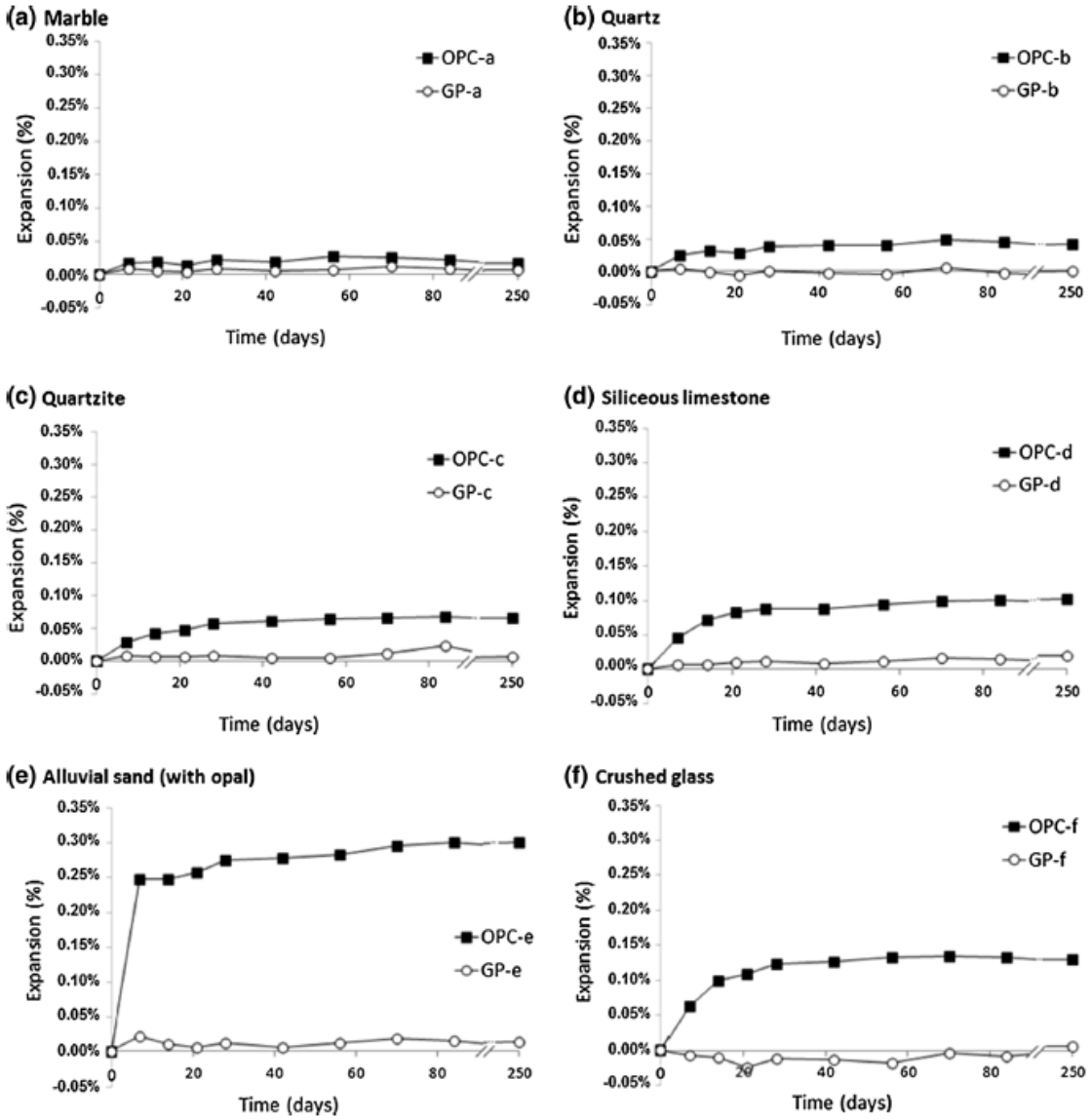


Figure 2-17. Expansion of geopolymer and OPC samples due to ASR (57)

They also studied the pore structure of the meta-kaolin geopolymer paste and compared it to a Portland cement paste by using the Mercury intrusion porosimetry test. Results from their studies showed that the geopolymer paste had a higher amount of total pore volume as well as a lower average pore diameter in comparison with the Portland cement paste (Table 2-7). In addition, lower calcium content in geopolymer paste compared to Portland cement paste resulted in formation of a low-viscosity ASR gel that could easily permeate into the pore structure of the

geopolymer paste without causing significant expansion.

García-Lodeiro et al. (58) conducted a study to compare the role of aggregate in undergoing alkali-silica reaction in geopolymer and portland cement mortars. In their study two types of aggregates with different mineralogy (opal aggregates and arkosic sandstone) were considered. The results of this study indicated that geopolymer mortars showed a much better performance compared to Portland cement mortars. However, the calcium content in the materials was recognized to be very important in the ASR-related expansion observed in the geopolymer mortars.

Xie et al. (59), conducted a comparative study on the ASR behavior of mixtures containing natural mineral aggregate and crushed glass aggregate in a fly ash based geopolymer mortar. Although the specimens with 100% percent glass aggregates showed some expansion, the specimens with the replacement level of 50% showed fairly low expansion after 14 days (less than 0.01%) in the accelerated mortar bar test. The authors also concluded that the calcium content and porosity of the geopolymer matrix are important parameters in formation of the ASR-related expansion in geopolymers. ASR gel with lower calcium content has a lower viscosity, which allows the gel movement through the porous media.

Table 2-7. Results of Mercury intrusion porosimetry of geopolymer and OPC pastes (57)

| | GP | OPC |
|---|---|---|
| Total pore volume ($mm^3/g$) | 181 | 56 |
| Total pore surface area ($m^2/g$) | 55.5 | 8.5 |
| Average pore diameter (nm) | 13.1 | 26.6 |
| Median pore diameter (nm) | 13.2 | 46.4 |

In conclusion, it was found that generally geopolymer samples show a significant lower ASR-related expansion when they were compared to the OPC samples. The main cause of this better performance can be related to 1) the lower level of calcium in their matrix, 2) higher total

pore volume with smaller pores size, and 3) further geopolymerisation of unreacted source materials when they are subjected in a high alkali environment as those that are typically being used for ASR study.

#### *2.2.7.2 Sulfate attack*

Sulfate resistance of geopolymer materials has been studied by several researchers. Sata et al. (60) studied the resistance of a lignite bottom ash geopolymer mortar against sulfate attack. Length changes of mortar bars exposed to 5% sodium sulfate solution were measured up to one year and were compared with Portland cement mortar samples, and the results showed the better performance of geopolymer mortars. The authors concluded that this better performance is due to the more stable cross-linked alumino-silicate polymer structure in geopolymer. However, it should be noted that the length change measurement may not exactly reflect the resistance of geopolymer against the sulfate attack, as the type and characteristics of the reaction product produced in the geopolymer might vary with those of OPC samples. For instance, the main reaction product from sulfate attack in portland cement mortars is gypsum and Ettringite, which result in either expansion or loss in mass and stiffness of the test specimen. However, gypsum and Ettringite are not the reaction products observed in the case of sulfate attack in geopolymers. Other studies have been conducted on the compressive strength behavior of geopolymer samples when subjected to a sulfate rich media.

Bakharev (41) studied the durability of geopolymer paste in $Na_2SO_4$, and $MgSO_4$ solutions. Fly ash was used as the source material while NaOH, KOH and $Na_2SiO_3$ were used separately for the activation process and change in compressive strength was monitored up to 200 days. The results showed that the samples immersed in $Na_2SO_4$ showed higher loss of compressive strength due to the migration of alkali from the matrix to the sulfate solution. Furthermore, loss of strength was seen to be higher in the samples made with KOH and then

$Na_2SiO_3$ because of their larger pore sizes. The results also showed that unlike the $Na_2SO_4$ solution, geopolymer samples that were immersed in $MgSO_4$ showed a slight compressive strength gain.

Bhutta et al. (20) studied the mass change and strength loss of geopolymer concrete made with palm oil fuel ash activated with NaOH and $Na_2SiO_3$. Weight and strength change were monitored up to 18 months. The strength change results showed changes from 28 to 30 MPa for geopolymer and from 27 to 10 MPa for a Portland cement concrete Figure 2-18. In addition, mass losses of 4 and 20% were seen for geopolymer and Portland cement concrete respectively.

In this study the better performance of geopolymer samples was related to lower calcium content of the geopolymer as well their stable crosslinked structure. It should be also noted that while XRD and TGA results confirmed the presence of gypsum in the sulfate attacked OPC samples, no sign of gypsum or ettringite was seen in the XRD results.

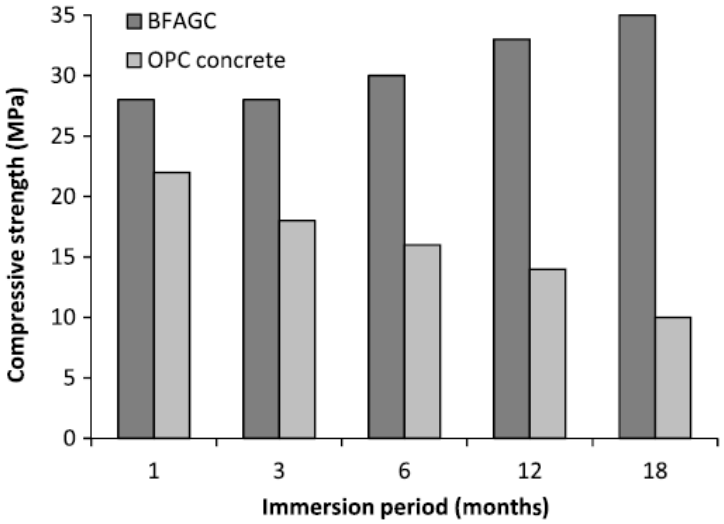


Figure 2-18. Change in the compressive strength of OPC and geopolymer samples (BFAGC) due to the sulfate attack (20)

In another study, Thokchom et al. (61), studied the Effect of $Na_2O$ content on durability of fly ash-based geopolymer pastes in magnesium sulfate solution. It was found that increase in

the $Na_2O$ content increase both initial and residual compressive strength. The results of this study showed that the compressive strength of the samples immersed in the 10% $MgSO_4$ solution were reduced significantly at the lower ages which then were followed by a strength gain as presented in Figure 2-19. The reason for this variation was explained by the migration of $Na^+$ from the samples to the solution and the diffusion of $Mg^{2+}$ ions to the samples which occur at a same time. Since ions such as $Ca^{2+}$ and $Mg^{2+}$ can act as a network-modifying cations, they will increase the compressive strength of the geopolymer sample. It also should be noted that the XRD results of the geopolymer samples that had been subjected to the sulfate solution identified the presence of gypsum and ettringite.

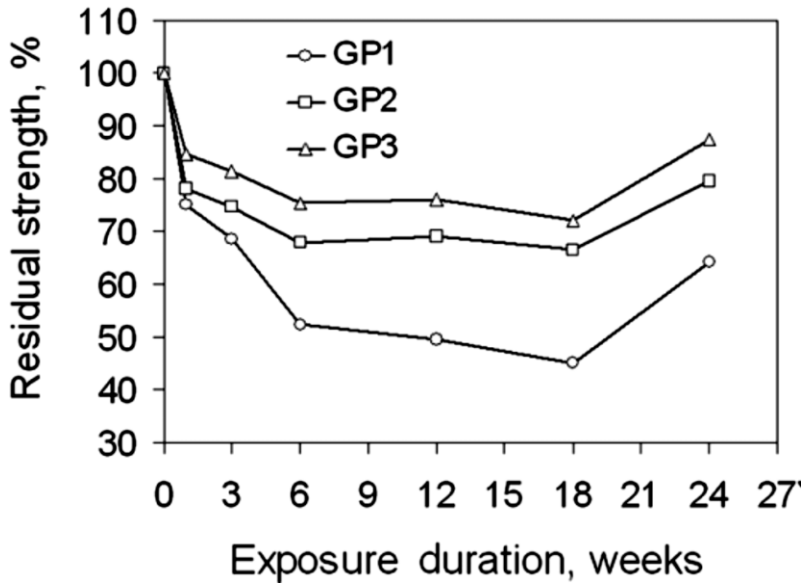


Figure 2-19. Residual compressive strength of geopolymer samples immersed in the $MgSO_4$ solution. Mix design with 5%, 6.5% and 8% $Na_2O$ content are named as GP1, GP2 and GP3 respectively (61)

In conclusion, it can be said that the sulfate attack mechanism in geopolymer systems is known to be different with OPC system. From the past studies of geopolymer samples tested in sulfate solution, both strength gain (20, 62) and strength loss has been reported (41, 61, and 63). In these works, the principal reason for strength gain was reported due to further geopolymerisation process while the main cause of strength loss is the dissolution of alkali in the

sulfate solution.

#### *2.2.7.3 Drying shrinkage*

Past researches on the shrinkage of geopolymer samples have indicated that this material has a relatively low shrinkage (43, 64) However, this is only true if they experience a high curing temperature during their curing process. Ridtirud et al. (65) studied the factors affecting the shrinkage of geopolymer samples. It was found that factors like curing temperature, liquid-to-binder ratio affect the shrinkage more while factors like sodium content and $Na_2SiO_3$ /NaOH have lesser effect. The results indicated that the higher temperatures cause lower shrinkage while higher liquid/binder, higher sodium content and higher $Na_2SiO_3$/NaOH causes the higher shrinkage. Nevertheless, the curing method, dry and steam curing didn't seem to have a significant effect on the shrinkage behavior of geopolymer concrete (64). In addition, it was noticed that the microstructure of geopolymer paste is unaffected due to water loss and the water loss is reversible, since geopolymer can gain water back from the humidity in air Fernández-Jiménez et al. (66).

# References:


1. R.T. Hemmings, R.D. Nelson, P.L. Graves, B.J. Cornelius,White pozzolan composition and blended cements containing same, US Patent US6776838 (2004)
2. Hemmings, R. Process for Converting Waste Glass Fiber into Value-added Products. DOE Report No. DE-FG36-03GO13015. Albacem, LLC, Peoria, Ill., 2005

A. Hossain, S.A. Shirazi, Properties of concrete containing vitreous calcium aluminosilicate pozzolan, J. Transp. Res. 2070 (2008) 32–38.

3. N. Neithalath, J. Persun, A. Hossain, Hydration in high-performance cementitious systems containing vitreous calcium aluminosilicate or silica fume, Cem. Concr. Res. 39 (2009) 473–481.
4. Kamali, M., & Ghahremaninezhad, A. (2016). An investigation into the hydration and microstructure of cement pastes modified with glass powders. Construction and Building Materials, 112, 915-924.
5. Tashima, M. M., Soriano, L., Payá, J., Monzó, J., & Borrachero, M. V. (2016). Assessment of pozzolanic/hydraulic reactivity of vitreous calcium aluminosilicate (VCAS). Materials & Design, 96, 424-430.
6. Chen, C. H., Huang, R., Wu, J. K., & Yang, C. C. (2006). Waste E-glass particles used in cementitious mixtures. cement and concrete research, 36(3), 449-456.
7. Davidovits, J. (1991). Geopolymers. Journal of thermal analysis, 37(8), 1633-1656.
8. Gartner, E. (2004). Industrially interesting approaches to “low-CO 2” cements. Cement and Concrete research, 34(9), 1489-1498.
9. Duxson, P., Fernández-Jiménez, A., Provis, J. L., Lukey, G. C., Palomo, A., & Van Deventer, J. S. J. (2007). Geopolymer technology: the current state of the art. Journal of Materials Science, 42(9), 2917-2933.
10. Davidovits, Joseph. "Chemistry of geopolymeric systems, terminology." Geopolymer. Vol. 99.

1999.

11. Duxson, P., Provis, J. L., Lukey, G. C., Mallicoat, S. W., Kriven, W. M., & Van Deventer, J. S. (2005). Understanding the relationship between geopolymer composition, microstructure and mechanical properties. Colloids and Surfaces A: Physicochemical and Engineering Aspects, 269(1), 47-58.
12. Barbosa, V. F., MacKenzie, K. J., & Thaumaturgo, C. (2000). Synthesis and characterization of materials based on inorganic polymers of alumina and silica: sodium polysialate polymers. International Journal of Inorganic Materials, 2(4), 309-317.
13. Singh, P. S., Bastow, T., & Trigg, M. (2005). Structural studies of geopolymers by $^{29}Si$ and $^{27}Al$ MAS-NMR. Journal of Materials Science, 40(15), 3951-3961.
14. Tossell, J. A., & Saghi-Szabo, G. (1997). Aluminosilicate and borosilicate single 4-rings: Effects of counterions and water on structure, stability, and spectra. Geochimica et Cosmochimica Acta, 61(6), 1171-1179.
15. Davidovits, J. (1994, October). Properties of geopolymer cements. In First international conference on alkaline cements and concretes (Vol. 1, pp. 131-149).
16. Klinowski, J. (1988). Recent advances in solid-state NMR of zeolites. Annual Review of Materials Science, 18(1), 189-218.
17. Anuar, K.A., Ridzuan, A.R.M. and Ismail, S., (2011) Strength characteristic of geopolymer concrete containing recycled concrete aggregate. International Journal of Civil & Environmental Engineering.
18. Xu, H. and Van Deventer, J.S., (2002) Geopolymerisation of multiple minerals. Minerals Engineering, 15(12), pp.1131-1139.
19. Bhutta, M.A.R., Hussin, W.M., Azreen, M. and Tahir, M.M., (2014) Sulphate resistance of geopolymer concrete prepared from blended waste fuel ash. Journal of Materials in Civil

Engineering, 26.

20. Pascual, A. B., Tognonvi, M. T., & Tagnit-Hamou, A. (2014). Waste glass powder-based alkali-activated mortar. In NTCC2014: International Conference on Non-Traditional Cement and Concrete.
21. Tashima, M. M., Soriano, L., Borrachero, M. V., Monzó, J., Cheeseman, C. R., & Payá, J. (2012). Alkali activation of vitreous calcium aluminosilicate derived from glass fiber waste. Journal of Sustainable Cement-Based Materials, 1(3), 83-93.
22. Nazari, A., Maghsoudpour, A. and Sanjayan, J.G., (2014) Characteristics of boroaluminosilicate geopolymers. Construction and Building Materials, 70, pp.262-268.
23. Palomo, A., Grutzeck, M.W. and Blanco, M.T., (1999) Alkali-activated fly ashes: a cement for the future. Cement and concrete research, 29(8), pp.1323-1329.
24. Van Jaarsveld, J.G.S., Van Deventer, J.S.J. and Lukey, G.C., (2003) The characterization of source materials in fly ash-based geopolymers. Materials Letters, 57(7), pp.1272-1280.
25. Xu, H., & Van Deventer, J. S. J. (2000). The geopolymerisation of alumino-silicate minerals. International Journal of Mineral Processing, 59(3), 247-266.
26. Wang, H., Li, H., & Yan, F. (2005). Synthesis and mechanical properties of metakaolinite-based geopolymer. Colloids and Surfaces A: Physicochemical and Engineering Aspects, 268(1), 1-6.
27. Granizo, M. L., Alonso, S., Blanco-Varela, M. T., & Palomo, A. (2002). Alkaline activation of metakaolin: effect of calcium hydroxide in the products of reaction. Journal of the American Ceramic Society, 85(1), 225-231.
28. Oh, J. E., Monteiro, P. J., Jun, S. S., Choi, S., & Clark, S. M. (2010). The evolution of strength and crystalline phases for alkali-activated ground blast furnace slag and fly ash-based geopolymers. Cement and Concrete Research, 40(2), 189-196.
29. Kumar, S., Kumar, R., & Mehrotra, S. P. (2010). Influence of granulated blast furnace slag on the

reaction, structure and properties of fly ash based geopolymer. Journal of Materials Science, 45(3), 607-615.

30. Tashima, M. M., Soriano, L., Monzo, J., Borrachero, M. V., & Paya, J. (2013). Novel geopolymeric material cured at room temperature. Advances in Applied Ceramics, 112(4), 179-183.
31. Hajimohammadi, A., Provis, J. L., & van Deventer, J. S. (2010). Effect of alumina release rate on the mechanism of geopolymer gel formation. Chemistry of Materials, 22(18), 5199-5208.
32. De Silva, P., Sagoe-Crenstil, K., & Sirivivatnanon, V. (2007). Kinetics of geopolymerization: role of Al 2 O 3 and SiO 2. Cement and Concrete Research, 37(4), 512-518.
33. Kouamo, H. T., Elimbi, A., Mbey, J. A., Sabouang, C. N., & Njopwouo, D. (2012). The effect of adding alumina-oxide to metakaolin and volcanic ash on geopolymer products: A comparative study. Construction and Building Materials, 35, 960-969.
34. Buchwald, A., Dombrowski, K. and Weil, M., (2005) The influence of calcium content on the performance of geopolymeric binder especially the resistance against acids. Proceedings of the world geopolymer.
35. Yip, C.K., Lukey, G.C. and Van Deventer, J.S.J., (2005) The coexistence of geopolymeric gel and calcium silicate hydrate at the early stage of alkaline activation. Cement and Concrete Research, 35(9), pp.1688-1697.
36. Lee, W. K. W., & Van Deventer, J. S. J. (2002). The effect of ionic contaminants on the early-age properties of alkali-activated fly ash-based cements. Cement and Concrete Research, 32(4), 577-584.
37. Dombrowski, K., Buchwald, A., & Weil, M. (2007). The influence of calcium content on the structure and thermal performance of fly ash based geopolymers. Journal of Materials Science, 42(9), 3033-3043.

38. Temuujin, J., Van Riessen, A., & Williams, R. (2009). Influence of calcium compounds on the mechanical properties of fly ash geopolymer pastes. Journal of hazardous materials, 167(1), 82-88.

39. Garcia-Lodeiro, I., Palomo, A., Fernández-Jiménez, A., & Macphee, D. E. (2011). Compatibility studies between NASH and CASH gels. Study in the ternary diagram Na 2 O–CaO–Al 2 O 3–SiO 2–H 2 O. Cement and Concrete Research, 41(9), 923-931.

40. Bakharev, T. (2005). Durability of geopolymer materials in sodium and magnesium sulfate solutions. Cement and Concrete Research, 35(6), 1233-1246.

41. Hardjito, D., & Fung, S. S. (2010). Parametric Study on the Properties of Geopolymer Mortar Incorporating Bottom Ash. Concrete Research Letters, 1(3), 115-124.

42. Hardjito, D., Wallah, S.E., Sumajouw, D.M. and Rangan, B.V., (2004). On the development of fly ash-based geopolymer concrete. ACI materials journal,101(6).

43. Rattanasak, U., & Chindaprasirt, P. (2009). Influence of NaOH solution on the synthesis of fly ash geopolymer. Minerals Engineering, 22(12), 1073-1078.

44. Morsy, M. S., Alsayed, S. H., Al-Salloum, Y., & Almusallam, T. (2014). Effect of sodium silicate to sodium hydroxide ratios on strength and microstructure of fly ash geopolymer binder. Arabian Journal for Science and Engineering, 39(6), 4333-4339.

45. Muñiz-Villarreal, M. S., Manzano-Ramírez, A., Sampieri-Bulbarela, S., Gasca-Tirado, J. R., Reyes-Araiza, J. L., Rubio-Ávalos, J. C., ... & Amigó-Borrás, V. (2011). The effect of temperature on the geopolymerization process of a metakaolin-based geopolymer. Materials Letters, 65(6), 995-998.

46. Chindaprasirt, P., Chareerat, T., & Sirivivatnanon, V. (2007). Workability and strength of coarse high calcium fly ash geopolymer. Cement and Concrete Composites, 29(3), 224-229.

47. Mo, B. H., Zhu, H., Cui, X. M., He, Y., & Gong, S. Y. (2014). Effect of curing temperature on

geopolymerization of metakaolin-based geopolymers. Applied Clay Science, 99, 144-148.

48. Nagral, M. R., Ostwal, T., & Manojkumar, V. C. Effect Of Curing Temperature And Curing Hours On The Properties Of Geo-Polymer Concrete.
49. Vora, P. R., & Dave, U. V. (2013). Parametric studies on compressive strength of geopolymer concrete. Procedia Engineering, 51, 210-219.
50. Satpute Manesh, B., Wakchaure Madhukar, R., & Patankar Subhash, V. (2012). Effect of duration and temperature of curing on compressive strength of geopolymer concrete. International Journal of Engineering and Innovative Technology, 1(5).
51. Adam, A. A., & Horianto. (2014). The effect of temperature and duration of curing on the strength of fly ash based geopolymer mortar. Procedia Engineering, 95, 410-414.
52. Van Jaarsveld, J. G. S., Van Deventer, J. S. J., & Lukey, G. C. (2002). The effect of composition and temperature on the properties of fly ash-and kaolinite-based geopolymers. Chemical Engineering Journal, 89(1), 63-73.
53. Kong, D. L., & Sanjayan, J. G. (2010). Effect of elevated temperatures on geopolymer paste, mortar and concrete. Cement and concrete research, 40(2), 334-339.
54. Kupwade-Patil, K. and Allouche, E.N., (2013). Impact of Alkali Silica Reaction on Fly Ash-Based Geopolymer Concrete. Journal of Materials in Civil Engineering, 25(1), pp.131-139.
55. Puertas, F., Palacios, M., Gil-Maroto, A. and Vázquez, T., (2009). Alkali-aggregate behaviour of alkali-activated slag mortars: Effect of aggregate type. Cement and Concrete Composites, 31(5), pp.277-284.
56. Pouhet, R. and Cyr, M., (2015). Alkali–silica reaction in metakaolin-based geopolymer mortar. Materials and Structures, 48(3), pp.571-583.
57. Fernández-Jiménez, A., Garcia-Lodeiro, I., & Palomo, A. (2007). Durability of alkali-activated fly ash cementitious materials. Journal of materials science, 42(9), 3055-3065.

58. Xie, Z., Xiang, W., & Xi, Y. (2003). ASR potentials of glass aggregates in water-glass activated fly ash and portland cement mortars. Journal of Materials in Civil Engineering, 15(1), 67-74.

59. Sata, V., Sathonsaowaphak, A., & Chindaprasirt, P. (2012). Resistance of lignite bottom ash geopolymer mortar to sulfate and sulfuric acid attack. Cement and Concrete Composites, 34(5), 700-708.

60. Thokchom, S., Mandal, K. K., & Ghosh, S. (2012). Effect of Si/Al ratio on performance of fly ash geopolymers at elevated temperature. Arabian Journal for Science and Engineering, 37(4), 977-989.

61. Hardjito, D., Wallah, S. E., Sumajouw, D. M., & Rangan, B. V. (2005). Fly ash-based geopolymer concrete. Australian Journal of Structural Engineering, 6(1), 77-86.

62. Sanni, S. H., & Khadiranaikar, R. B. (2012). Performance of geopolymer concrete under severe environmental conditions. International journal of civil and structural engineering, 3(2), 396.

63. Wallah, S. E. (2009). Drying shrinkage of heat-cured fly ash-based geopolymer concrete. Modern Applied Science, 3(12), 14.

64. Ridtirud, C., Chindaprasirt, P., & Pimraksa, K. (2011). Factors affecting the shrinkage of fly ash geopolymers. International Journal of Minerals, Metallurgy, and Materials, 18(1), 100-104.

65. Fernandez-Jimenez, A. M., Palomo, A., & Lopez-Hombrados, C. (2006). Engineering properties of alkali-activated fly ash concrete. ACI Materials Journal, 103(2), 106-112.

# CHAPTER 3

# EXPERIMENTAL WORK

In order to evaluate the properties of GGF when used as a SCM, or as a source materials in producing geopolymer, numbers of tests were conducted on mortar and concrete specimens. In the first case, utilization of GGF as a SCM, results were compared with two control mixtures; 1) a mixture with 100% Portland cement as the binder, and 2) a mixture having 25% fly ash as the cement replacement. In the second case, utilization of GGF in geopolymer production, all the results were compared with a fly ash-based geopolymer and in many cases with a glass-powder-based geopolymer. This chapter presents the materials and the tests methods that were used in this study.

## 3.1 Material

### *3.1.1 Portland cement*

In this study, two types of cements namely a Type I/II ordinary portland cement (OPC) with $Na_2O_{eq}$=0.38%, and a Type I high alkali Portland cement ($Na_2O_{eq}$=0.88%) meeting the requirements of ASTM C150 were used. While OPC was used for almost all the tests, the high alkali cement was used only in ASR related studies including miniature prism test (AASHTO TP110) and concrete prism test (ASTM C1293). The chemical compositions and physical properties of portland cement are presented Table 3-1 and Table 3-2. In addition, its particles size distribution and XRD pattern is presented in Figure 3-3 and Figure 3-4 respectively.

### *3.1.2 Ground Glass Fiber*

The Ground Glass Fiber (GGF) used in this study is a fine white powder as presented in Figure 3-1. This powder was prepared by milling the off-spec glass fiber in a ball mill to a fine powder with an average particle size of 4 microns. The chemical compositions and physical properties of

GGF are presented Table 3-1 and Table 3-2. In addition, its particles size distribution and XRD pattern is presented in Figure 3-3 and Figure 3-4 respectively.

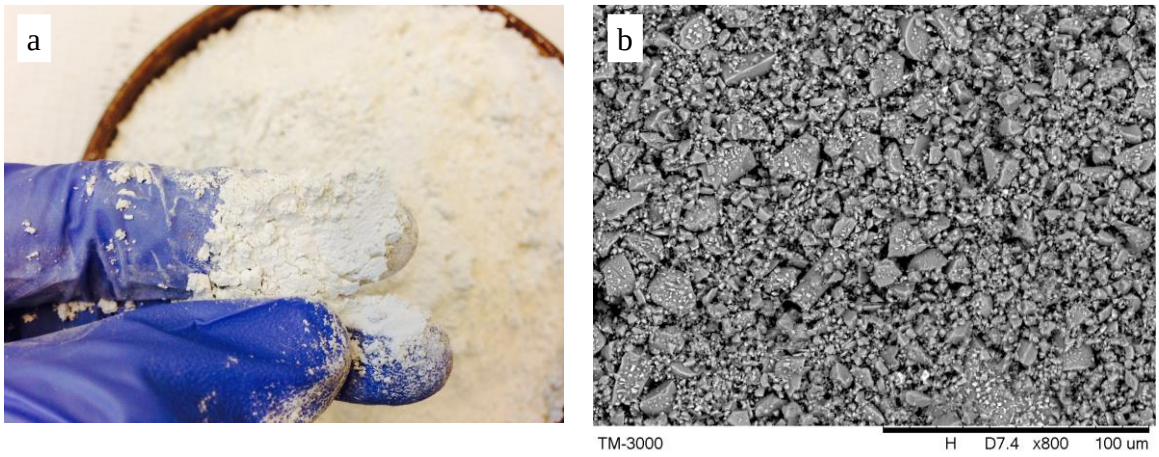


Figure 3-1. Appearance of GGF. a) normal view, and b) SEM image

### *3.1.3 Fly ash*

In this study, a class F fly ash (ASTM C618) was used as a SCM and a source material for geopolymer studies. The material had a specific gravity of 2.25 and average particle size of 28 microns. The chemical compositions and physical properties of the fly ash are presented Table 3-1 and Table 3-2. In addition, its particles size distribution and XRD pattern is presented in Figure 3-3 and Figure 3-4 respectively.

### *3.1.4 Glass-Powder*

A finely ground glass-powder (GLP) was used a source material for geopolymer studies. The glass-powder was obtained from a local source and was produced by grounding waste glass bottles. This material had specific gravity of 2.4 and average particle size of 17 microns. The appetence of GLP is presented in Figure 3-2. The chemical compositions and physical properties of the GLP are presented Table 3-1 and Table 3-2. In addition, its particles size distribution and XRD pattern is presented in Figure 3-3 and Figure 3-4 respectively.

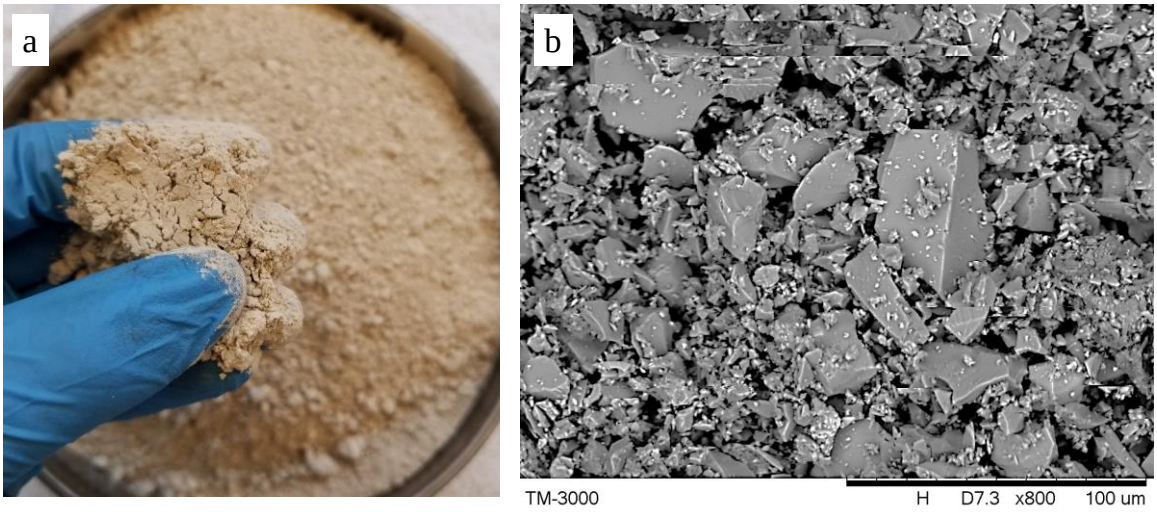


Figure 3-2. Appearance of GLP. a) normal view, and b) SEM image

Table 3-1. Chemical composition of the cementitious material

| Material | $SiO_2$ | $Al_2O_3$ | $Fe_2O_3$ | $CaO$ | $MgO$ | $Na_2O$ | $K_2O$ |
|---|---|---|---|---|---|---|---|
| Cement (%) | 19.93 | 4.77 | 3.13 | 62.27 | 2.7 | 0.06 | 0.48 |
| GGF (%) | 47.72 | 10.36 | 0.34 | 19.62 | 2.27 | 0.67 | 0.1 |
| Fly Ash (%) | 50.7 | 25.1 | 12.5 | 3.3 | 1.1 | 0.51 | 2.27 |
| Glass Powder (%) | 69.6 | 2.2 | 0.9 | 11.6 | 0.4 | 12.03 | 0.4 |

Table 3-2. Basic properties of the cementitous materials

| Material | Specific Gravity | Amount Passing #325 Sieve (%) | Loss On Ignition | Blaine's fineness ($cm^2/g$) |
|---|---|---|---|---|
| GGF | 2.6 | 96% | 1.0% | 10200 |
| Fly ash | 2.25 | 76% | 2.3% | 6040 |
| Glass Powder | 2.4 | 83% | 1.5% | 5920 |
| Cement | 3.15 | 98% | 2.6% | 4720 |

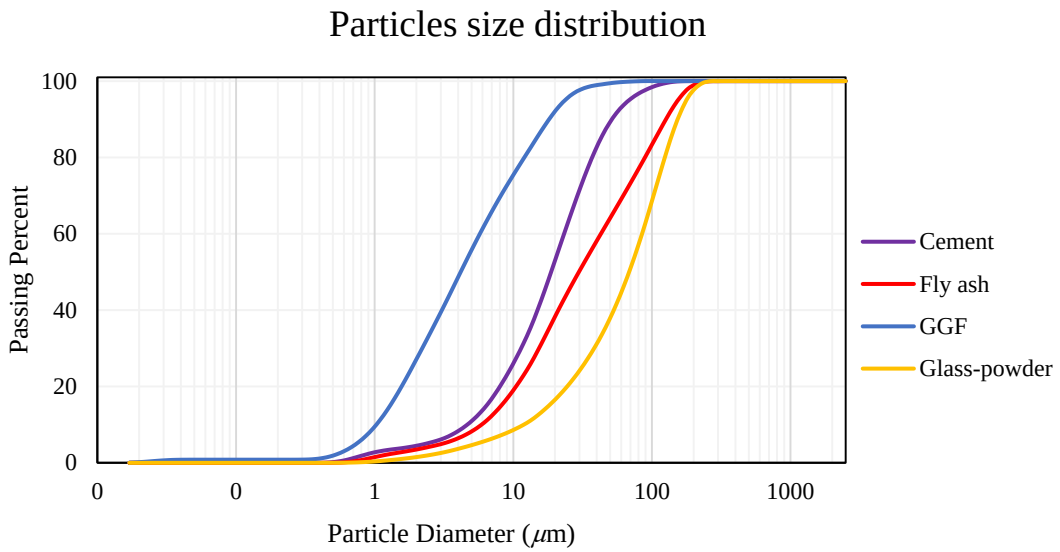


Figure 3-3. Particle size distribution of Cement, fly ash and GGF

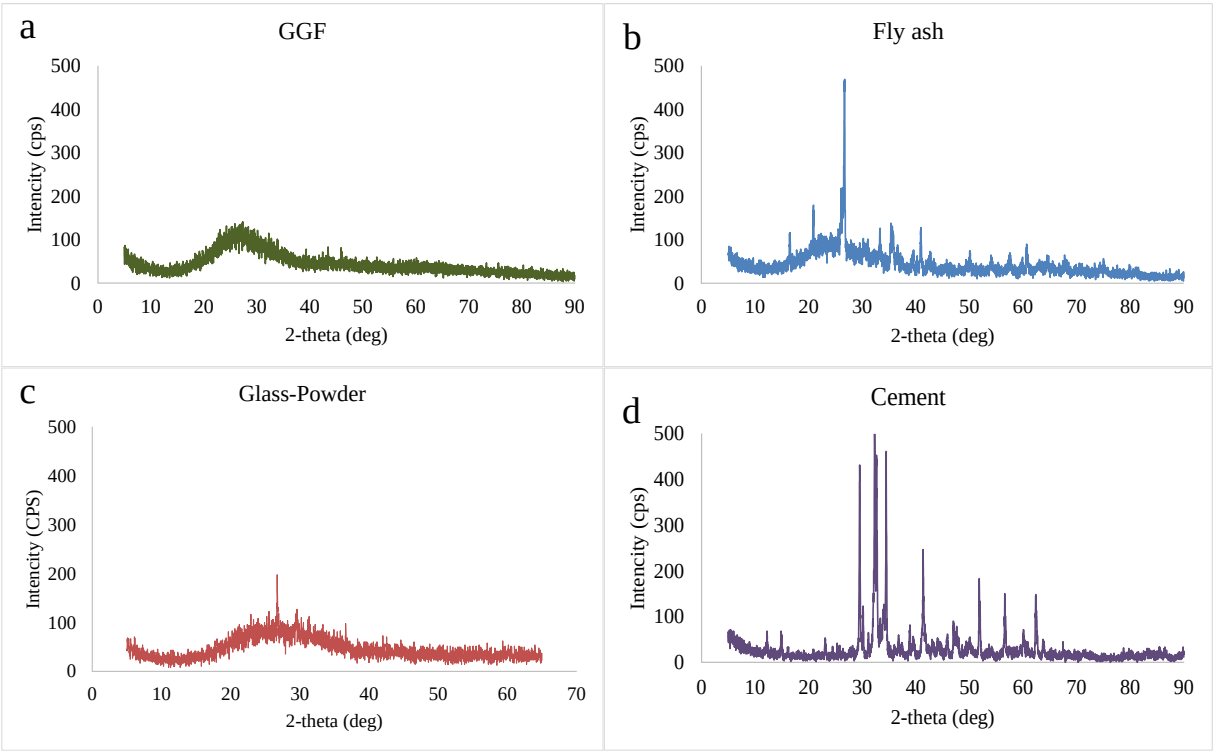


Figure 3-4. XRD pattern of a) GGF, b) Fly ash, c) Glass-powder and d) Cement.

### *3.1.5 Fine aggregate (siliceous sand)*

A mineral non-reactive siliceous river sand with an absorption value of 0.30% and an oven-dry

specific gravity of 2.67 was used in this study. The sand had the final modulus of 2.6.

### *3.1.6 Coarse aggregate*

In this study two types of coarse aggregates (i.e. Liberty and New-Mexico) were used depending on the purpose of the test. While reactive New-Mexico aggregates were used for the ASR related studies such as miniature concrete prism test (MCPT) and concrete prism test CPT; liberty aggregate was used for the other tests such as compressive strength, split tensile strength, rapid chloride penetration test etc. The specific gravity and abortion of liberty aggregate were 2.65 and 1% respectively. Also, the specific gravity and absorption of the New-Mexico aggregate were 2.6 and 1.09% respectively.

### *3.1.7 Crushed aggregate for ASR studies*

Crushed aggregates were used in order to study the ASR expansion of mortar mixtures. In this study several crushed aggregates i.e. New-Mexico, Spratt, Adairsville and crushed glass aggregate from waste bottles were used. All the aggregates were mechanically crushed using a pulverizer to meet the gradation specified by ASTM C 1260. The chemical composition of the aggregates are presented in Table 3-3. The specific gravity of NM, SP, AD, and glass aggregate is 2.60, 2.69, 2.83 and 2.42 respectively.

### *3.1.8 Chemicals*

In this study, different chemicals were used to study the durability properties of mortars and concretes mixtures made with GGF as the SCM. In addition, chemicals were used to produce the alkali activator solutions used to activate the source material of different geopolymer mixtures. These chemicals include, sodium sulfate ($Na_2SO_4$) anhydrous, magnesium sulfate ($MgSO_4$) powder, NaOH pellets and sodium silicate solution.

Table 3-3.Chemical composition of crushed aggregates

| Chemical parameter | Unit | Spratt | New-Mexico | Adairsville | Glass |
|---|---|---|---|---|---|
| $SiO_2$ | % | 10.47 | 75.14 | 7.01 | 69.6 |
| $Al_2O_3$ | % | <0.29 | 10.47 | <0.29 | 2.2 |
| $CaO$ | % | 85.17 | 4.20 | 58.90 | 11.6 |
| $Fe_2O_3$ | % | 0.63 | 3.40 | 0.68 | 0.9 |
| $MgO$ | % | 2.58 | 0.98 | 32.28 | 0.4 |
| $Na_2O$ | % | 0.93 | 2.82 | 0.52 | 12.03 |
| $K_2O$ | % | <0.13 | 2.42 | 0.62 | 2.27 |

The sodium sulfate anhydrous and magnesium sulfate anhydrous that used in this study were an ASC (American Society of Chemicals) grade which were obtained from AMERSCO Inc. An ASC grade sodium hydroxide pellets was obtained from AMERSCO Inc. with a 98% purity. This pellets were used to prepare the 1N NaOH solution in ASR study and also in preparation of the alkali solutions in activation of geopolymer mixtures. In addition, the sodium silicate solution was obtained from the CQ concept company and had the following chemical ratios as presented in Table 3-4. This sodium silicate solution was used in preparation of the activator solutions.

Table 3-4. Chemical composition ration in sodium silicate solution.

| Water content (%) | $Na_2O$ content (%) | $SiO_3$ content (%) |
|---|---|---|
| 60 | 9 | 31 |

## 3.2 Mixture proportion and curing

### *3.2.1 Mixture proportion for utilization of GGF as a SCM*

In this study, series of tests were conducted to evaluate the properties of GGF as a Supplementary Cementitious Martial (SCM). GGF that was employed in mortar and concrete as a partial substitute for cement at selected dosage levels of 10, 20 and 30% by mass replacement of cement. In addition, two control mixtures were tested for comparative purposes. The first control mixture

was consisted of plain Type I portland cement, while the second control mixture was consisted of binary blend of 75% Type I Portland cement with 25% Class F fly ash, by mass. Table 3-5 shows the mix ID and composition of the cementitious portion of the above-mentioned mixtures.

Table 3-5. Mix ID and mixture composition of the binder portion of concrete and mortar having GGF or Fly ash as a cement replacement

| Mix ID | Mixture Composition |
|---|---|
| CTRL-1 | 100% Cement |
| CTRL-2 | 75% Cement+ 25% Fly ash |
| GGF-10 | 90% Type I Cement+ 10% GGF |
| GGF-20 | 80% Type I Cement + 20% GGF |
| GGF-30 | 70% Type I Cement + 30% GGF |

To cast concrete samples, a standard concrete mixture with W/C ratio of 0.45 with a total cementitious materials content of 355 kg/m$^3$ (600 lb/yd$^3$) was employed. A #57 coarse aggregate was used in combination with siliceous river sand at 60:40 proportions. Also a high-range water reducer was used to achieve the desired slump to cast required test specimens. It should be noted that for other tests, the specified mixture design from the relevant test method (with the binder portion maintained as Table 3-5 were used. All the samples were cured at a standard curing room with 23$^o$C and RH> 95%.

### *3.2.2 Utilization of GGF in geopolymer production*

To study the effect of chemical composition of the activators on the fresh and hardened properties of geopolymers, relative proportions of NaOH and sodium silicate in the activator solution were varied to obtain a range of values for two different parameters. The first parameter is the mass ratio of total $Na_2O$ in the activator solution-to-source material (i.e. binder) which was studied at three different levels 5%, 7.5% and 10%. The second parameter is the mass ratio of $SiO_2/Na_2O$ in the activator solution which was used at three levels 0, 0.50 and 1.00. The sand content of the mortars was chosen to fill 55% of the total volume of the mixtures, and the water-to-binder ratio

of all the mixtures was maintained between 0.30 and 0.35. This range of water-to-binder was selected to maximize the compressive strength of the hardened mortars while requiring no water reducer to achieve the desired workability with the mixtures. Table 3-6 presents the details of the test plan and the mix ID of all the mixtures used in this study. The letter(s) in the mix IDs shows the source material, i.e. GGF for ground glass fiber, F for fly ash and GP for glass-powder. The first and second numbers show the $SiO_2/Na_2O$ ratio and percent of $Na_2O$-to-binder respectively. In present study, curing at 60°C for 24 h was used for all the geopolymer samples.

Table 3-6. Details of the mixtures proportion

| | | | | | | | | |
|---|---|---|---|---|---|---|---|---|
| GGF | Mix ID | GGF-0-10 | GGF-0.5-5 | GGF-0.5-7.5 | GGF-0.5-10 | GGF-1-5 | GGF-1-7.5 | GGF-1-10 |
| | $Na_2O$/Binder (%) | 10 | 5 | 7.5 | 10 | 5 | 7.5 | 10 |
| | $SiO_2/Na_2O$ | 0 | 0.5 | 0.5 | 0.5 | 1 | 1 | 1 |
| | W/Binder | 0.33 | 0.33 | 0.33 | 0.33 | 0.33 | 0.33 | 0.33 |
| Fly ash | Mix ID | F-0-10 | F-0.5-5 | F-0.5-7.5 | F-0.5-10 | F-1-5 | F-1-7.5 | F-1-10 |
| | $Na_2O$/Binder (%) | 10 | 5 | 7.5 | 10 | 5 | 7.5 | 10 |
| | $SiO_2/Na_2O$ | 0 | 0.5 | 0.5 | 0.5 | 1 | 1 | 1 |
| | W/Binder | 0.3 | 0.3 | 0.3 | 0.3 | 0.3 | 0.3 | 0.3 |
| Glass-Powder | Mix ID | GLP-0-10 | GLP-0.5-5 | GLP-0.5-7.5 | GLP-0.5-10 | GLP-1-5 | GP-1-7.5 | GLP-1-10 |
| | $Na_2O$ /Binder (%) | 10 | 10 | 7.5 | 5 | 10 | 7.5 | 5 |
| | $SiO_2/Na_2O$ | 0 | 0.5 | 0.5 | 0.5 | 1 | 1 | 1 |
| | W/Binder | 0.35 | 0.35 | 0.35 | 0.35 | 0.35 | 0.35 | 0.35 |

## 3.3 Test procedure

In this study different test methods were employed in order to identify the properties of raw materials and final products. Therefore, the test methods that were used in study of 1) the basic properties of raw materials, 2) utilization of GGF as a SCM and 3) Utilization of GGF in geopolymer production, are presented in following subsections. It should be noted that since some of these test methods were identical for both SCM and geopolymer related steadies, they have been introduced only once at the first possible location of this context.

### *3.3.1 Basic properties*

#### *3.3.1.1 X-Ray Fluorescence (XRF)*

In this study, the chemical composition of the cementitious materials were obtained by the X-Ray Fluorescence (XRF). The test was performed by the Argos cement laboratory. The results of XRF have been presented in Table 3-1.

#### *3.3.1.2 X-Ray Diffraction (XRD)*

The amorphous portion of the SCMs is the actual portion that is involved in the pozzolanic reaction. In order to identify the crystalline phase of each cementitious material, the X-Ray diffraction (XRD) technique was used in this study. To identify the structure of the samples, Rigaku Ultima IV multipurpose X-ray diffraction system was used. The tests parameters were set as, $2\theta$ changing from $5^{o}$ to $90^{o}$ (Cu Kalpha radiation) and the scan rate of 0.1 per minutes. The Inorganic Crystal Structure Database, NIST Crystal Data File and Powder Diffraction File electronic data base were used to match the best crystalline phase with the identified intensity peaks.

#### *3.3.1.3 Specific gravity, specific surface and amount passing #325 sieve*

Specific gravity of the samples were obtained using the ASTM C188. First kerosene with a specific gravity of 0.73 g/mL was introduced to a Le Chatelier flask until it reached to a point between 0 to 1-mL on the flask. Then a known amount of sample (i.e. 64 g) was introduced in the flask, flask were shacked to remove any trapped air, and the increase in the new volume of the suspension was recorded (volume of the sample). Finally, having the mass, and volume of the sample the specific gravity of each sample was calculated by dividing the mass to the volume of the sample.

Following ASTM C204, specific surface area of the samples were measured using the Blaine apparatus (Figure 3-5). Before testing the samples, the device was calibrated using the NIST Standard Reference Material No. 114. To perform the test, following steps were taken 1) required amount of the samples were placed in the top cell (notation "a" in the figure). 2) Using an aspirator bulb, air shall be evacuated until the monometer liquid gets to the point "b". 3) Valve shall be closed and monometer liquid is allowed to sink in the U-shape glass until it reaches point "c". 4) The time that takes for the liquid to reach point "d" is recorded as "T". 5) Finally, the Blaine surface area can be calculated as $S = S_s \sqrt{T} / \sqrt{T_s}$, wherein, $S$ is the specific surface of the test sample ($m^2/kg$), $S_s$ is the specific surface of the standard sample used in calibration of the apparatus ($m^2/kg$), and $T_s$ is the time needed for the liquid to drop from the point "c" to "d" for the standard sample.

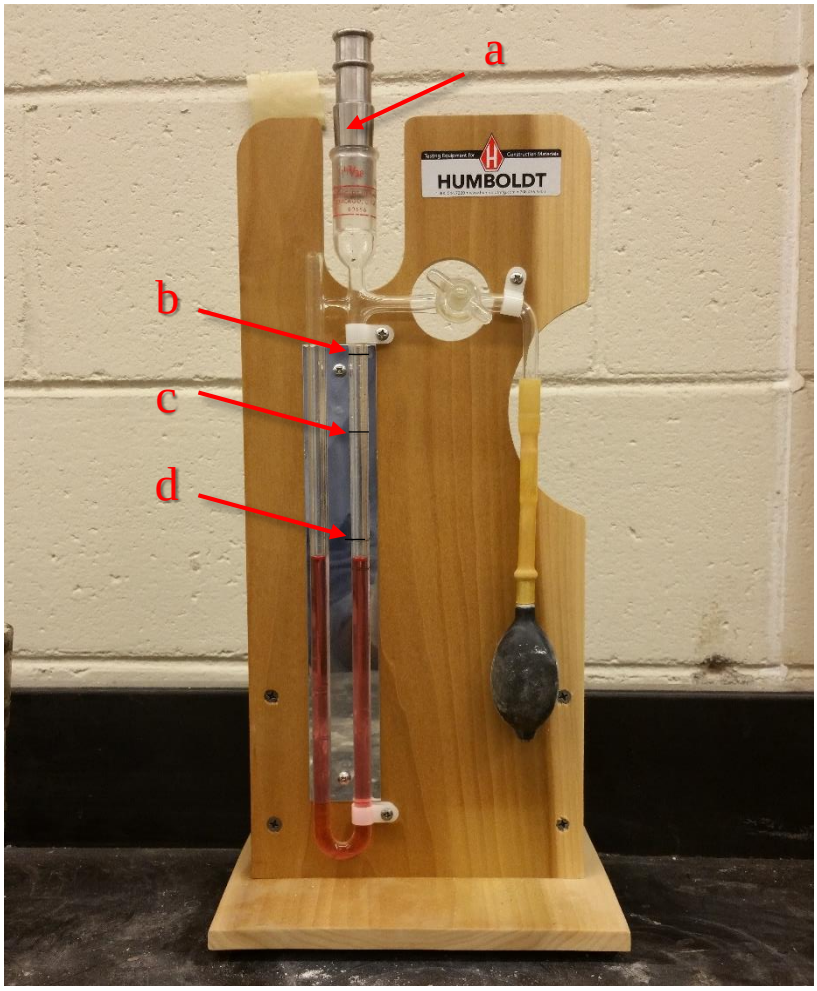


Figure 3-5. View of the Blaine apparatus

The amount passing #325 sieve was measured following the test method presented in ASTM C430. For the purpose of this, required amount of sample is placed in a standard #325 sieve and then the material is washed by water for 1 minute using a standard spray nozzle under the pressure range of $10 \pm 0.5$ psi. Material is then placed in an oven with 110°C to dry completely. Finally, dried material is weighed and the percent passing the #325 sieve is calculated.

#### *3.3.1.4 Laser Particle Size Distribution (PSD)*

In this study, the particle distribution size of the cement, fly ash and GGF were measured using a

Shimadzu SALD 2300 Laser Diffraction Particle Size Analyzer. The results of this test are used to plot the particles size distribution graph (Figure 3-3), and also the average size of each tested material.

### *3.3.2 Tests for utilization of GGF as a SCM*

This section, presents the test methods that were used in the studies related to the utilization of GGF as a SCM.

#### *3.3.2.1 Flow test (ASTM C1437)*

The effect of replacing cement with GGF on the workability of mortars was investigated using a flow table and using the method presented in ASTM C1437. In this study, the influence of GGF dosage were investigated at 10, 20 and 30% replacement levels and then were compared with two control mixtures i.e. a mix with 100% cement and a mix with 25% class F fly ash and 75% cement. For the purpose of this test, mortar mixes with abovementioned material and water-to-binder ratio of 48.5% were made and tested using a flow-table. For each of the mixes, prepared material was placed in a standard flow mold in two layers and was tamped 20 times for each layer by a standard tamper. The mold was then removed and the material was dropped 25 times in 15 seconds. Finally the spread of the mix was measured and recorded to calculate the flow percent.

#### *3.3.2.2 Strength activity Index (ASTM C311)*

In this study, the pozzolanic reactivity of GGF was examined by evaluating the strength activity index of the mixtures containing GGF as a cement replacement material using the ASTM C311 test procedure. In this test, 50 mm x 50 mm x 50 mm (2 in. x 2 in. x 2 in.) mortar cubes were cast for each mix design (0, 10, 20 and 30% GGF and 25% fly ash as the cement replacement) and the compressive strength of each mixture was evaluated at 7 and 28 days of curing. According to ASTM C311, a material can be considered as pozzolan if the mixture with replacement level of

20% can achieve 75% of the compressive strength of control mix (plain cement) after 7 or 28 days.

#### *3.3.2.3 Thermo Gravimetric Analysis (TGA)*

In order to evaluate the effectiveness of GGF in consumption of $Ca(OH)_2$, the Thermogravimetric analysis (TGA) was performed on the paste containing different dosage of the GGF. In this test method, the crushed paste samples are gradually heated from the ambient temperature to 800°C and the change in their mass is monitored and recorded. Decomposition of calcium hydroxide occurs in the temperature range between 440 to 520°C, causing a significant mass loss in the sample. The mass loss in this range can be used to calculate the amount of calcium hydroxide in the sample.

In present study, the TGA test was performed on the paste samples containing 10, 20 and 30% GGF and two control samples ( one with plain cement and the other with 25% fly ash as cement replacement) at their 28 and 56-day ages. At the testing date, the samples were removed from their molds and the paste sample was extracted from the core part of the sample. The paste were then mechanically crushed and sieved using a #200 sieve. The material that passed from the #200 sieve were then used to for the TGA test.

#### *3.3.2.4 Accelerated mortar bar test (AMBT-ASTM C1260 & ASTM C1567)*

To evaluate the ASR mitigation effectiveness of GGF, Accelerated Mortar Bar Test (AMBT) was conducted using crushed NM aggregate as a reactive fine aggregate. For CTRL-1 mixture, where no pozzolan was used, AMBT based on ASTM C1260 test procedure was conducted to serve as a reference. For all the other mixtures containing a pozzolan, AMBT based on ASTM C1567 test procedure was conducted. In this study, mortar bars with dimensions of 25 mm x 25 mm x 285 mm (1" × 1" × 11.25 ") were cast and cured for the initial 24 hours in a standard curing room.

The mortar bars were demolded after 24 hours and transferred into a water bath that was gradually heated to 80°C and cured for an additional 24 hours. Finally, the mortar bars samples were removed from the water bath and the zero-day reading was taken for each bar. The bars then were immersed in a 1N NaOH solution that was preheated to 80°C. The test was conducted up to 28 days and the length change in the mortar bars was recorded at selected time intervals to track the expansion

#### *3.3.2.5 Miniature Concrete Prism Test (MCPT-AASHTO TP110)*

Miniature Concrete Prism Test (MCPT), based on AASHTO TP-110, was performed on concrete prism specimens for all the mixtures. As per the test procedure, the cement content of the concrete mixtures is maintained at 420 kg/m3 and a water-to-cementitious materials ratio of 0.45 is used. In addition, the volume fraction of the dry-rodded coarse aggregate per unit volume in the concrete is fixed at 0.65. The coarse aggregate gradation calls for 57.5% of material that is passing 12.5 mm (1/2 in.) sieve and retained on 9.5 mm sieve (3/8 in.), and 42.5% of material that is passing 9.5 mm sieve (3/8 in.) and retained on No. 4 sieve. A non-reactive fine aggregate is used when a reactive coarse aggregate is evaluated in this study.

In preparing the concrete prisms for the MCPT, when the cement alkali content is less than 1.25% $Na_2O_{eq.}$, the alkali content of the concrete is boosted to 1.25% by weight of the cement by adding NaOH to the mix water. When evaluating supplementary cementitious materials (SCMs) in this test, the alkali content of the concrete is boosted to 1.25% only by the mass of the portland cement, and the SCMs are not considered in this calculation.

In this test, concrete prisms of 50 mm x 50 mm x 285 mm (2 in. x 2 in. x 11.25 in.) are used as test specimens. After demolding the concrete specimens after 24 hours of curing in a standard curing room, they are submerged in a sealed water bath and stored in a 60°C chamber for another 24-hours period. Finally, the prisms are removed from the water bath and the zero-day

reading is taken. The prisms are subsequently submerged in a 1N NaOH solution that has been preheated to 60ºC. The prisms are kept in a 60ºC chamber for the remainder of the test duration and their length-change is monitored up to 84 days by taking periodic measurement at selected intervals. An expansion of 0.040% or greater at 56 days is typically considered as indicative of an aggregate that is alkali-silica reactive. When evaluating the effectiveness of SCMs in this test method, a dosage of SCM that limits the expansion of concrete prisms to 0.020% or less at 56 days is considered to represent an effective SCM performance in mitigating ASR distress.

#### *3.3.2.6 Concrete prism test (CPT-ASTM C1293)*

Concrete prism test was conducted to study the effect of GGF in mitigation of long-term alkali-silica reaction. Following ASTM C1293 test method, for all the mix designs, concrete prisms with dimension of 75 mm x 75 mm x 75 mm (3" x 3" x 11.25") were cast using New-Mexico aggregate. Samples were removed after 24 h and were kept in sealed 5-gallons bucket at 38ºC. For the mitigation purposes, a mixture containing pozzolan should be able to meet the required 0.04% expansion limit after years.

#### *3.3.2.7 Expansion due sulfate attack (ASTM C1012)*

Formation of gypsum and Ettringite are the two main mechanisms that cause sulfate attack damages in concretes. Therefore, the pozzolans that could consume $Ca(OH)_2$ and also reduce the permeability can reduce the sulfate attack damages. In this study, expansion of mortar bars containing GGF were measured to evaluate their effectiveness in reducing the sulfate attack damages.

Following ASTM C1012 test method, 25 mm x 25 mm x 25 mm (1" x 1" x 11.25") mortar bars and sufficient amount of 50 mm x 50 mm x 50 mm (2" x 2" x 2") mortar cubes were cast for each mix design. The samples were removed from their molds after 24 h and were placed

in a saturated lime water until they reach compressive strength of 3000 psi. At this point, zero reading was performed on the mortar bars and then they were placed in a 5% $Na_2SO_4$ solution. Further readings were performed at the days specified by ASTM C1012 test method.

#### *3.3.2.8 Drying Shrinkage (ASTM C596)*

Drying shrinkage of mortars bars were measured in accordance with ASTM C596. To do the test 3 mortar bars from each mix were cast in a 1"×1"×11.25" prism mold. Samples were kept in a moisture room for 24 h and then were demoulded and placed in saturated lime solution for addition 48 hr. After this period, samples were removed from the solution, their length were measured and then were placed in a drying chamber to rest for the rest of the test period. The temperature and the relative humidity of the chamber were kept at 23°C and 50% respectively. In order to obtain the drying shrinkage percent, length change of the samples were measured periodically at the time spans indicated by ASTM C596.

#### *3.3.2.9 Scanning Electron Microscopy (SEM) and Energy-Dispersive X-Ray Spectral Analysis (EDX)*

In this study, the microstructure of the mortar and concrete samples were investigated. Selected specimens were cut using a slow-speed diamond saw and the testing surface was then polished with a resin-bonded diamond discs with grit size ranging from #80 to #2000. A Hitachi TM-3000 SEM in its back-scatter modes was used to take the SEM pictures. Along with this, an energy-dispersive X-ray (EDX) analysis was used to identify the chemical composition of the testing samples.

#### *3.3.2.10 Compressive strength (ASTM C39)*

Compressive strength of the concrete samples were measured in accordance with (ASTM C39).

For this mean 4” by 8” concrete cylinders were casted for each of the mixture GGF containing, and control mixtures. The specimens then were tested at 7, 28 and 56 days to obtain the compressive strength of each mix. The proportion of each mix is given in section 3.2.1.

### *3.3.2.11 Tensile strength (ASTM C496)*

For each mixture, tensile strength of 4” by 8” concrete cylinders were measured at 7, 28 and 56 days samples. Each sample was placed horizontally in the test machine (Figure 3-6 a) and tested with the load rate of 100-200 psi/min. As indicated by ASTM C496, two bearing bars were used in the top and bottom of the specimens to direct the load in a correct direction leading to tensile failure. A view of a broken sample after this test is shown in Figure 3-6 b.

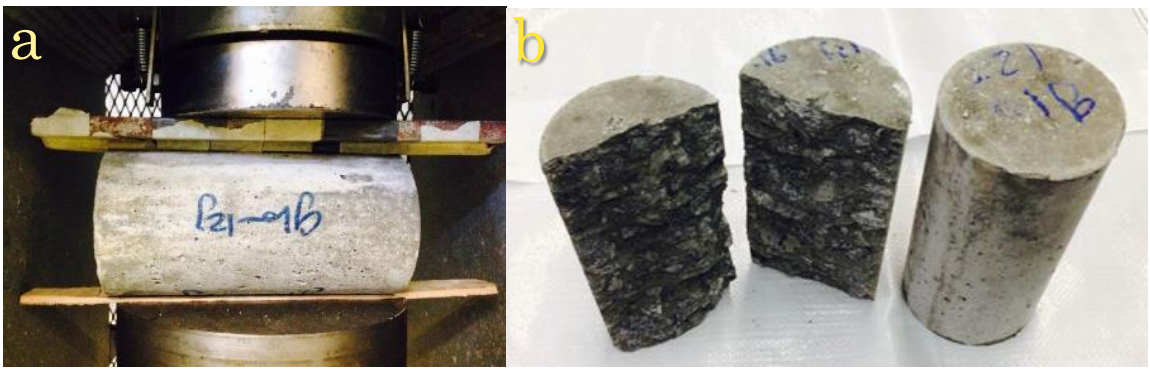


Figure 3-6. A view of tensile strength test a) under load in universal testing machine b) after the test

### *3.3.2.12 Modulus of elasticity (ASTM C469)*

The static modulus of elasticity (MOE) of the 28 days old specimens was determined using 4” by 8” cylinders and the test method presented in ASTM C469. Before starting the test, three samples of same age form the testing mixture were tested for their compressive strength (ASTM C39). Then the samples to be tested for (MOE) would be placed in a compressometer cage equipped with a dial gauge as shown in Figure 3-7. In order to calibrate the system, specimen were loaded twice before the actual loading was taken. Lastly, the spacemen was stressed to a stress equal to 40% of the averaged compressive strength of the samples that had tested earlier. The reading of

the gauge was recorded at this load and the MOE of each samples was calculated using the equation presented in ASTM C469.

Figure 3-7. View of sample in compressometer cage to measure the MOE

#### *3.3.2.13 Rapid chloride permeability test (RCPT-ASTM C1202)*

Rapid Chloride permeability test (RCPT) was performed on all concrete the mixtures (as presented in section 3-2). For the purpose of this test 4" by 8" concrete cylinders were cast and tested at 7, 28 and 56 days. According to the ASTM C1202, RCPT samples were cut in 2" discs, which then placed in a cell containing 3% $NaCl$ solution in one end and 0.3N $NaOH$ in the other end. Each cell were subjected to 60 V dc potential difference and the passing current were recorded for 6 hr. A view of the set-up of the test is presented in Figure 3-8.


Figure 3-8. View of the RCPT set-up

### *3.3.3 Tests for geopolymer*

In this section, the tests methods that were used exclusively for the geopolymer studies are presented. While other test methods that were used for geopolymer studies were as same as those that presented in section 3.3.2.1, they are not repeated in this section. It should be noted that in absence of any standard test methods for the geopolymer materials, the methods used in this phase were either originally developed, adopted from exciting literatures, or developed by alerting the existing standard test methods that are used for the Portland cement concrete.

#### *3.3.3.1 Extent of dissolution (source materials)*

As it was reviewed in the chapter 2 (literature review), solubility of source materials of geopolymer can affect the characteristic of the final material. In this study, solubility of raw material in high alkali media was determined by mixing 5g of each source material in 100ml of 5N NaOH solution. Solutions were mixed for 2 hr. at ambient temperature using a magnetic stirrer. The solution was filtered using micro fiber filters and then diluted to 1:100 using deionized water. Inductively coupled plasma (ICP) test was performed to analyze the filtered solution. The concentration of soluble Si, Al, Ca were measured for the diluted solution. The results were then back-calculated for the original concentration of the dissolved elements in the 5N NaOH solution.

#### 3.3.3.2 *Dissolution of Geopolymer Paste in HCl Acid*

To find the amount of unreacted GGF particles in the GGF-based geopolymer, dissolution of paste samples in an HCl solution was measured in this study. The HCl solution has been reported to dissolve the geopolymerisation products, while leaving the unreacted precursor's particles behind (1, 2). In this study, following Palomo et al. (1), dissolution of selected GGF-based paste samples were studied in a 1:20 HCl solution (i.e. 50 ml of 1N HCl solution in 1000 ml water). Geopolymer paste was crushed to a fine powder and the portion passing sieve #100 and retaining #200 sieved was collected for the test. To perform the test, 2 g of the paste powder was introduced into a 500 ml of the HCl solution. The solution was mixed for 3 h using a magnetic stirrer, and then was filtered using a 1.5 µm filter paper. Finally, the residue solids was collected, dried at 110$^{o}$C for 24 hours, and their dried weight was measured and recorded.

#### 3.3.3.3 *Solubility of geopolymer paste in water:*

To study the presence of any water-soluble phases in the GGF-based geopolymer pastes, the solubility of crushed pate in deionized water was examined. For this purpose, the 7-day old GGF-based geopolymer paste samples were mechanically crushed (using a hammer) and sieved. The portion that passed sieve #50 and retained on the sieve #100 was collected and dissolved in 100 ml of deionized water. A magnetic stirrer was used for this purpose; and each solution was mixed for 2 hours. Subsequently, the solutions were filtered using a micro-fiber filter (Whatman Grade 934-AH Glass Micro Fiber Filter), and ICP test was conducted on each filtered solution to measure the concentration of dissolved Si and Al in each solution.

#### 3.3.3.4 *Alkali silica reaction*

In this study the alkali silica reaction of geopolymer mortars were studied using different type of crushed aggregates. These crushed aggregates include New-Mexico, Spratt, Adairsville and glass

from waste bottles. Although, the overall procedure that was taken for this test was as same as the one that is presented in section 3.3.2.4; the temperature of curing was different for geopolymer samples and they were cured at 60°C for the first 24 hr.

In addition, to eliminate the effect of alkali solution, which can promote the hardening procedure of geopolymer paste, selected samples were tested in a 100% relative humidity and 80°C. For this purpose, enough amount of water was putt in the bottom of a sealed box and specimens were placed on supports in a manner that they have no contact with the water (almost 0.5 inch clearance). The box was then closed and placed in an 80°C oven for the remaining test period.

#### *3.3.3.5 Sulfate attack*

Formation of expansive Ettringite and gypsum are known to be the main mechanisms responsible for sulfate attack related damages in Portland cement-based concretes. Therefore, one of the common test methods for evaluation of the sulfate attack related damages is to monitor their length expansion as presented in section 3.3.2.7. However, in the case of geopolymer, the mechanism of sulfate attack is known to be different and is related to the dissolution of alkalis from the geopolymer paste into the sulfate solution (which might not be expansive). As a results, the expansion measurement might not be the best way to monitor the sulfate attack related damages.

In this study, therefore, the residual compressive strength and weight change of samples were measured to evaluate the resistance of geopolymer mortar samples against the sulfate attack. Mortar cubes with $50 \times 50 \times 50$ mm dimensions were cast and cured in accordant to section 3.1. Samples were removed from their molds after 24 h and kept at the ambient temperature for two additional days. After 3 days from the casting, all the samples were immersed in a 5% $Na_2SO_4$ solution and weight change, and compressive strength were measured at 7, 28, 56 and 120 days

after submerging. The old solutions were replaced by a new solution at 7, 14, 21, 28 and 56 days. View of the geopolymer mortar specimens in the 5% sodium sulfate solution is presented in Figure 3-9.

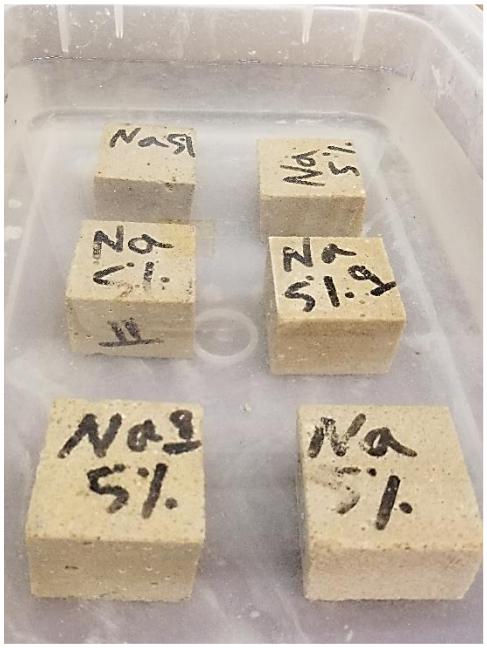

Figure 3-9. GGF-based geopolymer mortar cubes in a 5% sodium sulfate solution

### *3.3.3.6 Dissolution of geopolymer powder sample in sodium sulfate and magnesium sulfate solutions*

As it was reviewed in the chapter 2 (literature review), the main mechanism responsible for the sulfate attack of geopolymer samples is the dissolution of alkalis into the sulfate rich solution. In this research, to study the effect of dissolution of the other elements in a sulfate solution, selected geopolymer paste samples from each source material (i.e. GGF, fly ash and glass-powder based geopolymer) were tested. In this test, the paste samples were crushed mechanically (using a hammer) in to small powder and the portion that passes #100 and retains on #200 was collected. Five grams of this portion was then dissolved in 100 ml of a sulfate solution (5% $Na_2SO_4$ or $MgSO_4$) and kept in a sealed bottle. For each of the geopolymer specimens 6 samples were

prepared by the above-mentioned method. Each bottle was shacked vigorously for almost 1 minutes and then left in ambient temperature. The samples were shacked regularly up to the test date (i.e. 3, 7, 14, 28 and 56 days).

At the test day, each solution was filtered using a micro fiber filter. The filtered solution was collected for pH measurements and also ICP test to measure the amount of selected elements (i.e. Si, Al, Ca, Na, K, Fe etc.). The solid part of each sample was also collected, washed with 100 ml of desalted water and was allowed to dry in a drying shrinkage chamber at 23°C and 50% relative humidity to lose its water. When the samples was dry, it was gathered and sealed. Selected samples were sent for XRD test to check for the formation of gypsum and Ettringite. The view of the step of the test is presented in Figure 3-10.

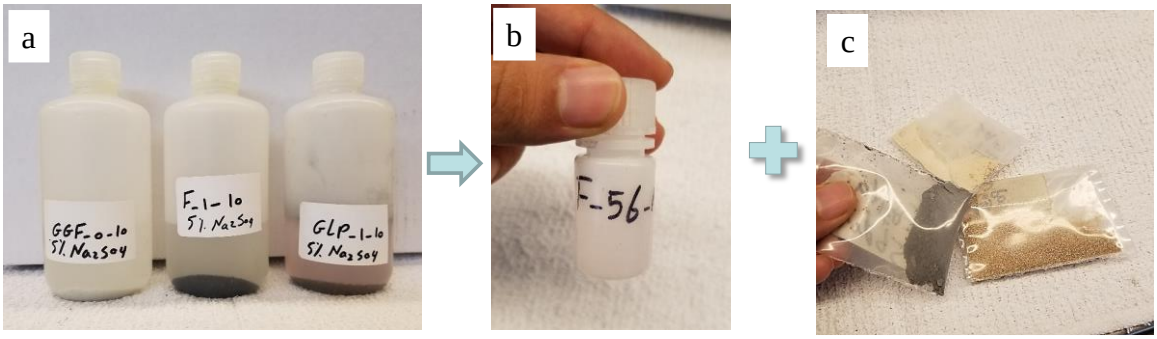


Figure 3-10. Dissolution of geopolymer powder sample in sulfate-rich solutions. a) The bottles containing crushed paste and the sulfate solution; b) filtered solution, c) filtered solids.

It should be noted that the 23°C temperature (for drying) was selected to avoid the decomposition of any gypsum or Ettringite that might have been possibly formed in the samples.

### *3.3.3.7 Drying shrinkage*

To study the drying shrinkage behavior of geopolymer samples, mortar bars with 25×25×254 mm dimensions were cast for each of the different source materials. Upon the casting, all samples were placed in sealed boxes and cured for 24 h at 60°C. The mold removed after 24 h curing, and the specimens placed in a chamber with 23°C and 50% RH. After specimens cooled to the

chamber temperature (almost 30 minutes), the reference reading was done, and they returned to the chamber and kept until the next testing dates. Length change of samples monitored up to 120 days at selected intervals.

#### *3.3.3.8 Rapid Chloride permeability test (RCPT)*

Rapid Chloride permeability test (RCPT) was performed on GGF and fly ash-based mortar samples (as presented in section 3.2.3.13). For the purpose of this test 4" by 8" concrete cylinders were cast and tested at 7, 28 and 56 days in Accordance to the ASTM C1202. For the comparison purposes the results were compared with two control portland cement-based mortar mixtures that had been cured in different condition. The specimens from the first control mixture, referred as Ctrl-23°C, were cured in the standard curing room (23°C and ~100 RH) and stayed there up to the test day. On the other hand the specimens of the second control mixtures, referred as Ctrl-60°C, were cured in a 60°C oven for 24 h, and then left in the ambient condition up to the test day.

#### *3.3.3.9 Chloride penetration test*

In order to evaluate the resistivity of geopolymer mortar samples against the Chloride ions penetration, the Chloride penetration test was performed on the two-inch geopolymer mortar discs. For the purpose of this test, discs were prepared by cutting two-inch discs from 4 by 8-inch mortar cylinders (three discs from each cylinder). The cut samples were sealed using a silicon glue, and a 10% NaCl solution was pounded on top of each disc. The samples would go through a 15-day long wet and dry cycles, and the Chloride penetration would be measured at the end each wetting and drying cycle (1 month). To do the wetting process the NaCl solution would be renewed for all the remaining samples. At the test day, two samples from each mixture were selected, crushed mechanically (using the compressive strength machine), and the depth of Chloride penetration was identified by spraying a silver ammonia solution on the cut surface of

the samples, and measuring the thickness of the bright colored sections.

# CHAPTER 4

# PROPERTIES AND PERFORMANCE OF GROUND GLASS FIBER AS A POZZOLAN IN PORTLAND CEMENT CONCRETE RESULTS ON UTILIZATION OF GGF AS A SCM[1]

## 4.1 Introduction

The use of waste glass, typically obtained from recycling of container glass, in Portland cement concrete has been widely investigated, both as a crushed granular aggregate material as well as in a finely ground form as a cement replacement material. However, glass waste derived from other waste forms such as window panes, fiber glass, abrasive material, etc. has not widely been investigated in Portland cement concrete. In particular, large volumes of glass fiber waste are produced due to strict requirements in the quality of the glass fiber. Also, the stringent chemical requirements of glass fiber production make it difficult to recycle the glass fiber back into production. As a result, significant quantities of glass fibers are disposed in landfills annually around the country.

Typically, crushed glass aggregates produced from soda-lime glass (often used in the production of container glass) are susceptible to a deleterious chemical reaction - alkali-silica reaction, in the presence of a highly alkaline portland cement paste. The extent of ASR with soda-lime glass inclusions in concrete is a function of the particle size of the glass and its chemical composition. In recent studies by Afshinnia and Rangaraju (1), it was found that even though the intensity of the deleterious ASR decreases with a decrease in the particle size of the soda-lime

[1] Rangaraju, H. Rashidian-Dezfouli, G. Nameni and G. Q. Amekuedi (2016). International Concrete Sustainability Conference

glass used in concrete, the high-alkali content of the soda-lime glass, typically 12% to 15% $Na_2O$, makes it virtually impossible to completely eliminate or mitigate ASR in concrete containing soda-lime glass, particularly in the long-term (1).

Although, glass fibers vary significantly in their chemical composition, depending on the specific purpose for which they are produced, bulk of the glass fiber is generally very low in its alkali content. Particular, a variety of glass fiber known as E-glass, which is widely produced and whose waste streams are largely disposed in landfills, contains very low level of alkali in its composition. From its chemical composition standpoint, E-glass is significantly superior glass for consideration as a pozzolanic material than the soda-lime glass. However, not much work has been conducted in the past and no significant literature is available to assess its value and use in concrete as a cement replacement material. In this study, a comprehensive investigation was conducted to study the role of processed glass fiber as a cement replacement material and its impact on a number of properties associated with cementitious pastes, mortar and concrete mixtures. This papers presents findings from this comprehensive study.

## 4.2 Materials, Mixture Proportions and Test Methods

**Materials.** In this study, a Type I/II Ordinary Portland Cement (OPC) meeting ASTM C150 specification was used, along with a finely powdered glass fiber, referred to as Ground Glass Fiber (GGF) and a Class F fly ash from a local source as pozzolans. The GGF was prepared by milling the off-spec glass fiber in a ball mill to a fine powder with an average particle size of 4 microns. The physical properties and the chemical composition of the cementitious materials are given in Tables 4-1 and 4-2. In addition, the X-ray diffraction (XRD) pattern of GGF and the Class F fly ash are presented in Figure 4-1.

Also, in this study a non-reactive siliceous river sand with an absorption value of 0.30% and an oven-dry specific gravity of 2.67 was used in preparing the mortar and concrete mixtures.

In studies pertaining to ASR, a highly reactive rhyolitic aggregate, Las Placitas gravel from New Mexico (NM) was used that had an absorption of 1.10% and an oven-dry specific gravity of 2.60. Although the NM aggregate was obtained as a coarse aggregate and used as such in concrete mixtures, a crushed form of this aggregate was used in mortar mixtures as a reactive fine aggregate in mortar bar tests.

Table 4-1. Basic properties of the cementitous materials

| Material | Specific Gravity | Amount Passing #325 Sieve (%) | Blaine's fineness ($cm^2/g$) | Loss On Ignition (LOI) |
|---|---|---|---|---|
| Cement | 3.15 | 98% | 4720 | 2.6% |
| GGF | 2.6 | 96% | 10200 | 1.0% |
| Fly ash | 2.25 | 76% | 6040 | 2.3% |

Table 4-2. Chemical composition of the cementitous materials

| | $SiO_2$ | $CaO$ | $Al_2O_3$ | $Fe_2O_3$ | $MgO$ | $Na_2O$ | $K_2O$ |
|---|---|---|---|---|---|---|---|
| Cement (%) | 19.93 | 62.27 | 4.77 | 3.13 | 2.7 | 0.06 | 0.48 |
| GGF (%) | 47.72 | 19.62 | 10.36 | 0.34 | 2.27 | 0.67 | 0.1 |
| Class F Fly Ash (%) | 50.7 | 3.3 | 25.1 | 12.5 | 1.1 | 0.51 | 2.27 |

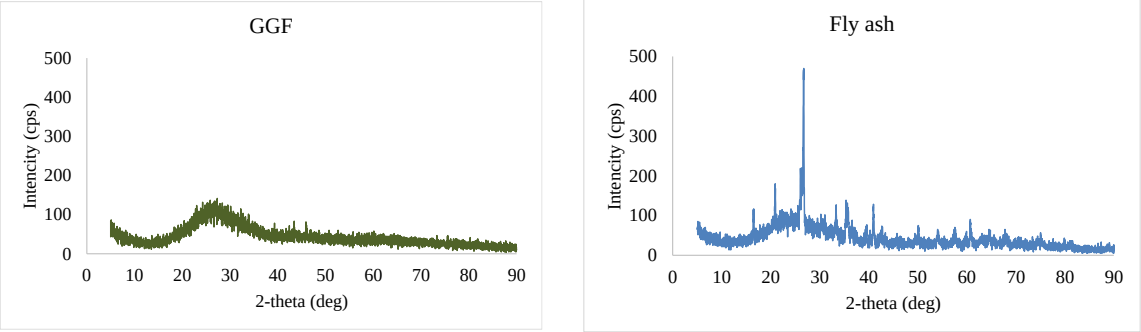


Figure 4-1. XRD results of GGF (left) and fly ash (right)

**Mixture Proportions.** In this study a total of 5 different cementitious blends were evaluated. Of the five mixtures, two mixtures – CTRL-1 and CTRL-2, were included as reference mixtures against which the performance of mixtures containing GGF as a partial cement replacement was evaluated. The first control mixture (CTRL-1) consisted of 100% Portland

cement, while the second control mixture (CTRL-2) consisted of binary blend of 75% Portland cement with 25% Class F fly ash, by mass. In this study, GGF was employed as a cement replacement material at selected dosage levels of 10, 20 and 30% by mass of cement. Table 4-3 shows the mix-ID and composition of the binder portion of the above-mentioned mixtures.

**Test Methods.** The following test procedures were conducted on either mortar or concrete mixtures containing each of the five blends of cementitious materials identified in Table 4-3.

Table 4-3. Mixture ID and their binder composition

| Mix ID | Mixture Composition |
|---|---|
| CTRL-1 | 100% Cement |
| CTRL-2 | 75% Cement+ 25% Fly ash |
| GGF-10 | 90% Type I Cement+ 10% GGF |
| GGF-20 | 80% Type I Cement + 20% GGF |
| GGF-30 | 70% Type I Cement + 30% GGF |

***Flow test (ASTM C1437).*** In this test, the effect of GGF, as a cement replacement material, on the workability of each mixture was examined using the flow test according to ASTM C1437 test procedure. The flow behavior of mixtures containing GGF was compared with the flow values obtained for CTRL-1 and CTRL-2 mixtures. Considering the specific surface area of GGF is more than twice that of the Portland cement (see Table 4-1), it can be anticipated that the flow behavior of mixtures containing GGF can be significantly different from that of the control mixtures. Also, with progressively increasing replacement levels of cement with GGF, the flow behavior of mixtures containing GGF can be expected to follow a trend.

***Strength activity index (ASTM C311).*** The pozzolanic reactivity of GGF was examined by evaluating the strength activity index of the mixtures containing GGF as a cement replacement material using the ASTM C311 test procedure. In this test, 50 mm x 50 mm x 50 mm (2 in. x 2 in. x 2 in.) mortar cubes were cast for each mix design and the compressive strength of each mixture

was evaluated at 7 and 28 days of curing.

***Accelerated Mortar Bar Test (ASTM C1260 and ASTM C1567).*** To evaluate the ASR mitigation effectiveness of GGF, Accelerated Mortar Bar Test (AMBT) was conducted using crushed NM aggregate as a reactive fine aggregate. For CTRL-1 mixture, where no pozzolan was used, AMBT based on ASTM C1260 test procedure was conducted to serve as a reference. For all the other mixtures containing a pozzolan, AMBT based on ASTM C1567 test procedure was conducted. In this study, mortar bars with dimensions of $25 \times 25 \times 285mm$ ($1" \times 1" \times 11.25"$) were cast and cured for the initial 24 hours in a standard curing room. The mortar bars were demolded after 24 hours and transferred into a water bath that was gradually heated to 80°C (176°F) and cured for an additional 24 hours. Finally, the mortar bars samples were removed from the water bath and the zero-day reading was taken for each bar. The bars then were immersed in a 1N NaOH solution that was preheated to 80°C (176°F). The test was conducted up to 28 days and the length change in the mortar bars was recorded at selected time intervals to track the expansion.

***Miniature Concrete Prism Test (AASHTO T110-14).*** In addition to AMBT, Miniature Concrete Prism Test (MCPT), based on AASHTO TP-110, was performed on concrete prism specimens for all the mixtures. Unlike the mortar samples used in AMBT, this procedure is conducted on concrete prisms. As per the test procedure, the cement content of the concrete mixtures is maintained at 420 kg/m$^3$ (708 lb/yd$^3$) and a water-to-cementitious materials ratio of 0.45 is used. In addition, the volume fraction of the dry-rodded coarse aggregate per unit volume in the concrete is fixed at 0.65. The coarse aggregate gradation calls for 57.5% of material that is passing 12.5 mm (1/2 in.) sieve and retained on 9.5 mm sieve (3/8 in.), and 42.5% of material that is passing 9.5 mm sieve (3/8 in.) and retained on 4.75 mm (No. 4) sieve. A non-reactive fine aggregate is used when a reactive coarse aggregate is evaluated in this study.

In preparing the concrete prisms for the MCPT, when the cement alkali content is less than 1.25% $Na_2O_{eq.,}$ the alkali content of the concrete is boosted to 1.25% by weight of the cement by adding NaOH to the mix water. When evaluating supplementary cementitious materials (SCMs) in this test, the alkali content of the concrete is boosted to 1.25% only by the mass of the portland cement, and the SCMs are not considered in this calculation.

In this test, concrete prisms of 50 mm x 50 mm x 285 mm (2 in. x 2 in. x 11.25 in.) are used as test specimens. After demolding the concrete specimens after 24 hours of curing in a standard curing room, they are submerged in a sealed water bath and stored in a 60°C (140°F) chamber for another 24-hours period. Finally, the prisms are removed from the water bath and the zero-day reading is taken. The prisms are subsequently submerged in a 1N NaOH solution that has been preheated to 60°C (140°F). The prisms are kept in a 60°C (140°F) chamber for the remainder of the test duration and their length-change is monitored up to 84 days by taking periodic measurement at selected intervals. An expansion of 0.040% or greater at 56 days is typically considered as indicative of an aggregate that is alkali-silica reactive. When evaluating the effectiveness of SCMs in this test method, a dosage of SCM that limits the expansion of concrete prisms to 0.020% or less at 56 days is considered to represent an effective SCM performance in mitigating ASR distress.

***Scanning Electron Microscope (SEM).*** In this study, the microstructure of the mortar samples subjected to AMBT was investigated to ascertain the location and the nature of the reaction products and evaluate the effectiveness of GGF in mitigating ASR. The 28-day old mortar bar specimens were cut using a slow-speed diamond saw and the testing surface was then polished with a resin-bonded diamond discs with grit size ranging from #80 to #2000. A Hitachi-3000 SEM was used in this study using a back-scatter detector along with energy-dispersive X-ray analysis capability to identify the chemical composition. This test was conducted on selected

mortar specimens, including CTRL-1, CTRL-2 and GGF-30.

## 4.3 Results and Discussion

**Flow Test.** Table 4-4 shows the flow results of all the mortar mixtures used in this study. As it can be seen in this table, replacement of cement with GGF increases the flow of the fresh mortar mixtures in comparison with the CTRL-1 mixture, and is almost equal to that of CTRL-2 mixture. However, the observation showed that the increase in the flow is not linearly related with the increase in the replacement level of GGF. While GGF-10 showed 97% flow, further replacement of cement with GGF didn't lead to significant change in the flow results.

Table 4-4. Flow results of fresh mortar mixtures

| Mix ID | CTRL-1 | CTRL-2 | GGF-10 | GGF-20 | GGF-30 |
|---|---|---|---|---|---|
| Flow (%) | 88 | 100 | 97 | 94 | 103 |

The increase in the flow in mixtures containing GGF can be attributed to the following parameters:

1. Generally SCMs are not as reactive as cement at very early ages and leave more water to act as a lubricant in the system.
2. SEM observation revealed a very smooth surface on GGF particles, which could lead to lower water absorption and hence better flow.
3. High negative z-potential of the GGF particles (2) can assist the flow as GGF particles repelling each other.

**Strength Activity Index.** To investigate the pozzolanic properties of the GGF, 50 mm x 50 mm x 50 mm (2 in. x 2 in. x 2 in.) mortar cubes were cast in accordance with ASTM C311. The samples were tested for their compressive strength after 7 and 28 days. The results of compressive strength and strength activity index (SAI) are presented in Table 4-5. As it can be seen in this table, the GGF-20 mixture showed the SAI values of 104% and 110% after 7 and 28

days, respectively. Since these values are higher than 75%, the GGF is considered as a pozzolanic material (ASTM C618). Moreover, as the results revealed, the SAI value of all GGF containing mixtures showed higher values than CTRL-2 mixture at both 7 and 28 days.

The better performance of the GGF containing mixtures in comparison to fly ash containing mixture (CTRL-2) could be attributed to the fact that GGF particles are much finer ($4\mu m$) in comparison to fly ash ($28\mu m$) and can get engaged in the pozzolanic reaction faster. Furthermore, the results of XRD test revealed that the structure of GGF powder is very amorphous. This amorphous structure accelerates the pozzolanic reaction by allowing silica ions to be released faster in the mixture and form the C-S-H gel. As a result of the pozzolanic reaction all the GGF containing mixtures have surpassed the compressive strength of the CTRL-1 mixture after 28 days (see Table 4-5).

Table 4-5. Compressive strength and Strength Activity Index of mortar cubes for 7 and 28 days

| Age (days) | | CTRL-1 | CTRL-2 | GGF-10 | GGF-20 | GGF-30 |
|---|---|---|---|---|---|---|
| 7 | Compressive strength MPa (psi) | 42.2 (6125) | 34.3 (4970) | 37.5 (5445) | 43.9 (6365) | 41 (5945) |
| | SAI | 100 | 81 | 89 | 104 | 97 |
| 28 | Compressive strength MPa (psi) | 54.1 (7850) | 48.3 (7010) | 55.7 (8080) | 59.9 (8685) | 57.5 (8340) |
| | SAI | 100 | 89 | 103 | 110 | 106 |

**Resistance against ASR.** In order to evaluate the effect of GGF in the mitigation of ASR, two different test methods were followed in this research. The first method is the Accelerated Mortar Bar Test (ASTM C1260 and ASTM C1567), which was performed on the mortar mixtures and the second method is the Miniature Concrete Prism Test (AASHTO TP-110) which was performed on concrete prisms. In this section, the test results of each method are presented separately, and then a discussion of results from both the test methods is presented.

**a. Accelerated Mortar Bar Test (AMBT).** The accelerated mortar bar test was carried

out in accordance with ASTM C1260 and ASTM C1567 to investigate the performance of GGF containing mixtures against the alkali silica reaction. The expansion of the mortar bars was measured up to 28 days and the results are presented in Figure 4-2. As it can be seen in this figure, CTRL-1 mortar bars showed a significant expansion of 0.81% at 14 days, which is far above the 0.10% limit for an aggregate to be considered as reactive. The CTRL-1 mortar bars showed continued expansion through the rest of the test period, and further measurements showed the expansion of 1.15% after 28 days. In the case of GGF-10 mixture, although the mortar bars showed significant expansion, above the 0.10% limit, a significant reduction in expansion can also be seen when compared to the unmitigated control mixture, CTRL-1. The expansion of GGF-10 mixture was found to be 0.43% and 0.75% for 14 and 28 days respectively.

At the other GGF replacement levels, GGF-20 and GGF-30 showed a better performance in comparison to the CTRL-1 and CTRL-2 mixtures. The results showed a significant decrease in the expansion of mortar bars, as GGF-20 and GGF-30 mixtures succeeded to keep the expansion to below 0.10% limit at 14 days and only reached 0.04% and 0.02%, respectively. However, the 28-day expansion indicated the superior performance of GGF-30 mixture in terms of the expansion mitigation compared to other GGF mixtures. As it can be seen after 28 days of submersion, the GGF-30 mixture expansion reached 0.05% which is still lower than the 0.10% limit.

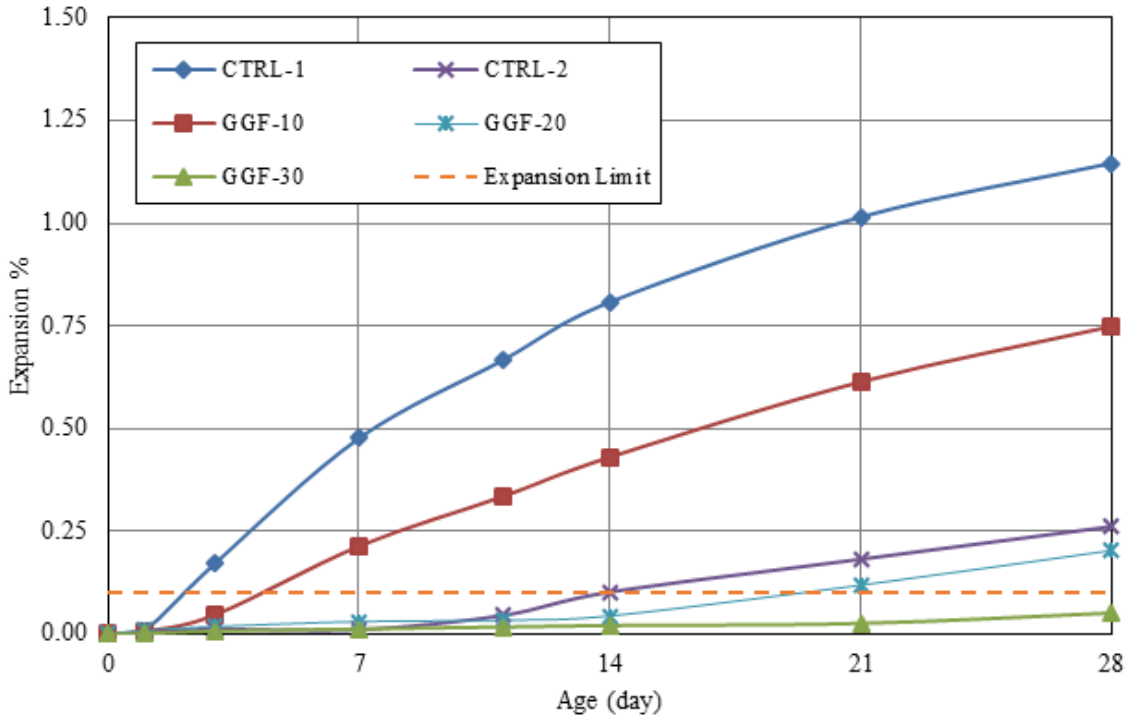


Figure 4-2. Expansion curve of the mortar bras (AMBT)

After 28 days of exposure to alkali hydroxide solution, the mortar bar specimens were removed from the 1N NaOH solution, and a visual observation was conducted to document any significant damage in the specimens. The appearances of the mortar bars after 28 days are presented in Figure 4-3. As presented in Figure 4-3a, the CTRL-1 mixtures showed severe cracks due to the ASR expansion while smaller cracks were seen on GGF-10 mortar. However, as presented in Figure 4-3c and Figure 4-3d, the visual examination of GGF-20 and GGF-30 bars did not show any signs of damage or cracks.

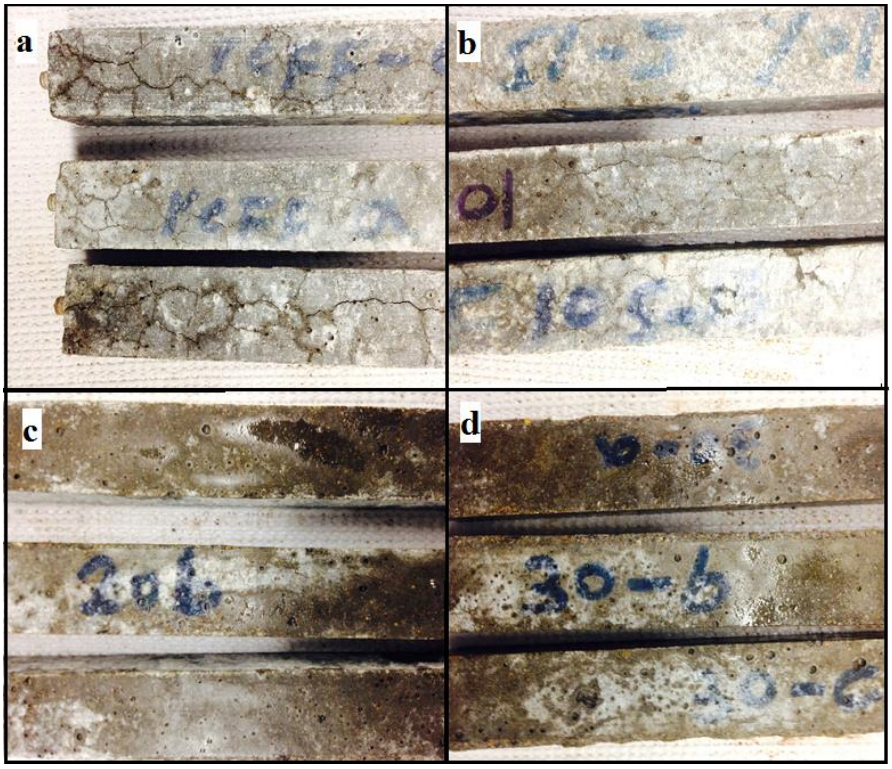


Figure 4-3. Visual appurtenance of mortar bars after 28 days

In addition to the visual observation, SEM images of the polished samples showed the effect of GGF in reducing ASR damage. The SEM pictures of CTRL-1, CTRL-2 and GGF-30 are presented in Figure 4-4. As it can be seen the severe cracks have been formed in the aggregate of the CTRL-1 samples while no sign of crack is observed in CTRL-2 and GGF-30 samples.

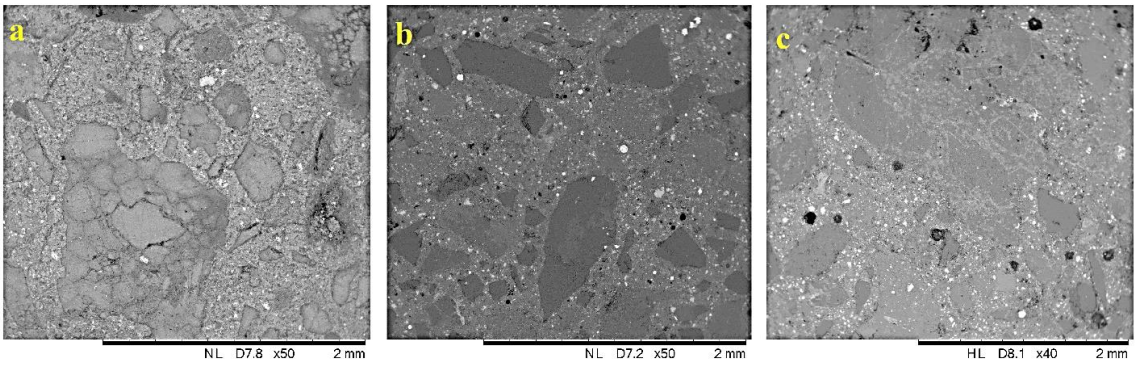


Figure 4-4. SEM observation on polished mortar bars a) CTRL-1 b) CTRL-2 and C) GGF-30 mixtures.

**b. Miniature Concrete Prism Test (MCPT).** The expansion results from the Miniature Concrete prism Test (MCPT) are presented in Figure 4-5. The expansion limit for this test is considered as 0.04% at 56 days. As it can be seen in Figure 4-5, all the mixtures met the expansion limit with the exception of CTRL-1 mixture. In all the GGF containing mixtures, the final expansion at 84 days was less than 0.01%. Although the expansion results from the AMBT showed higher expansion of GGF-10 in compare to other GGF mixtures, the results of MCPT indicated comparable expansion with GGF-20 and GGF-30 samples.

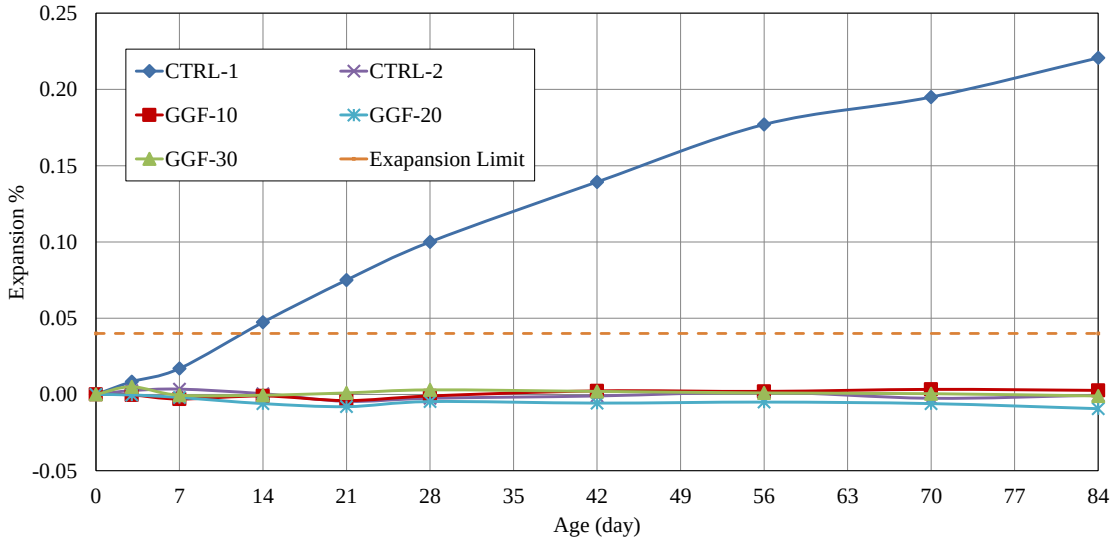


Figure 4-5. Expansion curves of concrete bars (MCPT)

**c. Mitigation mechanism.** The good performance of the GGF containing mixtures in mitigation of ASR-related expansion could be explained due to the following mechanisms:

1) *Reduction in available calcium for newly formed ASR gel*. Calcium hydroxide is one of the main reaction products of the cement hydration, which will eventually react with the ASR gel to calcify the gel. The freshly produced low-viscosity ASR gel is unstable in the presence of calcium and exchanges its alkali with Ca ions to produce hardened (higher viscosity) gel (3). The formation of this hardened ASR gel can induce significant expansion upon sorption of moisture and cause cracks in the vicinity of the reactive aggregates. Addition of reactive silica

in the form of GGF or fly ash will reduce the level of this material through the well know pozzolanic reaction which consumes the free calcium hydroxide. Reduction of calcium hydroxide avoids the easy access of ASR gel to calcium and would reduce the ASR-related damages.

2) *Reduction in Ca/Si ratio*. It is known that C-S-H gels with lower Ca/Si ratios retain more alkali than those with higher Ca/Si ratios (4-6). It is also clear that addition of reactive silica will consume the calcium hydroxide due to the pozzolanic reaction. As a result, introduction of materials such as GGF and fly ash reduces the Ca/Si ratio in the C-S-H gel. The reduction of Ca/Si ratio takes place in two ways. First reaction of silica with the calcium hydroxide and production of secondary C-S-H gel with lower Ca/Si ratio. Second by refining the structure of existing C-S-H gel and formation of a gel with lower Ca/Si ratio.
3) To measure the effect of addition of GGF and fly ash on the Ca/Si ratio, EDX analysis was conducted on CTRL-1, CTRL-2 and GGF-30 samples. The results from the EDX analysis confirmed the reduction of Ca/Si ratio of C-S-H gel in CTRL-2 and GGF-30 samples in comparison to CTRL-1 samples. The measurement of chemical analysis showed the Ca/Si ratio of 1.41, 1.26 and 1.10 for CTRL-1, CTRL-2 and GGF-30, respectively.
4) *Effect of alumina in reducing ASR*. Presence of alumina in SCMs is known to increases their effectiveness against the ASR (7, 8). Two suggested reasons by which alumina plays a role in reduction of ASR damage are, the higher alkali binding of C-A-S-H gel in comparison to C-S-H gel (9) and reduction in the rate of silica dissolution from the reactive aggregates (10).
5) Regardless of the mechanism responsible for the role of alumina, the higher amount of Al was seen in the paste matrix of CTRL-2 and GGF-30 in comparison to the CTRL-1 sample. The EDX results showed the Al atomic weight percent of 3.09%, 6.81% and 7.25% for CTRL-1, CTRL-2 and GGF-30 samples respectively. Despite the XRF results, which showed

a lower amount of Al in GGF in comparison with fly ash, the comparable amount of Al released from GGF and fly ash could be attributed to more amorphous structure of GGF and the easy availability of Al (Figure 4-1).

6) *Reduction in paste permeability*. Both GGF and fly ash introduce a large amount of silica into the binder. The pozzolanic reaction takes place by consuming CH and producing C-S-H gel, thus refining the paste structure and reduce the permeability. Reduction in permeability will lower the amount of available water and therefore, cause less expansion of ASR gel. In this study, although no direct test was performed to measure the permeability but Ca/Si for GGF-30 and CTRL-2 mixtures showed lower values in compare to the CTRL-1 mixture. These results could be related to the consumption of CH and production of C-S-H gel. The newly formed C-S-H gel reduces the permeability by filling the pores in the paste matrix as well as reducing their connectivity.

The better performance of GGF in comparison to fly ash mixture (CTRL-2) could be attributed to the following factors. Firstly, the more amorphous structure of GGF accelerates the pozzolanic reaction. This leads to early strength gain and also reduction in permeability by refining the paste structure in its earlier ages. As SAI index results show (Table 4-5) in all the mixtures containing GGF, SAI is higher than the SAI of CTRL-1 mixture at both 7 and 28 days. This indicates the faster reaction of GGF in comparison with fly ash. Secondly, the GGF powder used in this study had a finer particle size (of 4$\mu$m) compared to the fly ash (of 28$\mu$m) which also leads to better refinement of the paste structure.

Finally, presence of higher alumina content as well as lower Ca/Si ratio in the reaction product of GGF containing mixtures assists the better ASR mitigation. According to the results of Hong and Glasser (9), presence of alumina is more effective in binding alkali in the paste with lower Ca/Si ratios. Thus, it could be assumed that the C-A-S-H gel in GGF retains more alkali

since it has a lower Ca/Si ratio in compare with the fly ash mixture.

## 4.4 Conclusion

Based on the results of this study, following conclusions can be drawn:

1) Addition of GGF improved the workability of the fresh mortar mixtures at all levels of cement replacement.
2) GGF used in this study showed a clear pozzolanic behavior as evidenced by the SAI results. The SAI results revealed the faster strength gain in mixtures containing GGF in comparison to the mixture having fly ash as the cement replacement.
3) Addition of GGF showed a significant decrease in ASR related expansion in both mortar and concrete test specimens. The effectiveness of GGF in reducing ASR-induced expansion increased with the increase in the dosage of GGF from 10% to 30% mass replacement of cement.
4) The better performance of GGF in comparison to fly ash can be attributed to its more amorphous structure and its finer particle size. In addition, presence of higher amount of Al and lower Ca/Si ratio in the reaction products of GGF mixtures assists the ability of GGF containing mixture to retain more alkali in the paste matrix compared to mixture containing fly ash.

## References


1. Afshinnia, K. and Rangaraju, P.R. 2015. Effectiveness of Ground Glass Powder From Recycled Glass In Mitigating Alkali-Silica Reaction In Concrete, Transportation Research Record: The Journal of Transportation Research Board, Concrete Materials, Vol. 2508, p. 11.
2. Bismarck, A., Boccaccini, A.R., Egia-Ajuriagojeaskoa, E., Hülsenberg, D. and Leutbecher, T., 2004. Surface characterization of glass fibers made from silicate waste: Zeta-potential and contact angle measurements. Journal of materials science, 39(2), pp.401-412.

3. Taylor, H.F.W., Cement Chemistry, Academic Press, London, 1990.
4. Muhammad, S.B., 1985. Mechanism of pozzolanic reactions and control of alkali-aggregate expansion. Cement, concrete and aggregates, 7(2), pp.69-77.
5. Stade, H., 1989. On the reaction of CSH (di, poly) with alkali hydroxides. Cement and Concrete Research, 19(5), pp.802-810.
6. Hong, S.Y. and Glasser, F.P., 1999. Alkali binding in cement pastes: Part I. The CSH phase. Cement and Concrete Research, 29(12), pp.1893-1903.
7. Duchesne, J. and Bérubé, M.A., 2001. Long-term effectiveness of supplementary cementing materials against alkali–silica reaction. Cement and concrete research, 31(7), pp.1057-1063.
8. Ramlochan, T., Thomas, M.D.A. and Hooton, R.D., 2004. The effect of pozzolans and slag on the expansion of mortars cured at elevated temperature: Part II: Microstructural and microchemical investigations. Cement and Concrete Research, 34(8), pp.1341-1356.
9. Hong, S.Y. and Glasser, F.P., 2002. Alkali sorption by CSH and CASH gels: Part II. Role of alumina. Cement and Concrete Research, 32(7), pp.1101-1111.
10. Chappex, T. and Scrivener, K.L., 2012. The influence of aluminium on the dissolution of amorphous silica and its relation to alkali silica reaction. Cement and Concrete Research, 42(12), pp.1645-1649.

# CHAPTER 5

# ROLE OF GROUND GLASS FIBER AS A SCM IN IMPROVING SELECTED PROPERTIES OF PORTLAND CEMENT CONCRETE[1]

## 5.1 Introduction:

Utilization of ground glass powder, typically obtained from processing of recycled glass containers made of soda-lime glass, as an SCM has been the subject of many studies (1-4). Due to the high amount of alkali present in these glass powders, susceptibility of concrete mixtures containing glass-derived pozzolans to Alkali-Silica Reaction (ASR) has been always a big concern. On the other hand, ground glass fiber (GGF), a pozzolan derived from finely grinding fiber glass (commonly referred to as E-glass) that has very low alkali content. Due to its chemical composition, GGF can potentially serve as a valuable pozzolan without the negative effects often associated with the use of high-alkali glass powders such as soda-lime glass, particularly in reducing the risk of ASR in the concrete mixtures.

Presence of reactive silica is essential for any supplementary cementitious material (SCM) to cause the pozzolanic reaction. Although like other SCMs, GGF has high enough combined silica, iron and aluminum oxide (S+A+F) content (i.e. > 50%) and can serve as a good pozzolan, unlike other SCMs such as fly ash, GGF is an engineered material which is produced in a controlled environment. This results in a uniform chemical composition of the material which lends itself to a consistent quality SCM for use in concrete.

Utilization of GGF as an SCM in concrete construction is a relatively new concept and unlike the conventional SCMs like fly ash, slag, meta-kaolin and silica fume, which are known to

[1] - Rashidian-Dezfouli, H., & Rangaraju, P. R. (in press). Role of Ground Glass Fiber as A SCM in Improving Selected Properties of Portland Cement Concrete (No. 17-04237).

be used for several decades, the first use of this material as pozzolan was patented in 2004 by Hemmings et al (5). According to a report by the US Department of Energy in 2005, the total amount of waste glass fiber in United States that ends up in landfills was about 250,000 tons per year, which can be reclaimed for beneficial uses. This amount can be further increased to 500,000 tons/year if the waste streams from the users of glass fibers are also considered (6).

Past studies on the utilization of waste glass fiber as a SCM, have shown the advantages of using this material in improving some fresh and hardened properties of mortar and concrete mixtures. Chen et al. (7), investigated the utilization of E-glass particles in concrete mixtures. It was seen that the replacement of E-glass as cementitious material, up to 40% by mass of the cement showed pozzolanic reactivity. Furthermore, it was observed that the addition of E-glass as a cement replacement improved durability characteristics of concrete such as resistance against sulfate attack and chloride penetration. Hossein et al. (8), studied the fresh and hardened properties of the concrete mixture containing glass fiber particles. It was reported that utilization of this material as a cement replacement increased the workability of the fresh concrete mixtures (higher slump), increased the plastic shrinkage and also reduced chloride ion permeability.

A few studies have been performed on the hydration mechanism of the mixtures having glass fiber as a cement replacement. A comprehensive study on the pozzolanic properties of milled glass fiber was performed by Neithalath et al. (9). It was reported that although the glass fiber powder did not show any cementitious properties, it had a significant pozzolanic effect. In addition, it was seen that addition of glass fiber (as cement a replacement) was very beneficial in reducing the calcium hydroxide level. In another study, Kamali and Gharemaninezhad (10) investigated the hydration and microstructure of cement pastes modified with glass fiber powder. It was found that addition of fiber-glass powder as cement replacement, improved the early hydration of the cement and also showed pozzolanic reactivity at later ages (i.e. 91 days).

Furthermore, it was observed that the addition of fiber-glass reduced the porosity.

This paper presents selected findings from a comprehensive study conducted to evaluate the material characteristics of a ground glass fiber produced from E-glass and its role in affecting a range of fresh and hardened properties of pastes, mortars and concrete. Findings from the material characterization of GGF and its effects on fundamental material and selected mechanical properties of cementitious matrices are published elsewhere (11). The focus of this paper is to report findings from studies conducted to evaluate the impact of a specific GGF of defined fineness on selected mechanical and durability properties of mortars and concrete mixtures. To evaluate the mechanical properties, concrete specimens were tested for their compressive strength, splitting tensile strength, and modulus of elasticity. In addition, durability properties of the mixtures containing GGF were evaluated by conducting alkali-silica reaction, sulfate attack and, rapid chloride penetration test (RCPT). Furthermore, to assess the pozzolanic behavior of the GGF, strength activity index (SAI), and thermo gravimetric analysis (TGA) were performed on mixtures containing various level of GGF.

## 5.2 EXPRIMENTAL PROGRAM

### *5.2.1 Materials:*

Following materials were used in this study:

### *5.2.2 Cement*

In this study, a Type I/II (ASTM C 150) ordinary portland cement (OPC) with a specific gravity of 3.15 and an average particle size of 17 microns was used. The chemical composition of the portland cement and its selected physical properties are presented in Table 5-1.

### *5.2.3 Ground Glass Fiber*

The Ground Glass Fiber (GGF) used in this study was a fine white powder that was prepared by milling the off-spec glass fiber in a ball mill to a fine powder with an average particle size of 4

microns. The scanning electron microscope (SEM) observation showed that the GGF particles were angular with a smooth surface texture. The chemical composition of the GGF and its selected physical properties are presented in Table 5-1.

### *5.2.4 Fly Ash*

A class F fly ash (ASTM C618) with a specific gravity of 2.25 and an average particle size of 28 microns was used as an SCM. The chemical composition of the fly ash and its selected physical properties are presented in Table 5-1.

Table 5-1. Chemical Composition and Physical Properties of the Cementitious Materials

| Chemical composition/Physical properties | | Cement (%) | GGF (%) | Fly ash (%) |
|---|---|---|---|---|
| Chemical composition | $SiO_2$ | 19.9 | 47.7 | 50.7 |
| | $CaO$ | 62.3 | 19.6 | 3.3 |
| | $Al_2O_3$ | 4.8 | 10.4 | 25.1 |
| | $Fe_2O_3$ | 3.1 | 0.3 | 12.5 |
| | $MgO$ | 2.7 | 2.3 | 1.1 |
| | $Na_2O_{eq}$ | 0.38 | 0.70 | 2.0 |
| | $SO_3$ | 3.23 | 0.02 | 0.70 |
| | | | | |
| Physical properties | Specific Gravity | 3.15 | 2.60 | 2.25 |
| | Amount Passing #325 Sieve (%) | 98% | 96% | 76% |
| | Blaine's fineness ($cm^2/g$) | 4720 | 10200 | 6040 |
| | Loss On Ignition (LOI) | 2.6% | 1.0% | 2.3% |

### *5.2.5 Fine Aggregate (Siliceous Sand)*

A non-reactive siliceous river sand meeting ASTM C33 gradation requirements with a fineness modulus of 2.60, absorption of 0.30% with an oven-dry specific gravity of 2.67 was used in this study.

### *5.2.6 Coarse Aggregate:*

In concrete mixtures, a #57 (ASTM C33) granitic aggregate with the specific gravity of 2.65 and absorption of 1% was used.

### *5.2.7 Crushed reactive aggregates:*

To study the ASR-related expansion of the mortar mixtures (using standard ASTM C1260 and ASTM C1567 tests), a highly reactive rhyolitic crushed gravel aggregate from Las Placitas gravel pit from New Mexico (NM) was used. The NM aggregate had an absorption of 1.10% and an oven-dry specific gravity of 2.60.

## 5.3 Mixture Properties

In this study, GGF was employed in the mortar and concrete mixtures as a partial substitute for cement by mass at selected dosage levels of 10, 20 and 30%. In addition, two control mixtures were tested for comparative purposes. The first control mixture (CTRL-1) consisted of 100% plain Type I portland cement as the binder, while the second control mixture (CTRL-2) consisted of a binary blend of 75% Type I Portland cement with 25% Class F fly ash, by mass, as the binder. Table 5-2 shows the mixture ID and the composition of the cementitious portion of the above-mentioned mixtures. Specified mixture proportions from the relevant test methods were used for designing mortar mixtures.

Table 5-2. Mixture ID and Composition of the Binder Portion of Concrete and Mortar

| Mix ID | Paste Composition |
|---|---|
| CTRL-1 | 100% Cement |
| CTRL-2 | 75% Cement+ 25% Fly ash |
| GGF-10 | 90% Type I Cement+ 10% GGF |
| GGF-20 | 80% Type I Cement + 20% GGF |
| GGF-30 | 70% Type I Cement + 30% GGF |

In the case of concrete mixtures, water-to-cementitious materials ratio was maintained at 0.45 and a total cementitious materials content of 355 kg/m3 was employed. A #57 coarse aggregate (ASTM C33) was used in combination with siliceous river sand at 60:40 proportions by mass.

## 5.4 Experimental Test Methods

### *5.4.1 Mechanical Properties:*

In this study, 100 mm by 200 mm (4 in. by 8 in.) concrete cylinders were cast to test the mechanical properties of the concrete mixtures. The tested properties are compressive strength (ASTM C39), split-tensile strength test (ASTM C496) and modulus of elasticity (ASTM C469). The compressive strength test and split-tensile strength tests were conducted on 7, 28 and 56-days old samples and modulus of elasticity test was performed only on 28-days old specimens.

### *5.4.2 Pozzolanic Activity*

The pozzolanic reactivity of the mixtures was evaluated by conducting strength activity index on the mortar and thermogravimetric analysis (TGA) of paste specimens.

**Strength activity index**: The pozzolanic reactivity of GGF was examined by evaluating the strength activity index of mixtures containing GGF as a cement replacement material using the ASTM C311 test procedure. In this test, 50 mm x 50 mm x 50 mm (2 in. x 2 in. x 2 in.) mortar cubes were cast for each mix design (0, 10, 20 and 30% GGF and 25% fly ash as the cement replacement) and the compressive strength of each mixture was evaluated at 7 and 28 days of curing.

**Thermogravimetric analysis**: Effectiveness of GGF in consumption of calcium hydroxide, was evaluated by performing TGA on the paste specimens containing different dosage levels of the GGF as SCM. In this test method, crushed paste samples were gradually heated from ambient temperature to 800ºC and the change in their mass was monitored and recorded. Decomposition of calcium hydroxide occurs in the temperature range between 440 to 520ºC, causing a significant mass loss in the sample. The mass loss in this temperature range can be used to calculate the amount of calcium hydroxide in the sample.

In the present study, the TGA test was performed on the paste samples containing 10, 20

and 30% GGF as SCM and two control samples (one with plain cement and the other with 25% fly ash as cement replacement) at 28 and 56-day of ages. In addition, TGA test was performed on 200-day old mortar bars that were used in the sulfate attack test.

### *5.4.3 Resistance Against Alkali-Silica Reaction*

Effectiveness of GGF in mitigation of ASR related expansion was evaluated by performing the accelerated mortar bar test (ASTM C1260 and ASTM C1567) using reactive crushed NM aggregate. The test method of ASTM C1260 was used for the CTRL-1 mixture, which had no pozzolan. For all the other mixtures, which had pozzolan in their mix design, ASTM C1567 test method was used.

### *5.4.4 Sulfate Attack Resistance*

Following ASTM C1012 test method, 25 mm x 25 mm x 285 mm (1 in. x 1 in. x 11.25 in.) mortar bars and sufficient numbers of 50 mm x 50 mm x 50 mm (2 in. x 2 in. x 2 in.) mortar cubes were cast for each mix design. The samples were removed from their molds after 24 hours and were placed in a saturated lime water bath until they reach the required compressive strength of 3000 psi. At this point, zero-day reading for length-change measurement was taken on the mortar bar specimens. They were then placed in a 5% sodium-sulfate solution at ambient temperature. Further length-change readings were taken on days specified by ASTM C1012 test method. After each reading, the old solution would be replaced with a fresh one.

### *5.4.5 Rapid Chloride Penetration Test*

Rapid Chloride penetration test (RCPT) was performed on all the concrete mixtures (as presented in Table 5-2). For the purpose of this test, 100 mm by 200 mm (4 in. x 8 in.) concrete cylinders were cast and tested at 7, 28 and 56 days. According to the ASTM C1202, RCPT samples were cut in 50 mm (2 in.) thick discs and prepared before placing them in the RCPT cell containing 3% sodium chloride solution on one end and 0.3N sodium hydroxide solution on the other end. Each

cell was subjected to 60 V DC potential difference and the charge passing through the specimens was monitored for 6 hours.

## 5.5 RESULTS AND DISCUSSION

### *5.5.1 Mechanical Properties:*

Results of the compressive strength and split-tensile strength are presented in Figure 5-1. As it can be observed from Figure 5-1, the compressive strength of CTRL-2 samples (with 25% fly ash) was lower at early ages (7 days), however by 56 days reached to a similar level as CTRL-1. However, in the case of mixtures containing GGF, at dosage levels of 10% and 30% the compressive strength of the mixtures were similar to that of CTRL-1 samples at all ages. However, at 20% dosage of GGF the observed compressive strength was lower than that of the control mixtures. The precise reason for the observed trend in the GGF samples, i.e. lower strength at 20% dosage level compared to that at 10% and 30% is not entirely evident at this time. It is hypothesized that perhaps the competing influences of micro-filler effect and the pozzolanic reactivity effect of GGF may be different at different dosage levels. Further investigation is needed to ascertain the underlying reasons for this unexpected trend in the results.

In the case of split-tensile strength test, while lower strength at 7 days were observed in mixtures containing 20% and 30% GGF, the 28-day and 56-day values of all the mixtures containing GGF were similar to that of CTRL-1 samples. As a general observation, it appears that the use of GGF as a cement replacement material does not affect the split-tensile strength at the dosage levels evaluated, particularly at 28 days and beyond.

Modulus of elasticity of all the specimens was measured at 28 days. The results of this test were 33.1, 32.5, 33.2, 31.2 and 32.6 GPa for CTRL-1, CTRL-2, GGF-10, GGF-20 and GGF-30 mixtures respectively [1 GPa is equal to 145 ksi]. From these results it can be concluded that the modulus of elasticity of all mixtures containing pozzolans were very similar to the value

obtained for CTRL-1 mixture.

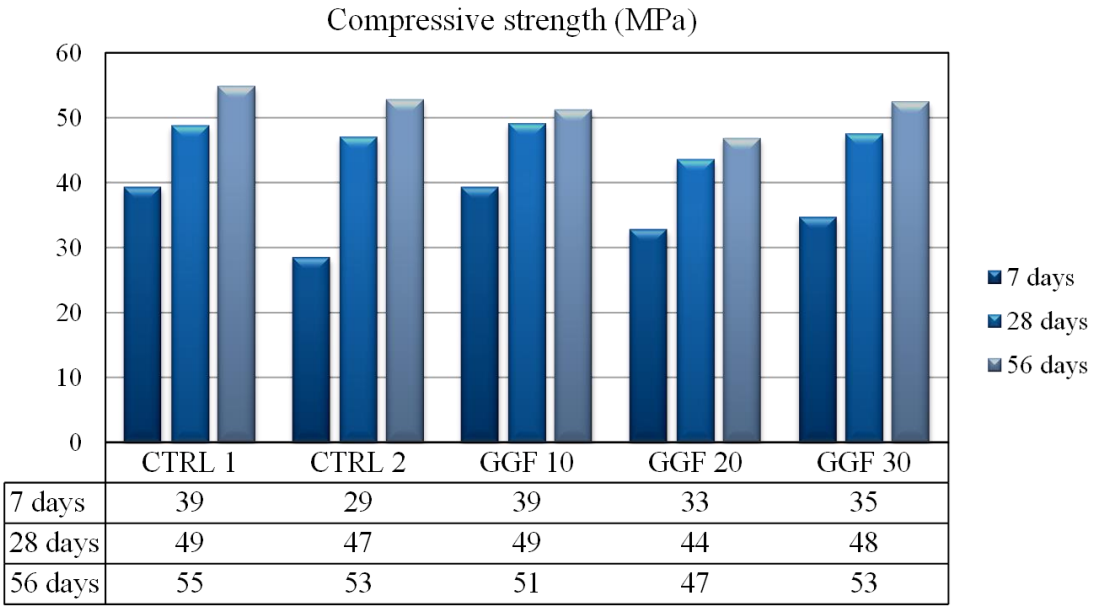


| | CTRL 1 | CTRL 2 | GGF 10 | GGF 20 | GGF 30 |
|---|---|---|---|---|---|
| 7 days | 39 | 29 | 39 | 33 | 35 |
| 28 days | 49 | 47 | 49 | 44 | 48 |
| 56 days | 55 | 53 | 51 | 47 | 53 |

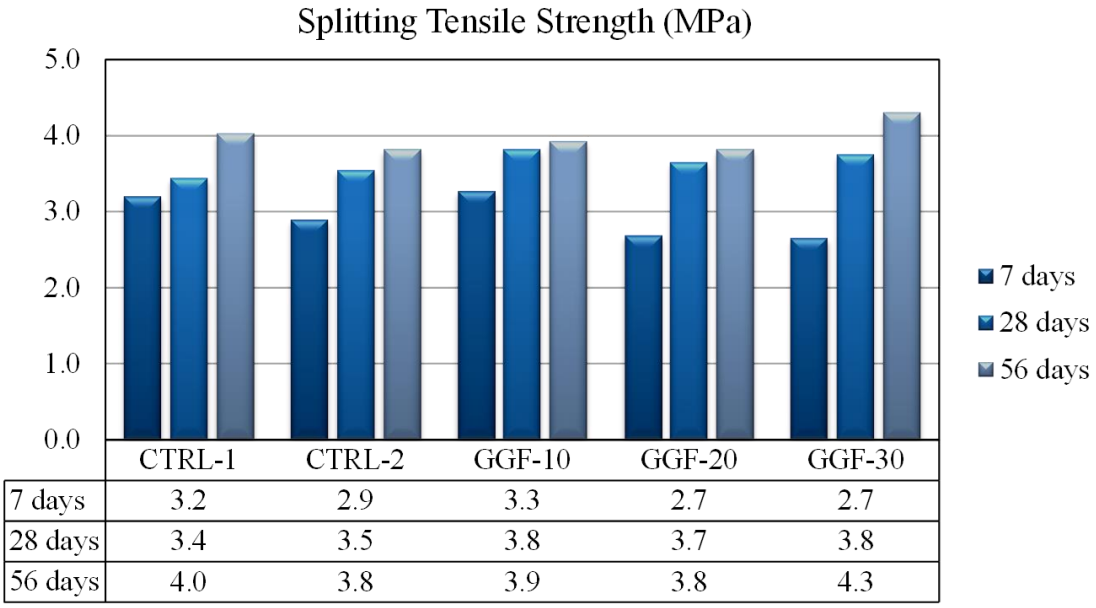


| | CTRL-1 | CTRL-2 | GGF-10 | GGF-20 | GGF-30 |
|---|---|---|---|---|---|
| 7 days | 3.2 | 2.9 | 3.3 | 2.7 | 2.7 |
| 28 days | 3.4 | 3.5 | 3.8 | 3.7 | 3.8 |
| 56 days | 4.0 | 3.8 | 3.9 | 3.8 | 4.3 |

Figure 5-1. Compressive strength (top) and splitting tensile strength (bottom) of concrete samples [1 MPa is equal to 145 psi].

### *5.5.2 Pozzolanic Reactivity*

#### *5.5.2.1 Strength Activity Index*

The results from testing compressive strength of mortar cube specimens and the resultant strength activity index (SAI) values are presented in Table 5-3. As it can be seen in this table, the GGF-20 mixture showed the SAI values of 104% and 110% after 7 and 28 days, respectively. Since these values are higher than 75%, the GGF is considered as a pozzolanic material (ASTM C618). Moreover, as the results revealed, the SAI value of all GGF containing mixtures showed higher values than CTRL-2 mixture at both 7 and 28 days.

Table 5-3. Compressive Strength and Strength Activity Index of Mortar Cubes for 7 and 28 Days

| Age (days) | | CTRL-1 | CTRL-2 | GGF-10 | GGF-20 | GGF-30 |
|---|---|---|---|---|---|---|
| 7 | Compressive strength (MPa) | 42 | 34 | 38 | 44 | 41 |
| | SAI (%) | 100 | 81 | 89 | 104 | 97 |
| 28 | Compressive strength (MPa) | 54 | 48 | 56 | 60 | 58 |
| | SAI (%) | 100 | 89 | 103 | 110 | 106 |

The better performance of mixtures containing GGF in comparison with CTRL-2 mixture (having 25% fly ash) can be explained by the smaller size of the GGF particles that are much finer ($4\mu m$) than the size of fly ash ($28\mu m$) particles which can refine the porosity, and can be engaged in the pozzolanic reaction faster. Furthermore, the results of XRD test revealed that the structure of GGF powder is very amorphous. This amorphous structure accelerates the pozzolanic reaction by allowing silica to react and form C-S-H gel. As a result of the pozzolanic reaction all the GGF containing mixtures have surpassed the compressive strength of the CTRL-1 mixture after 28 days (see Table 5-3). It should be noted that the strength activity index is not necessarily a complete reflection of the pozzolanic reactivity of the pozzolan such as GGF rather it also includes any micro-filler effect imparted by the pozzolan in the test mixtures. Further, with materials such as GGF, due to the particle size and the surface texture characteristics of the GGF

grains, to ensure a constant flow, the w/c ratio of mixtures containing GGF at different dosage levels is significantly lower than that of the control mixture, which can also influence the SAI.

#### *5.5.2.2 TGA Results*

The TGA results from crushed paste powder with different dosage of GGF replacement are presented in Figure 5-2 for the ages of 28 and 56 days. As it can be seen, the amount of calcium hydroxide significantly decreases with the increase in GGF dosage. The reduction occurs as a result of a combination of both dilution effects of GGF, which reduces the total amount of calcium hydroxide in the systems and the pozzolanic reaction, which consumes the calcium hydroxide to form C-S-H gel. It is evident from Figure 5-2 that the pozzolanic effect increases with the increase in the replacement dosage and time of curing. The results of 28-days samples showed the values of 1%, 2% and 7% for GGF-10, GGF-20 and GGF-30 for the amount of calcium hydroxide that was consumed through the pozzolanic reaction respectively. In the case of 56-days old samples, the pozzolanic effect caused 3%, 4% and 17% reduction in the calcium hydroxide for GGF-10, GGF-20 and GGF-30 respectively.

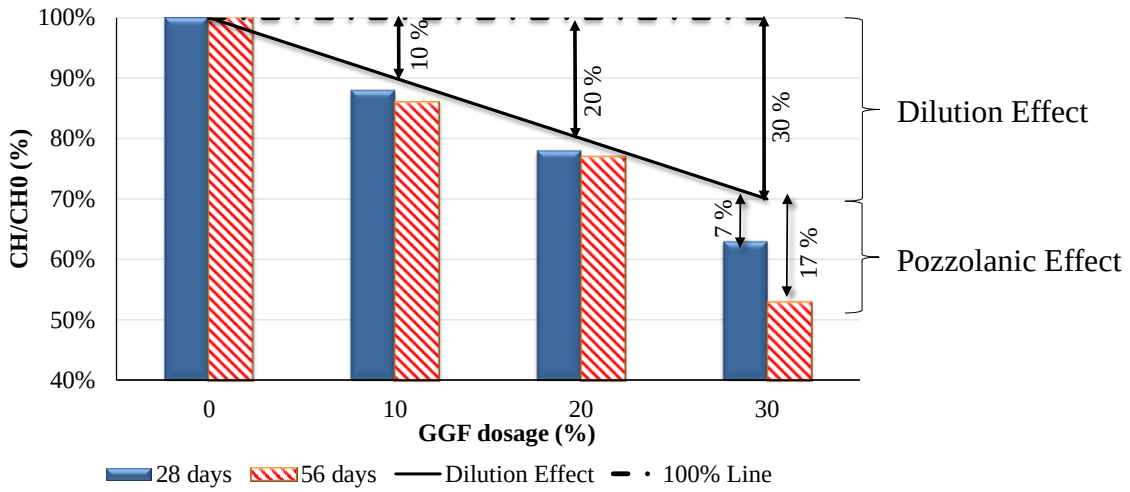


Figure 5-2. Effect of GGF dosage on the TGA result [where CH is calcium hydroxide content of the sample and CHo is the calcium hydroxide content of the CTRL-1 (100% Cement)]

### *5.5.3 Alkali-Silica Reaction:*

The effect of GGF in the mitigating ASR related expansion was studied by conducting the accelerated mortar bar test (ASTM C1260 and ASTM C1567). Figure 5-3, shows the expansion of the mortar bars up to 28 days. It is evident from Figure 5-3 that the addition of GGF as an SCM significantly reduced the ASR-related expansion, while the CTRL-1 mixture, which has no pozzolan, showed a significant expansion. At 14 days, the expansion of CTRL-1 mortar bars reached 0.90%, which is significantly higher than the 0.10% threshold limit as identified in ASTM C33 to identify reactive aggregates. Beyond 14 days, the expansion of CTRL-1 samples continued further and reached 1.40% at 28 days. In the case of GGF-10 mixture, although a considerable reduction in expansion was observed in comparison to CTRL-1 mixture, the 14-day expansion of this mixture was still far above the 0.10% limit.

At the higher dosage of GGF, i.e. GGF-20 and GGF-30, the expansion results showed a significant reduction in comparison to the CTRL-1 mixture. Replacement levels of 20% and 30%, successfully mitigated the expansion of the mortar bars and kept it below the 0.10% limit at 14 days. At this age, the expansion of GGF-20 and GGF-30 mixtures reached 0.04% and 0.03% respectively. The CTRL-2 mixture was also able to mitigate the expansion of the mortar bars and showed an expansion of 0.10% at 14 days. However, the expansion of this mixture was higher than GGF-20 and GGF-30 mixtures. The results from this investigation also indicated that among all the mixtures, the GGF-30 mixture had the best performance in terms of expansion mitigation. It can be observed from Figure 3 that even after 28 days of testing, the expansion of GGF-30 mortar specimens was only 0.06%, which is significantly lower than the 0.10% limit.

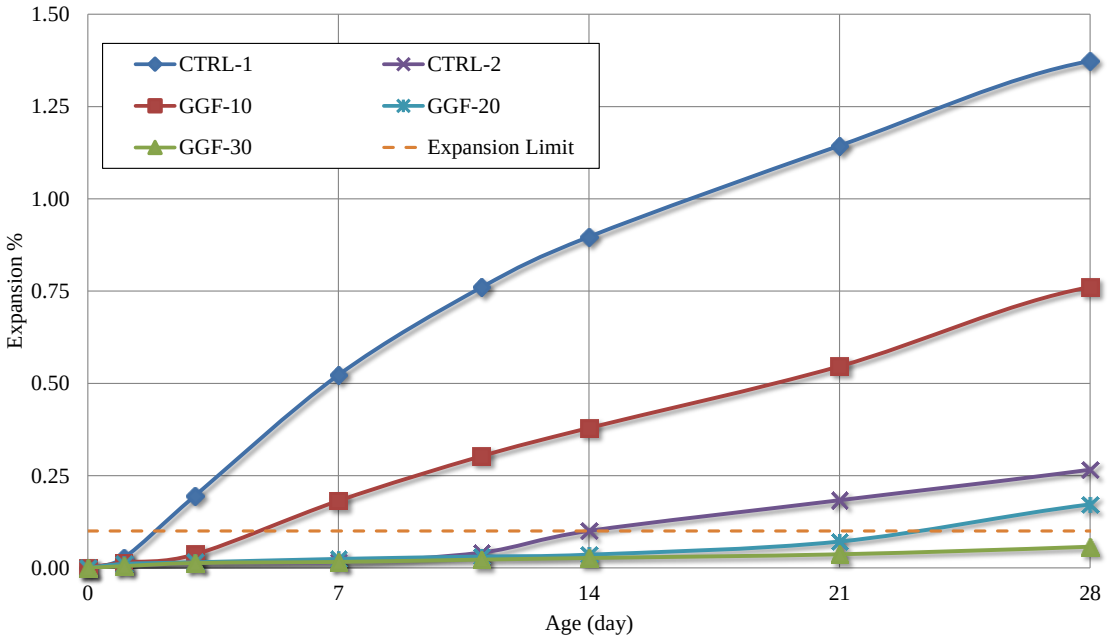


Figure 5-3. Expansion of the mortar bar versus time

The mitigation mechanism of the GGF containing mixtures in terms of ASR-related expansion has been discussed in detail elsewhere (11). However, the main mechanisms for the mitigation can be summarized as follow:

*Reduction in available calcium for newly formed ASR gel*. As it was presented in the TGA results, GGF containing mixtures have a lower level of calcium hydroxide, which is essential for triggering ASR-associated expansion and damage. It has been shown that calcium hydroxide reacts with freshly produced low-viscosity ASR gels (by exchanging calcium ions with alkalis) forming a more viscous ASR gel, that can induce significant tensile stress on the mortar matrix upon absorption of moisture and expansion (12). As result, addition of fine and highly reactive silica glass in the form of GGF or fly ash will reduce the risk of ASR damage as the level of calcium hydroxide will be lowered through the dilution and pozzolanic reaction effects.

*Reduction in Ca/Si ratio*. Addition of glassy silica in the form of GGF or fly ash, leads to the formation of a C-S-H gel with a lower Ca/Si ratio. Past studies have shown that the C-S-H

gels with lower Ca/Si ratio will retain a higher amount of alkalis in comparison to the gels with greater Ca/Si ratio (13-14). As a result, the C-S-H gel in the GGF containing samples is likely to retain more alkalis in its structure. The EDX analysis of the paste portion of GGF samples showed that Ca/Si ratio was 22% lower than the Ca/Si ratio in the CTRL-1 samples (For more information see the reference (11)).

*Effect of alumina in reducing ASR.* It is known that the presence of Al in SCMs increases their effectiveness against the ASR (15-16). Two suggested mechanisms for the role of Al are: 1) better performance of C-A-S-H gel in binding alkali in comparison to C-S-H gel (17). And 2) reduction in the rate of solubility of Si from the reactive aggregates (18). Regardless of the responsible mechanism for reducing ASR, a higher amount of aluminum was observed in GGF-30 samples compared to other samples. The EDX results performed on at least three points of the paste portion of each sample showed a higher aluminum content of the GGF-30 in comparison to the CTRL-1 sample. According to the EDX results, the aluminum atomic percent in the GGF-30 and CTRL-1 samples were 7.25% and 3.09% respectively (11).

*Reduction in paste permeability*. Addition of pozzolans in terms of cement replacement, introduces a large amount of reactive silica into the system. In the presence of reactive silica, the pozzolanic reaction takes place by consuming CH and producing C-S-H gel, thus refining the paste structure and reducing the permeability. In addition, small particles of GGF are thought to refine the pore structure of the paste and hence reduce the permeability. Although no specific test was conducted in this study to test the effectiveness of addition of GGF on reducing the permeability of the samples, other studies have reported that using glass fiber in a powder form (as a pozzolan) caused a reduction in the permeability of mortar mixtures (8).

### *5.5.4 Sulfate Attack:*

Resistance of mortar bar specimens containing GGF replacement to sulfate attack was evaluated

by studying their length change when submerged in a 5% sodium-sulfate solution at ambient temperature. From Figure 5-4 it is evident that the addition of GGF was seen to effectively reduce the rate of expansion, especially at later ages (i.e. after 28 days). As it can be seen, higher levels of replacement resulted in a lower expansion, as GGF-20 and GGF-30 samples showed the lowest level of expansion after 180 days.

The lower expansion of samples with GGF as the cement replacement can be attributed to their pozzolanic reactivity resulting in lower calcium hydroxide content of mixtures in comparison to CTRL-1 mixture (TGA results). Presence of CH is known to have a deleterious effect on the sulfate attack-related expansion. Calcium hydroxide is known to react with the sulfate and form the expansive gypsum, which, in the presence of a sufficient amount of alumina can form Ettringite. Formation of Ettringite is an expensive process and can lead to cracking and resultant strength-loss of the samples. In addition, other factors that reduce the expansion of GGF containing samples are the smaller particle size of GGF (in comparison to portland cement and fly ash), as well as its pozzolanic reactivity, that can refine the microstructure of the paste. Refinement of the paste structure reduces the permeability of the matrix and hence reduces the penetration of the sulfate ions into the samples.

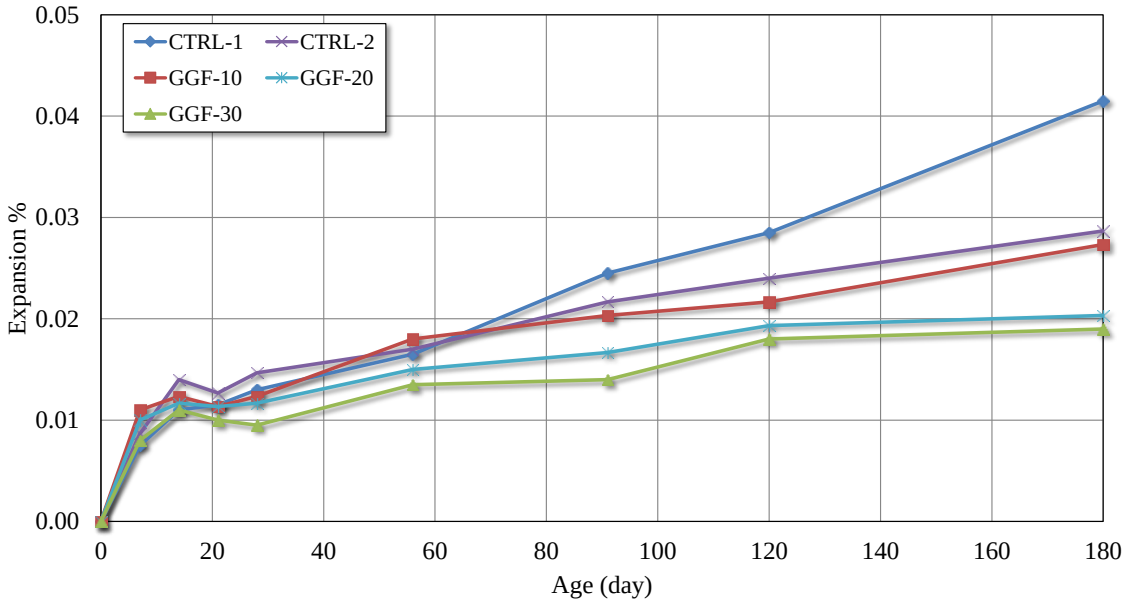


Figure 5-4. Expansion results of mortar bars subjected to 5% sodium sulfate solution.

Results from TGA tests conducted on mortar samples after 200 days of submersion in the 5% sodium-sulfate solution for CTRL-1 (a), CTRL-2 and GGF-30 samples are presented in Figure 5-5(a) through 5-5(c), respectively. Two distinct peaks in the differential analysis of the TGA curve can be identified in each of the graphs after 100°C. The first peak which is located between 120°C to 150°C is thought to be as a result of decomposition of gypsum, which ideally occurs between 110°C to 150°C (19). The second peak which is located between 420°C to 500°C is known to be as a result of the decomposition of calcium hydroxide crystals from the cement hydration. Decomposition of calcium hydroxide has been reported to occur between 440°C to 520°C (20). The percent weight loss for the gypsum decomposition (first peak) and CH decomposition (second peak) for CTRL-1, CTRL-2 and GGF-30 curves progressively decreases from CTRL-1, CTRL-2 to GGF-30 curves as seen in Figure 5-5. The smallest peaks were seen in the case of GGF-30 samples, indicating that the lowest amount of gypsum and calcium hydroxide are present in this sample after 200 days of testing.

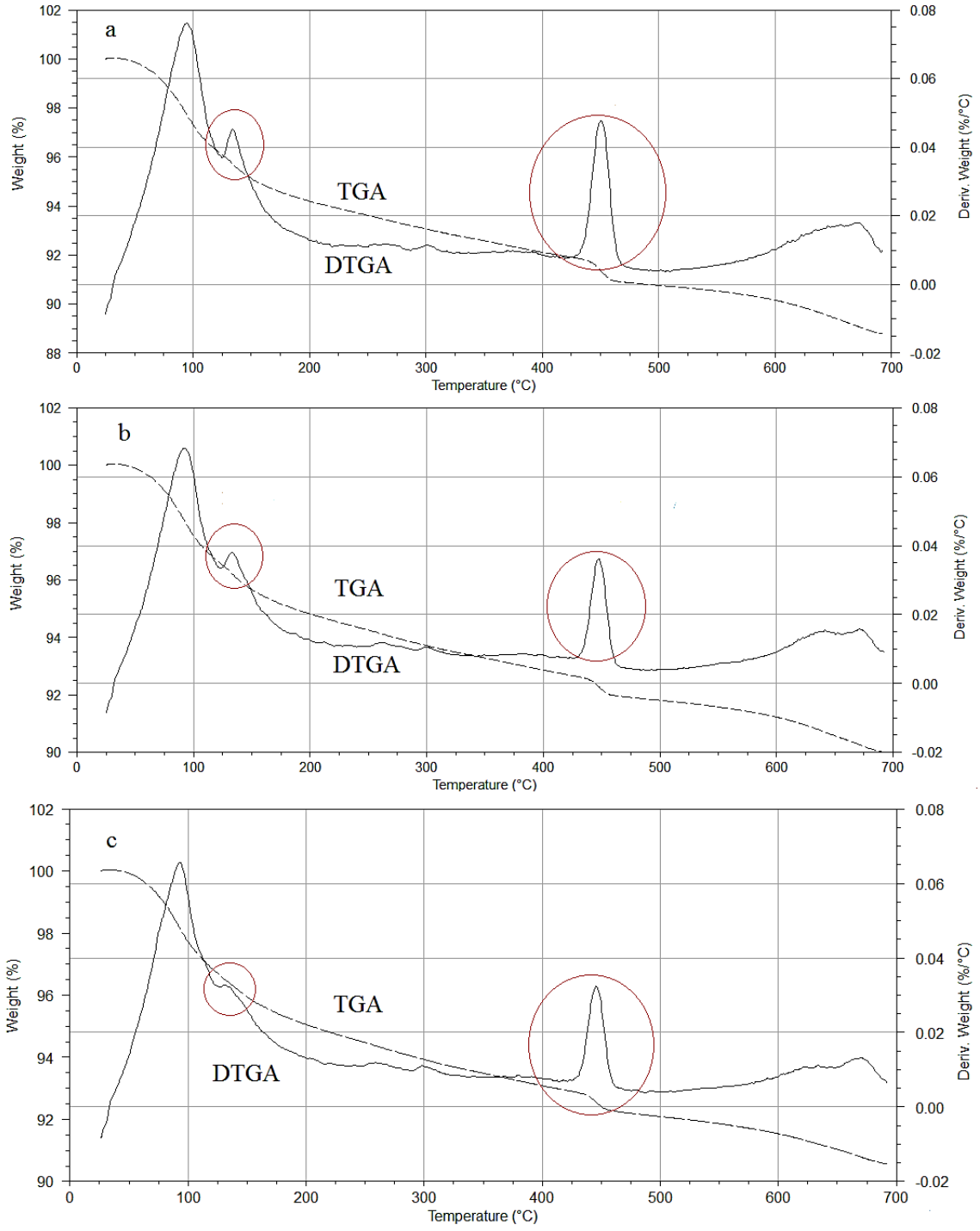


FIGURE 5-5. TGA and DTGA results of mortar samples immersed in 5% sodium-sulfate solution for 200 days: (a) CTRL-1 (b) CTRL-2 (c) GGF-30

### *5.5.5 Chloride Permeability*

The results from Rapid Chloride penetration Test (RCPT) at 7, 28 and 56 days are presented for all the mixtures in Figure 5-6. These results show the clear advantage of using GGF in the concrete mixtures in reducing the penetration of chloride ions. From the results, it is evident that the amount of charge passing decreases with the increase in the replacement level of GGF dosage. As it can be seen in this figure, GGF-20 and GGF-30 samples showed very low chloride ion permeability (in the range of 100-1000 Coulombs based on the ASTM C1202) at 28 days. In the case of CTRL-2 samples, although test results showed a high amount of passing charge at 7 days, a lower value for the passing charge was registered at later ages (i.e. 56 or 28 days) in comparison to the CTRL-1 sample. The comparison between CTRL-2 samples and GGF-10 samples indicates better performance of GGF in reducing the Coulomb value, as the measured values of this parameter for GGF-10 were lower than CTRL-2 at all the measured ages.

The improved performance of GGF samples is thought to be mainly as a result of refinement in the paste pore structure. As it has been discussed earlier, this is the result of fine particle size of the GGF as well as the pozzolanic reactivity. Moreover, the results of earlier studies on mixtures containing glass fiber powder have shown its effect in reducing pore content and electrical resistivity, which can cause lower ion permeability of the GGF containing mixtures (10).

It is also thought that the lower chloride ion penetrability could be related to the presence of a relatively high amount of Al compounds in GGF. It is known that the availability of the Al compounds in the paste structure increases its ability in binding the chloride ions by the formation of insoluble Friedel's salt. Earlier studies have reported that the capacity of the chloride binding in binders increases with the increase in the total aluminum content of the binder (21-22).

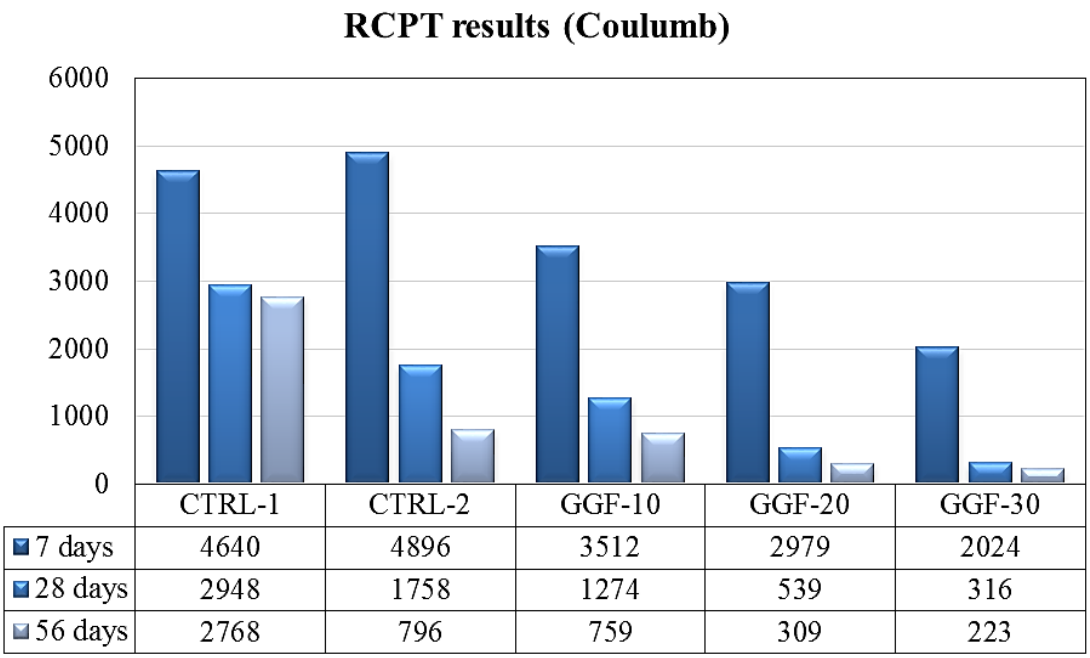


| | CTRL-1 | CTRL-2 | GGF-10 | GGF-20 | GGF-30 |
|---|---|---|---|---|---|
| 7 days | 4640 | 4896 | 3512 | 2979 | 2024 |
| 28 days | 2948 | 1758 | 1274 | 539 | 316 |
| 56 days | 2768 | 796 | 759 | 309 | 223 |

Figure 5-6. Result of rapid chloride penetration on concrete samples

## 5.6 CONCLUSION

The results from characterization and use of GGF as an SCM in portland cement concrete can be summarized as follows:

1) At all the cement replacement levels (i.e. 10, 20 and 30%) evaluated in this study, the use of GGF showed a strength activity index greater than 100% at 28 days.
2) Results of TGA up to 56 days did not show any significant pozzolanic reaction for 10 and 20% replacement levels. The maximum reduction in the CH content was 17%, which occurred for the 30% replacement level after 56 days
3) The results from tests conducted to evaluate mechanical properties showed that addition of GGF at cement replacement levels up to 30% did not lead to any significant reduction in the compressive strength, split-tensile strength and modulus of elasticity.
4) At replacement levels of 20% and 30%, GGF was able to meet the expansion limit of 0.10% after 14 days in the accelerated mortar bar test to indicate its ability to mitigate ASR. Both

these replacement levels showed better performance in ASR mitigation compared to control mixtures (CTRL-1 and CTRL-2 mixtures).

5) Results from sulfate attack studies revealed that at all levels of cement replacement, GGF containing samples showed a lower level of expansion compared to control (CTRL-1 and CTRL-2) mixtures.
6) Use of GGF at all levels of cement replacement reduced chloride ion permeability values in concrete significantly (2768 coulomb for CTRL-1 versus 223 coulomb for GGF-30, after 56 days).

Overall, it can be concluded from this study that a finely ground GGF with an average particle size of 4 microns can be successfully used as an SCM at cement replacement levels as high as 30% by mass of cement with no loss in mechanical properties compared to control concrete mixtures, while significantly improving the durability properties of concrete mixtures. In all regards, the performance of GGF as a pozzolan was better compared to a typical Class F fly ash at comparable dosage levels.

## References


1. Shao Y, Lefort T, Moras S, Rodriguez D. Studies on concrete containing ground waste glass. *Cement and Concrete Research*, Vol. 30 No. 1, 2000, pp. 91-100.
2. Dyer TD, Dhir RK. Chemical reactions of glass cullet used as cement component. *Journal of Materials in Civil Engineering*, Vol. 13, No. 6, 2001, pp. 412-417.
3. Shayan A, Xu A. Value-added utilisation of waste glass in concrete. *Cement and concrete research,* Vol. 34, No. 1, 2004, pp. 81-89.
4. Afshinnia K, Rangaraju PR. Efficiency of ternary blends containing fine glass powder in mitigating alkali–silica reaction. *Construction and Building Materials,* Vol. 100, 2015, pp. 100:234-245.
5. Hemmings RT, Nelson RD, Graves PL, Cornelius BJ, inventors; Albacem, Llc, assignee. White pozzolan composition and blended cements containing same. United States patent US 6776838, 2004.
6. Hemmings RT. Process for Converting Waste Glass Fiber into Value Added Products, Final Report. Albacem LLC; 2005.
7. Chen CH, Huang R, Wu JK, Yang CC. Waste E-glass particles used in cementitious mixtures. *Cement and Concrete Research*, Vol. 36, No. 3, 2006, pp. 449-456.
8. Hossain A, Shirazi S, Persun J, Neithalath N. Properties of concrete containing vitreous calcium aluminosilicate pozzolan. *Transportation Research Record: Journal of the Transportation Research Board, No. 2070,* 2008 pp. 32-38.
9. Neithalath N, Persun J, Hossain A. Hydration in high-performance cementitious systems containing vitreous calcium aluminosilicate or silica fume. *Cement and Concrete Research,* Vol. 39, No. 6, 2009 pp. 473-481.
10. Kamali M, Ghahremaninezhad A. An investigation into the hydration and microstructure of

cement pastes modified with glass powders. *Construction and Building Materials,* 2016 Vol. 112, pp. 915-924.

11. Prasad Rangaraju, Hassan Rashidian, Gordon Nameni and Godwin Amekuedi. Properties and Performance of Ground Glass Fiber as a Pozzolan in Portland Cement Concrete. *Proceedings of the International Concrete Sustainability Conference,* Washington DC 2016.
12. Taylor, H.F.W., Cement Chemistry, *Academic Press*, London, 1990.
13. Bhatty MS. Mechanism of pozzolanic reactions and control of alkali-aggregate expansion. *Cement, concrete and aggregates,* Vol. 7, No. 2, pp. 69-77.
14. Stade H. On the reaction of CSH (di, poly) with alkali hydroxides. *Cement and Concrete Research,* Vol. 19, No. 5, pp. 802-810.
15. Duchesne J, Bérubé MA. Long-term effectiveness of supplementary cementing materials against alkali–silica reaction. *Cement and concrete research,* Vol. 31, No. 7, 2001, pp. 1057-1063.
16. Ramlochan T, Zacarias P, Thomas MD, Hooton RD. The effect of pozzolans and slag on the expansion of mortars cured at elevated temperature: Part I: Expansive behaviour. *Cement and Concrete Research,* Vol. 33, No. 6, 2003, pp. 807-814.
17. Hong SY, Glasser FP. Alkali sorption by CSH and CASH gels: Part II. Role of alumina. Cement and Concrete Research. 2002 Jul 31;32(7):1101-1111.
18. Chappex T, Scrivener KL. The influence of aluminium on the dissolution of amorphous silica and its relation to alkali silica reaction. *Cement and Concrete Research,* Vol. 34, No. 12, 2012, pp. 1645-1649.
19. Borrachero MV, Payá J, Bonilla M, Monzó J. The use of thermogravimetric analysis technique for the characterization of construction materials. *Journal of thermal analysis and Calorimetry*, Vol. 91, No. 2, 2008, pp. 503-509.

20. Pane I, Hansen W. Investigation of blended cement hydration by isothermal calorimetry and thermal analysis. *Cement and Concrete Research,* Vol. 35, No. 6, 2005, pp. 1155-1164.
21. Dhir RK, El-Mohr MA, Dyer TD. Chloride binding in GGBS concrete. *Cement and Concrete Research,* Vol. 26, No. 12, 1996, pp. 1767-1773.
22. Delagrave A, Marchand J, Ollivier JP, Julien S, Hazrati K. Chloride binding capacity of various hydrated cement paste systems. *Advanced cement based materials,* Vol. 6, No. 1, 1997, pp. 28-35.

# CHAPTER 6

# EFFICIENCY OF GROUND GLASS FIBER AS A CEMENTITIOUS MATERIAL, IN MITIGATION OF ALKALI-SILICA REACTION OF GLASS AGGREGATES IN MORTARS AND CONCRETE[1]

## 6.1 Introduction

According to a report by the Environment Protection Agency on the Municipal Solid Waste (MSW), published in 2013, around 11.5 million tons of waste glass are produced in the US (1). Although the amount of recycled glass has considerably increased from 0.16 million tons in 1970 to 3.15 million tons in 2013, almost 74% of the total waste glass is discarded in landfills (1). Some of the difficulties in increased recycling level of waste glass are due to the combination of different colors of waste glass as well as difficulties in removing dirt, paper, or other contaminants from the glass products.

One of the proposed solutions to reduce the large stream of the waste glass that is dumped in landfills is to incorporate waste glass as an aggregate in portland cement concrete in place of natural mineral aggregates. Several research studies have investigated different aspects of utilizing glass aggregate in concrete mixtures, either as a fine or a coarse aggregate replacement. In these studies, issues such as reduction in the workability and compressive strength, (for the replacement levels of higher than 25 to 30%) were reported (2-5). However, the susceptibility of glass aggregate to deleterious alkali-silica reaction (ASR) has been the main concern that

[1] - Hassan Rashidian-Dezfouli, Kaveh Afshinnia[a], Prasada Rao Rangaraju. Efficiency of Ground Glass Fiber as a cementitious material, in mitigation of alkali-silica reaction of glass aggregates in mortars and concrete. Submitted to Journal of Building Engineering (under review).

hampered its extensive use (6-9). In this study, we have focused on evaluating the efficiency of different cement replacement materials (ground glass fiber, ground glass powder, and meta-kaolin) in reducing the damaging effects of ASR caused by the use of crushed glass aggregate in mortar and concrete mixtures.

### *6.1.1 Background:*

Use of waste glass aggregate as a replacement material for natural mineral aggregate in portland cement concrete has been the subject of a number of previous research studies (2, 4, 10-14). Several studies also have been conducted to evaluate mitigation of ASR-related damages of glass aggregates by replacing cement with different types of supplementary cementitious materials (SCMs) and their combinations (15-19).

A study by Shafaatian et al. on the ASR mitigation mechanisms of several types of Class C fly ash in mortars containing glass aggregates (15) showed that fly ash reduces the ASR-related damages by reducing the alkali content of the pore solution through alkali binding, as well as reducing the dissolution rate of silica from glass aggregates. It was also found that using fly ash increases the tensile strength of mortars; which, reduces or delays the ASR-related expansion. Efficiency of fly ash and meta-kaolin in the mitigation of ASR expansion of concrete blocks containing glass cullets of different sizes as aggregate material was investigated by Lee et al. (18) using accelerated mortar bar tests. It was found that both fly ash, and meta-kaolin effectively reduced the ASR-related expansion of mortar bars. Further, it was reported that the size of the glass aggregate have a significant effect on the ASR-expansion; and the larger aggregate size resulted in a higher ASR-related expansion (18). Afshinnia and Rangaraju studied the efficiency of ternary blends containing fine glass powder in mitigating alkali–silica reaction (19). It was found that both the ternary blends of Class C fly ash and GLP, and ternary blends of slag and GLP, showed a better ASR mitigation performance compared to that of the individual components

(i.e. Class C fly ash or slag) at an equivalent dosage level.

In addition to the studies performed on the concrete and mortar mixtures containing glass aggregate, several studies have been performed on the utilization of recycled glass powder from soda-lime glass (GLP) as cement replacement material (11, 20-24). In a finely ground form, GLP shows pozzolanic reactivity and can be used an SCM. A study by Parghi and Alam was carried out to investigate the pozzolanic reactivity of glass powder derived from waste glass bottle. It was found that the 7-, 28- and 56-day Strength Activity Index (SAI) values of the mortar mixtures containing 20% glass powder were 120%, 127% and 131%, respectively (23). Pozzolanic reactivity and ASR mitigation performance of glass powder are related to its fineness. A study by Afshinnia and Rangaraju was carried out to investigate the influence of glass powder fineness on its pozzolanic reactivity and ASR mitigation performance using two glass powders with average particle sizes of 17 and 70 microns (24). It was found that the 28-day strength activity index value of the mortar specimens containing 20% of the 17-micron glass powder was 37% more than that of the mortar mixture containing 20% of the 70-micron glass powder. This clearly indicates the higher level of pozzolanic reactivity of finer glass powder size compared to the coarser glass powders.

Glass powder, when used at an appropriate dosage level can mitigate ASR distress in concrete (19, 23-28). However, similar to the pozzolanic reactivity of glass powder, the finer glass powder showed more promising ASR mitigation performance compared to that of the coarser ones (24, 25). A study by Zheng was carried out to evaluate the ASR mitigation performance of two glass powders with maximum particle sizes of 50 and 200 microns. It was found that while the 180-day expansion value of the control mortar bars (without glass powder) subjected to the ASTM C227 test method was around 0.6%, values of the same age mortar bars containing 30% finer glass powder and 30% coarser glass powder were 0.1% and 0.2%,

respectively (25). A study by Jang et al. was carried out to evaluate the beneficial influence of using waste glass powder derived from thin-film transistor liquid-crystal display (TFT-LCD) glass in mortar and concrete. The mortar bars containing 10% of TFT-LCD showed 43% less ASR expansion compared to that of the control specimens (22).

Ground glass fiber is one of the relatively new types of SCMs that can be used as a cement replacement if waste glass fiber is milled in to a fine powder form. According to a report by US Department of Energy in 2005 (29), the total amount of waste glass fiber in United States that ends up in landfills is about 250,000 tons per year, which can be further increased to 500,000 tons if the waste streams from the users of glass fibers are also considered. However, unlike more conventional SCMs such as fly ash, slag, and meta-kaolin, which have been a subject of the large number of studies, only few studies have been performed on the utilization of this material as a cement replacement material (29).

Available studies on utilization of the powdered glass fiber have shown an excellent performance of this material in improving mechanical and durability properties of mortars and concrete mixtures (30-34). A study by Chen et al. evaluated the pozzolanic reactivity and ASR mitigation performance of E-glass powder that was derived by grinding the electronic grade glass fiber scrap to small particle size (30). It was seen that the replacement of E-glass as cementitious material, by 40% of the mass of cement, revealed a clear sign of pozzolanic reactivity by showing 117%, 127% and 143% strength activity index after 28, 91 and 356 days. Moreover, no potentially deleterious ASR expansion was observed within the mortar bars containing 10% to 50% E-glass powder. The opposing effects of E-glass powder and bottle glass powder (GLP) in influencing ASR behavior of mortar and concrete specimens can be attributed to the level of sodium oxide present in the glass, which is significantly lower in E-glass powder compared to that of the bottle glass powder. According to a DOE report in 2005, replacement of cement with a

powdered form of glass fiber (average particle size of 3 microns) effectively reduced the ASR expansion (29). The test results showed an excellent performance of the mixture having 20% glass fiber powder as cement replacement material by mass over the control sample. It was also reported that when the mixtures were tested in accordance to ASTM C441 method, a significant difference was seen in the 14-day expansion (0.0045% for a mixture with 20% vitrified calcium aluminate silica glass (VCAS) and 0.337% for the control mixture). Recent studies by Rangaraju et al. and Rashidian-Dezfouli and Rangaraju, have shown the benefits of using waste ground glass fiber (GGF) in reducing the ASR-related expansion of a mineral reactive natural aggregate. It was seen that replacement of cement with GGF at 20% and 30% by the mass significantly reduced the expansion of mortar bars and concrete bars (35, 36).

### *6.1.2 Significance of this research*

Earlier studies on the usage of crushed glass aggregates in mortars and concretes have reported ASR as the main problem of using glass aggregates. On the other hand, replacement of cement with ground glass powders (from recycled bottles), or ground glass fibers, has shown the promise of pozzolanic reactivity of this material. However, the efficiency of ASR mitigation offered by the ground glass powders seems to largely depend on the chemical composition of the glass, particularly its alkali content. The significance of the present research is to evaluate the potential of using a large amount of waste glass in concrete by incorporating crushed waste glass as aggregate as well as ground waste glass as cement replacement material in an effort in mitigate the potential ASR distress resulting from the crushed glass aggregate. In this study, the performance of ground glass powder from both glass containers as well as glass fibers in mitigating ASR distress was compared along with meta-kaolin as a cement replacement material. The ASR induced expansion in both mortar and concrete test specimens were measured by performing Accelerated Mortar Bar Test (AMBT) and Miniature Concrete Prism Test (MCPT),

respectively. In addition, Scanning Electron Microscope (SEM) and Energy X-Ray Dispersive analysis (EDX) were conducted to investigate the microstructure of the mortar samples.

## 6.2 Experimental Procedure

### *6.2.1 Materials:*

The following materials have been used in this study:

### *6.2.2 Cement:*

In this study a Type I/II cement (ASTM C150), with alkali content of 0.38% $Na_2O_{eq.}$ and a Blaine fineness of 482 $m^2/kg$ was used. The cement had a 0.018% autoclave expansion, which is significantly lower than the 0.2% maximum limit given in ASTM C 1260. The chemical composition of the Portland cement is given in Table 6-1.

#### *6.2.2.1 Ground Glass Fiber:*

In this study, Ground Glass Fiber (GGF) with a specific gravity of 2.6 was used as the cement replacement material. This material had the average particles size of 4 $\mu m$ and a Blaine fineness of 1020 $m^2/kg$. The GGF was received in the form of a fine white powder, which was produced by milling the off-spec glass fiber in a ball mill. The chemical composition of the GGF is presented in Table 6-1.

#### *6.2.2.2 Ground Bottle Glass:*

The ground glass powder from recycled bottles (GLP) used in this study was obtained from grinding waste bottle glass of different colors in a ball mill. This material had an average particle size of 17 $\mu m$, Blaine fineness of 604 $m^2/kg$ and a specific gravity of 2.45. The chemical compositions of the glass powder are shown in the Table 6-1.

#### 6.2.2.3 *Meta-kaolin:*

A highly reactive meta-kaolin (MK) with a specific gravity of 2.2, average particle size of 1.4 microns and Blaine fineness of 2174 $m^2$/kg was used in this study as an SCM. The chemical composition of meta-kaolin is presented in Table 6-1.

Table 6-1. Chemical composition of cementitious material

| Cementitious material | $SiO_2$ | $Al_2O_3$ | $Fe_2O_3$ | $CaO$ | $MgO$ | $Na_2O$ | $K_2O$ |
|---|---|---|---|---|---|---|---|
| Cement (%) | 19.93 | 4.77 | 3.13 | 62.27 | 2.71 | 0.06 | 0.48 |
| GGF (%) | 47.72 | 10.36 | 0.34 | 19.62 | 2.27 | 0.67 | 0.10 |
| GLP (%) | 69.60 | 2.20 | 0.90 | 11.60 | 0.40 | 12.03 | 0.40 |
| MK (%) | 52.4 | 44.3 | 0.50 | 0.02 | 0.12 | * | ** |

* The $Na_2O_{eq}$ content of meta-kaolin was not measured, although literature shows values ranging between 0.25% to 2.45% (37)

** The $K_2O_{eq.}$ content of meta-kaolin was not measured, although literature shows values ranging between 2.5% to 3.5% (37)

#### 6.2.2.4 *Glass aggregate:*

Crushed glass aggregate produced from waste soda bottles was obtained from a local source. This material had an oven-dry specific gravity of 2.42 and an absorption value of 0.03%. In order to meet the required gradation per ASTM C1260, the glass aggregates were prepared by crushing them using a Bico disc-pulverizer with 8-inch ceramic grinding plates.

#### 6.2.2.5 *Non-reactive fine aggregate:*

A non-reactive siliceous sand was obtained from a local source in South Carolina. Fine aggregate used in this study had a specific gravity of 2.6, with an absorption of 1% and fineness modulus of 2.58.

### 6.2.3 *Test procedure:*

#### 6.2.3.1 *Flow test:*

In this study, workability of mortar mixtures was measured by following the ASTM C1437

method. Although the workability of a mixture does not affect its effectiveness in mitigating ASR expansion, however, a good workability is required to ensure the proper mixing and consolidation of the test samples. In this study, workability of mortar mixtures containing 20% GGF, GLP and meta-kaolin as cement replacement materials were measured and compared to the workability of a control mixture with no cement replacement.

#### *6.2.3.2 Strength activity index (ASTM C311)*

The pozzolanic reactivity of each supplementary cementitious material was evaluated using the strength activity index test. Comparative tests were performed on a control mixture containing 100% portland cement and mixtures containing GGF at 10%, 20% and 30% cement replacement level; GLP at 10%, 20% and 30% cement replacement level and MK at 10% and 20% cement replacement level. Following ASTM C311 procedure, 50 mm x 50 mm x 50 mm mortar cubes of each mixture were cast and cured in a curing room, with the temperature of 23ºC and relative humidity of ~100%, for 24 h. The test specimens were demolded after 24 h and mortar cubes were kept in the curing room up to the testing day. Finally, the compressive strength of mortar cubes were measured 28 days after casting. The Mix ID and paste composition of all the mixtures are presented in Table 6-2.

#### *6.2.3.3 Thermogravimetric Analysis*

In order to evaluate the effectiveness of each SCM in consumption of calcium hydroxide, the Thermogravimetric analysis (TGA) was performed on representative samples of pastes containing 20% dosage of GGF, GLP and MK at 28 and 56 days. For this purpose a TGA Instrument (2950 model), employing a platinum pan with nitrogen purge gas was used. The temperature was raised from ambient to 800 degrees Celsius at a temperature ramp of 10 degrees per minute. In this test, representative crushed paste samples passing #200 sieve were gradually heated and change in

their mass was monitored and recorded. Decomposition of calcium hydroxide occurs within the temperature range between 440 to 520°C, causing a significant mass loss in the sample (38). The mass loss in this range can be used to calculate the amount of calcium hydroxide in the sample. Furthermore, to evaluate the degree of pozzolanic reactivity of GLP, GGF and MK the test results were compared with results from a control sample containing no SCMs. The calcium hydroxide content of each sample was normalized for per gram of the paste and reported.

#### *6.2.3.4 Accelerated Mortar bar test (ASTM C1567)*

Following ASTM C1567 procedure, Accelerated Mortar Bar Tests (AMBT) were conducted to evaluate the effectiveness of GLP, GGF and MK as cement replacement materials in mitigating ASR-related expansion. In these test methods, 25 x 25 x 285 mm mortar bars were cast and cured in a curing room for 24 h. The samples were then placed in water and cured for a further 24 h period at 80°C. After 24 h, samples were removed from the water, and a zero-day length measurement was taken and placed back in a preheated 1N sodium hydroxide solution bath. The submerged samples were kept in an 80°C oven, and additional length-change measurements were taken at selected intervals of time up to 28 days. In this test method, for each combinations of the aggregate, cement, and SCMs, mortar bar expansion less than 0.10% at 14 days is considered to indicate a mixture with a low risk of ASR deterioration.

In this study, crushed glass aggregates meeting the gradation requirements of the ASTM C1260 were used as the reactive aggregates in preparing the mortar bar samples for the test. Using glass aggregates, samples containing 10, 20 and 30% dosage of GLP and GGF, and 10% dosage of MK were cast, and the expansion results were compared with a control mixture having no cement replacement material. It should be noted that due to the very low workability of MK-containing mixtures, the maximum dosage of MK in the AMBT mixtures was limited to 10%.Miniature Concrete Prism Test (AASHTO TP110-14)

It has been reported that the larger glass aggregate size causes a higher ASR-expansion in comparison to those with the smaller size (18). Therefore, in this study, Miniature Concrete Prism Test (MCPT) is used to assess the alkali-silica reactivity of coarse glass aggregate in concrete specimens. The concrete mixtures are prepared using a high alkali cement (0.9 ± 0.1% $Na_2O_{eq.}$), a reactive coarse aggregate and a non-reactive sand. The cement content of the concrete mixture is maintained at 420 kg/m$^3$ with the water-to-binder ratio of 0.45; while the volume fraction of the coarse aggregate is fixed at 0.65 of per unit volume of the mixture. The alkali content of the concrete is further boosted to 1.25% $Na_2O_{eq}$ by weight of cement by adding sodium hydroxide to mixing water. When SCMs are evaluated using MCPT method to study their ability to mitigate ASR, portland cement in concrete mixture is replaced by SCM on a mass basis. The alkali content of the concrete is boosted to 1.25% $Na_2O_{eq.}$ based only on the mass of portland cement employed in the concrete mixture.

In this test method 50 x 50 x 285 mm concrete prisms are cast and cured for 24 in a curing room. The samples are then removed from the molds, submerged in water and subjected to a 24 h of additional curing at 60$^o$C. The samples are then removed from the water, and zero-day length measurement is taken. Subsequently, concrete prisms are soaked in a preheated 1N sodium hydroxide solution and kept in the 60$^o$C chamber. The change in the length of the samples is monitored at selected time intervals up to 56 or 84 days, depending on the length change observed. Typically, when evaluating aggregate reactivity (i.e. without any SCM in the concrete) a length-change of less than 0.04% at 56 days represents a non-reactive aggregate. However, when evaluating ASR mitigation potential of SCMs, a length change of 0.02% or lower at 56 days is considered as the limit to indicate the effectiveness of SCMs.

In this study, crushed glass aggregates with particle size ranging between 9.5 mm and 4.75 mm were used as coarse aggregates and a non-reactive siliceous sand is used as fine

aggregate. In control mixtures, 100% portland cement was used, while in mixtures containing SCMs, different dosage levels of GLP, GGF and meta-kaolin were used as cement replacement materials by mass.

#### *6.2.3.5 Scanning Electron Microscope and energy-dispersive X-ray spectral analysis*

In this study, Scanning Electron Microscopy (SEM) and the energy-dispersive X-ray spectral analysis (EDX) were used to study the microstructure and the chemical compositions of the ASR gel in the AMBT samples. The mortar samples were removed from the sodium hydroxide solution after 28 days and were cut using slow-speed diamond saw with mineral oil as the lubricant and isopropyl alcohol to clean the cut samples. The cut samples were then ground and polished using propylene glycol lubricant using resin-bonded diamond discs with grit size changing form #80 to #4000. The SEM examination was performed on the prepared samples using a Hitachi TM 3000 microscope in back-scatter mode equipped with a Swift EDX silicon-drift detector.

### *6.2.4 Mixture proportion*

In this study, the mixture proportions of mortar bars and concrete prisms were based upon the requirements per ASTM C1567 and AASHTO TP110 procedures, respectively. The cement was replaced based on mass for all the SCMs evaluated in this study. In addition, to ensure the adequacy of consolidation, flow test (ASTM C143) was performed on all the mortar mixtures. To study the effectiveness of SCMs on the mitigation of the ASR-related expansion of the mortar and concrete samples, crushed glass aggregate was used as the reactive aggregate in the mixtures. Table 6-2 shows the mix ID and composition of the cementitious portion of the above-mentioned mixtures. For each test, the aggregate portion of the mixture was proportioned as the suggested values by the relevant test method. It should be noted that in the case of MCPT, AASHTO TP 110 indicates the gradation of the coarse aggregate as 57.5% for the fraction between 12.5 mm to 9.5 mm, and 42.5% for the fraction 9.5 mm to 4.75 mm; however, due to the unavailability of the

larger size fraction of glass aggregate, all the coarse aggregates used for the concrete samples had a size between 9.5 mm to 4.75 mm.

Table 6-2. Mix ID and composition of the of the mixtures

| Mix ID | Paste composition (mass %) | Proportion for different size of crushed glass aggregates for AMBT* (mass %) | | | | | Aggregate proportion for MCPT** (volume %) | |
|---|---|---|---|---|---|---|---|---|
| | | #4 to #8 | #8 to #16 | #16 to #30 | #30 to #50 | #50 to #100 | Glass | Sand |
| CTRL | 100% Cement | 10% | 25% | 25% | 25% | 15% | 65% | 35% |
| GLP-10 | 90% Cement + 10% GLP | 10% | 25% | 25% | 25% | 15% | Not performed | |
| GLP-20 | 80% Cement + 20% GLP | 10% | 25% | 25% | 25% | 15% | 65% | 35% |
| GLP-30 | 70% Cement + 30% GLP | 10% | 25% | 25% | 25% | 15% | 65% | 35% |
| GGF-10 | 90% Cement + 10% GGF | 10% | 25% | 25% | 25% | 15% | 65% | 35% |
| GGF-20 | 80% Cement + 20% GGF | 10% | 25% | 25% | 25% | 15% | 65% | 35% |
| GGF-30 | 70% Cement + 30% GGF | 10% | 25% | 25% | 25% | 15% | 65% | 35% |
| MK-10 | 90% Cement + 10% MK | 10% | 25% | 25% | 25% | 15% | 65% | 35% |
| MK-20 | 80% Cement + 20% MK | Not used for AMBT (low workability) | | | | | Not performed (low workability) | |

*- The water-to-binder ratio for AMBT mixtures: 0.47.

**- The water-to-binder ratio for MCPT mixtures: 0.45.

## 6.3 Results and discussion

### *6.3.1 Flow test:*

The results of flow test on the mortar samples containing 20% of GGF, GLP and MK are presented in Figure 6-1. As it can be seen, while GLP-20 and GGF-20 had a higher workability in comparison to CTRL mixture, addition of meta-kaolin caused a significant drop in the workability of the mixture. The low workability of the MK-20 was the main limitation in using this mixture for the ASR study. The mix was very stiff, and it was difficult to work with. The flow of CTRL, GGF-20, GLP-20 and MK-20 were 83%, 96%, 92% and 7% respectively.

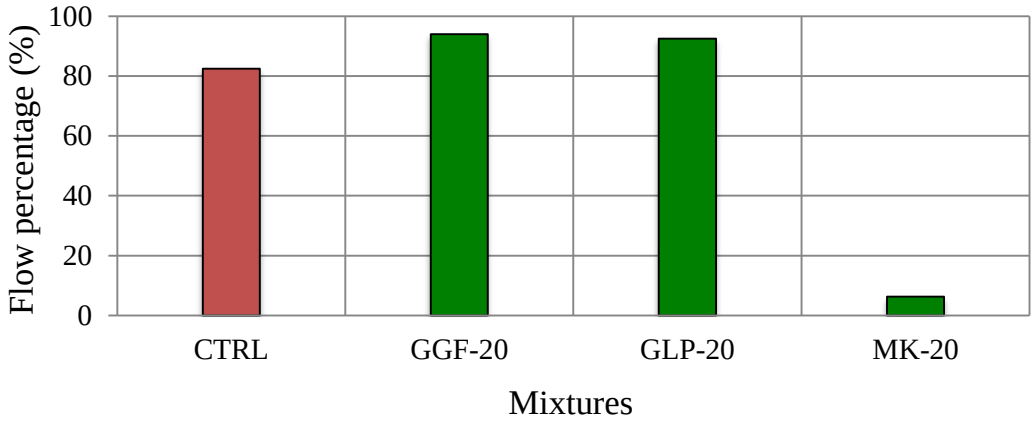


Figure 6-1. Flow test results of control mixture and mixtures containing 20% SCM

While the effect of meta-kaolin in reducing the workability is related to its high specific surface area, the improvement in the workability of the fresh mortar containing GGF and GLP is thought to be due to smooth surface texture of the particles with little to no absorption. Figure 6-2 shows the particle morphology of GGF and GLP particles. Moreover, GGF and GLP are not as reactive as portland cement at early ages, thus leaving more water to lubricate the system and increases the workability.

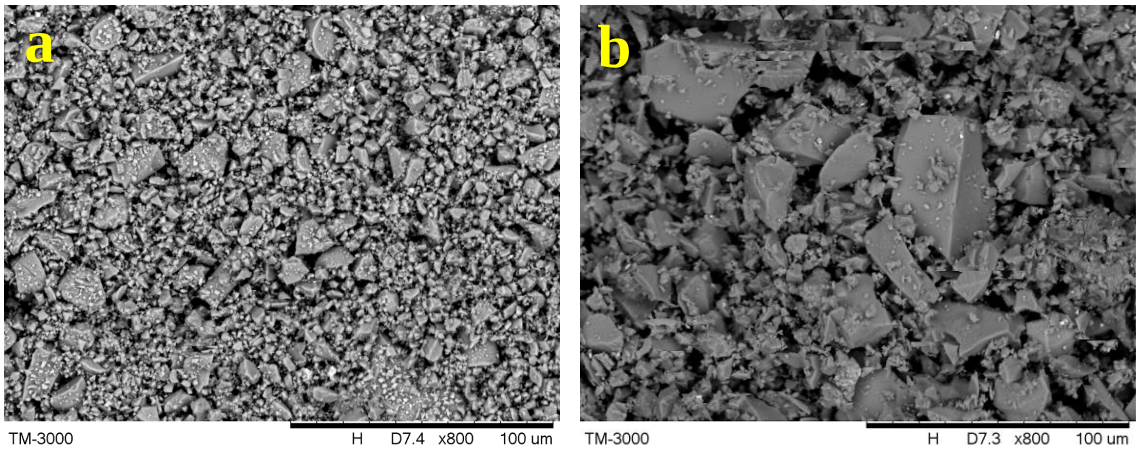


Figure 6-2. Particle shape of GGF (a) and glass-powder (b)

### *6.3.2 Pozzolanic reactivity*

#### *6.3.2.1 Strength Activity Indices (ASTM C311)*

Pozzolanic reactivity of each of SCMs was evaluated by the Strength Activity Index (SAI) test (ASTM C311). The results of SAI for 28-day old samples are presented in Figure 6-3. It was observed that with increase in dosage of GGF, the SAI increased; as GGF-20 and GGF-30 showed higher SAI values in comparison to GGF-10. However, in case of mixtures with GLP, as the replacement level increased from 10% to 30%, the SAI decreased.

Moreover, it was seen that while using GLP resulted in the reduction of compressive strength of mortar cubes at all replacement levels, use of GGF improved the compressive strength compared to control mixture at all replacement levels, as the 28-day SAIs of all mixtures with GGF were higher than 100%.

The better performance of GGF can be related to its smaller particle size (4 $\mu m$), which results in a higher specific surface (1020 $m^2$/kg for GGF versus 604 $m^2$/kg for GLP). The smaller size of the GGF particles can also help the refinement of the paste matrix. While it was not measured in this study, other studies have indicated a higher level of cement hydration and a lower level of total porosity in the samples with cement replacement, in comparison to the control

samples with 100% cement (32, 34). In addition, the better performance of GGF in comparison to GLP, in terms of reducing the total porosity of the paste matrix, was observed by Kamali and Ghahremaninezhad (33).

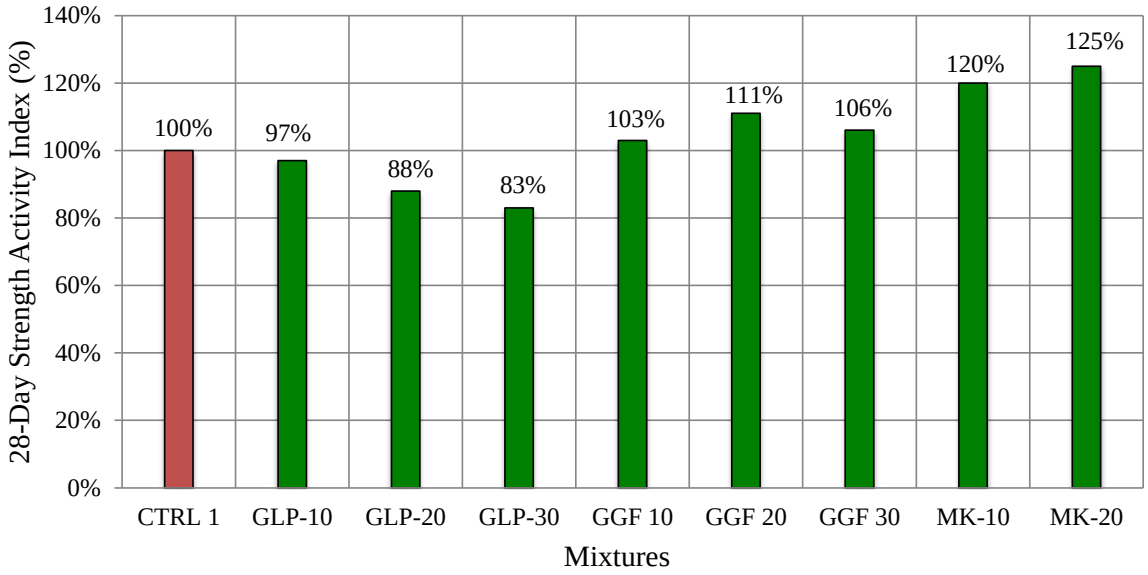


Figure 6-3. Strength activity index of mortar cubes containing GGF, GLP and meta-kaolin at 28 days

### *6.3.2.2 Thermo-gravimetric analysis*

In order to compare the pozzolanic reactivity of the SCMs that were used in this work, TGA was performed on paste sample, containing 20% SCM. The results of the paste samples containing 20% GLP, GGF and MK are presented in Figure 6-4. In all mixtures containing SCMs, the amount of CH content was found to be lower than the control mixture. However, among the different SCMs employed in this study, GLP and MK were found to be the least and most effective SCMs, respectively. Mixtures containing GLP reduced the CH content by 16% and 20% after 28 and 56 days, respectively, compared to the control mixture. However, replacing cement with 20% GGF reduced the CH content by 22% and 24% after 28 and 56 days, respectively. Although better results were seen in the case of GGF in comparison with GLP, the principal source of reduction in the CH content was due to the dilution effect. In the case of meta-kaolin, a

significant reduction in CH content was seen in comparison to the other tested mixtures. Replacement of 20% of cement with meta-kaolin, caused 48% and 56% reduction in the CH content of this mixture in comparison to the control sample after 28 days and 56 days, respectively. The TGA result of mixtures containing meta-kaolin showed a considerable amount of reductions of CH content was due to the pozzolanic reactions, which were 28% and 36% after 28 and 56 days respectively.

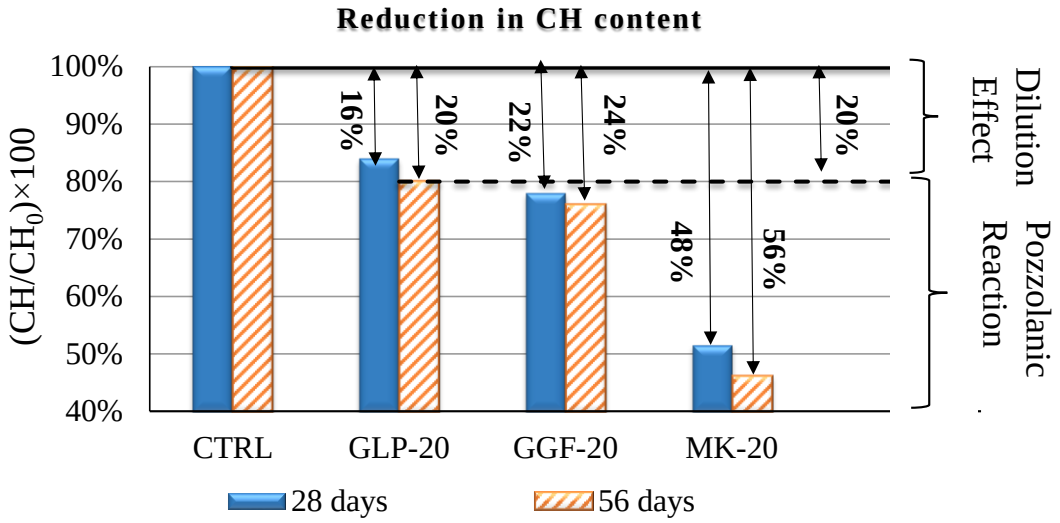


Figure 6-4. Normalized Calcium hydroxide content of paste samples containing 20% GGF, GLP and meta-kaolin. (CH is the calcium hydroxide content of the samples, and, $CH_0$ is the calcium hydroxide content of the control sample)

### *6.3.3 ASR Mitigation Performance*

#### *6.3.3.1 AMBT*

Expansion results of mortar samples subjected to ASTM C1260 and ASTM C1567 tests are presented in Figure 6-5. It is evident from Figure 6-5 that the control mortar bars (i.e. without any SCMs) show an expansion of 1% after 14 days, which further increased to almost 1.6% at 28 days. Clearly, this level of expansion in the mortar bars indicates that the crushed glass aggregate used in the mortar bars in highly reactive. Replacing cement with GLP showed a considerable

reduction in the ASR-related expansion of the mortar mixtures. However, none of the GLP containing mixtures could reduce the expansion to below 0.10% expansion limit at 14 days (ASTM C1567). On the other hand, mixtures containing MK and GGF showed a very good performance in the mitigation of the ASR-related expansion. Addition of 10% meta-kaolin as the cement replacement reduced the expansion of the mortar mixture to 0.03% and 0.30% after 14 days and 28 days, respectively.

The expansion results showed that at all the tested levels of replacement, GGF was able to reduce the expansion below the 0.10% limit. In the case of GGF-10 mixture, expansions of 0.01% and 0.06% were observed at 14 and 28 days, which were lesser than measurements made for MK-10 mixture. In the case of GGF-20 and GGF-30 mixtures, the 14-days expansion was less than 0.01%, and the 28-days results showed an almost 0.01% expansion for both mixtures.

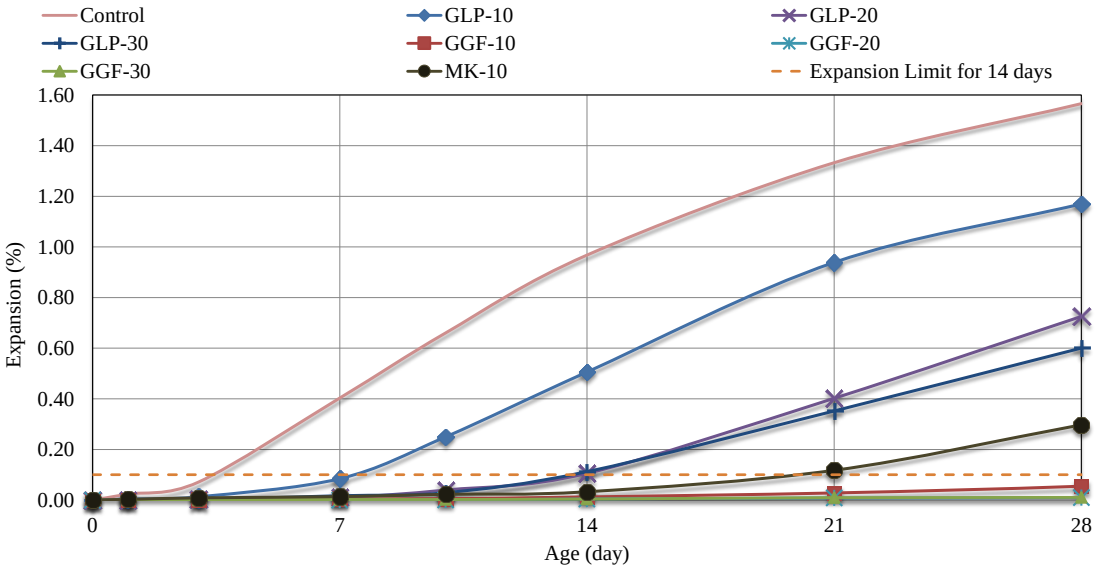


Figure 6-5. Expansion behavior of mortar bars (ASTM C1567)

It should be noted that despite the ASTM C1260 has initially be developed to test the mineral aggregates rather than the artificial aggregates, such as the glass aggregate. Hence, the difference between the chemical compositions of glass aggregate and natural aggregates,

especially due to its high level alkali can influence the test results (19, 24). As it can be seen in Figure 5, while addition of SCMs (except for GLP-10 mixture) could reduce the 14-day ASR expansion under the 0.10% limit, however, a dramatic expansion after 14 days was observed in specimens containing GLP and MK. The reason for such a behavior (delayed expansion), as discussed in details by Afshinnia and Rangaraju (19, 24), could be explained by the high alkali content of the glass aggregate; which act as a secondary source of alkalis. Owing the high temperature associated with the AMBT test condition (80°C), alkalis would leach from the glass aggregate, acting as an internal source of alkali, and causing expansion (19, 24). Therefore, to reduce the effect of the secondary source of alkalis (leached from glass aggregate), the MCPT test was performed on concrete specimens. This test is performed in a relatively lower temperature, 60°C, and also utilizes aggregate with a larger size. Thus, could provide us with more realistic expansion results.

#### *6.3.3.2 MCPT*

The expansion results of concrete mortar bars (MCPT) are presented in Figure 6. According to this method, when evaluating aggregate, the expansion limit of 0.04% at 56 days or 84 days (depending on the aggregate reactivity) are considered as the expansion limit of the test; however, in evaluating SCMs for ASR mitigation, the expansion limit is 0.02% at 56 days is considered. As seen in Figure 6-6, almost similar trend in the expansion curves can be observed in MCPT as with the AMBT results shown in Figure 6-5. While control mixture showed a dramatic expansion of 0.76% and 1.12% after 56 and 84 days respectively, replacement of cement with SCMs reduces the ASR-related expansion. In the case of replacement of cement with GLP, a slight reduction in the expansion was observed for mixtures containing GLP-20 and GLP-30. However, expansions of these mixtures were far above the 0.02% limit at 56 days and showed 0.68% and 57% after 56 days, respectively. In the case of meta-kaolin, a considerable reduction in the expansion of MK-

10 mixture was seen. Although, replacement of cement with 10% meta-kaolin reduced the 56-days expansion considerably, it was still above the 0.02% limit at 56 days, with further increase in expansion up to 84 days. The expansion of MK-10 samples was 0.040% and 0.204% after 56 days and 84 days respectively.

Replacing cement with GGF showed a significant reduction in expansion in comparison with control and GLP containing mixtures at all the tested levels of cement replacement, and a similar performance as MK-10 at 10% cement replacement level. Results from these tests showed that the expansion of MK-10 and GGF-10 mixtures at 56 days were 0.040% and 0.075%, respectively, which failed to meet the 0.02% expansion limit at 56 days. However, mixtures containing GGF at 20% and 30% cement replacement level (i.e. GGF-20 and GGF-30) showed concrete prism expansion levels below 0.02% at 56 days, and continued to show minimal increase in expansion even up to 84 days. The expansion of GGF-20 and GGF-30 was 0.015% and 0.006% at 56 days, and 0.030% and 0.012% at 84 days respectively.

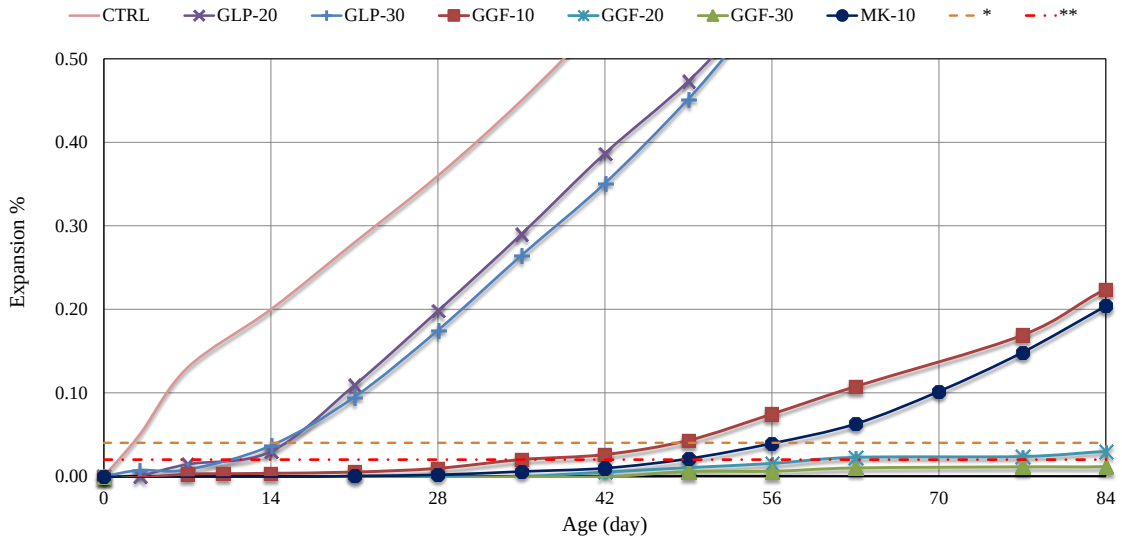


Figure 6-6. Expansion behavior of miniature concert prisms (AASHTO-TP110)
**- Expansion Limit for CTRL at 56 days, **- Expansion limit for SCM containing samples at 56 day*

#### *6.3.3.3 Scanning Electron Microscopy (SEM)*

The microstructure of CTRL, GLP-30, GGF-30 and MK-10 samples from the accelerated mortar bar tests were analyzed to determine the presence or absence of ASR-induced damage in the test specimens, nature of the reaction products that formed, and the relative effectiveness of the SCMs used in mitigating the ASR damage in the test specimens. These results are presented in Figures 6-7 through 6-9.

Figure 6-7 shows the backscatter SEM image from a polished section of the CTRL mortar, containing 100% glass aggregate after 28 days of evaluation in the ASTM C1260 test. The microstructural observations from CTRL sample showed extensive cracking and presence of ASR gel. In this image, a significant number of cracks can be observed within the structure of glass aggregate. In addition, it is clear from Figure 6-7 that most of these internal cracks are filled with ASR gel, which indicates the initiation of ASR reaction within the matrix of the glass aggregate particles. The preferred formation of ASR gel within the glass structure, and not at the interface of the glass aggregate and the cement paste can be explained by two hypotheses. Firstly, the presence of internal cracks within the glass particles resulting from the crushing operations which provides a ready pathway for the alkaline pore solution in the mortar to penetrate the glass particles and trigger the ASR reaction. The presence of these internal cracks within crushed glass aggregate particles was documented earlier by Maraghechi et al. (13). Secondly, the alkalis required to sustain the alkali-silica reaction may likely be derived from the glass aggregate particles themselves as they start to degrade, owing to the alkali-rich nature of the soda-lime glass material used in preparing the aggregate particles.

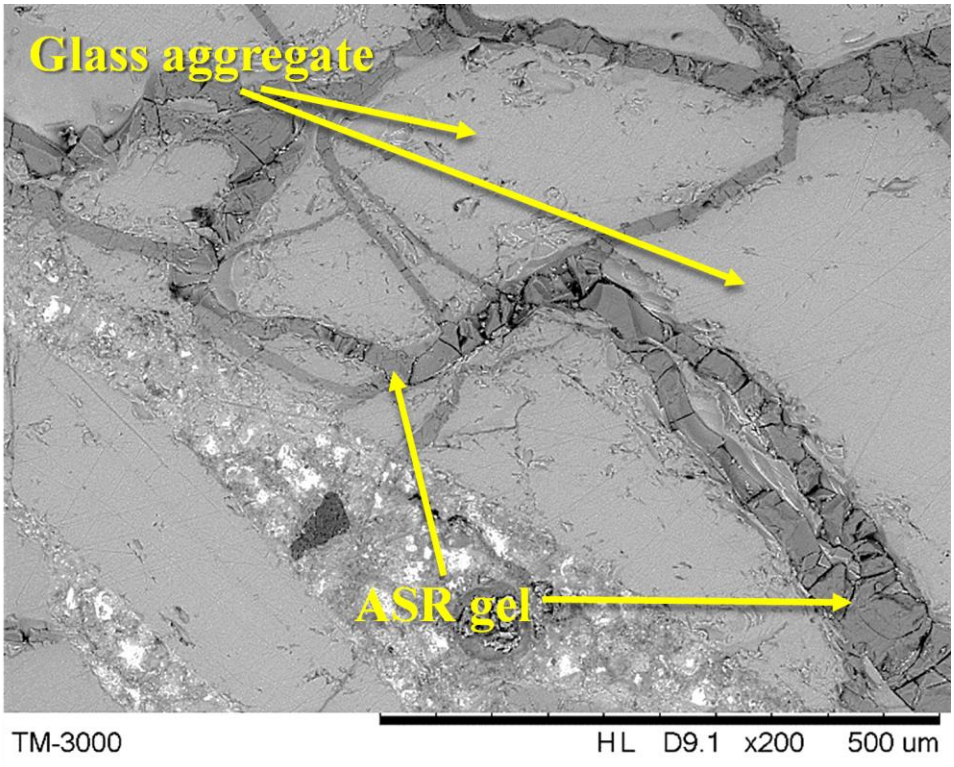


Figure 6-7. Formation of ASR gel within glass aggregate in the control samples without SCMs

Figure 6-8 shows the backscatter SEM image from a polished section of a GLP-30 specimen after 28 days of testing per the ASTM C1567 method. It is clear from this figure that the ASR gel formed predominantly within the paste matrix itself and at the interface of the glass aggregate and cement paste. Although there is some level of cracking that is observed in the glass particles and the associated presence of some ASR gel, the extent of ASR gel formation within the glass aggregate particles is comparatively less in the GLP-30 sample compared to the CTRL sample. The reasons for this pattern of damage appear to be due to the presence of highly reactive GLP particles within the paste that preferentially react with the alkaline pore solution and form localized ASR gel deposits within the paste. Figure 6-8 shows a sample of GLP particles that have reacted and the resulting ASR gel residing next to these reacted GLP particles. On a relative basis, it can be observed that the large glass aggregate particles that are much farther away from the reaction sites of GLP particles are less affected in the GLP-30 sample. It is conceivable that the

mobility of the alkali ions to penetrate larger glass aggregate particles to cause internal damage is minimized in the presence of GLP particles within the paste matrix (19, 24).

As presented in expansion curves shown in Figure 6-5, the relatively small increase in the expansion of the GLP-10, GLP-20 and GLP-30 mortar bars within the first 7 to 14 days may be explained by the following two reasons: (a) The small grain size of GLP particles (17 um) and their presence throughout the matrix of the mortar bars would have likely created ASR gel that is dispersed throughout the mortar bar. This is evident in Figure 6-8. The role of glass powder as a sacrificial reacting silica to protect larger reactive aggregate particles was shown earlier by Afshinnia and Rangaraju (24). (b) Also, the high alkalinity of the pore solution at initial stages of the test (with little to no soluble calcium being available in the pore solution) would likely have generated an ASR gel with significantly lower viscosity, which could easily permeate through the pore structure without causing significant expansive stress. In combination, these two reasons would have an effect of shielding the larger glass aggregate particles from undergoing ASR at early ages. Beyond 7 days in the case of GLP-10 mortar bars and beyond 14 days in the case of GLP-20 and GLP-30 mortar bars, a significant onset of expansion was observed as seen in Figure 6-5. The later age expansion in these mortar bars is likely due to the continued reaction of the large glass particles with the alkalis supplied by the external soak solution, whose migration into the mortar bar is unhindered as the GLP particles would have completely reacted before 14 days and lose any ability to trap the alkalis.

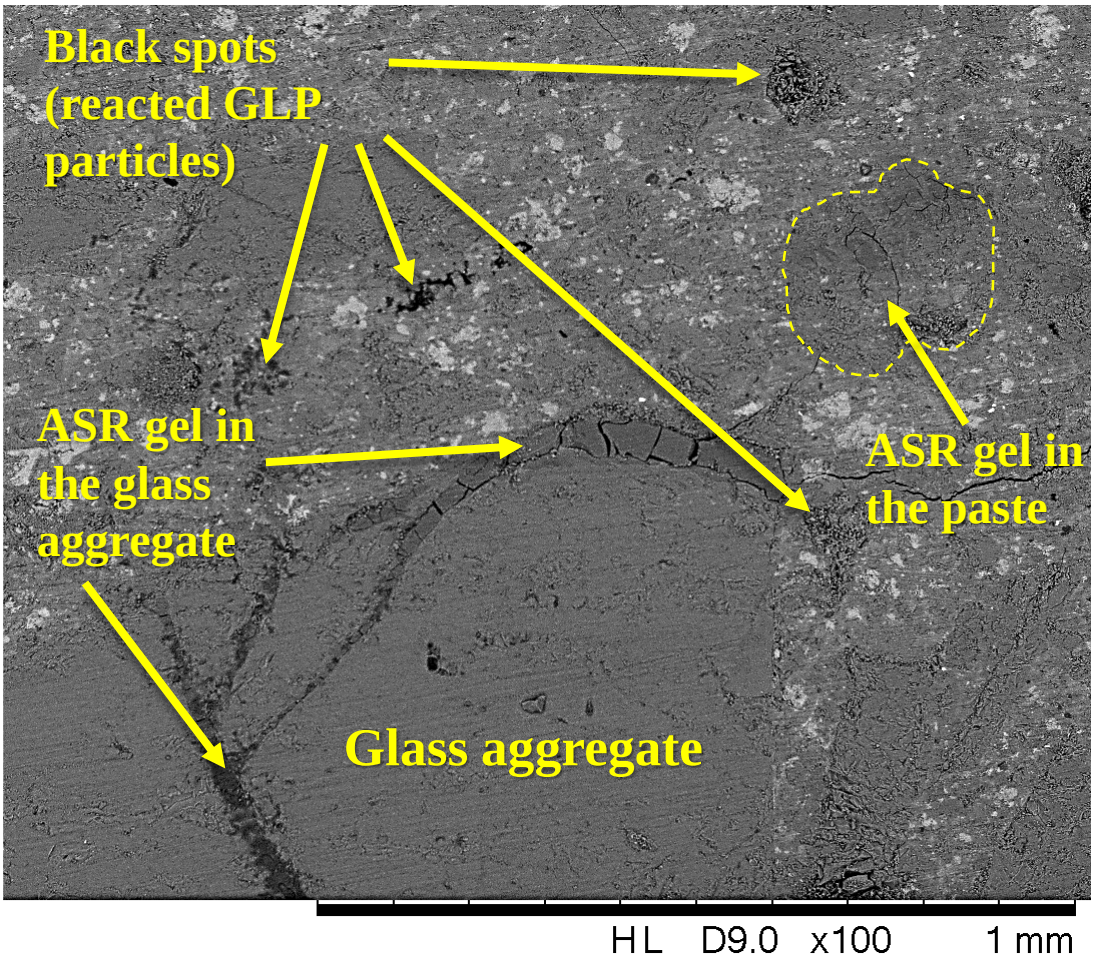


Figure 6-8. SEM image from GLP-30 mortar bar section

The SEM images of polished sections of MK-10 and GGF-30 samples are shown in Figure 6-9a and Figure 6-9b, respectively. In the cases of meta-kaolin and GGF containing mortar bars, no significant cracking was observed either in the paste or in the glass aggregate particles. It can be observed in Figure 6-9a and Figure 6-9b that the glass aggregate particles did not show any distress within themselves in the form of cracking or presence of ASR gel, either inside or at the interface between glass aggregate particles and the paste. The effectiveness of meta-kaolin and GGF in mitigating ASR in mortar bars is discussed in section 6.3.3.4.

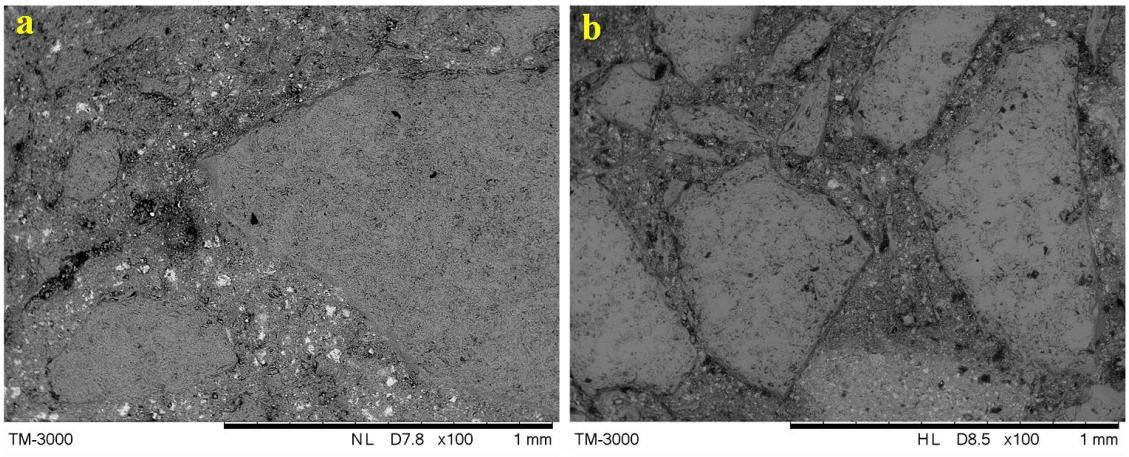


Figure 6-9. SEM images from mortar bar section a) MK-10 and b) GGF-30

#### 6.3.3.4 *Effectiveness of GGF and meta-kaolin in mitigation of ASR damage*

Although replacement of cement with GLP reduced the ASR-related expansion in mortar bars and concrete prisms at all replacement levels evaluated in this study even at a dosage of 30% replacement level, GLP was unable to control the expansions of test specimens below the prescribed limits. However, GGF containing mixtures showed a significant reduction in the expansion of mortar and concrete specimens at all dosage levels, and particularly at high enough dosage levels (i.e. 20% and 30% replacement levels) was able to completely mitigate the expansions to levels below the required limits. While the use of 10% dosage level of meta-kaolin was effective in reducing the mortar bar expansions below the prescribed expansion limit in ASTM C1567 test, this dosage level was found to be not adequate in mitigating expansion of concrete prisms to below 0.02% at 56 days. However, due to the lack of adequate workability in mixtures containing high dosages of meta-kaolin (i.e. 20%), replacement of cement with meta-kaolin beyond 10% was found to be impractical and hence no additional miniature concrete prism tests were conducted at higher dosage levels of meta-kaolin. Unlike meta-kaolin, increase in GGF dosage in mortars and concrete mixtures, even up to 30% cement replacement level, did not negatively affect the workability and therefore, test specimens could be easily fabricated and

handled. Based on the results of mortar bar and concrete prism tests, the best performance of all mixtures was seen in the case of mixtures containing GGF at 20% and 30% dosage levels. The good performance of the GGF containing mixtures in mitigating ASR-related expansion could be explained by the following mechanisms:

*Reduction in the level of calcium hydroxide:* TGA results shown in Figure 6-4 present the relative efficiency of each SCMs in reducing the amount of the calcium hydroxide, which is one of the key factors in the promotion of expansion due to ASR. The ASR gel that forms at early stages of the reaction is highly alkaline, having little to no calcium in its structure, and has a low viscosity. (39-42) However, with continued formation of ASR gel, alkalinity of the pore solution progressively decreases causes increase in dissolution of calcium from calcium hydroxide into the pore solution. The interaction of the ASR gel with the calcium in pore solution calcifies the low-viscosity ASR gel and converts it into a higher viscosity gel that is dense and is of low permeability (42, 43). Whether the calcified ASR gel at the periphery of the ASR gel mass generates higher levels of stress upon absorption of moisture or whether it acts as a barrier around the low-viscosity ASR gel present within the confines of the reacted glass aggregate particle, causing osmotic stresses to build up the internal pressure and cause cracking is not clear at the present time. Regardless, the addition of GGF as an SCM, which has a high amount of silica can reduce the calcium hydroxide level in the paste due to pozzolanic reactivity and dilution. The TGA results showed that the calcium hydroxide content of the GGF-30 paste was equal to the 63% and 53% of the calcium hydroxide content of the control mixture after 28 and 56 days respectively.

*Effect of alumina in reducing ASR:* Presence of alumina in SCMs is known to increases the resistance of the mixture against the ASR damages (44, 45). Two suggested mechanisms for the role of alumina in the reduction of ASR damage are: (i) formation of C-A-S-H gel which

binds higher amount of alkali in comparison to C-S-H gel (46) and (ii) reduction in the rate of dissolution of silica from the reactive aggregates (47). Regardless of the mechanism by which alumina plays its role, the higher amount of Al was seen in the paste matrix of MK-10 and GGF-30 in comparison to the CTRL and GLP-30 samples. The EDX results, performed on at least three points of the paste of each mixture showed the Al atomic weight percent of 9.86%, 7.21% for MK-10 and GGF-30 samples, respectively. The atomic weight percent of Al in the paste portion of the CTRL and GLP-30 samples was 2.66% and 2.63%, respectively.

The EDX results for sodium and potassium content of the paste portion of the mortar bars tested in ASTM C1567 test for 28 days are shown in Table 6-3. From these results, it can be seen that while the amount of sodium is almost in the same range for all test specimens (i.e. 8% to 9%), the amount of potassium varied significantly across the test specimens. The rather uniform level of sodium in the paste across the test specimens is likely caused by the flooding of the paste with external sodium hydroxide soak solution. The results showed that amount (atomic weight percent) of potassium in the paste of CTRL and GLP-30 specimens was 0.16% and 0.31%, respectively, which is significantly lower than 3.05% and 2.53% observed for MK-10 and GGF-30 mixtures, respectively. The higher amount of bound potassium in MK-10 and GGF-30 signifies the higher binding capacity of alkalis in the paste matrix of these mixtures. The slightly higher amount of bound potassium observed in MK-10 test specimen compared to GGF-30, is thought to be related to two factors. Firstly, meta-kaolin does contain higher amount of potassium than any of the cementitious materials used in this study. Although the alkali levels of meta-kaolin were not measured in this study, literature indicates potassium oxide levels in meta-kaolin range between 2.5% and 3.5% (37). Secondly, MK-10 mixture has 20% more cement compared to GGF-30 mixture. The principal alkali present in portland cement being potassium, it is likely that the MK-10 mixture with 90% cement in its binder has a larger source of potassium and can be

absorbed by the C-A-S-H gel produced in MK-10 specimens. It should be noted again, that due to the poor workability of the mixture containing meta-kaolin, addition of MK to mixtures at dosage levels higher than 10% is not considered to be practical.

Table 6-3. Average sodium and potassium content in the paste portion of AMBT samples

| Sample ID | CTRL | GLP-30 | GGF-30 | MK-10 |
|---|---|---|---|---|
| Na (atomic %) | 9.12% | 8.43% | 8.48% | 9.22% |
| K (atomic %) | 0.16% | 0.31% | 2.53% | 3.05% |

## 6.4 Conclusion

In this study, the effectiveness of ground glass fiber (GGF) was compared with ground glass powder (GLP) and meta-kaolin (MK) in mitigating ASR distress in mortar and concrete. Also, the flow characteristics of the fresh mortar mixtures (with or without SCMs) and the pozzolanic reactivity of these mixtures (at 28 days) were investigated. The following conclusions are drawn based on the research conducted in this investigation:

1) Mixtures containing either GGF or GLP showed better workability based on flow measurements compared to control mixture or mixture containing MK, at all dosage levels of supplementary cementitious materials considered in this study.
2) Mixtures containing GLP, GGF and MK showed a strength-activity index greater than 75% at 28 days; although increasing dosage of GLP from 10% to 30% cement replacement level reduced the strength-activity index values. In contrast, test specimens containing GGF and MK exceeded 100% at all dosage levels evaluated and performed better than the control mixture.
3) Based on ASTM C1567 tests conducted to evaluate ASR mitigation efficiency of these SCMs using reactive crushed glass aggregate, it can be concluded that:
    a. GGF was effective in reducing the mortar bars expansions to below 0.10% at 14 days at

10%, 20% and 30% cement replacement levels. In addition, the expansion levels of these mortar bars remained below 0.10% even at 28 days in the test at all cement replacement levels.

b. GLP was found to be ineffective in reducing the mortar bar expansions to below 0.10% at 14 days, at 10%, 20% and 30% cement replacement levels.

c. MK was found to be effective at 10% cement replacement level to reduce the expansion of mortar bars to below 0.10% at 14 days. However, a considerable increase in expansion was observed between 14 and 28 days.

4) Based on the Miniature Concrete Prism Test with a crushed glass aggregate as the reactive aggregate, to evaluate the ASR mitigation effectiveness of SCMs, it can be concluded that:

a. The use of GGF at 20% and 30% cement replacement level was effective in reducing concrete prism expansion to below 0.02% at 56 days. However, GGF at 10% replacement level was not effective.

b. GLP was found to be ineffective in mitigating expansion in concrete prisms to below 0.02% at 56 days, at 10%, 20% and 30% cement replacement levels.

c. The use of MK at 10% was found to be ineffective in reducing the concrete prism expansion to below 0.02% at 56 days; however, the performance of MK at 10% was significantly better than GLP, regardless of its dosage.

1) Microstructural observations on polished sections of mortar bars subjected to ASTM C1567 tests showed that in mixtures that were highly susceptible to ASR (i.e. CTRL and GLP-30), significant cracking in the glass aggregate particles could be observed with extensive amount of ASR gel filling the cracks. However, in mixtures that were effective against ASR (i.e. GGF-30 and MK-10), the glass aggregate particles showed no cracking and no deposits of ASR gel could be observed.

## Reference


1. U.S. Environmental Protection Agency Office of Resource Conservation and Recovery. (2015). Advancing Sustainable Materials Management: Fact and Figures 2013.
2. Topcu, I. B., & Canbaz, M. (2004). Properties of concrete containing waste glass. Cement and Concrete Research, 34(2), 267-274.
3. Shi, C., & Zheng, K. (2007). A review on the use of waste glasses in the production of cement and concrete. Resources, Conservation and Recycling, 52(2), 234-247.
4. Park, S. B., Lee, B. C., & Kim, J. H. (2004). Studies on mechanical properties of concrete containing waste glass aggregate. Cement and concrete research, 34(12), 2181-2189.
5. Adaway, M., & Wang, Y. (2015). Recycled glass as a partial replacement for fine aggregate in structural concrete–Effects on compressive strength. Electronic Journal of Structural Engineering, 14(1), 116-122.
6. Meyer, C., Egosi, N., & Andela, C. (2001, March). Concrete with waste glass as aggregate. In Proceedings of the international symposium concrete technology unit of ASCE and University of Dundee, Dundee (pp. 179-87).
7. Jin, W., Meyer, C., & Baxter, S. (2000). "Glascrete"-Concrete with Glass Aggregate. ACI Materials Journal, 97(2), 208-213.
8. Topçu, İ. B., Boğa, A. R., & Bilir, T. (2008). Alkali–silica reactions of mortars produced by using waste glass as fine aggregate and admixtures such as fly ash and Li 2 CO 3. Waste Management, 28(5), 878-884.
9. Cota, F. P., Melo, C. C. D., Panzera, T. H., Araújo, A. G., Borges, P. H. R., & Scarpa, F. (2015). Mechanical properties and ASR evaluation of concrete tiles with waste glass aggregate. Sustainable Cities and Society, 16, 49-56.
10. Limbachiya, M. C. (2009). Bulk engineering and durability properties of washed glass sand

concrete. Construction and Building Materials, 23(2), 1078-1083.

11. Shayan, A., & Xu, A. (2004). Value-added utilisation of waste glass in concrete. Cement and concrete research, 34(1), 81-89.
12. Lam, C. S., Poon, C. S., & Chan, D. (2007). Enhancing the performance of pre-cast concrete blocks by incorporating waste glass–ASR consideration. Cement and Concrete Composites, 29(8), 616-625.
13. Maraghechi, H., Fischer, G., & Rajabipour, F. (2012). The role of residual cracks on alkali silica reactivity of recycled glass aggregates. Cement and Concrete Composites, 34(1), 41-47.
14. Taha, B., & Nounu, G. (2008). Properties of concrete contains mixed colour waste recycled glass as sand and cement replacement. Construction and Building Materials, 22(5), 713-720.
15. Shafaatian, S. M., Akhavan, A., Maraghechi, H., & Rajabipour, F. (2013). How does fly ash mitigate alkali–silica reaction (ASR) in accelerated mortar bar test (ASTM C1567)?. Cement and Concrete Composites, 37, 143-153.
16. Dhir, R. K., Dyer, T. D., & Tang, M. C. (2009). Alkali-silica reaction in concrete containing glass. Materials and structures, 42(10), 1451-1462.
17. Schwarz, N., Cam, H., & Neithalath, N. (2008). Influence of a fine glass powder on the durability characteristics of concrete and its comparison to fly ash. Cement and Concrete Composites, 30(6), 486-496.
18. Lee, G., Ling, T. C., Wong, Y. L., & Poon, C. S. (2011). Effects of crushed glass cullet sizes, casting methods and pozzolanic materials on ASR of concrete blocks. Construction and Building Materials, 25(5), 2611-2618.
19. Afshinnia, K., & Rangaraju, P. R. (2015). Efficiency of ternary blends containing fine glass powder in mitigating alkali–silica reaction. Construction and Building Materials, 100, 234-245.

20. Omran, A., & Tagnit-Hamou, A. (2016). Performance of glass-powder concrete in field applications. Construction and Building Materials, 109, 84-95.
21. Khmiri, A., Samet, B., & Chaabouni, M. (2012). A cross mixture design to optimise the formulation of a ground waste glass blended cement. Construction and Building Materials, 28(1), 680-686.
22. Jang, H., Jeon, S., So, H., & So, S. (2015). Properties of different particle size of recycled TFT-LCD waste glass powder as a cement concrete binder. International Journal of Precision Engineering and Manufacturing, 16(12), 2591-2597.
23. Parghi, A., & Alam, M. S. (2016). Physical and mechanical properties of cementitious composites containing recycled glass powder (RGP) and styrene butadiene rubber (SBR). Construction and Building Materials, 104, 34-43.
24. Afshinnia, K., & Rangaraju, P. R. (2015). Influence of fineness of ground recycled glass on mitigation of alkali–silica reaction in mortars. Construction and Building Materials, 81, 257-267.
25. Zheng, K. (2016). Pozzolanic reaction of glass powder and its role in controlling alkali-silica reaction. Cement and Concrete Composites, 67, 30-38.
26. Dyer, T. D., & Dhir, R. K. (2001). Chemical reactions of glass cullet used as cement component. Journal of Materials in Civil Engineering, 13(6), 412-417.
27. Afshinnia, K., & Rangaraju, P. R. (2015). Mitigating alkali–silica reaction in concrete: Effectiveness of ground glass powder from recycled glass. Journal of the Transportation Research Board, (2508), 65-72
28. Liu, S., Wang, S., Tang, W., Hu, N., & Wei, J. (2015). Inhibitory effect of waste glass powder on ASR expansion induced by waste glass aggregate. Materials, 8(10), 6849-6862.
29. Hemmings, R. T. (2005). Process for Converting Waste Glass Fiber into Value Added

Products, Final Report (No. DOE GO13015-1). Albacem LLC.

30. Chen, C. H., Huang, R., Wu, J. K., & Yang, C. C. (2006). Waste E-glass particles used in cementitious mixtures. Cement and Concrete Research, 36(3), 449-456.
31. Hossain, A., Shirazi, S., Persun, J., & Neithalath, N. (2008). Properties of concrete containing vitreous calcium aluminosilicate pozzolan. Transportation Research Record: Journal of the Transportation Research Board, (2070), 32-38.
32. Neithalath, N., Persun, J., & Hossain, A. (2009). Hydration in high-performance cementitious systems containing vitreous calcium aluminosilicate or silica fume. Cement and Concrete Research, 39(6), 473-481.
33. Kamali, M., & Ghahremaninezhad, A. (2016). An investigation into the hydration and microstructure of cement pastes modified with glass powders. Construction and Building Materials, 112, 915-924.
34. Tashima, M. M., Soriano, L., Payá, J., Monzó, J., & Borrachero, M. V. (2016). Assessment of pozzolanic/hydraulic reactivity of vitreous calcium aluminosilicate (VCAS). Materials & Design, 96, 424-430.
35. Rangaraju, P. R., Rashidian-Dezfouli, H., Nameni G., Amekuedi, G. (2016). Properties and Performance of Ground Glass Fiber as a Pozzolan in Portland Cement Concrete. Proceedings of the International Concrete Sustainability Conference, Washington DC 2016.
36. Rashidian-Dezfouli, H., & Rangaraju, P. R. (in press). Role of Ground Glass Fiber as A SCM in Improving Selected Properties of Portland Cement Concrete (No. 17-04237).
37. Velosa, A. L., Rocha, F., & Veiga, R. (2009). Influence of chemical and mineralogical composition of metakaolin on mortar characteristics. Acta Geodynamica et Geomaterialia, 153(6), 121-126.
38. Pane, I., & Hansen, W. (2005). Investigation of blended cement hydration by isothermal

calorimetry and thermal analysis. Cement and Concrete Research, 35(6), 1155-1164.

39. Bleszynski, R. F., & Thomas, M. D. (1998). Microstructural studies of alkali-silica reaction in fly ash concrete immersed in alkaline solutions. Advanced Cement Based Materials, 7(2), 66-78.
40. Urhan, S. (1987). Alkali silica and pozzolanic reactions in concrete. Part 1: Interpretation of published results and an hypothesis concerning the mechanism. Cement and concrete research, 17(1), 141-152.
41. Lindgård, J., Andiç-Çakır, Ö., Fernandes, I., Rønning, T. F., & Thomas, M. D. (2012). Alkali–silica reactions (ASR): literature review on parameters influencing laboratory performance testing. Cement and Concrete Research, 42(2), 223-243.
42. Detwiler, R. (1997). The Role of Fly Ash Composition in Reducing Alkali-Silica Reaction. Portland Cement Association.
43. Taylor, H. F. W. Cement Chemistry, Academic Press, London, 1990.
44. Duchesne, J., & Bérubé, M. A. (2001). Long-term effectiveness of supplementary cementing materials against alkali–silica reaction. Cement and concrete research, 31(7), 1057-1063.
45. Ramlochan, T., Zacarias, P., Thomas, M. D. A., & Hooton, R. D. (2003). The effect of pozzolans and slag on the expansion of mortars cured at elevated temperature: Part I: Expansive behaviour. Cement and Concrete Research, 33(6), 807-814.
46. Hong, S. Y., & Glasser, F. P. (2002). Alkali sorption by CSH and CASH gels: Part II. Role of alumina. Cement and Concrete Research, 32(7), 1101-1111.
47. Chappex, T., & Scrivener, K. L. (2012). The influence of aluminium on the dissolution of amorphous silica and its relation to alkali silica reaction. Cement and Concrete Research, 42(12), 1645-1649.

# CHAPTER 7

# COMPARISON OF STRENGTH AND DURABILITY CHARACTERISTICS OF A GEOPOLYMER PRODUCED FROM FLY ASH, GROUND GLASS FIBER AND GLASS POWDER[1]

## 7.1 Introduction

Each year, a large amount of glass fiber is produced around the world for use in various applications. However, this process generates hundreds of thousands of tons of waste glass fiber. It has been reported that, in the U.S., around 250,000 to 500,000 tons of waste glass fiber end-up in landfills each year (1). This waste material is rich in silica, alumina, and calcium and if ground to a fine powder, might potentially be used as supplementary cementitious material (SCM) or as a precursor for production of geopolymer. Chen et al. (2) studied the utilization of waste E-glass (the most commonly used type of fiber glass) as cement replacement material. In addition, a number of studies were also conducted on the utilization of vitreous calcium aluminosilicate (which is a commercially produced pozzolan made from by-products of fiber glass) as cement replacement material (3, 4) or as a precursor for geopolymer production (5, 6).

So far, a large number of waste or industrial by-product materials have been studied as precursors to produce geopolymer concrete. Among them, fly-ash, slag, and meta-kaolin and their combinations are the most widely used materials (7-14). In addition, other materials like kaolinite and albite (15), waste paper sludge ash (16), palm oil fuel Ash (17), spent fluid catalytic cracking

[1] Hassan Rashidian-Dezfouli and Prasada Rao Rangaraju (in press). Comparison of Strength and Durability Characteristics of a Geopolymer produced from Fly ash, Ground Glass Fiber and Glass Powder. Journal of Material de construction.

catalyst (18), waste glass-powder (19), blends of clay and fly ash (20), a combination of fly ash and anhydrous borax (21), and combination of natural pozzolan and slag (22) were studied by other authors. Thus far, no studies have been conducted on the use of GGF in geopolymer systems.

Earlier studies, performed mostly on fly-ash or metakaolin based geopolymer mixtures, have revealed some of the important parameters that affect the mechanical properties of final geopolymer products. It has been reported that parameters, such as type and concentration of the alkali solution (23, 24), ratio of $SiO_2/Na_2O$ in the alkali activator solution (24, 26), availability of calcium compounds (10, 27, 28), extent of dissolution of precursors in an alkali media (15, 29), and the molar ratio of Si:Al in the final product (30-32) are parameters that can affect mechanical properties of final geopolymer products.

Several studies have also been conducted on durability aspects of geopolymers. Considering the high amount of alkali present in geopolymers, the potential for Alkali Silica Reaction (ASR) in aggregates used in geopolymers has always been a big concern. Susceptibility of fly ash-based geopolymer mixtures to ASR have been studied in several works (33-37). Results of these studies showed a better ASR-resistance of geopolymer mixtures in comparison to a portland cement based mixture. The better performance of geopolymer mixtures in reduction of ASR-related expansion has been attributed to: lower calcium content of the geopolymer paste in comparison to portland cement based mixtures (33, 35, 36), further geopolymerisation of geopolymer mixtures in the ASR-test condition (33, 34, 36), and the higher amount of total porosity (with smaller pore diameter) of the geopolymer paste in comparison to portland cement paste (37).

In this study, the activation process for three different materials, i.e. class F fly ash, Ground Glass Fiber (GGF), and ground bottle glass in a powder form, was investigated. The

activators used in this study were combinations of NaOH and $Na_2SiO_3$ solutions in various concentrations and proportions of activators. In addition, accelerated curing for 24 h at 60°C was used in this study for all the mixtures evaluated.

The first objective of this study was to investigate the effect of using different dosages of activator as measured by the mass ratio of $Na_2O$-to-binder and the ratio of sodium hydroxide and sodium silicate in the activator solution as measured by $Si_2O/Na_2O$ mass ratio on workability and compressive strength of the geopolymer concretes. The second objective of this study was to evaluate the performance of mixtures that resulted in the highest compressive strength under the first objective to determine their resistance to ASR.

## 7.2 EXPERIMENTAL PROCEDURE

### *7.2.1 Materials*

The materials used in this study were:

a. Alumino-siliceous precursors for geopolymers including GGF, class F fly ash and glass powder with average particle size of 4, 28 and 17 microns, respectively.
b. For conducting comparative studies with for portland cement mixtures an ASTM C150 (38) Type I cement was selected.
c. Locally available siliceous river sand with oven-dry specific gravity of 2.67 and absorption of 0.30% was used as a fine aggregate in preparing the mortar mixtures. Reactive rhyolitic gravel from Las Placitas gravel pit was used in studies related to ASR mitigation.
d. The alkali activators used in this study were 40% sodium-silicate solution ($SiO_2/Na_2O$=3, weight ratio) and anhydrous NaOH pellets.

The GGF used in this study is a fine white powder produced by grinding waste fiber glass. The fly ash in this study is a Class F fly ash obtained from a local source. The glass powder

was obtained from finely ground recycled glass bottles. Basic physical properties and chemical composition of the precursors can be seen in Table 7-1 and Table 7-2, respectively. In addition, the XRD pattern of the cementitious materials that were used in this study are presented in Figure 7-1.

Table 7-1. Basic properties of the precursors

| Material | Specific Gravity | Amount Passing #325 Sieve (%) | Loss On Ignition | Blaine's fineness ($cm^2/g$) |
|---|---|---|---|---|
| GGF | 2.6 | 96% | 1.0% | 10200 |
| Fly ash | 2.25 | 76% | 2.3% | 6040 |
| Glass Powder | 2.4 | 83% | 1.5% | 5920 |
| Cement | 3.15 | 98% | 2.6% | 4720 |

Table 7-2. Chemical composition of the precursors

| | $SiO_2$ | $Al_2O_3$ | $Fe_2O_3$ | $CaO$ | $MgO$ | $Na_2O$ | $K_2O$ |
|---|---|---|---|---|---|---|---|
| GGF (%) | 47.72 | 10.36 | 0.34 | 19.62 | 2.27 | 0.67 | 0.1 |
| Fly Ash (%) | 50.7 | 25.1 | 12.5 | 3.3 | 1.1 | 0.51 | 2.27 |
| Glass Powder | 69.6 | 2.2 | 0.9 | 11.6 | 0.4 | 12.03 | 0.4 |
| Cement (%) | 19.93 | 4.77 | 3.13 | 62.27 | 2.7 | 0.06 | 0.48 |

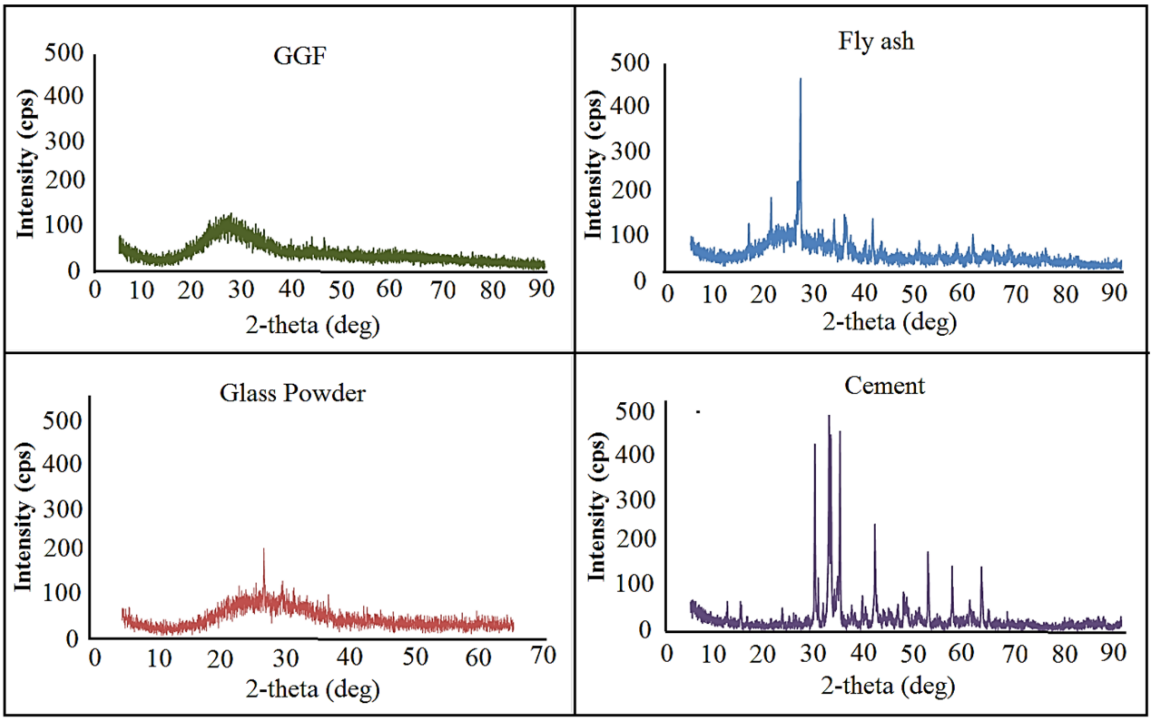


Figure 7-1. XRD pattern of the cementitious materials: GGF (top left), Fly ash (top right), Glass-powder (bottom left) and Cement (bottom right)

### *7.2.2 Mixture Proportions*

Effect of the relative proportion of the two activators (sodium silicate and sodium hydroxide) on the fresh and hardened properties of geopolymers was studied by changing two parameters. Firstly, the mass ratio of total $Na_2O$-to-binder at three different levels – 5%, 7.5% and 10% – was used. Secondly, the mass ratio of $SiO_2/Na_2O$ at three levels – 0, 0.50 and 1.00 – was used. In all the mixtures, the sand content was selected to fill 55% of the total volume, and the water-to-binder ratio was maintained between 0.30 and 0.35. This range was chosen to get the highest possible strength while the mixtures were workable without the need for any water reducers. The details of the test plan are presented in Table 7-3.

Table 7-3. Mixture proportions

| | | | | | | | | |
|---|---|---|---|---|---|---|---|---|
| GGF | Mix ID | GGF-0-10 | GGF-0.5-5 | GGF-0.5-7.5 | GGF-0.5-10 | GGF-1-5 | GGF-1-7.5 | GGF-1-10 |
| | $Na_2O$/Binder (%) | 10 | 5 | 7.5 | 10 | 5 | 7.5 | 10 |
| | $SiO_2/Na_2O$ | 0 | 0.5 | 0.5 | 0.5 | 1 | 1 | 1 |
| | W/Binder | 0.33 | 0.33 | 0.33 | 0.33 | 0.33 | 0.33 | 0.33 |
| Fly-ash | Mix ID | F-0-10 | F-0.5-5 | F-0.5-7.5 | F-0.5-10 | F-1-5 | F-1-7.5 | F-1-10 |
| | $Na_2O$/Binder (%) | 10 | 5 | 7.5 | 10 | 5 | 7.5 | 10 |
| | $SiO_2/Na_2O$ | 0 | 0.5 | 0.5 | 0.5 | 1 | 1 | 1 |
| | W/Binder | 0.3 | 0.3 | 0.3 | 0.3 | 0.3 | 0.3 | 0.3 |
| Glass-Powder | Mix ID | GLP-0-3 | GLP-0.5-5 | GLP-0.5-7.5 | GLP-0.5-10 | GLP-1-5 | GLP-1-7.5 | GLP-1-10 |
| | W/Binder | 10 | 10 | 7.5 | 5 | 10 | 7.5 | 5 |
| | $SiO_2/Na_2O$ | 0 | 0.5 | 0.5 | 0.5 | 1 | 1 | 1 |
| | $Na_2O$/Binder (%) | 0.35 | 0.35 | 0.35 | 0.35 | 0.35 | 0.35 | 0.35 |

### *7.2.3 Flow test and compressive strength*

The water-to-binder ratio employed in geopolymer mixtures is generally between 0.20-0.40 which is lower than the normal water-to-binder ratios used in conventional portland cement concrete and mortar. To examine the effect of different precursors and the chemical ratios (alkali-to-binder ratio and $SiO_2/Na_2O$) on the flowability of the geopolymer mixtures, flow test (ASTM C1437) (39) was done on each of the blends. To evaluate the compressive strength, 50×50 x 50 mm mortar cubes were cast. The mixing procedure began with dissolving required amount of NaOH in water. The sodium-silicate solution was then added, and mixing process continued until all the NaOH pellets were completely dissolved. Immediately after the dissolution of all NaOH pellets, the precursor was added to the solution and mixed for 1 additional minute. Lastly, the fine aggregate was introduced into the mixer and mixing process continued until uniform mix was achieved. The material was then placed in the cube molds and transferred to a 60°C chamber for a 24-hour period of heat curing. After 24 hours, cubes were removed from molds and placed inside an environmental chamber, maintained at 23°C temperature and 50% relative humidity, until the time of testing. The compressive strength was measured at 3, 7 and 28 days following the ASTM C109 (40) procedure. Additional mortar prisms were also cast to investigate the microstructure using scanning electron microscopy (SEM).

### *7.2.4 Dissolution of paste in HCl acid solution*

In this study, HCl solution is used to find the amount of unreacted GGF particles of geopolymer mixtures. This solution is known to dissolve the geopolymer structure and leave the unreacted precursor particles behind (41, 42). In this study, following Palomo et al (42), dissolution of selected paste were studied in a 1:20 HCl solution (i.e. 50 ml of 1N HCl solution in 1000 ml water). Geopolymer paste was crushed to a fine powder and the amount passing sieve #100 and retaining #200 sieved was selected for the test. To perform the test, 2 grams of the paste powder

was introduced into 500 ml of HCl solution and the solution was mixed for 3 h using a magnetic stirrer. The solution then was filtered using 1.5 µm filter paper. The residue was dried at 110°C for 24 hours, then weighed and recorded.

### *7.2.5 Extent of dissolution*

Solubility of raw material in high alkali media was determined by mixing 5 grams of each precursor in 100 ml of 5N NaOH solution. Solutions were mixed for 2 hr. at ambient temperature using a magnetic stirrer. The solution was filtered using micro fiber filters and then diluted to 1:100 using deionized water. Inductively coupled plasma (ICP) test was performed to analyze the filtered solution. The concentration of soluble Si, Al, Ca and Fe was measured for the diluted solution. The results were then back-calculated for the original concentration of the dissolved elements in the 5N NaOH solution.

### *7.2.6 Alkali-silica reactivity of aggregates in geopolymers*

Accelerated mortar bar test using ASTM C1260 (43) procedure was followed to study the ASR behavior in geopolymer mortar specimens. A known alkali-silica-reactive aggregate, Las Placitas gravel from New-Mexico, was crushed to meet the gradation requirements of ASTM C1260 and was used as the fine aggregate in all the mixtures. Following the ASTM C1260 procedure, the binder-to-aggregate ratio was selected such that for 1 part by weight of dry source-materials (i.e. GGF, fly ash or glass-powder), 2.25 parts by weight for the crushed aggregate by mass were used.

In this study, ASTM C1260 test was used, realizing that even though the test is being run on geopolymer mortars rather than portland cement mortars, as no suitable test method is presently available to evaluate ASR behavior of aggregates in geopolymers. The binder portion of the geopolymer test specimens followed the proportions given in Table 7-3. Same mixing and curing procedure as described in section 7.2.3 were followed in preparing the mortar prisms for ASR study. The specimens were removed after 24 h in 60°C environment and submerged in water

at 80ºC for addition 24 h. Finally, the mortar bars were immersed in 1N NaOH solution and kept in 80ºC oven for the remaining duration of the test. The length change in the mortar bars was monitored up to 28 days after submerging in the solution. The ASR performance of geopolymer samples was compared with that of portland cement mortar samples with a water/cement ratio of 0.35 and same content of aggregate in the mixture as in the case of geopolymer samples. It should be noted that portland cement mixture had gone through identical curing procedure, 24 h in 60ºC followed by ambient curing (23ºC and 50% RH), as geopolymer samples for the purposes of this investigation.

## 7.3 RESULTS AND DISCUSSION

### *7.3.1 Flow test*

Figure 7-2 shows the flow results of geopolymer samples. As it can be seen, GGF-based geopolymer mortar showed the highest flow while glass powder-based geopolymer mortar had the lowest flow. The workability of fresh geopolymer mixtures has been reported to vary with the change in the alkali content of the solution as well as its $SiO_2/Na_2O$ ratio (44-46). According to these studies, increase in Na concentration and $SiO_2/Na_2O$ ratio will reduce the workability of the mixture. In the present study, however, increase in the alkali content of the activator solution from 5 to 10% ($Na_2O$-to-binder mass ratio) did not seem to have a considerable effect on the flow results of fly ash and GGF-based mixtures but caused improvement in the workability of glass-powder-based mixtures. On the other hand, increase in $SiO_2/Na_2O$ ratio showed a clear improvement in the workability of the mixtures, which is in agreement with the earlier mentioned studies.

The main mechanism by which increase in $SiO_2/Na_2O$ ratio improved the workability is thought to be related to the mixing procedure that was followed in this study. As presented in section 7.2.3, the first step of the mixing procedure was to dissolve NaOH pellets in the required

amount of water, which is followed by the addition of the precursors. The dissolution of NaOH pellets is an exothermic reaction and increases the temperature of the mixture which lowers the workability. However, addition of soluble Si was done by using pre-mixed sodium silicate (ambient temperature), and therefore, cooling the mixture. The lower temperature of the mixture with higher $SiO_2/Na_2O$ ratio is thought to be the main reason for the better workability of these mixtures. A same observation has been also reported by (47), in which NaOH solution was not allowed to cool down.

It was also observed that GGF mixtures had the highest viscosity in the flow test (based on visual observation of the stickiness of the mixtures). The fly-ash based material, however, showed the lowest viscosity and was easier to work with. For mixtures with very low workability (Glass-powder based samples), a High Range Water Reducer (HRWR, MasterGlenium® 7500) was used to ensure an adequate flow for proper compaction of test specimens for other tests. The amount of HRWR was measured to be 1.5% of the weight of the glass-powder and no HRWR was needed for the GGF and fly ash-based geopolymer samples.

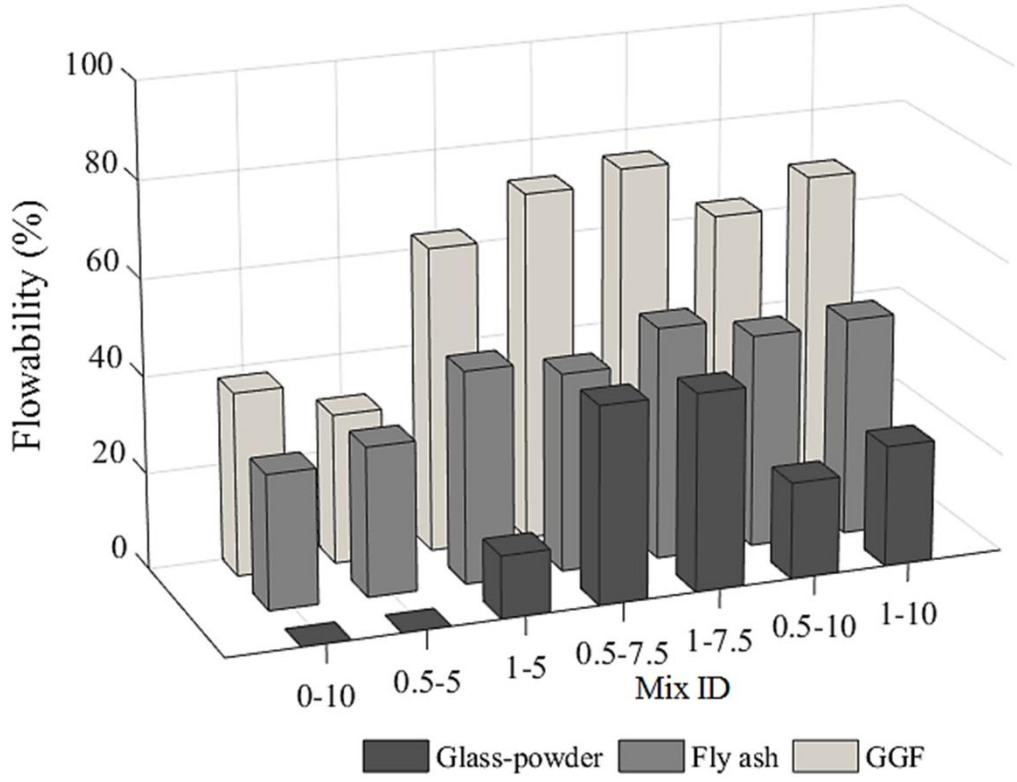


Figure 7-2. Flow results of geopolymer mortars

### *7.3.2 Compressive strength*

Compressive strength of geopolymer samples are presented in Table 7-4 and Figure 7-3. As it can be seen for all the precursors, compressive strength increases with an increase in the Na content of the mixture. At 28 days, the compressive strength of GGF samples having $SiO_2/(Na_2O)$=0.5 (GGF-0.5) and $SiO_2/(Na_2O)$=1.0 (GGF-1) showed an increase from 29 to 72 MPa and 28 to 67 MPa respectively, when the Na content of the mixture was increased from 5% to 10%. Similarly, the compressive strength of geopolymer samples containing fly ash having $SiO_2/(Na_2O)$=0.5 (F-0.5) and $SiO_2/(Na_2O)$=1.0 (F-1) showed an increase in compressive strength from less than 5 MPa to 46 MPa and 24 to 59 MPa, respectively, when the Na content of the mixture was increased from 5% to 10%.

Except for the glass-powder geopolymer mixture with $SiO_2/Na_2O$ = 0.5 and $Na_2O$ content

of 10% (GLP-0.5-10 sample), an almost similar trend as observed with GGF and fly ash can be seen in other geopolymers prepared with glass-powder. However, the difference in the compressive strength between glass powder-based geopolymer mixtures containing 7.5% and 10% $Na_2O$ content were smaller than observed with geopolymers prepared with other precursors. This could be attributed to the large amount of alkalis that are already present in glass-powder. It is assumed that glass particles release Na+ into the surrounding media and act as an internal source of alkalis, which reduces the effect of the external source of alkalis.

The effect of soluble Si content in the activator solution seems to be very important in fly ash and glass-powder-based geopolymer samples, while it is less significant in the case of GGF. In 28 day-old fly ash samples with 10% Na2O content, for $SiO_2/(Na_2O)$ ratios of 0, 0.5, and 1, the compressive strength values were 25, 46, and 59 MPa respectively. In the case of glass-powder samples, for $SiO_2/(Na_2O)$ ratios of 0, 0.5, and 1, the compressive strength values were 14, 33, and 43 MPa respectively. However, as can be seen, GGF samples do not follow this trend, and an increase in the $SiO_2/(Na_2O)$ ratio from 0 to 1 causes reduction in compressive strength from 82 MPa to 67 MPa. The highest strength observed was in the case of GGF-0-10, which has no Si in the activator solution.

Addition of soluble Si to mixtures also affects the rate of strength gain. Samples with larger Si content showed high early-age strengths (i.e. 3 days) and no significant improvement in the strength was observed at later ages, indicating much of the strength gain was achieved within the first 3 days. It was also seen that GGF samples had the highest compressive strength for all levels of activator dosage in comparison to fly ash and glass-powder-based geopolymer samples.

The higher compressive strength of GGF-0-10 specimens (with no added soluble silica) in comparison to GGF-0.5-10 and GGF-1-10 specimens (with silica-to-binder ratio of 5 and 10%) can be related to the lower level of unreacted GGF particles in GGF-0-10 specimens. Higher

amount of available soluble Si (from sodium silicate solution) is thought to reduce the solubility of the GGF particles in these mixtures and cause reduction in the compressive strength. To evaluate the amount of unreacted GGF particles in GGF-0-10 and GGF-1-10, two grams of paste from each of the mixtures were dissolved in an HCl solution using the method described in section 8.2.4. Results of this test are presented in Table 7-5. As it can be seen a higher amount of residue (unreacted GGF particles) was measured in GGF-1-10 paste specimens. Therefore, the better performance of GGF-0-10 specimens can be related to the higher level of GGF particles in this mixture.

Table 7-4.Compressive strength of geopolymer cubes (MPa)

| Precursor | | GGF | | | Fly ash | | | Glass-Powder | | |
|---|---|---|---|---|---|---|---|---|---|---|
| $Na_2O$/(Source-material), % | | 5 | 7.5 | 10 | 5 | 7.5 | 10 | 5 | 7.5 | 10 |
| Age | $SiO_2/Na_2O$ | Compressive Strength, MPa | | | | | | | | |
| 3 days | 0 | - | - | 79 | - | - | 14 | - | - | 7 |
| | 0.5 | 27 | 53 | 67 | NA | 16 | 35 | 7 | 22 | 19 |
| | 1 | 25 | 58 | 69 | 16 | 43 | 58 | 21 | 30 | 37 |
| 7 days | 0 | - | - | 78 | - | - | 20 | - | - | 11 |
| | 0.5 | 28 | 54 | 75 | NA | 17 | 36 | 9 | 32 | 22 |
| | 1 | 27 | 53 | 72 | 21 | 44 | 60 | 29 | 40 | 40 |
| 28 days | 0 | - | - | 82 | - | - | 25 | - | - | 14 |
| | 0.5 | 29 | 55 | 72 | NA | 22 | 46 | 16 | 28 | 33 |
| | 1 | 28 | 56 | 67 | 24 | 45 | 59 | 35 | 36 | 43 |

Table 7-5. Residue percent of GGF-0-10 and GGF-1-10 paste after dissolution in HCl solution

| Mix ID | Residue (weight %) |
|---|---|
| GGF-0-10 | 47 |
| GGF-1-10 | 55 |

Presence of Ca in geopolymer systems is known to accelerate the hardening process (27). It is thought that Ca+2 ions balance the negative charge associated with $Al(OH)^{4-}$ and leave more Na in the system, which further accelerates the geopolymerisation. Higher strength of GGF samples even with low Na content might be explained by the presence of Ca in the GGF matrix. Although other mechanisms such as the formation of calcium-silicate-hydrate and calcium-aluminum-silicate-hydrate, have been proposed by others (48), however, the study of the mechanisms by which calcium improves the compressive strength of the GGF geopolymer was not investigated in this study, which needs to be investigated in the future.

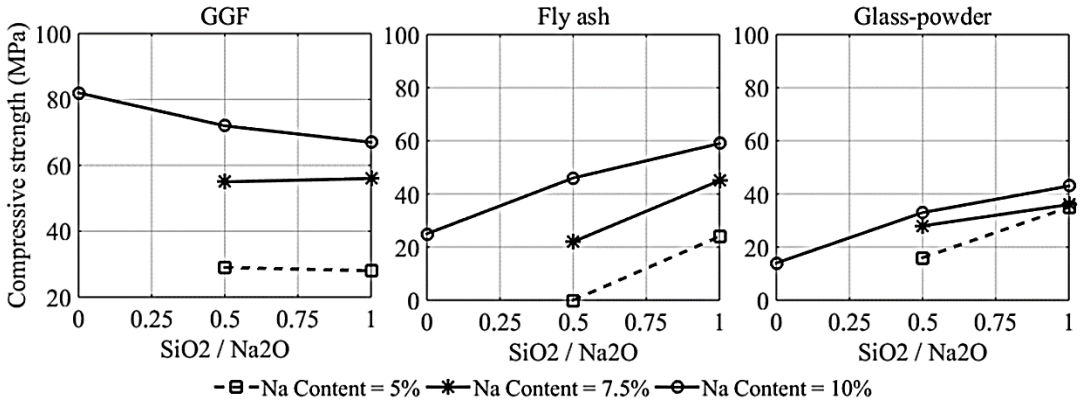


Figure 7-3. Change in the compressive strength of geopolymers mortar at 28 days due to the change in Na content and $SiO_2/Na_2O$

The solubility test was performed on all the precursors to measure the extent of dissolution of Si, Al and Ca in a high alkali solution of 5M NaOH solution (Table 7-6). As shown in this table, GGF releases a higher amount of Si and Ca in comparison to fly-ash, while they both produce a higher amount of Al in comparison to glass-powder. While the XRF result showed higher Al content in fly ash, the amount of dissolved Al for GGF was in the same range as the fly ash sample. Therefore, it could be concluded that, in comparison to GGF, Al in fly ash is bound more strongly, which could be attributed to the presence of mullite in fly ash.

The lower solubility of Si and Al in fly ash can be related to the presence of quartz and

mullite crystals. Mullite and quartz are known to be stable and do not easily dissolve in a high alkali solution (49, 50). As a result, compressive strength of the fly ash-based geopolymer can be affected by the presence of crystals of quartz and mullite in the fly ash particles. According to Temuujin and Van Riessen (51) presence of mullite in the fly ash lowers the reactivity of fly ash and decreases the level of geopolymerisation. In this study, the XRD test was conducted on virgin fly ash particles and F-1-10 geopolymer paste. The results showed that mullite and quartz peaks in fly ash specimens remain intact even after the reaction process (Figure 7-4), which can be attributed to the lower degree of geopolymerisation of the fly ash based geopolymer.

Table 7-6. Extent of the Dissolution of GGF, Fly ash and GLP in a High Alkali Media (5N NaOH Solution, for 2 h)

| Sample | Ca (ppm) | Al (ppm) | Si (ppm) |
|---|---|---|---|
| Fly ash | 315 | 141 | 748 |
| GGF | 696 | 142 | 1156 |
| Glass Powder | 816 | 28 | 724 |

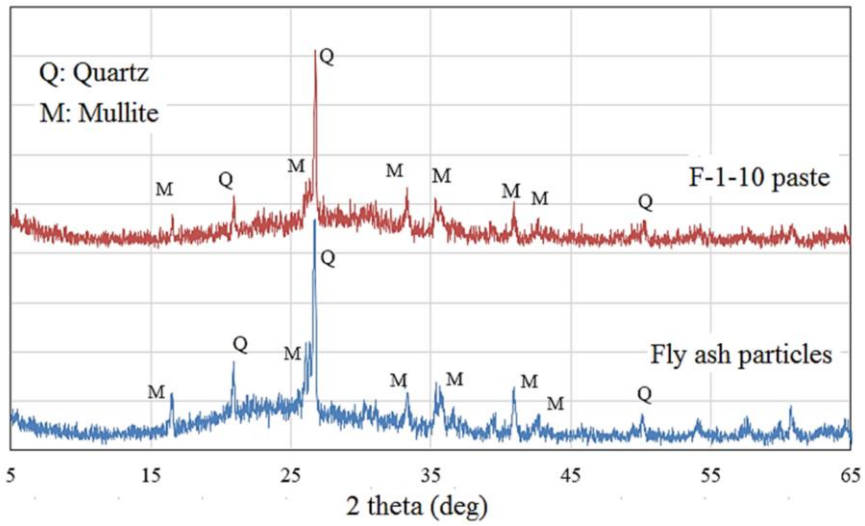


Figure 7-4. XRD pattern of fly ash particles and F-1-10 paste

Glass-powder samples, however, released an even lower amount of Al in the solution compared to GGF and fly ash. Glasser and Harvey as well as Xu et al. indicated that Al

compounds do not readily combine with the small highly charged silicate monomers, instead they form silica-alumina complexes with long-chain silicate oligomers (29, 52). In such cases when the Si/Al ratio is so high (higher than 15), the geopolymeric material shows more polymeric characterization (53). It should also be noted that presence of Al in the geopolymer structure can bind the alkali as they are required to balance the negative charge associated with Al(OH)_4^-. As a result, the low Al content leaves higher free alkali in the system, which may end up in ASR gel in the paste matrix of glass-powder-based geopolymers.

Samples with the highest compressive strength from each precursor were selected to investigate the microstructure using back-scatter SEM. These samples were GGF-0-10, F-1-10, and GLP-1-10, which showed 82, 59, and 43 MPa at their 28 days. Pictures showing the general appearances of each sample are presented in Figure 7-5. As presented in this picture, severe damages in the form of voids and cracks can be seen in GLP-1-10 sample. The cracks and voids could be related to the high shrinkage tendency of glass-powder geopolymer cured at elevated temperature and also, presence of high dosage of alkali which resulted in formation of ASR gel. Although the shrinkage tests are on-going and are not presented or discussed in detail in this paper, the 28-day results of the drying shrinkage test of geopolymer mortars showed the high shrinkage of glass-powder-based samples. Results of the 28 days old GLP-1-10 mortar sample was measured to be 2700 micro-strain, while GGF-0-10 and F-1-10 sample showed 620 and 700 micro-strain respectively. This shows the higher shrinkage tendency of the GLP-1-10 mixture.

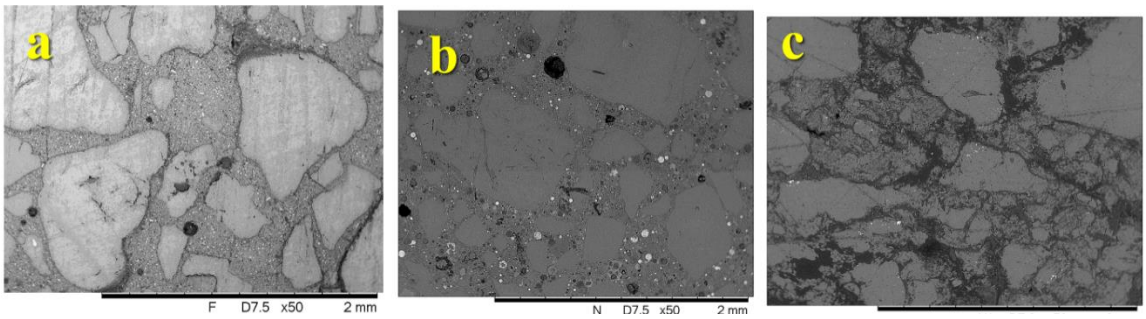

Figure 7-5. General appearance of GGF-0-10 (a), F-1-10 (b) and GLP-1-10 (c)

Figure 7-6 presents the microstructure of GGF-0-10 and F-1-10 paste. As it can be seen in this picture, unreacted GGF particles are observed as discrete particles in the paste, while reaction products connect them together. Considering the rigid nature of these particles, they act as an internal reinforcement in the paste matrix which leads to higher compressive strength of the GGF samples. The EDX results showed a higher amount of Na in the reaction products, while the other compounds had an almost same proportion in both unreacted particles and surrounding products. As presented in this picture, unreacted particles of fly ash were observed in F-1-10 samples. Nevertheless, the structure of fly ash grains did not appear to be as rigid as GGF grains since micro cracks observed to pass through the un-reacted materials. In the case of glass-powder geopolymer however, an ASR-like gel in the matrix caused cracks in the weak gel as presented in Figure 7-7.

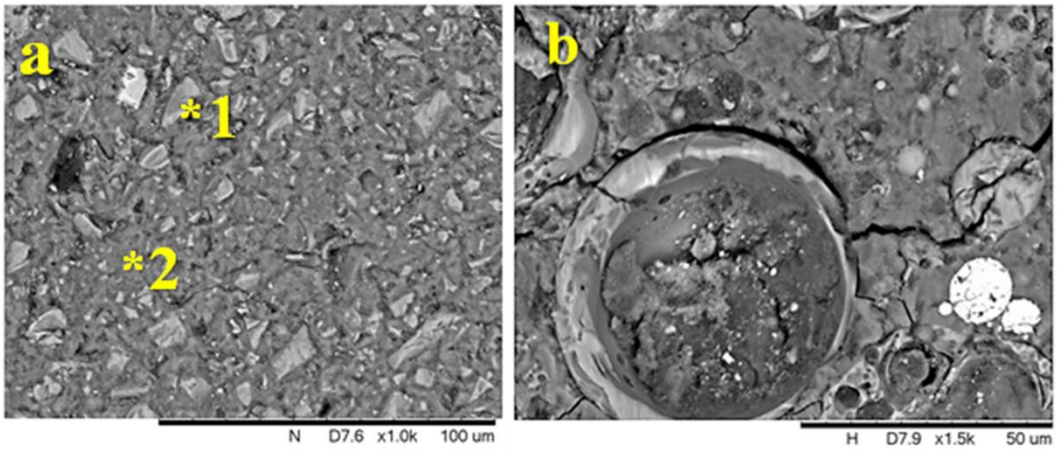


Weight Percentage of Elements

| | Na | Mg | Al | Si | K | Ca | Fe |
|---|---|---|---|---|---|---|---|
| Spectrum 1 | 5.61 | 2.98 | 11.41 | 52.75 | 0.13 | 26.67 | 0.46 |
| Spectrum 2 | 14.98 | 2.14 | 9.96 | 47.38 | 0.89 | 24.99 | 0.47 |

Figure 7-6. Microstructure of a) GGF-0-10 and b) F-1-10 Paste

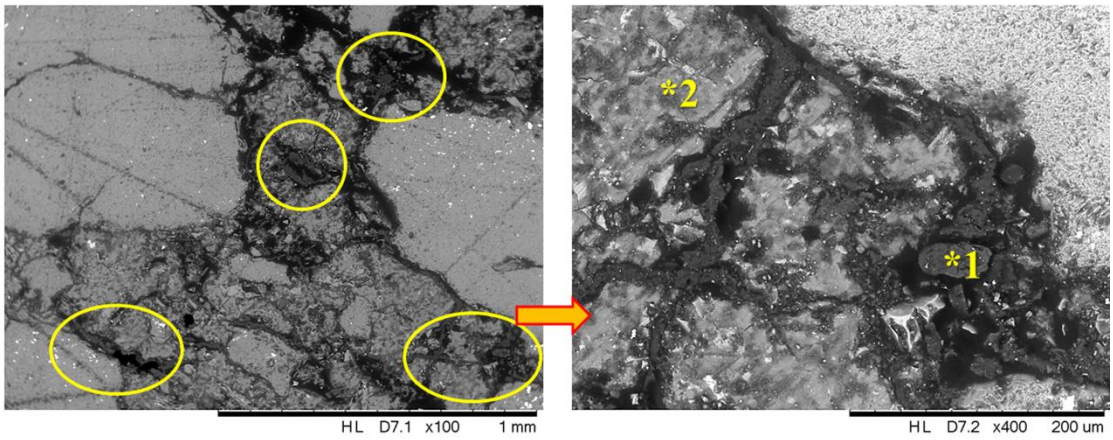


Weight Percentage of Elements

| | Na | Al | Si | K | Ca | Fe |
|---|---|---|---|---|---|---|
| Spectrum 1 | 11.29 | 2.04 | 74.31 | 0.17 | 9.05 | 3.13 |
| Spectrum 2 | 16.07 | 1.33 | 68.05 | 1.07 | 12.21 | 1.26 |

Figure 7-7. Formation of ASR gel in the paste matrix of GLP-1-10 Paste

### *7.3.3 Alkali-silica reaction*

Expansion results of the ASR test are presented in Figure 7-8. As it can be seen in this graph, GLP-1-10 shows a rapid expansion which exceeds 1% length change after only 3 days of submerging in 1N NaOH solution. As a result, the samples cracked severely at an early age and length-change measurements were not practical at 7 days. The expansion observed in other geopolymer samples was much less than that observed with portland cement mortars. After 28 days of exposure, the expansion of GGF-0-10 and F-1-10 samples reached 0.04% and 0.06% respectively, while the expansion of portland cement mortars reached 0.84%.

The dramatic expansion of GLP-1-10 samples could be attributed to a number of factors, like the lesser amount of Al content in the matrix, the high amount of calcium content, and a large amount of readily available voids and cracks in the hardened matrix. Considering the results presented in Table 7-6, the amount of Al released in glass-powder geopolymers is very low, which results in low binding levels of alkalis in the geopolymer structure. Furthermore, presence of a high amount of calcium in the system leads to the formation of more rigid ASR gel, which causes

more cracks and eases the attacking process in aggregates. In addition to these, as seen in Figure 7-8, as a result of the high amount of already available alkalis in the glass-powder geopolymers, ASR gel was observed in samples with non-reactive aggregate and no exposure to ASR accelerating conditions. Consequently, it is thought that ASR reaction contributing to such high expansion is taking place in the paste matrix of the glass-powder geopolymer itself rather than the aggregate surface. Although not presented in this paper, the SEM results of the samples made with reactive aggregates validated this assumption, as the aggregates were uncracked even in severely cracked mortar bars after 3 days of exposure to ASR accelerating conditions (Figure 7-9).

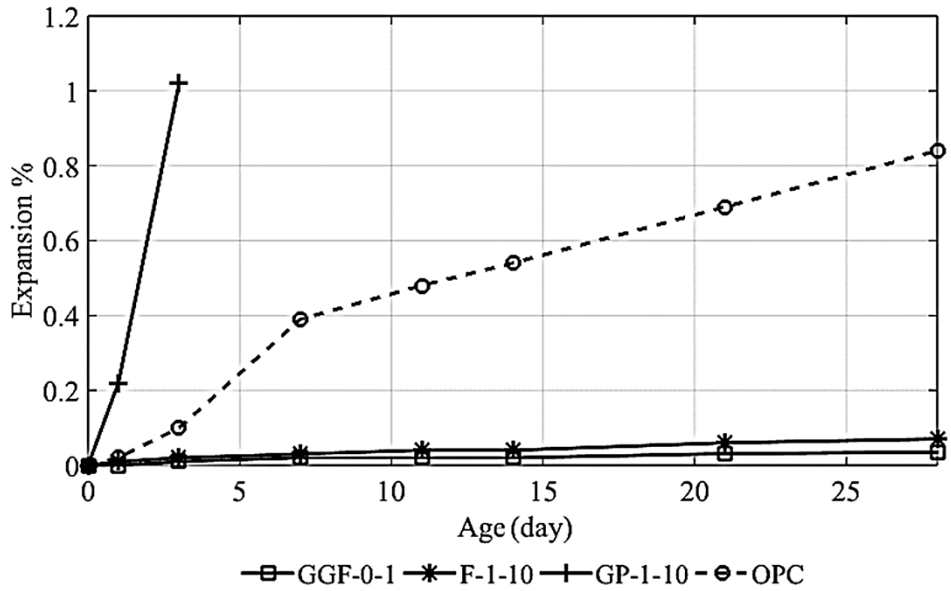


Figure 7-8. Expansion due to ASR

On the other hand, lower expansions of F-1-10 and GGF-1-10 samples are related to densification of the paste matrix in the presence of NaOH solution. Un-reacted material can go through the reaction process again forming stronger and more uniform paste, which limits the alkali attack on aggregates. Although availability of Ca in cementitious mixtures is known to be deleterious for ASR resistance; and the lower ASR-related expansion of fly ash-based

geopolymers has been explained by this parameter (33, 35, 37), GGF samples did not follow this trend. The low expansion of GGF-based sample might be related to its very low porosity as well as low $Ca(OH)_2$ content. Results of Mercury Intrusion Porosimetry (MIP) test on 3-days old mortar samples showed a much lower total porosity of the GGF-0-10 mixture (33 mm3/g) in comparison to F-1-10 (100 $mm^3/g$) and GLP-1-10 (74 $mm^3/g$) mixtures. In addition, it should also be noted that not all the Ca content of the paste (i.e. already fixed Ca) can participate in the formation of ASR gel, and therefore studies such as TGA might be useful to measure the amount of $Ca(OH)_2$ in the GGF-based geopolymer paste. It is thought that the higher amount of $Ca(OH)_2$ in the paste can increase the potential of the formation of a more rigid ASR gel, which will cause larger expansion. The TGA results showed a very low level of $Ca(OH)_2$ in both fly ash-based (0.7% of total weight) and GGF based geopolymer (1.1% of total weight) paste samples (Figure 7-10).

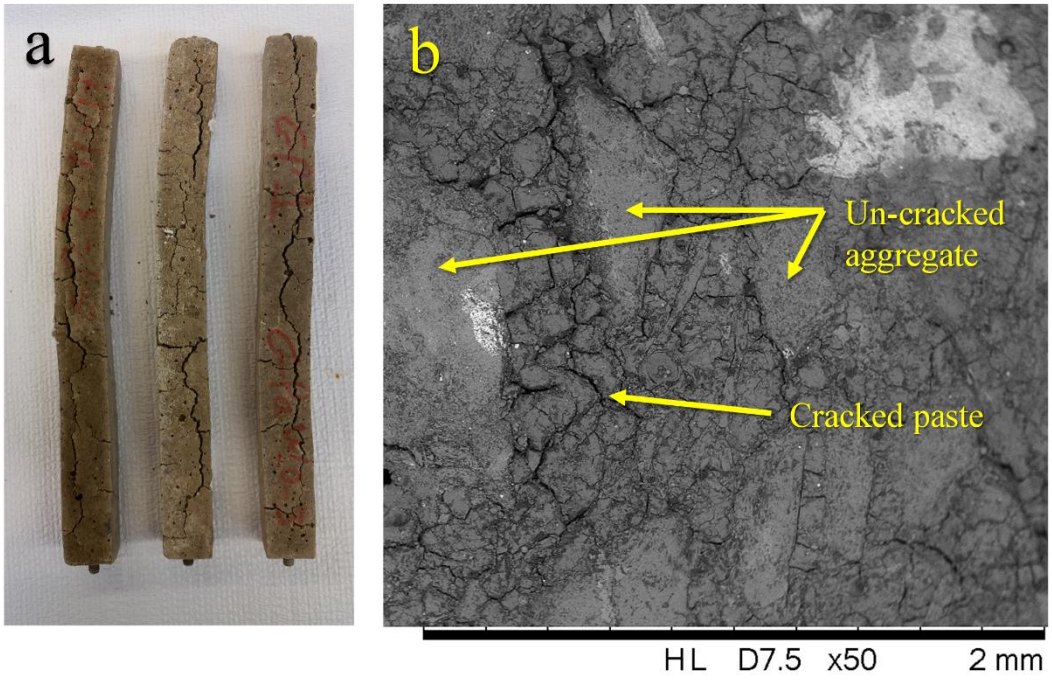


Figure 7-9. a) Severely cracked mortar bars after 7 days of exposure to ASR accelerating condition, and b) SEM picture of GLP-1-10 sample after 3 days of exposure to ASR accelerating condition

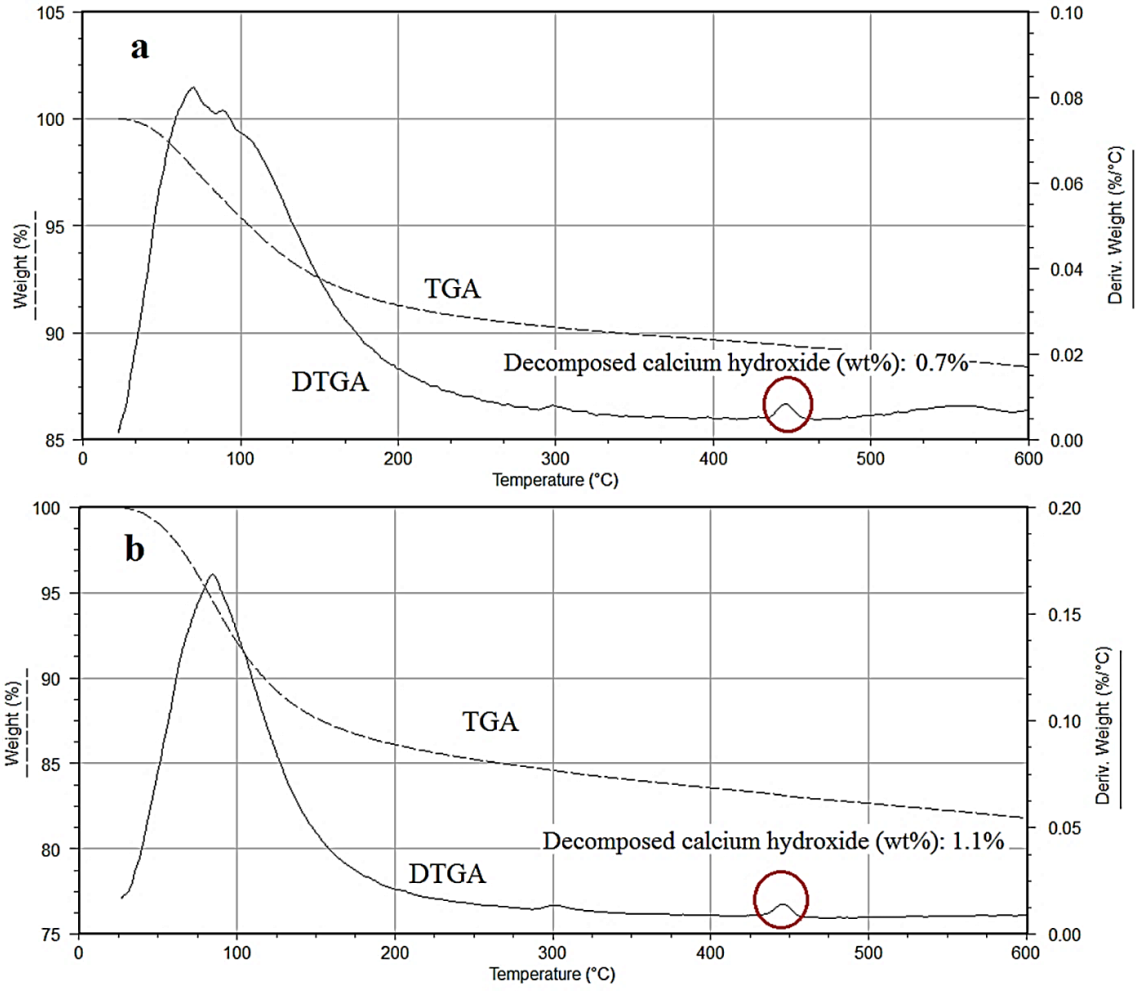


Figure 7-10. TGA and DTGA curve of 7-days old paste samples. a) F-1-10 paste, and b) G-0-10 paste.

SEM pictures taken from the GGF-0-10 sample and the F-1-10 sample after 14 days of exposure are presented in Figure 7-11. As presented, no significant signs of cracks can be seen in both samples. Interestingly, the paste matrix of GGF samples remained intact as unreacted GGF particles can clearly be seen in Figure 7-11b. For the case of the F-1-10 sample, more reacted particles were seen in the paste matrix in comparison to the unexposed samples. This indicates the role of high alkali media in the secondary reaction of unreacted particles. The lower amount of alkali-silica reaction in both cases can be attributed to the stabilization of alkalis by unreacted material, the lower level of available calcium in form of $Ca(OH)_2$, as well as the rigid structure of

GGF-0-10 paste which reduces the permeability. It should also be noted that no visible ASR gel was observed around the aggregates.

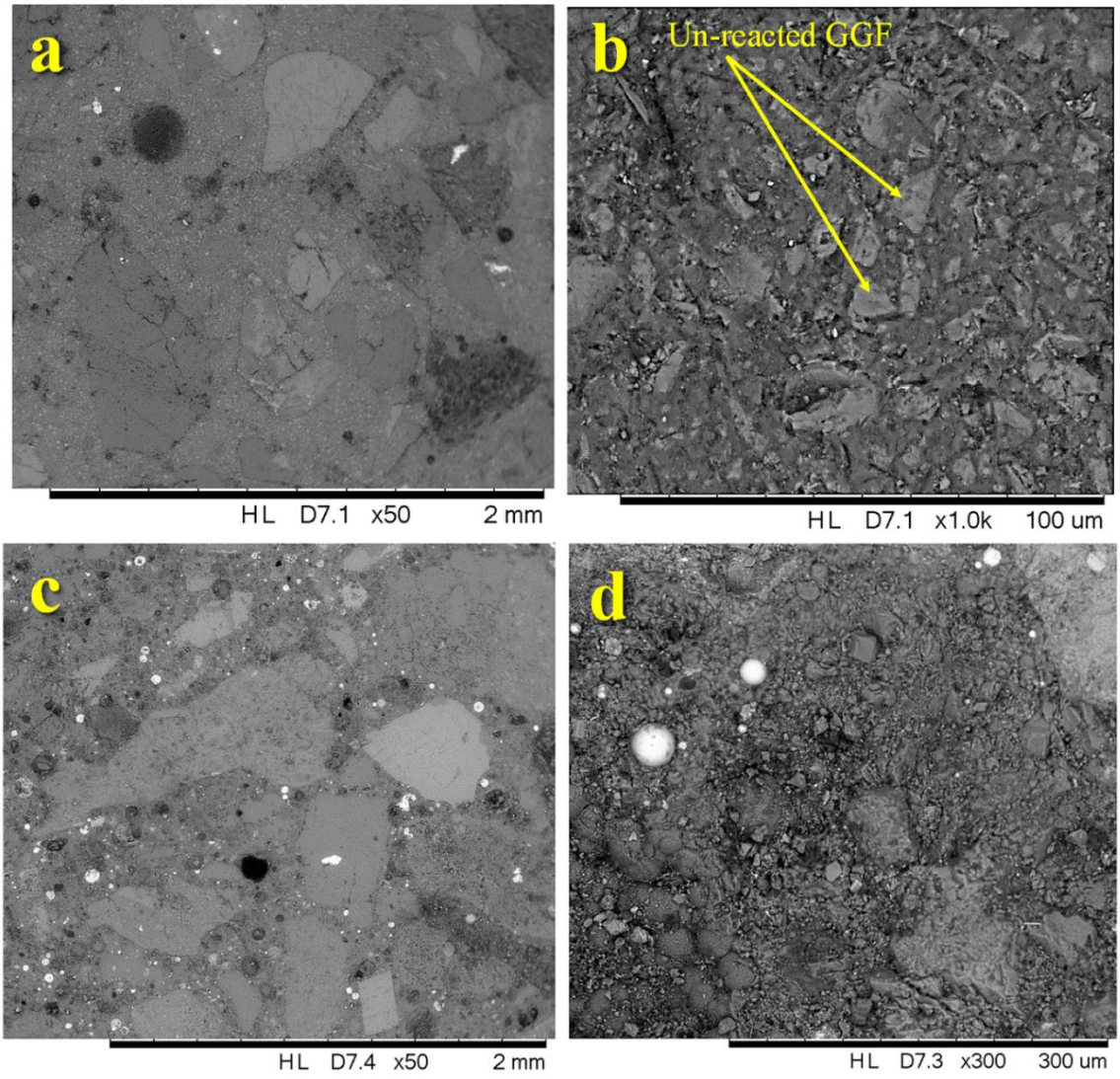


Figure 7-11. SEM of GGF-0-10, a) Uncracked aggregate, and b) paste matrix. SEM of F-1-10, c) Uncracked aggregate, and d) Paste Matrix

## 7.4 Conclusion

Based on the findings from this investigation, the following conclusions were drawn:

1) Increase in the Na content of the activator solution did not seem to have a considerable effect on the workability of the GGF and fly ash-based mixtures, but caused improvement in the

workability of glass-powder-based mixtures. On the other hand, increase in the soluble Si content, in terms of $SiO_2/Na_2O$ content caused improvement in the workability.

2) The role of Na content was observed to be significant in affecting the compressive strength of all the geopolymer mixtures investigated in this study. The 28-day compressive strength increased with an increase in Na levels in all mixtures.
3) While addition of soluble Si (i.e. increase in $SiO_2/Na_2O$) to mixtures improved compressive strength of fly ash and glass-powder-based geopolymers, it reduced the compressive strength of GGF geopolymer samples. The highest compressive strength in GGF geopolymers was observed in samples with no added silica, i.e. $SiO_2/Na_2O=0$. This is thought to be because of the higher degrees of geopolymerisation of GGF particles in the GGF-0-10 samples, with no addition of sodium silicate in the activator solution.
4) In terms of alkali-silica reaction, the glass-powder-based geopolymer showed a very poor resistance against ASR as mortar bars showed severe cracking and significant expansion. However, fly ash and GGF-based geopolymer mortar bars showed a much lower expansion in comparison to portland cement mortar specimens. Also, results from SEM analysis of polished specimens from GGF and fly ash mortar bars subjected to ASR tests showed a dense paste matrix with little cracking.

## Reference


1. Hemmings, R. T. (2005) Process for Converting Waste Glass Fiber into Value Added Products, Final Report (No. DOE GO13015-1). Albacem LLC.
2. Chen, C. H.; Huang, R.; Wu J. K.; Yang, C. C. (2006) Waste E-glass particles used in cementitious mixtures. Cem. Concr. Res. 36 [3], 449-456. http://dx.doi.org.libproxy.clemson.edu/10.1016/j.cemconres.2005.12.010
3. Hossain, A.; Shirazi, S.; Persun, J.; Neithalath, N. (2008) Properties of concrete containing vitreous calcium aluminosilicate pozzolan. J Transp. Res. Record. (2070), 32-38. http://dx.doi.org/10.3141/2070-05.
4. Neithalath, N.; Persun, J.; Hossain, A. (2009) Hydration in high-performance cementitious systems containing vitreous calcium aluminosilicate or silica fume. Cem. Concr. Res. 39 [6], 473-481. http://dx.doi.org/10.1016/j.cemconres.2009.03.006.
5. Tashima, M. M.; Soriano, L.; Borrachero, M. V.; Monzó, J.; Cheeseman C. R.; Payá, J. (2012) Alkali activation of vitreous calcium aluminosilicate derived from glass fiber waste. Journal of Sustainable Cement-Based Materials. 1 [3], 83-93. http://dx.doi.org/10.1080/21650373.2012.742610.
6. Tashima, M. M.; Soriano, L.; Monzo, J.; Borrachero, M. V.; Paya, J. (2013) Novel geopolymeric material cured at room temperature. Adv. App. Ceram. 112 [4], 179-183. http://dx.doi.org/10.1179/1743676112Y.0000000056.
7. Duxson, P.; Fernández-Jiménez, A.; Provis, J.L.; Lukey, G.C.; Palomo, A.; Van Deventer, J.S.J. (2007) Geopolymer technology: the current state of the art. J. Mater. Sci. 42 [9], 2917-2933. http://dx.doi.org/10.1007/s10853-006-0637-z.
8. Ganesan, N.; Abraham, R.; Raj, S.D.; Sasi, D.; (2014) Stress–strain behaviour of confined Geopolymer concrete. Constr. Build. Mater. 73, 326-331.

http://dx.doi.org/10.1016/j.conbuildmat.2014.09.092.

9. Morsy, M.S.; Alsayed, S.H.; Al-Salloum, Y.; Almusallam, T. (2014) Effect of sodium silicate to sodium hydroxide ratios on strength and microstructure of fly ash geopolymer binder. Arab. J Sci. Eng. 39 [6], 4333-4339. http://dx.doi.org/10.1007/s13369-014-1093-8.
10. Van Jaarsveld, J.G.S.; Van Deventer, J.S.J; Lukey, G.C. (2003) The characterization of source materials in fly ash-based geopolymers. Mater. Lett. 57 [7], 1272-1280. http://dx.doi.org/10.1016/S0167-577X (02)00971-0.
11. Ryu, G.S.; Lee, Y.B.; Koh, K.T; Chung, Y.S. (2013) The mechanical properties of fly ash-based geopolymer concrete with alkaline activators. Constr. Build. Mater. 47, 409-418. http://dx.doi.org/10.1016/j.conbuildmat.2013.05.069.
12. Li, C.; Sun, H.; Li, L. (2010) A review: The comparison between alkali-activated slag (Si+ Ca) and metakaolin (Si+Al) cements. Cem. Concr. Res. 40 [9], 1341-1349. http://dx.doi.org/10.1016/j.cemconres.2010.03.020.
13. Kumar, S.; Kumar, R.; Mehrotra, S.P.; (2010) Influence of granulated blast furnace slag on the reaction, structure and properties of fly ash based geopolymer. J. Mater. Sci. 45 [3], 607-615. http://dx.doi.org/10.1007/s10853-009-3934-5.
14. Oh, J.E.; Monteiro, P.J.; Jun, S.S.; Choi, S; Clark, S.M. (2010) The evolution of strength and crystalline phases for alkali-activated ground blast furnace slag and fly ash-based geopolymers. Cem. Concr. Res. 40 [2], 189-196. http://dx.doi.org/10.1016/j.cemconres.2009.10.010.
15. Xu, H.; Van Deventer, J.S. (2002) Geopolymerisation of multiple minerals. Miner. Eng. 15 [12], 1131-1139. DOI: http://dx.doi.org/10.1016/S0892-6875 (02)00255-8.
16. Anuar, K.A.; Ridzuan, A.R.M.; Ismail, S. (2011) Strength characteristic of geopolymer concrete containing recycled concrete aggregate. International Journal of Civil and Environment. http://dx.doi.org/10.1061/(ASCE)HZ.2153-5515.0000312.

17. Bhutta, M.A.R.; Hussin, W.M.; Azreen, M; Tahir, M.M. (2014) Sulphate resistance of geopolymer concrete prepared from blended waste fuel ash. J Mater Civil Eng. 26. http://dx.doi.org/10.1061/(ASCE)MT.1943-5533.0001030.
18. Trochez, J. J.; Mejía de Gutiérrez, R.; Rivera, J.; Bernal, S. A. (2015). Synthesis of geopolymer from spent FCC: Effect of SiO2/Al2O < 3 and Na2O/SiO2 molar ratios. Mater. Construcc. 65 [317]. http://dx.doi.org/10.3989/mc.2015.00814
19. Pascual, A. B.; Tognonvi, M. T.; Tagnit-Hamou, A. (2014). Waste glass powder-based alkali-activated mortar. In NTCC2014: International Conference on Non-Traditional Cement and Concrete.
20. Sukmak, P.; Horpibulsuk, S.; Shen, S.L. (2013) Strength development in clay–fly ash geopolymer. Constr. Build. Mater. 40, 566-574. DOI: http://dx.doi.org/10.1016/j.conbuildmat.2012.11.015.
21. Nazari, A.; Maghsoudpour, A. and Sanjayan, J.G. (2014) Characteristics of boroaluminosilicate geopolymers. Constr. Build. Mater. 70, 262-268. http://dx.doi.org/10.1016/j.conbuildmat.2014.07.087.
22. Robayo, R. A.; Mejía de Gutiérrez, R.; Gordillo, M. (2016) Natural pozzolan-and granulated blast furnace slag-based binary geopolymers. Mater. Construcc. 66 [321], http://dx.doi.org/10.3989/mc.2016.03615.
23. Wang, H.; Li, H.; Yan, F. (2005) Synthesis and mechanical properties of metakaolinite-based geopolymer. Colloids and Surfaces A: Physicochemical and Engineering Aspects, 268 [1], 1-6. http://dx.doi.org/10.1016/j.colsurfa.2005.01.016.
24. Hardjito, D.; Wallah, S.E.; Sumajouw, D.M; Rangan, B.V. (2004). On the development of fly ash-based geopolymer concrete. ACI materials journal, 101 [6].
25. Phair, J.W; and Van Deventer, J.S.J. (2002) Effect of the silicate activator pH on the

microstructural characteristics of waste-based geopolymers. Int. J Miner. Process. 66 [1]. http://dx.doi.org/10.1016/S0301-7516 (02)00013-3.

26. Palomo, A.; Grutzeck, M.W.; Blanco, M.T. (1999) Alkali-activated fly ashes: a cement for the future. Cem. Concr. Res. 29 [8],1323-1329. http://dx.doi.org/10.1016/S0008-8846(98)00243-9.
27. Buchwald, A.; Dombrowski, K; Weil, M. (2005) The influence of calcium content on the performance of geopolymeric binder especially the resistance against acids. Proceedings of the world geopolymer. St. Quentin, France (2005).
28. Lee, W. K. W.; Van Deventer, J. S. J. (2002) The effect of ionic contaminants on the early-age properties of alkali-activated fly ash-based cements. Cem. Concr. Res. 32 [4], 577-584. http://dx.doi.org/10.1016/S0008-8846(01)00724-4.
29. Xu, H.; Van Deventer, J. S. J. (2000) The geopolymerisation of alumino-silicate minerals. Int. J Miner. Process. 59 [3], 247-266. http://dx.doi.org/10.1016/S0301-7516(99)00074-5.
30. De Silva, P.; Sagoe-Crenstil, K.; Sirivivatnanon, V. (2007) Kinetics of geopolymerization: role of Al2O3 and SiO2. Cem. Concr. Res. 37 [4], 512-518. http://dx.doi.org/10.1016/j.cemconres.2007.01.003.
31. Kouamo, H. T.; Elimbi, A.; Mbey, J. A.; Sabouang, C. N.; Njopwouo, D. (2012) The effect of adding alumina-oxide to metakaolin and volcanic ash on geopolymer products: A comparative study. Constr. Build. Mater. 35, 960-969. http://dx.doi.org/10.1016/j.conbuildmat.2012.04.023.
32. Duxson, P.; Provis, J. L.; Lukey, G. C.; Mallicoat, S. W.; Kriven, W. M.; Van Deventer, J. S. (2005). Understanding the relationship between geopolymer composition, microstructure and mechanical properties. Colloids and Surfaces A: Physicochemical and Engineering Aspects, 269 [1], 47-58. http://dx.doi.org/10.1016/j.colsurfa.2005.06.060.
33. Kupwade-Patil, K.; Allouche, E.N. (2013) Impact of Alkali Silica Reaction on Fly Ash-Based Geopolymer Concrete. J Mater Civil Eng. 25 [1], 131-139.

http://dx.doi.org/10.1061/(ASCE)MT.1943-5533.0000579.

34. Puertas, F.; Palacios, M.; Gil-Maroto; A. and Vázquez, T. (2009) Alkali-aggregate behaviour of alkali-activated slag mortars: Effect of aggregate type. Cem. Concr. Comp. 31 [5], 277-284. http://dx.doi.org/10.1016/j.cemconcomp.2009.02.008.
35. Fernández-Jiménez, A.; Garcia-Lodeiro, I.; Palomo, A. (2007) Durability of alkali-activated fly ash cementitious materials. J. Mater. Sci. 42(9), 3055-3065. http://dx.doi.org/10.1007/s10853-006-0584-8.
36. Xie, Z.; Xiang, W.; Xi, Y. (2003) ASR potentials of glass aggregates in water-glass activated fly ash and portland cement mortars. J Mater Civil Eng. 15 [1], 67-74. http://dx.doi.org/10.1061/(ASCE)0899-1561(2003)15:1(67).
37. Pouhet, R.; Cyr, M. (2015) Alkali–silica reaction in metakaolin-based geopolymer mortar. Mater Struct, 48 [3], 571-583. http://dx.doi.org/10.1617/s11527-014-0445-x.
38. ASTM International: Standard Specification for Portland cement (ASTM C150) (2016). http://dx.doi.org/10.1520/C0150_C0150M-16.
39. ASTM International: Standard Test Method for Flow of Hydraulic Cement Mortar (ASTM C1437) (2013). http://dx.doi.org/10.1520/C1437-13.
40. ASTM International: Standard Test Method for Compressive Strength of Hydraulic Cement Mortars (Using 2-in. or [50-mm] Cube Specimens) (ASTM C109) (2013). http://dx.doi.org/10.1520/C0109_C0109M-13.
41. Struble, L; Hicks, J. K. (2013) Geopolymer Binder Systems, ASTM International. New York, (2013).
42. Palomo, A.; Alonso, S., Fernandez-Jiménez, A.; Sobrados, I.; Sanz, J. (2004) Alkaline activation of fly ashes: NMR study of the reaction products. J Am. Ceram. Soc. 87 [6], 1141-1145. http://dx.doi.org/10.1111/j.1551-2916.2004.01141.x.

43. ASTM International: Standard Test Method for Potential Alkali Reactivity of Aggregates (Mortar-Bar Method) (ASTM C1260) (2014). http://dx.doi.org/10.1520/C1260-14.
44. Sathonsaowaphak, A.; Chindaprasirt, P.; Pimraksa, K. (2009) Workability and strength of lignite bottom ash geopolymer mortar. J Hazard. Mater. 168 [1], 44-50. http://dx.doi.org/10.1016/j.jhazmat.2009.01.120.
45. Malkawi, A. B.; Nuruddin, M. F.; Fauzi, A.; Almattarneh, H.; Mohammed, B. S. (2016) Effects of Alkaline Solution on Properties of the HCFA Geopolymer Mortars. Procedia Engineering. 148, 710-717. http://dx.doi.org/10.1016/j.proeng.2016.06.581.
46. Chindaprasirt, P.; Chareerat, T.; Sirivivatnanon, V. (2007) Workability and strength of coarse high calcium fly ash geopolymer. Cem. Concr. Comp. 29 [3], 224-229. http://dx.doi.org/10.1016/j.cemconcomp.2006.11.002.
47. Bhowmick, A.; Ghosh, S. (2012) Effect of synthesizing parameters on workability and compressive strength of fly ash based geopolymer mortar. International journal of civil and structural engineering, 3 [1], Doi: 10.6088/ijcser.201203013016.
48. Yip, C.K.; Lukey, G.C.; Van Deventer, J.S.J. (2005) The coexistence of geopolymeric gel and calcium silicate hydrate at the early stage of alkaline activation. Cem. Concr. Res. 35 [9],1688-1697. DOI: http://dx.doi.org/10.1016/j.cemconres.2004.10.042.
49. Yao, Z.; Ye, Y.; Xia, M. (2013) Synthesis and characterization of lithium zeolites with ABW type from coal fly ash. Environmental Progress & Sustainable Energy. 32 [3], 790-796. http://dx.doi.org/10.1002/ep.11689.
50. Fernández-Jiménez, A.; Palomo, A.; Sobrados, I.; Sanz, J. (2006) The role played by the reactive alumina content in the alkaline activation of fly ashes. Micropor. Mesopor. Mat. 91 [1], 111-119. http://dx.doi.org/10.1016/j.micromeso.2005.11.015.
51. Temuujin, J.; Van Riessen, A. (2009) Effect of fly ash preliminary calcination on the properties of

geopolymer. J Hazard. Mater. 164 [2], 634-639. http://dx.doi.org/10.1016/j.jhazmat.2008.08.065.

52. Glasser, L.S.D.; Harvey, G. (1984) The unexpected behaviour of potassium aluminosilicate solutions. Journal of the Chemical Society, Chem. Commun. 10, 664-665. http://dx.doi.org/10.1039/c39840000664.

53. Davidovits, J. (1999) Chemistry of geopolymeric systems, terminology. In: Proceedings of 99 International Conference. France. 9-40.

# CHAPTER 8

# INFLUENCE OF SELECTED PARAMETERS ON PERFORMANCE OF GEOPOLYMER PRODUCED FROM GROUND GLASS FIBER[1]

## 8.1 Introduction:

In recent years the use of geopolymer concrete as a potential replacement for portland-cement based concrete is attracting more attention to not only address growing environmental concerns (1-5) but also to provide a better alternative as a construction material of choice in resisting aggressive chemical environments (5-7). Utilization of geopolymer concrete in precast concrete products, including sewer pipes, culverts, railway sleepers, pre-fabricated units for housing market, etc. (8-12), repair or a retrofitting material for existing portland-cement-concrete elements or structures (13-15), using as a fire resisting material (16, 17) and as a repair coating or a construction material in marine sites (18-21) are some examples of the geopolymer applications.

To produce geopolymers, silica and alumina-rich precursors are chemically activated using alkaline activators such as sodium hydroxide or sodium silicate solutions. This process results in the formation of an amorphous three-dimensional alumino-silicate network, which is known as the geopolymer (4). Thus far materials such as slag, fly-ash, meta-kaolin, and various combinations of these materials are the most widely used precursors to produce geopolymer concrete (22-28). However, in recent years, several other waste or industrial by-products such as: waste paper sludge ash (29), glass produced from the DC plasma treatment of air pollution

---

1 - Hassan Rashidian-Dezfouli, Prasada Rao Rangaraju, Venkat Sai Kumar Kothala. Influence of Selected Parameters on Performance of Geopolymer Produced from Ground Glass Fiber Submitted to Journal of Construction and Building material (under review).

control residue (30), spent fluid catalytic cracking catalyst (31), Oil palm shell (32) sugar cane straw ash (33), waste glass-powder (34, 35), combination of sugarcane bagasse ash and blast furnace slag (36), palm oil fuel Ash (37), combinations of natural pozzolan and slag (38), blends of clay and fly ash (39), and vitreous calcium alumino-silicate (40) have been used as a precursor for geopolymer. In addition to these materials, recent studies have shown that ground glass fiber (GGF) can be effectively activated by an alkali activator to produce a geopolymer mortar (35).

Each year, a large amount of glass fiber is commercially produced to be used in various applications. However, this process generates millions of tons of waste glass fiber around the world. According to a 2005 report by Hemmings (41), each year around 250,000 to 500,000 tons of waste glass fiber end-up in landfills of the U.S. This waste glass fiber has a chemical composition which is rich in glassy silica, alumina, and calcium. Therefore, if milled to a fine powder, this material might potentially be used as supplementary cementitious material (SCM) or as a precursor to produce geopolymers. Chen et al. (42) investigated the use of waste E-glass (the most commonly used type of fiber glass) as cement replacement material in concrete mixtures. Utilization of GGF as a cement replacement and its effect on the mechanical and durability properties of concrete are also reported by Rangaraju et al. and Rashidian-Dezfouli and Rangaraju (43, 44). Furthermore, recent research by the authors has shown that GGF can be effectively activated by sodium hydroxide solution, producing a geopolymer mortar mixture with the high early strength as high as 79 MPa after 3 days (35).

The purpose of this work is to study the influence of several activation parameters that affect the strength gain of GGF-based geopolymer mixtures. Earlier studies on geopolymer mixtures have identified some of a large number of parameters that can affect the mechanical properties of the final product (9, 11, 20, 23, 28, 45- 52). Based on their characteristics, some of the most important parameters can be divided into three main categories: (i) parameters related to

the properties of the activator solutions, such as combination and concentration of activator solutions (11, 45-47); (ii) parameters related to the physical and chemical properties of precursors, such as fineness and chemical composition (9, 23-28, 48); and (iii) parameters related to the curing condition such the temperature and duration of the heat curing process, have been reported to affect the mechanical properties of the geopolymers considerably (11, 46, 49-52)

The alkali concentration of the activator solution is one of the most important parameters that affect the strength of geopolymers. Generally, it has been reported that increase in the alkali concentration results in the increase in the mechanical properties of the geopolymers (11, 32, 45-47, 53-55). However, it also has been reported that the excessive amount of alkali content of the activator solution will negatively influence their strength (16, 32, 54-56). In addition to the alkali content, presence of soluble Si, mostly in the form of sodium silicate solution, in the activator solution can influence the compressive strength of the geopolymer mixtures. Several works have shown that the manufacturing of geopolymer mixtures using combinations of sodium hydroxide (NaOH) and sodium silicate solution resulted in a higher compressive strength in comparison to the mixtures that were activated using sodium hydroxide alone (36, 46, 47, 57).

It has been shown that the $SiO_2/Na_2O$ ratio of the activator (or mixtures) plays an important role in the final compressive strength of geopolymer mixtures. According to Hardjito et al. (11), increase in the sodium silicate/NaOH liquid mass ratio from 0.4 to 2.5 resulted in the higher compressive strength ratio for both NaOH concentration of 8M and 14M. Nonetheless, it should be noted that despite its beneficial effect at lower dosage levels, addition of too much sodium silicate solution to mixtures has been found to reduce compressive strength of the geopolymer samples (24, 26, 55, 57-59). Therefore, some studies have suggested an optimum range or ratio for the sodium silicate/NaOH of the activator solution based on the particular precursor used in their study (57, 58).

Physical and chemical characteristics of the precursors have a significant influence on the compressive strength of the geopolymers. Several studies have shown that a finer particles size of a precursor can result in a higher compressive strength of the final geopolymer product; mainly due to the higher surface area of the precursors (54, 60, 61) and smaller pore sizes in the geopolymer matrix (60). Despite this, other studies have indicated no clear trend between the particles size of precursors and the mechanical properties of geopolymers (25, 62).

Chemical composition of precursors plays an important role in determining the structure and mechanical properties of geopolymers. According to Davidovits (63), the lower atomic ratio of Si/Al (Si/Al <3) leads to the formation of a rigid three-dimensional network and the higher Si/Al ratios (Si/Al > 15) gives a polymeric characteristic to the geopolymer systems. Effect of Si/Al and the ratio or the Al content of the geopolymer mixtures on the mechanical properties of geopolymers has been investigated in a number of studies (64-69). Based on these studies, it is evident that Si/Al ratio plays a significant role in affecting the compressive strength and Young's modulus of elasticity of geopolymer concrete, with Si/Al ratio (~ 2.0) being optimal for providing the highest mechanical properties.

In addition to the Si/Al ratio, presence of calcium oxides also affects the fresh and hardened properties of geopolymer mixtures (25, 70). While the exact mechanism is not yet clear, several works have shown that the presence of calcium oxide accelerates the setting procedure (59, 71-73) and also improves the mechanical properties of geopolymer mixtures (2, 5, 70, 71, 74-80). In efforts to explain the role of calcium oxides in geopolymer systems, several mechanisms have been proposed, such as: 1) formation of C-S-H (calcium silicate hydrate) or C-A-S-H gel (calcium aluminosilicate hydrate) which densifies the structure of the paste (2, 28, 75, 80), 2) effect of calcium compounds in creating a nucleation site for the precipitation of the geopolymer compound (71, 77, 81, 82), and 3) charge balancing capacity of Ca in the alumino-

silicate structure (73, 76, 78, 79, 83, 84).

Effect of temperature and duration of heat curing on the mechanical properties of geopolymer mixtures have been discussed in several studies (11, 46, 49, 58). Based on these studies it is generally observed that compressive strength of geopolymer mixtures increases with an increase in the temperature. However, the effect is more significant in lower temperature ranges (i.e. up to 60 to 75°C); and the further increase in the heat-curing temperature did not show a notable increase in the strength (11, 52, 53). However, in other studies (49-51, 58), it was shown that very high curing temperatures (i.e. more than 80°C to 90°C) could lead to the reduction in the strength of geopolymer. According to Muñiz-Villarreal et al. (49), the reduction in the compressive strength at the higher temperature can be explained through the fast evaporation of water in the system that occurs, which not only increases the porosity but also causes geopolymerisation to take place on the surface of precursors which hinders the further dissolution of Si and Al. Prolongation of the heat-curing of samples has been shown to improve the mechanical properties of geopolymers, as more time is provided for the polymerisation to take place (11). Nonetheless, it should also be mentioned that a few studies performed on the fly ash-based geopolymers have reported a reduction in the compressive strength with the extension in the heat-curing period (58).

This work follows our previous research (35, 72), in which utilization of GGF as a precursor to manufacture a novel geopolymer was described. The focus of this work is to evaluate the parameters that can affect the compressive strength and microstructure of the GGF-based geopolymer systems. For comparison purposes, fly ash-based geopolymer mixtures were prepared using a class F fly ash. The effect of parameters such as) alkali content and combination of activator solutions on the compressive strength of the GGF and fly ash-based mixtures were investigated and compared. Furthermore, the influence of temperature and duration of the heat-

curing on the compressive strength and the micro-structure of GGF-based geopolymers was studied. This study provides a new insight and information on the potential usages of GGF as a precursor to in production of geopolymer concrete.

## 8.2 Materials

### *8.2.1 Ground Glass Fiber (GGF):*

GGF used in this study was obtained from a commercial source that produces a powdered form of glass fiber by milling it to the average particles size of 4 microns. The specific gravity, Blain's fineness, and Loss of Ignition (LOI) of GGF were measured to be 2.6, 10,200 $cm^2/g$, and 1% respectively. The chemical composition of GGF is presented in Table 8-1. In addition, the appearance and the shape of its particles are presented in Figure 8-1. Moreover, the XRD pattern of the raw GGF is presented at Figure 8-2.

### *8.2.2 Fly ash:*

A local source of class F fly ash with an average particle size of 28 microns and used in this study. The fly ash used in this study had the specific gravity of 2.25, LOI of 2.3, and the Blain's fineness of 6040 $cm^2/g$. The chemical composition of the fly ash, and its XRD pattern are shown in the Table 8-1 and Figure 8-2 respectively.

Table 8-1. Chemical composition of the precursors

| | $SiO_2$ | $Al_2O_3$ | $Fe_2O_3$ | $CaO$ | $MgO$ | $Na_2O$ | $K_2O$ |
|---|---|---|---|---|---|---|---|
| GGF (%) | 47.72 | 10.36 | 0.34 | 19.62 | 2.27 | 0.67 | 0.10 |
| Fly Ash (%) | 50.70 | 25.10 | 12.50 | 3.30 | 1.10 | 0.51 | 2.27 |

### *8.2.3 Activator solutions:*

To prepare activator solutions, ASC grade sodium hydroxide pellets with 98% purity was obtained from AMERSCO Inc. In addition, a sodium silicate solution with a 40% solids-to-liquid ratio and the $SiO_3$-to-$Na_2O$ weight ratio of 3.4 was obtained from the CQ concept company.

Measured amount of sodium hydroxide pallets and sodium silicate solution would be dissolved in a required amount of water to prepare the alkali solution.

### *8.2.4 Fine aggregate (siliceous sand):*

To produce the mortar specimens, a mineral non-reactive siliceous river sand with an absorption value of 0.30% and an oven-dry specific gravity of 2.67 was used in this study. The sand had the final modulus of 2.6.

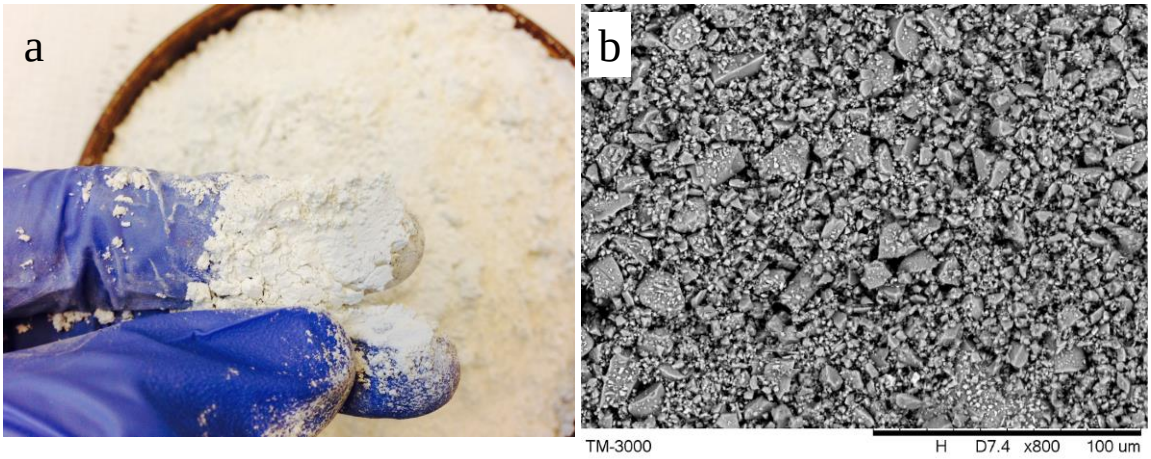


Figure 8-1. Raw GGF, (a). Normal appearance, (b). SEM image

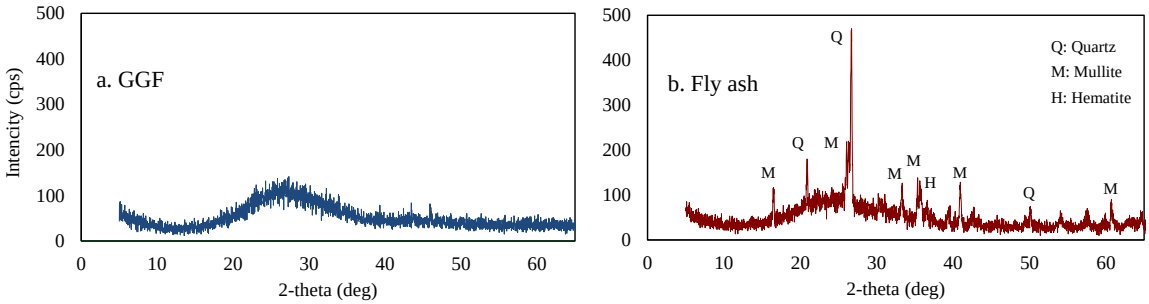


Figure 8-2. XRD pattern of precursors, (a). GGF, and (b). Fly ash

## 8.3 Experimental program.

### *8.3.1 Mixture proportions:*

To study the effect of chemical composition of activators on the properties of geopolymers, specific proportions of sodium hydroxide solution and sodium silicate solution were combined

together to produce the activator solutions of specific compositions. The two characteristic of activator solutions that were considered in this study were the mass ratio of $SiO_2/Na_2O$ and the mass ratio of total $Na_2O$ in the activator solution-to-precursors (i.e. binder). The first parameter, $SiO_2/Na_2O$ in the activator, was investigated at three levels 0, 0.50 and 1.00, while the second parameter, $Na_2O$-to-binder was studied at three different dosages 5%, 7.5% and 10%.

The sand content of the mortars was chosen to fill 55% of the total volume of the mixtures, and the water-to-binder ratio of all the mixtures was maintained at 0.30 for fly and 0.33 for the GGF-based geopolymers. These values of water-to-binder was selected to maximize the compressive strength of the hardened mortars, while requiring no water reducer to achieve the desired workability with the mixtures. Table 8-2 presents the details of the mixture proportions and the mix ID of all the mixtures used in this study. The letter(s) in the mix IDs shows the source material, i.e. GGF for ground glass fiber and F for fly ash, while the first and second numbers show the $SiO_2/Na_2O$ and the percent of $Na_2O$-to-binder respectively.

Table 8-2. Mixture proportion of the geopolymer pastes (to produce mortars, fine aggregate was added to fill 55% of the volume of the mixtures)

| Proportions | Mix ID for GGF-based mixtures | | | | | | |
|---|---|---|---|---|---|---|---|
| | GGF-0-10 | GGF-0.5-5 | GGF-0.5-7.5 | GGF-0.5-10 | GGF-1-5 | GGF-1-7.5 | GGF-1-10 |
| $Na_2O$/Binder | 10% | 5% | 7.5% | 10% | 5% | 7.5% | 10% |
| $SiO_2/Na_2O$ | 0 | 0.5 | 0.5 | 0.5 | 1 | 1 | 1 |
| Water/Binder | 0.33 | 0.33 | 0.33 | 0.33 | 0.33 | 0.33 | 0.33 |
| | Mix ID for fly ash-based mixtures | | | | | | |
| | F-0-10 | F-0.5-5 | F-0.5-7.5 | F-0.5-10 | F-1-5 | F-1-7.5 | F-1-10 |
| $Na_2O$/Binder | 10% | 5% | 7.5% | 10% | 5% | 7.5% | 10% |
| $SiO_2/Na_2O$ | 0 | 0.5 | 0.5 | 0.5 | 1 | 1 | 1 |
| Water/Binder | 0.3 | 0.3 | 0.3 | 0.3 | 0.3 | 0.3 | 0.3 |

### *8.3.2 Mixing procedure and compressive strength test*

To examine the effect of change in the characteristics of activator solution(i.e. $Na_2O$/precursors, and $SiO_2/Na_2O$ in the activator solution), on the compressive strength of the geopolymer mixtures, mortars were mixed and then cast in 50×50×50 mm cube molds. The first step in the mixing procedure involved dissolving the required amount of sodium hydroxide pellets and sodium-silicate solution in water to achieve the desired activator composition. The mixing process was continued until all the sodium hydroxide pellets were completely dissolved. At this point, the source material was added to the solution and was mixed for an additional minute. Finally, the sand was introduced into the mixer and the mixing process was continued until a desired consistency was achieved. The material was then cast into cube molds and placed in a 60$^{o}$C curing chamber. After 24 hours, specimens were removed from their molds and were placed inside an environmental chamber with the controlled temperature of 23$^{o}$C and the relative humidity of 50%. Subsequently, the compressive strength of the cubes was measured at 3, 7 and 28 days from the casting day in accordance with the test procedure described in ASTM C109.

In addition to the reference curing temperature of 60$^{o}$C and 24 hour curing duration, the effect of extended curing durations and other curing temperatures on the compressive strength of a GGF-based geopolymer mixture was also evaluated. For this purpose, the geopolymer mixture that had resulted in the highest 28 days compressive strength based on the variations in the compositions of the activator solutions was selected for further evaluation. To evaluate the effect of extended curing duration, the 7-day and the 28-day compressive strength of the mixture that was cured at 60$^{o}$C for 24 h was compared to the specimens that were cured at the same temperature for 48 h, 72 h and 168 h. In addition, to examine the effect of the curing temperature, the compressive strength of mixture was also compared to the specimens that were cured at 23$^{o}$C, 38$^{o}$C, 80$^{o}$C and 110$^{o}$C (for 24 hours). The influence of curing temperature was evaluated by

testing the cubes at 3, 7 and 28 and 56 days from the casting day.

### *8.3.3 Extent of dissolution of precursors*

To evaluate the solubility of each precursor in a high alkali media, 5g of each precursor was dissolved in 100 ml of a 5N Sodium hydroxide solution. A magnetic stirrer was used to mix the solutions for 2 h at the ambient temperature. A 1.5 µm glass micro fiber filter (Whatman Grade 934-AH Micro Fiber Filter) was used to filter the solution. The filtered solution would then be diluted to 1:100 using deionized water. The concentration of soluble Si, Al, and Ca in the solution was measured using the Inductively Coupled Plasma (ICP) test method. Finally, concentration of dissolved elements was back-calculated for the 5N Sodium hydroxide solution before the dilution.

### *8.3.4 Dissolution of Geopolymer Paste in HCl Acid*

To find the amount of unreacted GGF particles in the GGF-based geopolymer, dissolution of paste samples in an HCl solution was measured in this study. The HCl solution has been reported to dissolve the geopolymerisation products, while leaving the unreacted precursor's particles behind (52, 85). In this study, following Palomo et al. (52), dissolution of selected GGF-based paste samples were studied in a 1:20 HCl solution (i.e. 50 ml of 1N HCl solution in 1000 ml water). Geopolymer paste was crushed to a fine powder and the portion passing sieve #100 and retaining #200 sieved was collected for the test. To perform the test, 2 g of the paste powder was introduced into a 500 ml of the HCl solution. The solution was mixed for 3 h using a magnetic stirrer, and then was filtered using a 1.5 µm filter paper. Finally, the residue solids was collected, dried at 110$^{o}$C for 24 hours, and their dried weight was measured and recorded.

### *8.3.5 Solubility of geopolymer paste in water:*

To study the presence of any water-soluble phases in the GGF-based geopolymer pastes, the solubility of crushed pate in deionized water was examined. For this purpose, the 7-day old GGF-

based geopolymer paste samples were mechanically crushed (using a hammer) and sieved. The portion that passed sieve #50 and retained on the sieve #100 was collected and dissolved in 100 ml of deionized water. A magnetic stirrer was used for this purpose; and each solution was mixed for 2 hours. Subsequently, the solutions were filtered using a micro-fiber filter (Whatman Grade 934-AH Glass Micro Fiber Filter), and ICP test was conducted on each filtered solution to measure the concentration of dissolved Si and Al in each solution.

### *8.3.6 SEM, XRD-EDX and TGA*

To investigate the microstructure and the chemical composition of the geopolymer specimens, the scanning electron microscopy (SEM) and the energy-dispersive X-ray spectral analysis (EDX) were used in this study. Geopolymer specimens were cut using a slow-speed diamond saw with mineral oil as the lubricant. The cut samples were then polished using resin-bonded diamond discs with grit size changing form #80 to #4000. The SEM examination of the prepared specimens was performed in back-scatter mode, using a Hitachi TM 3000 microscope that was equipped with a Swift EDX silicon-drift detector.

To study the microstructural characterization, and to measure the amount of calcium hydroxide (CH) of the geopolymer samples, X-Ray diffraction (XRD) and thermogravimetric analysis (TGA) were performed on the crushed geopolymer pastes, respectively. For the XRD analyses, a Rigaku Ultima IV multipurpose X-ray diffraction system with a test parameters being set as 2θ changing from 5$^{o}$ to 65$^{o}$ (Cu Kalpha radiation), and the scan rate of 0.1 per minutes, was used. For the purpose of the TGA test, a TA instrument Model TGA 2950employing a platinum pan with nitrogen purge gas was used. In this test, representative crushed paste samples were gradually heated from the ambient temperature to 700$^{o}$C. Decomposition of CH is known to occur within the temperature of 440 to 520$^{o}$C, causing a mass loss in the sample (86). In this study, the mass loss in this range was measured and used to calculate the amount of CH in the

geopolymer samples.

### *8.3.7 Quantification of Unreacted Precursor Using Image Analysis*

Image analysis of SEM images taken in back-scatter mode was conducted on paste specimens to quantify the unreacted precursor present in the test specimens. To conduct the image analysis, a stepwise image processing algorithm was designed to detect and quantify the amount of GGF present in the paste test specimens. The SEM images were acquired using a Hitachi TM-3000 Electron Microscope and then pre-processed in MATLAB software. A unique segmentation technique known as Adaptive K-means Clustering (AKM) based on the work by Chen et al. and Darken and Moody, was implemented in this study to segment the GGF particles (87, 88). Adaptive k-means clustering is an operation where the given image is divided into different clusters automatically based on cluster centers unlike normal k-means where number of clusters must be specified. As the number of clusters may vary in different images, the algorithm was designed in such a way to detect the brightest cluster and binarize it to detect the GGF particles. Consequently, the segmented GGF particles are quantified in terms of percentage over the entire image and used for further analysis in the present study.

## 8.4 Results and discussion

In this study, the effect of different parameters on the mechanical strength of hardened GGF-based geopolymer mortar specimens was investigated. Parameters such as: effect of precursor's type (GGF and fly ash) and the effect of composition of activator solutions such as $SiO_2/Na_2O$ ratio in the activator solution and $Na_2O$-to-binder ratio on the compressive strength of the GGF and fly ash-based geopolymers were investigated. Moreover, effects of the heat-curing temperature and its duration, on the compressive strength of the GGF-based geopolymers were examined in this study.

### *8.4.1 Effect of precursor type on the compressive strength (GGF versus fly ash)*

The compressive strength of the GGF and fly ash-based geopolymer mortar cubes at 3, 7 and 28 days are shown Table 8-3. To evaluate the performance of GGF as a precursor, the compressive strength of GGF-based geopolymer mortar mixtures was compared to the compressive strength of fly ash-based geopolymer mixtures that were prepared in the same manner with the GGF-based specimens. As it can be seen, for all the tested mixtures, compressive strength of the GGF-based mortar cubes were higher than the fly ash-based specimens that were synthesized using a same activator solution. While the effect of composition of activator solutions on the compressive strength of geopolymer cubes made from each precursor will be discussed in the section 8.4.2, this section deals with the effect of the precursors themselves on the strength of the geopolymer specimens.

Table 8-3. Compressive strength of the GGF and fly ash-based geopolymer mortar cubes (MPa)

| Age | Compressive strength of GGF-based mortar cubes (MPa) | | | | | | |
|---|---|---|---|---|---|---|---|
| | GGF-0-10 | GGF-0.5-5 | GGF-0.5-7.5 | GGF-0.5-10 | GGF-1-5 | GGF-1-7.5 | GGF-1-10 |
| 3 days | 79 | 27 | 53 | 67 | 25 | 58 | 69 |
| 7 days | 78 | 28 | 54 | 75 | 27 | 53 | 72 |
| 28 days | 82 | 29 | 55 | 79 | 28 | 56 | 67 |
| | Compressive strength of fly ash-based mortar cubes (MPa) | | | | | | |
| | F-0-10 | F-0.5-5 | F-0.5-7.5 | F-0.5-10 | F-1-5 | F-1-7.5 | F-1-10 |
| 3 days | 14 | NA | 16 | 35 | 16 | 43 | 58 |
| 7 days | 20 | NA | 17 | 36 | 21 | 44 | 60 |
| 28 days | 25 | NA | 22 | 46 | 24 | 45 | 59 |

The particle size of precursors has been reported to play a key role in the mechanical properties of the fly ash based geopolymers (57). Small particles size of the precursors not only provides a higher specific surface area but also causes the activated material to have a lower porosity, which enhances the compressive strength of geopolymers (60). In this study, the first

factor that can explain the higher compressive strength of the GGF-based geopolymer mortars is the smaller particle size of the GGF (4 μm) in comparison to fly ash (27 μm). As presented in sections 8.2.1 and 8.2.2, the Blaine's fineness of GGF and fly ash was measured to be 10,200 $cm^2/g$ and 6040 $cm^2/g$, respectively.

To measures the total porosity of a GGF and fly ash-based geopolymer, MIP test was conducted on the seven-day old mortar samples with the highest compressive strength from each of the GGF (G-0-10) and fly ash-based geopolymers (F-1-10). The outcome of this test showed the lower porosity of the GGF-based mortars (0.03 cc/g) in comparison to the fly ash-based mortars (0.10 cc/g).

Unreacted precursors in the geopolymer matrix can act as a reinforcement (30, 89). Therefore, it can be assumed that a precursor with a harder nature can enhance the mechanical properties of a geopolymer mixture. To better understanding the role of unreacted GGF particles in improving the compressive strength of the mortar samples the microstructure of cracked geopolymers was studied. In order to obtain cracked specimens, geopolymer specimen were stressed to 75% to 85% of their ultimate compressive strength. The samples were then cut using a slow speed saw and analyzed using an SEM machine. Figure 8-3, shows SEM images of a GGF and a fly ash-based geopolymer specimen that was prepared with this method. As it can be seen Figure 8-3a, in the case of GGF-based geopolymer, the cracks would either stop or bypass the GGF particles, but do not pass through them. For crack to circumvent the particles would require additional energy, thus increasing the stress required for the failure of the sample. On the other hand, as presented in Figure 8-3b, cracks formed in the fly ash-based samples passed through the fly particles. This suggests that fly ash particles do not provide the same reinforcing effect as GGF particles.

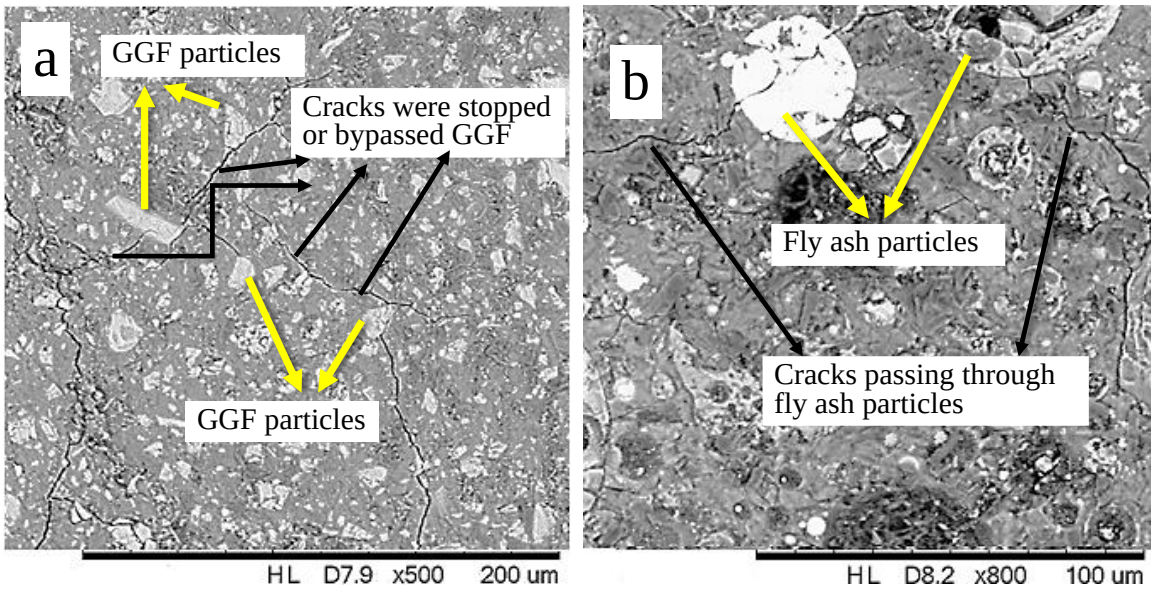


Figure 8-3. SEM images of cracked surface of geopolymer samples. a). GGF-based specimen, b). Fly ash-based specimen

Extent of dissolution of a certain precursor in a high alkali media has been used as a parameter to evaluate the compressive strength of geopolymers (59, 70, 89). It has been suggested that a higher leaching rate of a precursor will results in the faster gelation, setting, which in most of the cases, will lead to the higher compressive strength of the resultant geopolymer (89). To measure the extent of solubility of the precursors in a high alkali media, a solubility test was conducted on each of the precursors in accordance to the procedure described in the section 8.3.3 (Table 8-4). As presented in Table 8-4, in comparison to the fly ash, GGF released a higher amount of Si and Ca into the alkali solution; while they both showed an almost same amount for the case of Al leachate. It should be noted that although the XRF result (Table 8-1) showed a higher amount of Al content in the fly ash in comparison with GGF, the amount of Al that released from both materials were in a close range. Therefore, it could be concluded that the Al in the fly ash sample is more strongly bound with the original material in comparison with GGF.

The lower level of dissolution of Si and Al ions from the fly ash particles compared to the GGF particles into the alkali solution can be related to the presence of quartz and mullite crystals

in the structure of the raw fly ash. These phases do not readily dissolve in a high alkali solution and are known to be stable in such media (90, 91). According to Temuujin and Van Riessen, presence of mullite in the fly ash reduces the reactivity of fly ash and decreases the level of geopolymerisation (77). Therefore, presence of these phases, i.e. mullite and quartz, in the original fly ash is thought to negatively affect the compressive strength of the final geopolymer. As it can be observed in the XRD pattern of the virgin fly ash and F-1-10 geopolymer paste (Figure 8-4), the mullite's and quartz's peaks in the original fly ash remained almost intact, even after the activation with the high alkali solution (solution with a $Na_2O$-to-binder =10%) and can be observed in the XRD pattern of the F-1-10 specimen. Thus, these results can explain the low amount of dissolution of Si and Al in the alkali solution (Table 8-5), despite the relatively high amount of Si and Al in its chemical composition. It should be noted that the chemical composition of the raw fly ash showed values of 50.0% for Si and 25.1% for Al in comparison to the values of 47.72% for Si and 10.36% for Al in GGF (Table 8-1).

Table 8-4. Extent of dissolution of GGF and Fly ash in a High Alkali Media (5N NaOH solution, for 2 h)

| Precursors | Si (ppm) | Al (ppm) | Ca (ppm) |
|---|---|---|---|
| GGF | 1156 | 142 | 696 |
| Fly ash | 748 | 141 | 315 |

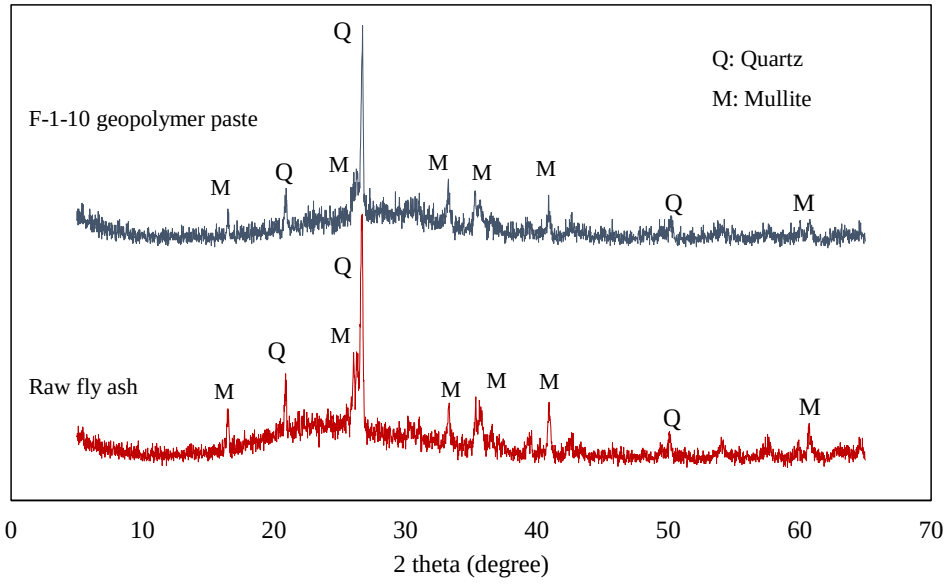


Figure 8-4. XRD pattern of the raw fly ash and F-1-10 geopolymer paste

An important parameter that can affect the strength gain behavior of the geopolymer systems, is the amount of calcium content in the used original precursors. Presence of calcium in the precursors is known to shorten the setting time (71-73), and hence increase the rate of strength gain of the geopolymer samples. The exact mechanism by which calcium affects the mechanical properties of the geopolymer systems is not clear yet. However, many studies have reported that the addition or presence of calcium caused an increase in the compressive strength of the geopolymer mixtures (2, 25, 71, 76, 77).

One of the suggested mechanisms by which Ca affects the structure of the geopolymers, is the substitution of the Na ions in the N-A-S-H (sodium aluminosilicate hydrate) structure by Ca ions (83). According to (92), considering the similar electronegativity potential and ionic radius between Ca and Na, Ca ions will replace Na ions in the N-A-S-H gels causing the formation of (C-N)-A-S-H gels ((calcium-sodium)-aluminosilicate-hydrate) in the geopolymer structure. Therefore, given the presence of the relatively high amount of Ca in the of GGF, it was concluded in this study that in GGF-based geopolymers, negative charge associated with $Al(OH)_4^-$ is

balanced with the Ca and therefore more sodium ions are left free in the system to accelerate the geopolymerisation process. Thus, the higher compressive strength of GGF-based samples in comparison to the fly ash-base ones, especially for the case of mixtures with the lower Na-to-binder ratios (i.e. 5% and 7.5%), can be explained by the presence of calcium in the matrix of GGF based geopolymers.

### *8.4.2 Effect of activator solutions*

#### *8.4.2.1 Effect of sodium content*

The compressive strength of the GGF and fly ash-based geopolymer mortar cubes at 3, 7 and 28 days are shown Table 8-3. Based on these results, for both the GGF and fly ash-based mixtures the compressive strength increased with the increase in the sodium content of the activator solution. In the case of GGF-based geopolymers, the 28-day compressive strength of mixtures with $SiO_2/Na_2O$ = 0.5 and $SiO_2/Na_2O$ =1, showed an increase from 29 to 79 MPa and 28 to 67 MPa, respectively, when the sodium content was increased from 5% to 10% by the weight of the binder. The fly ash-based specimens showed a same trend as same as the GGF-based mixtures. For the fly ash based mixtures, the compressive strength of the 28 days old specimens showed an increase from less than 5 MPa to 46 MPa, and 24 to 59 MPa for $SiO_2/Na_2O$ = 0.5 and $SiO_2/Na_2O$ =1 respectively, when the $Na_2O$-to-binder weight ratio was increased from 5% to 10%. The effect of $Na_2O$-to-binder weight ratio on the 28-day compressive strength of the GGF and fly ash-based mortar samples are presented in Figure 8-5.

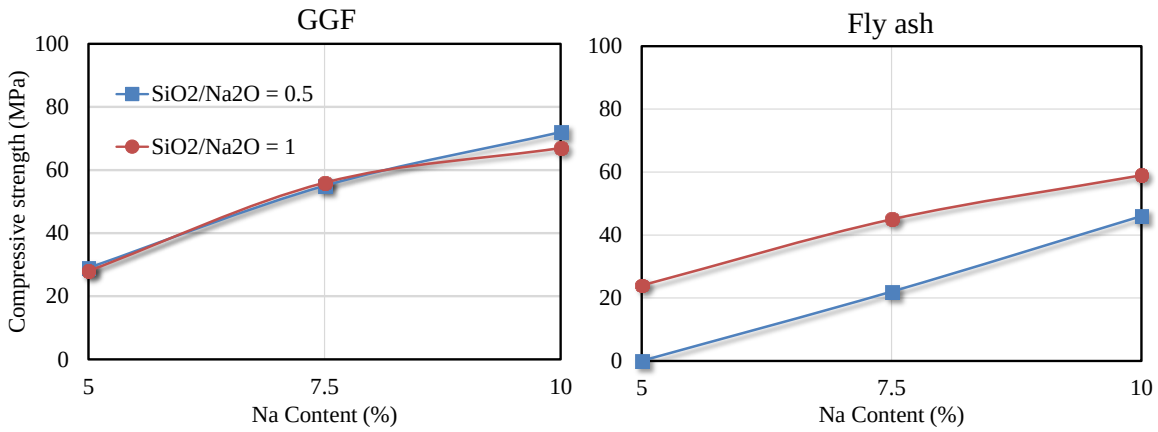


Figure 8-5. Effect of sodium content of the activator solution on the compressive strength of the GGF and fly ash-based geopolymer mortar mixtures.

The higher compressive strength of the mixtures made with the $Na_2O$-to-binder ratio of 10% in comparison to the mixtures with the lower Na content, can be related to the higher dissolution rate of the precursors in a higher pH (70). Based on the earlier studies made on precursors such as meta-kaolin and fly ash-based geopolymer, employing an activator with a higher sodium content causes an increase in the breakage of the glassy chains in the precursor which leads to a higher compressive strength (26, 45, 53). More detailed discussion on the effect of the alkali concentration of the activator solution on the compressive strength of GGF based mixtures is presented in the section 8.4.2.3.

### *8.4.2.2 Effect of silica content*

As it can be observed from Table 8-3, the compressive strength of geopolymer mortar mixtures is affected by the amount of added silica ($SiO_2/Na_2O$ ratio of the activator solution). The influence of this parameter (in terms of $SiO_2/Na_2O$ ratio) on the 28-days compressive strength of GGF and fly ash-based mixtures, at a fixed Na content of 10%, is presented in Figure 8-6. As shown in this figure, rise in the silica content of the activator solutions resulted in the higher compressive strength in the fly ash-based geopolymers. However, it showed a negative influence on the compressive strength of GGF-based specimens.

In fly ash-based mixtures with 10% sodium content, the compressive strengths values of 28-days specimens increased from 25 MPa to 59 MPa, when $SiO_2/Na_2O$ was increased from 0 to 1. However, the compressive strength of GGF-based mixtures decreased from 82 MPa to 67 MPa when $SiO_2/Na_2O$ ratio of the activator solution was increased from 0 to 1. The highest compressive strength in the GGF-based samples (82 MPa) was observed in the case of GGF-0-10 mixture which had no added silica in the activator solution. The increase in the compressive strength of the fly ash-based mixture with the increase in the Si content of activator is in agreement with the earlier studies conducted on fly ash-based geopolymer mixtures (11, 46, 59).

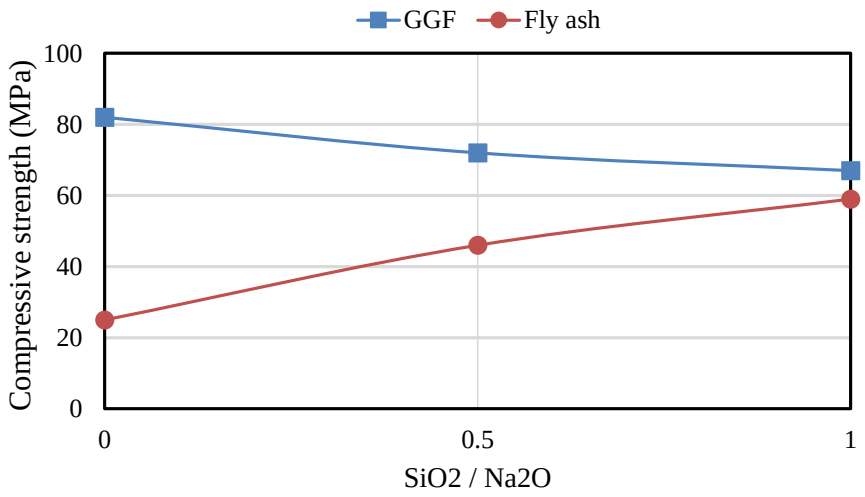


Figure 8-6. Effect of silica content of the activator solution on the compressive strength of GGF and fly ash-based geopolymers

In the present study, the reduction seen in the compressive strength of GGF-based geopolymers with the rise in the soluble Si content of the solution (higher $SiO_2/Na_2O$ values) is thought to be due the following two reasons:

(a) *Si/Al ratio:* Presences of Al in geopolymers is essential, as it links the silica chains together and produces the 3-D network of the final material (63). Studies performed on the geopolymer mixtures with varying amount of Si/Al ratios have shown the significance of this parameter on the mechanical properties of the final product (64-69) According to these

studies, the optimum value of the Si/Al molar ratio in the geopolymer mixture is around two, and either low, or high amounts of Si/Al ratio of the mixture causes the reduction in the compressive strength. In the present study, the Si/Al molar ratio of the GGF-0-10 and GGF-1-10 mixtures was calculated to be equal to 4.06 and 4.92 respectively. Thus, the lower compressive strength of the GG-1-10 specimens can be related to the higher Si/Al ratio.

*(b)* Unreacted particles: The higher compressive strength of GGF-0-10 specimens (with no added soluble silica) in comparison to the mixtures with added soluble Si (i.e. GGF-0.5-10 and GGF-1-10) can also be attributed to the lower level of unreacted GGF particles in this mixture. Presence of soluble Si (from sodium silicate solution) in the activator solution of the GGF-0.5-10 and GGF-1-10 mixtures, is thought to affect the solubility of the GGF particles negatively; and causes a reduction in the compressive strength of these mixtures. In this study, to evaluate the amount of unreacted GGF particles in the GGF-0-10 and GGF-1-10 mixtures, two methods namely dissolution in HCl acid, as described by Palomo et al. (52), and an image analysis technique were used.

Results of the first test, dissolution in HCl acid, are presented in Table 8-5. These results show the amount of the residue that did not dissolve into the HCl solution and hence are considered as the unreacted particles. As it can be seen a higher amount of residue was measured for the case of GGF-1-10 paste specimens. Therefore, the better performance of GGF-0-10 specimens in comparison to the GGF-1-10 specimens can be explained by the lower level of unreacted GGF particles in this mixture.

Table 8-5. Results of dissolution in HCl solution for GGF-0-10 and GGF-1-10 pastes

| Mix ID | Added paste (g) | Residue (g) | Residue (weight %) |
|---|---|---|---|
| GGF-0-10 | 2.00 | 0.95 | 48.3% |
| GGF-1-10 | 2.00 | 1.04 | 52.0% |

To perform the image analyses, three SEM images were taken from the different locations of the GGF-0-10 and GGF-1-10 pastes. Using image analysis technique, the ratio of unreacted particles to the total paste area was calculated for each of the images. These ratios were then averaged and reported as the unreacted particles ratio of each of the mixtures. In this method, the higher ratio means more unreacted particles in the geopolymer paste and can be related to the lower compressive strength. Example of one of the images from GGF-0-10 and GGF-1-10 used for the image analyses are presented in Figure 8-7. As it can be observed, unreacted particles have occupied a higher area in the GGF-1-10 paste (20.1%) in comparison to the GGF-0-10 paste (16.6%). Thus the higher strength of the GGF-1-10 samples can be explained by the lower amount of unreacted particles.

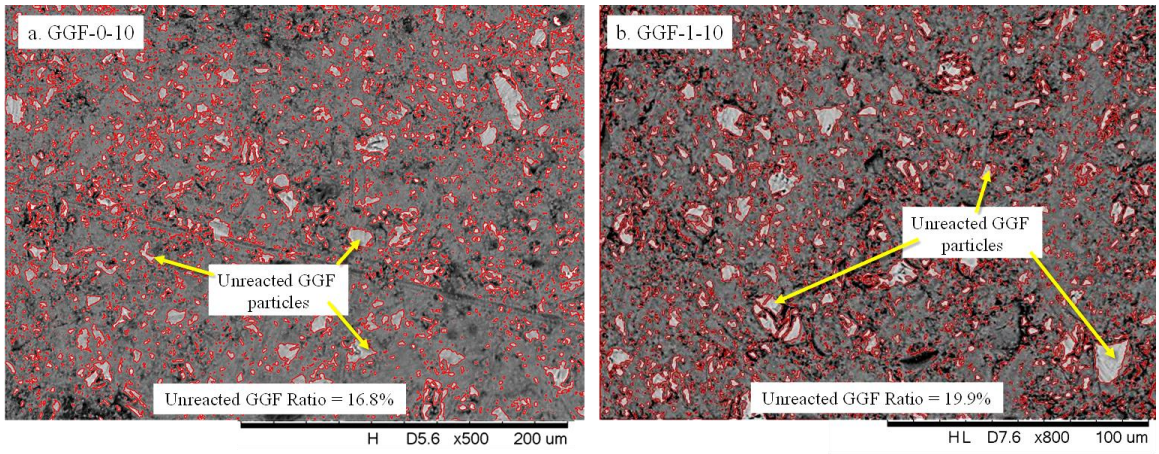


Figure 8-7. Image analysis results: a) performed on GGF-0-10, and b) Performed on GGF-1-10 pastes. (The unreacted GGF ratio is defined as: area of the unreacted particles" divided by the total area of the pate and unreacted particles)

Although, studying the potential environmental benefits of using GGF-based geopolymers is beyond the scope of this work and could be associated to several other factors. It is worth mentioning that, according to Weil et al. (1) and Turner and Collins (93), it is known that the usage of sodium silicate has a significant effect in increasing the amount $CO_2$ emission for the production of geopolymers. Thus, using the material that can be activated with no need for

sodium silicate might have potential environmental benefits.

#### *8.4.2.3 Optimum alkali content for GGF-based geopolymer*

To investigate the optimum alkali content of activator solutions which results in the highest compressive strength, solutions with varying amount of $Na_2O$-to-binder mass ratio were prepared to produce GGF-based geopolymer mortars. The solutions were prepared by dissolution of required amount of NaOH pellets in water to produce mixtures with $Na_2O$-to-binder ratio of 5, 10, 15 and 20% (No sodium silicate solution was used). A water-to-binder ratio of 0.33 and sand content of 55% (volume based) were used in these mixtures. The same labeling method as presented in section 8.3.1 (Table 8-2) was used to identify the mixtures. Therefore a mixture with the $\alpha$% $Na_2O$-to-binder ratio was named as GGF-0-$\alpha$ (i.e. the mixture with $Na_2O$-to-binder ratio of 15% was labeled as GGF-0-15).

The 28-days compressive strength of GGF-based geopolymer samples which were synthesized using the above mentioned proportions are presented in Figure 8-8. As it can be seen, increase in the alkali content of the solution, up to the $Na_2O$-to-binder ratio of 10%, resulted in the higher compressive strength of the mortar samples. However, the further increase in the alkali content (i.e. 15% and 20%) led to the reduction of the compressive strength. The same behavior, reduction in the mechanical properties with the rise in the alkali content of the solution, was also seen in the earlier studies conducted on various precursors (32, 54, 56, 94).

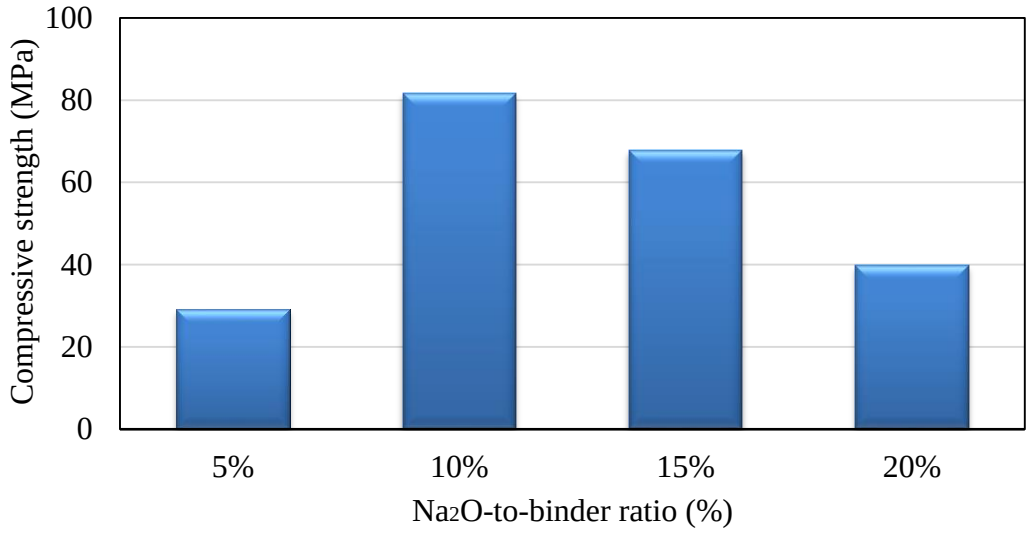


Figure 8-8. Effect of $Na_2O$-to-binder ratio on the compressive strength of GGF-based geopolymer samples (after 28 days)

The higher compressive strength of the GGF-0-10 specimens in comparison to the GGF-0-5 specimens could be related the higher content of alkali in the mixture; which; promote the dissolution of Si and Al from the GGF particles. Using the same method presented in the section 8.4.2.2, the image analyses technique was used to find the ratio of unreacted GGF particles in GGF-05, GGF-0-20 (Figure 8-9). Based on these results, the ratio of the unreacted particles is strongly related to the alkali content of the activator solutions. The average ratio of the unreacted GGF particles of GGF-0-5, GGF-0-10, and GGF-0-20 were measured to be 22.6%, 16.6%, and 9.6% respectively. Therefore, the lower compressive strength of the GGF-0-5 specimens in comparison to the GGF-0-10 can be explained by the lower dissolution of the GGF particles.

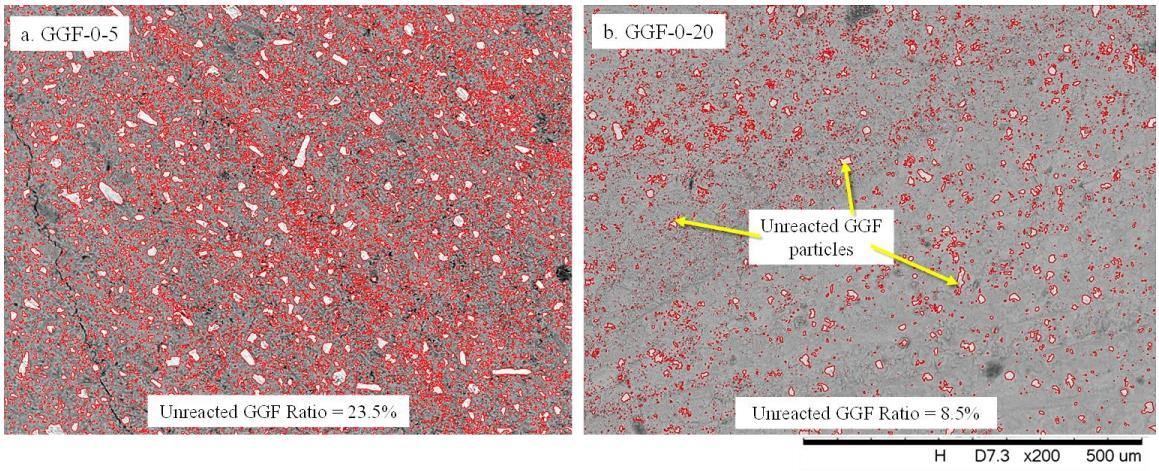


Figure 8-9. Image analysis results: a) performed on GGF-0-5, and b) Performed on GGF-0-20 pastes. (The unreacted GGF ratio is defined as: area of the unreacted particles" divided by the total area of the pate and unreacted particles)

The decrease in the compressive strength in the GGF-0-15 and GGF-0-20 mixtures could be explained by the extremely high alkali content of solution. The geopolymerisation process consists of the dissolution of Si and Al monomers from the precursor into the activator solution, which is then followed by the saturation of the solution, gelation, reorganization, polymerization, and hardening (3). According to Alonso and Palomo (56), in a high pH solution, the anionic silicate ($SiO_3^{2-}$) is a more stable form than the molecular one; and hence delaying the geopolymerisation. Alternatively, it is thought that in the high alkali mixture such as GGF-0-15 and GGF-0-20, the polymerisation and hardening cannot take place favorably as the Si and Al monomers tend to dissolve into the high pH solution.

In this situation, with the excessive amount of Na in the mixture, the Na ions that have not been fixed in the geopolymer matrix are present in the pore solution. This increases the pH of the pore solution; leading to the dissolution of more Si and Al from the GGF particles. It is thought that in this situation, the amount of Al is not sufficient to fix the Na ions; thus, due to the high pH of the pore solution a super-saturated solution (rich in Na and Si) will form in the GGF-0-15 and GGF-0-20 mixtures, which delays the setting process. Results of initial, and final setting

times (ASTM C191 - Vicat needle) are presented in Table 8-6.

Table 8-6. Final setting time of GGF-based geopolymer paste (minutes)

| Paste ID | GG-0-10 | GGF-0-15 | GGF-0-20 |
|---|---|---|---|
| Final setting time (min) | 70 | 105 | 125 |

As the curing process continues, the water evaporates from the geopolymer matrix. However, considering the mechanism of geopolymerisation (3), the geopolymerisation process can only take place, when water is available to act as a transporting media for the Si and Al monomers. Therefore, in the absence of a transporting media, the Si and Na ions that have remained in the pore solution will react together, forming a sodium silicate-like gel.

As it is known, sodium silicate is soluble in the water, and if such a gel is available in the system, the GGF-0-15 and GGF-0-20 should have a higher solubility in the water in comparison to GGF-0-10. To examine this, according to the procedure described in section 8.3.5, two grams of GGF-0-10, GGF-0-15 and GGF-0-20 were dissolved in 100 ml of deionized water. The solution was then filtered using a micro-fiber filter, and ICP test was conducted on each filtered solution. The results of ICP test are presented in Figure 8-10. As it can be seen the amount of dissolved Si in all the cases is much higher than the Al. This support the theory that most of the released Al have been fixed in the geopolymer structure and hence do not dissolve in the water. In addition, as it could be seen, the amount of Si dissolved shows a significant increase for the case of GGF-0-20, in comparison to GGF-0-10 and GGF-0-15. Thus, it was concluded that the gel (sodium silicate-like gel) is forming in the GGF-based geopolymers with the high alkali content (i.e. GGF-0-15 and GGF-0-20).

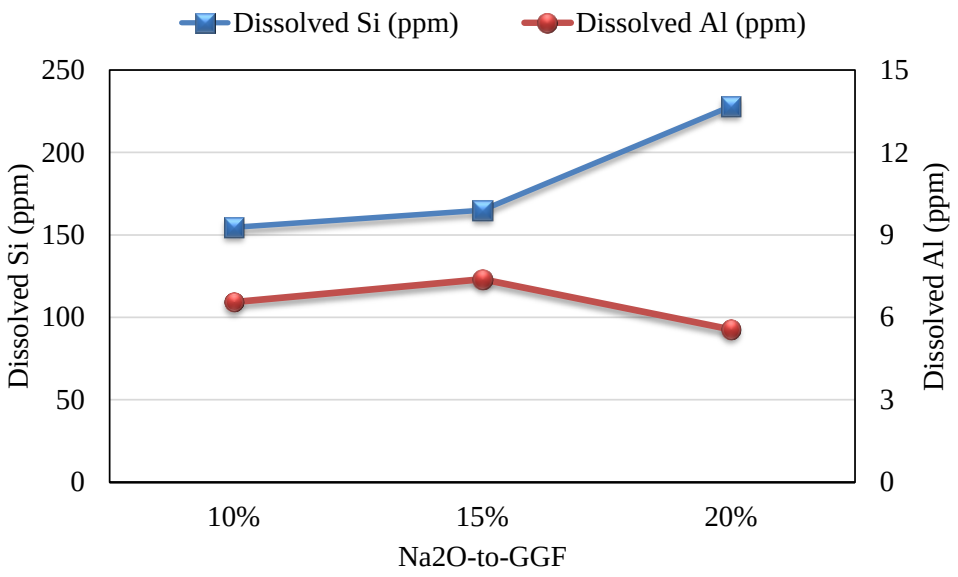


Figure 8-10. Dissolution of Si and Al from GGF-based geopolymer paste into deionized water

### *8.4.3 Effect temperature and duration of heat curing*

#### *8.4.3.1 Effect of temperature of curing*

In order to investigate the effect of curing temperature on the compressive strength of GGF-based geopolymers, the GGF-0-10 mixture was selected as it showed the highest compressive strength among the tested mixtures. To investigate the effect of curing temperature, this mixture was prepared using the method described at section 8.3.2 and then cured at 23ºC, 38ºC, 60ºC, 80ºC and 110ºC for the initial 24 h. After the initial 24 hour curing at the respective temperatures, the samples were aged at 23ºC and 50% relative humidity up to the day of testing. The effect of curing temperature on the compressive strength of the GGF-based geopolymer is presented in Figure 8-11.

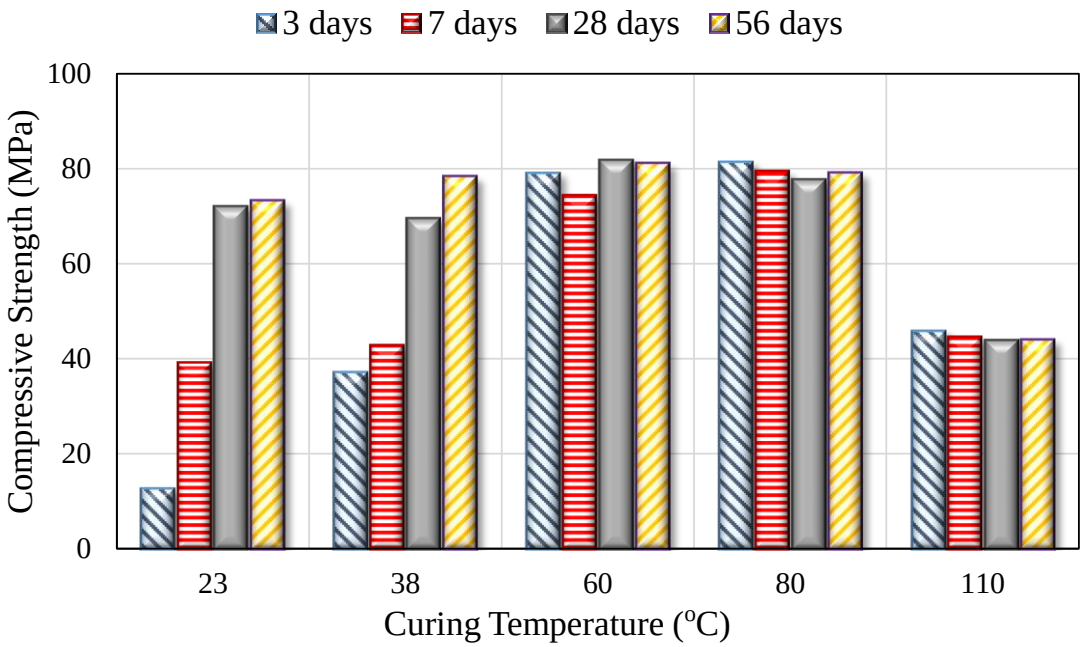


Figure 8-11. Effect of curing temperature on the compressive strength of GGF-0-10 mortar cubes

As it can be seen in the Figure 8-11, for all the different tested ages, the highest compressive strength occurred at the 60°C and 80°C curing temperatures. As presented in this figure, the specimens that were cured at lower temperatures (i.e. 23°C and 38°C) showed a gradual strength gain between 3 days and 56 days from 13 to 73 MPa (at 23°C) and 37 to 78 MPa (at 38°C) However, the compressive strength of the mortar cubes that were cured at 60°C, 80°C and 110°C remained almost constant between 3 days and 56 days. In the case of specimens cured at 60°C and 80°C the compressive strength was measured to be in the range of 74 to 82 MPa at all the tested ages, while in the case 110°C the strength of the tested specimens was around 45 MPa at all the measured ages. It should be mentioned that, except for the specimens that were cured at the 110°C, the effect of curing temperature on the compressive strength of the specimens was seen to be negligible at the later ages (i.e. 28 days and 56 days), as the compressive strength of the specimens that were cured at 23°C, 38°C, 60°C and 80°C was in the range of 70 to 80 MPa.

The lower compressive strength of the specimens cured at 110°C can be related to the

following factors. 1) Formation of cracks in the paste due to plastic shrinkage, and 2) low dissolution of the precursors. Figure 8-12 shows SEM images of the geopolymer paste cured at 60°C and 110°C after 28 days. As it can be seen while no significant sign of cracking was seen in the case of the samples cured at 60°C, however wide cracks were clearly seen in the samples cured at 110°C. The cracks formed in these samples (cured at 110°C) are thought to be as a result of the shrinkage that occurred due to the evaporation of water at the high curing temperature. The main reason for the lower compressive strength of the 28 days old samples cured at 110°C in comparison to the specimens, cured at the other temperatures, is attributed to the presence of these cracks.

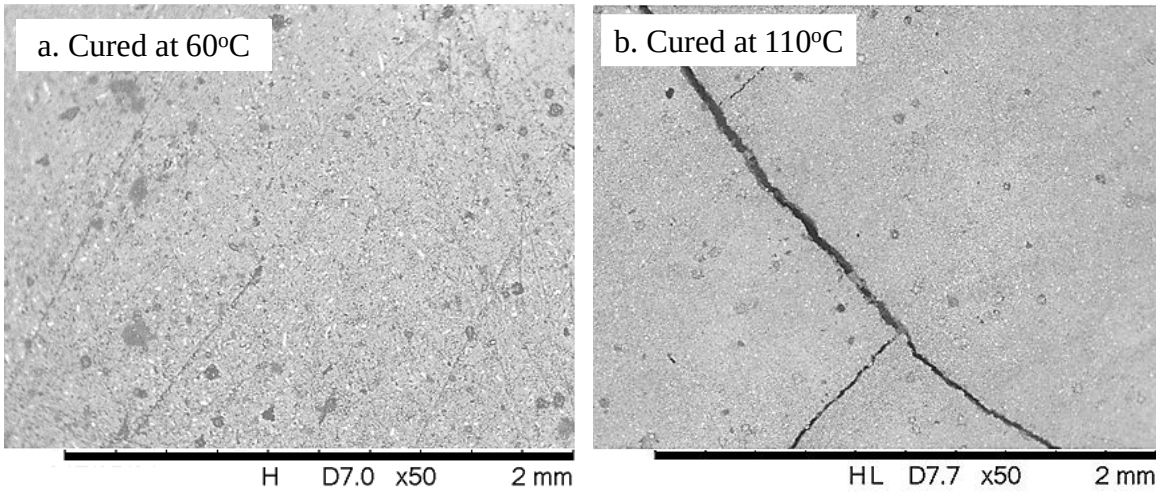


Figure 8-12. SEM image of geopolymer paste samples: a). cured at 60°C, b). cured at 110°C

Lower degree of dissolution of the precursors in the solution is another factor that affected the compressive strength of the specimens cured at 110°C. To compare the dissolution rate of the specimens cured at different temperatures, 7 and 28 days old paste samples cured at each of the temperatures were dissolved in HCl acid per the procedure described in the section 8.3.4. The results of the HCl dissolution test for both 7 and 28-day samples are presented in Table 8-6. As it can be seen the samples cured at 110°C showed the highest amount of residue (unreacted particles) after being dissolved in HCl acid. The higher amount of unreacted particles

in the case of specimens curd at 110°C can be related to the rapid evaporation of the moisture which shortens the available time for the dissolution process to take place.

Table 8-7. Results of HCl dissolution test for the GGF-0-10 paste cured at different temperatures

| Curing temperature | Amount of residue (%) | |
|---|---|---|
| | After 7 days | After 28 days |
| 23°C | 56% | 56% |
| 38°C | 53% | 54% |
| 60°C | 53% | 50% |
| 80°C | 54% | 54% |
| 110°C | 67% | 65% |

Compressive strength of the specimens cured in lower temperatures can be related to the lower degree of the polymerisation at these ages. While moisture is needed to act as a transporting media for the dissolved Si and Al monomers, presence of moisture in a geopolymer system has reported to delay the polymerisation. According to Bing-hui et al. (50), the geopolymers mixtures cured in the lower temperatures showed a gelatinous and moist structure in the early ages. Moreover, as presented in Table 8-7, the curing temperature, does not seem to have a notable influence on the dissolution rate of these specimens, as the specimens cured at lower temperatures showed almost same values of dissolution with specimens cured at 60°C for both 7 and 28-day ages. Thus, the low early-age strength of the specimens cured at 23°C, and 38°C could be related to the delayed geopolymerisation.

Finally, it should be added that the curing GGF-based mixture at different temperatures did not seem to affect the phases formed in the final products. Figure 8-13 presents the XRD patterns of the GGF-based geopolymers cured at 23°C and 110°C. As it can be observed, despite small variations in the peaks' intensity, the overall patterns of both samples are in a close match. Therefore, it could be concluded that the main reasons for the variation in the compressive

strength of the samples cured at different temperatures are attributed to their different micro-structure (i.e. effect of cracks and unreacted particles).

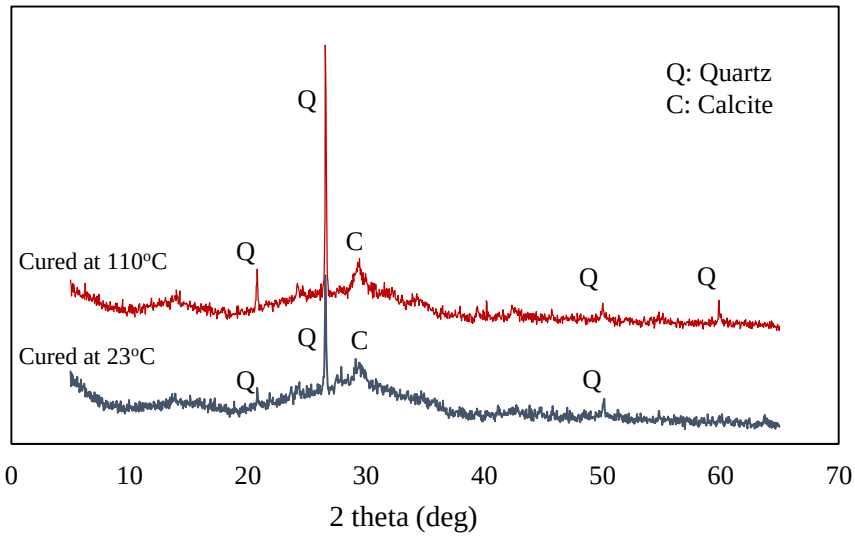


Figure 8-13. Comparison of XRD patterns of GGF-0-10 paste cured at 23°C and 110°C

### *8.4.3.2 Effect of heat-curing duration*

To investigate the effect of heat curing duration, the GGF-0-10 specimens were cured at 60°C for different time periods, including 24 h, 48 h, 72 h and 168 h (7 days). The effect of heat curing duration on the compressive strength of these specimens are presented in Figure 8-14. As it is obvious from this figure, prolongation of the heat-curing duration caused a slight increase in the compressive strength of the geopolymer mortar samples. For the tested mixture (GGF-0-10 mixture), increase in the heat-curing duration from 24 h to 168 h (7 days), led to the increase in the 7-days compressive strength from 74 MPa to 79 MPa (6.7% increase). However, this process was seen to be more effective in the case of the 28-days strength, as the compressive strength was raised from 81 MPa, for the 24 h heat-curing duration, to 95 MPa for the specimen that heat-cured for 168 h (16.4% increase).

The higher compressive strength of the samples with the longer heat-curing duration has

been also reported in other studies performed on fly ash based geopolymers (11, 46, 95). According to Hardjito et al. (11), the higher strength of the specimens that cured for the longer durations is related with their higher level of polymerisation. Therefore, it was concluded that the slight increase in the compressive strength of GGF-based specimens that were heat-cured for higher durations, could be related to their higher degree of geopolymerisation which causes a denser structure, and hence increases strength of the samples.

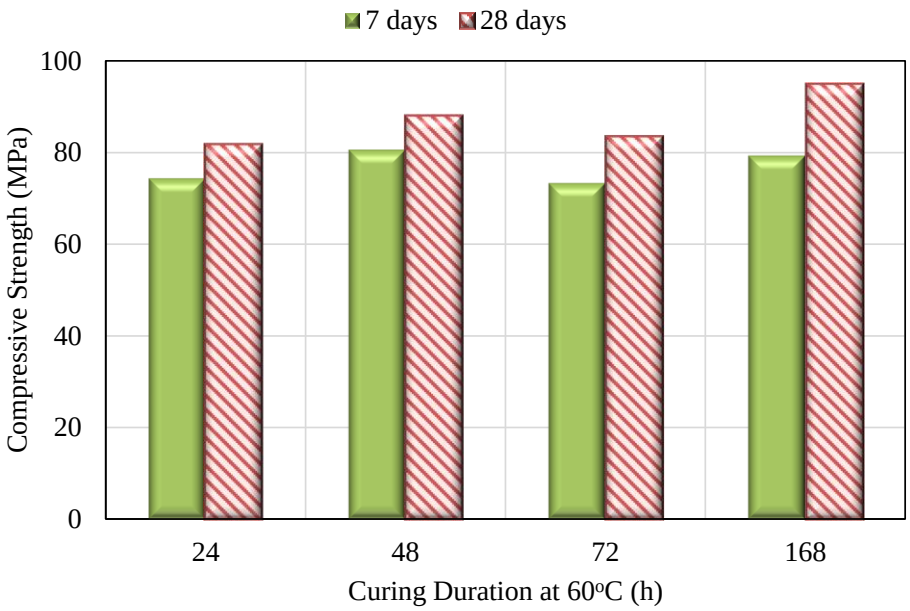


Figure 8-14. Effect of heat-curing duration on the compressive strength of GGF-0-10 mortar cubes

## 8.5 Conclusion

In this study, the influence of various factors that affect the activation of GGF as a precursor for geopolymer was investigated. Effect of activator solution composition (i.e. combinations of NaOH solution and sodium silicate solution to achieve different $Na_2O$-to-binder and $Na_2O$-to-$SiO_2$ ratios) on the compressive strength of GGF-based geopolymer mortars was explored, and the results were compared with a fly ash-based geopolymer. Further, the effect of the temperature of the heat-curing and its duration on the microstructure and compressive strength of GGF-based mixtures were studied. The most significant findings from this work can be summarized as

follows:

1) GGF can be effectively activated using a NaOH solution with no need for sodium silicate solution. GGF-based specimen showed a high compressive strength of 79 MPa after 3 days, when GGF was activated using an activator solution having $Na_2O$-to-binder ratio of 10%, and cured at the temperature of 60$^oC$ for 24 h.
2) For all the tested mixtures, GGF-based geopolymer showed a higher compressive strength than fly ash-based mixtures that were prepared using a same activator solution. In this study, the higher compressive strength of GGF-based geopolymers in comparison to fly ash based ones, was related to the smaller particles size of GGF, harder nature of GGF particles that can act as an internal reinforcing, higher extent of dissolution in an alkali media, and their higher Ca content.
3) Increase in the alkali content of the activator solution up to the $Na_2O$-to-binder ratio of 10% showed an increase in the compressive strength of GGF-based specimens. However, the rise in the alkali content beyond this point (i.e. $Na_2O$-to-binder ratios of 15 and 20%) showed a reduction in the compressive strength of the GGF-based geopolymers.
4) Change in the curing temperature from 23$^oC$ to 80$^oC$ did not seem to affect the later age (i.e. 28-day and 56-day) strength of the GGF-based geopolymer specimens. However, specimens that were cured at 23$^oC$ and 38$^oC$ showed lower early-age strength (i.e. 3-day and 7-day results). The gradual strength gain observed in the low-temperature cured GGF mixtures can be explained by the lower degree of geopolymerisation at early ages in these specimens. On the other hand, curing at a high temperature such as 110$^oC$ caused a significant reduction in the compressive strength of the GGF-based samples. The lower strength in this case, can be mainly related to the very fast evaporation of water from the mixture, which resulted in cracking in the geopolymer's matrix.

5) Prolonging the curing duration led to a gradual rise in the strength of geopolymer samples. Extending the heat curing (60$^{o}$C) period from 24 h to 168 h (7 days) for GGF-0-10 specimens, resulted in the increase in the 28-day compressive strength from 81 MPa to 95 MPa.

6) Based on the results of this work, GGF-based geopolymer showed a comparable, or better compressive strength results when compared to fly ash-based geopolymer. Their strength gain was not dependent on the presence of sodium silicate solution, and good compressive strengths were achieved using NaOH solution alone as the activator solution.

7) Finally, it should be noted that, while the results of compressive strength revealed the potential of utilization of GGF-based geopolymer in precast or in-site applications; further researches, particularly on the durability properties of this material, are needed before using GGF-based geopolymers in the field.

# Reference:


1. Weil M, Dombrowski K, Buchawald A. Life-cycle analysis of geopolymers. In: Provis J, Van Deventer J, editor. Geopolymers, structure, processing, properties and applications. UK; 2009. p. 194–210 [ISBN -13: 978 1 84569 449 4].Woodhead Publishing Limited Abington Hall, Cambridge,
2. Dombrowski, K., Buchwald, A., & Weil, M. (2007). The influence of calcium content on the structure and thermal performance of fly ash based geopolymers. Journal of Materials Science, 42(9), 3033-3043.
3. Duxson, P., Fernández-Jiménez, A., Provis, J. L., Lukey, G. C., Palomo, A., & Van Deventer, J. S. J. (2007). Geopolymer technology: the current state of the art. Journal of Materials Science, 42(9), 2917-2933.
4. Li, Z., Ding, Z., & Zhang, Y. (2004, May). Development of sustainable cementitious materials. In Proceedings of international workshop on sustainable development and concrete technology, Beijing, China (pp. 55-76).
5. Komnitsas, K., & Zaharaki, D. (2007). Geopolymerisation: A review and prospects for the minerals industry. Minerals engineering, 20(14), 1261-1277.
6. Baš˘carevic, Z. (2014). The resistance of alkali-activated cement-based binders to chemical attack. Handbook of Alkali-Activated Cements, Mortars and Concretes, 373-396 (Eds) Pacheco-Torgal, F.; Labrincha, J.; Palomo, A.; Leonelli, C.; Chindaprasirt, P., WoodHead Publishing-Elsevier, Cambridge.
7. Duxson, P., Provis, J. L., Lukey, G. C., & Van Deventer, J. S. (2007). The role of inorganic polymer technology in the development of ‘green concrete’. Cement and Concrete Research, 37(12), 1590-1597.
8. Rangan, B. V. (2014). Geopolymer concrete for environmental protection. Indian Concr. J, 88(4),

41-59.

9. Gourley, J. T., & Johnson, G. B. (2005). Developments in geopolymer precast concrete. In World Congress Geopolymer (pp. 139-143).
10. Cheema, D., Lloyd, N., & Rangan, B. V. (2009). Durability of geopolymer concrete box culverts-A green alternative. In Proceedings of 34th Conference on Our World in Concrete and Structures (pp. 85-92). CI Premier Pty Ltd.
11. Hardjito, D., Wallah, S. E., Sumajouw, D. M., & Rangan, B. V. (2004). Factors influencing the compressive strength of fly ash-based geopolymer concrete. civil engineering dimension, 6(2), pp-88.
12. Aldred, J., & Day, J. (2012, August). Is geopolymer concrete a suitable alternative to traditional concrete. In 37th Conference on our world in concrete & structures, Singapore (pp. 29-31).
13. Balaguru, P., Kurtz, S., & Rudolph, J. (1997). Geopolymer for repair and rehabilitation of reinforced concrete beams. St Quentin, France, Geopolymer Institute, 5.
14. Pacheco-Torgal, F., Abdollahnejad, Z., Miraldo, S., Baklouti, S., & Ding, Y. (2012). An overview on the potential of geopolymers for concrete infrastructure rehabilitation. Construction and Building Materials, 36, 1053-1058.
15. Vasconcelos, E., Fernandes, S., de Aguiar, J. B., & Pacheco-Torgal, F. (2011). Concrete retrofitting using metakaolin geopolymer mortars and CFRP. Construction and Building Materials, 25(8), 3213-3221.
16. Cheng, T. W., & Chiu, J. P. (2003). Fire-resistant geopolymer produced by granulated blast furnace slag. Minerals Engineering, 16(3), 205-210.
17. Temuujin, J., Rickard, W., Lee, M., & van Riessen, A. (2011). Preparation and thermal properties of fire resistant metakaolin-based geopolymer-type coatings. Journal of non-crystalline solids, 357(5), 1399-1404.

18. Zhang, Z., Yao, X., & Zhu, H. (2010). Potential application of geopolymers as protection coatings for marine concrete: II. Microstructure and anticorrosion mechanism. Applied clay science, 49(1), 7-12.
19. Reddy, D. V., Edouard, J. B., & Sobhan, K. (2012). Durability of fly ash–based geopolymer structural concrete in the marine environment. Journal of Materials in Civil Engineering, 25(6), 781-787.
20. Chindaprasirt, P., & Chalee, W. (2014). Effect of sodium hydroxide concentration on chloride penetration and steel corrosion of fly ash-based geopolymer concrete under marine site. Construction and Building Materials, 63, 303-310.
21. Oslakovic, I. S., Bjegovic, D., & Mikulic, D. (2010). Evaluation of service life design models on concrete structures exposed to marine environment. Materials and structures, 43(10), 1397-1412.
22. Duxson, P., Fernández-Jiménez, A., Provis, J. L., Lukey, G. C., Palomo, A., & Van Deventer, J. S. J. (2007). Geopolymer technology: the current state of the art. Journal of Materials Science, 42(9), 2917-2933.
23. Ganesan, N., Abraham, R., Raj, S. D., & Sasi, D. (2014). Stress–strain behaviour of confined Geopolymer concrete. Construction and building materials, 73, 326-331.
24. Morsy, M. S., Alsayed, S. H., Al-Salloum, Y., & Almusallam, T. (2014). Effect of sodium silicate to sodium hydroxide ratios on strength and microstructure of fly ash geopolymer binder. Arabian Journal for Science and Engineering, 39(6), 4333-4339.
25. Van Jaarsveld, J. G. S., Van Deventer, J. S. J., & Lukey, G. C. (2003). The characterisation of source materials in fly ash-based geopolymers. Materials Letters, 57(7), 1272-1280.
26. Ryu, G. S., Lee, Y. B., Koh, K. T., & Chung, Y. S. (2013). The mechanical properties of fly ash-based geopolymer concrete with alkaline activators. Construction and Building Materials, 47, 409-418.

27. Kumar, S., Kumar, R., & Mehrotra, S. P. (2010). Influence of granulated blast furnace slag on the reaction, structure and properties of fly ash based geopolymer. Journal of Materials Science, 45(3), 607-615.
28. Oh, J. E., Monteiro, P. J., Jun, S. S., Choi, S., & Clark, S. M. (2010). The evolution of strength and crystalline phases for alkali-activated ground blast furnace slag and fly ash-based geopolymers. Cement and Concrete Research, 40(2), 189-196.
29. Anuar, K. A., Ridzuan, A. R. M., & Ismail, S. (2011). Strength characteristics of geopolymer concrete containing recycled concrete aggregate. International Journal of Civil & Environmental Engineering, 11(1), 59-62.
30. Kourti, I., Devaraj, A. R., Bustos, A. G., Deegan, D., Boccaccini, A. R., & Cheeseman, C. R. (2011). Geopolymers prepared from DC plasma treated air pollution control (APC) residues glass: properties and characterisation of the binder phase. Journal of hazardous materials, 196, 86-92.
31. Trochez, J. J., de Gutiérrez, R. M., Rivera, J., & Bernal, S. A. (2015). Synthesis of geopolymer from spent FCC: Effect of SiO 2/Al 2 O< 3 and Na2O/SiO2 molar ratios. Materiales de Construcción, 65(317), 046.
32. Kupaei, R. H., Alengaram, U. J., & Jumaat, M. Z. (2014). The effect of different parameters on the development of compressive strength of oil palm shell geopolymer concrete. The Scientific World Journal, 2014.
33. de MORAES, J. C. B., de Araújo Queiroz, D. C., AKASAKI, J. L., MELGES, J. L. P., BORRACHERO, M. V., PAYÁ, J., & TASHIMA, M. M. (2016). Possibilities of reusing sugar cane straw ash in the production of alternative binders. Key Engineering Materials, 668.
34. Pascual, A. B., Tognonvi, M. T., & Tagnit-Hamou, A. (2014). Waste glass powder-based alkali-activated mortar. Int. J. Res. Eng. Technol, 3(13), 32-36.

35. Rashidian-Dezfouli, H., & Rangaraju, P. R. (in press). Comparison of Strength and Durability Characteristics of a Geopolymer produced from Fly ash, Ground Glass Fiber and Glass Powder. Materiales de Construcción.
36. Pereira, A., Akasaki, J.L., Melges, J.L., Tashima, M.M., Soriano, L., Borrachero, M.V., Monzó, J. and Payá, J. (2015). Mechanical and durability properties of alkali-activated mortar based on sugarcane bagasse ash and blast furnace slag. Ceramics International, 41(10), 13012-13024.
37. Bhutta, M. A. R., Hussin, W. M., Azreen, M., & Tahir, M. M. (2014). Sulphate resistance of geopolymer concrete prepared from blended waste fuel ash. Journal of Materials in Civil Engineering, 26(11), 04014080.
38. Robayo, R. A., de Gutiérrez, R. M., & Gordillo, M. (2016). Natural pozzolan-and granulated blast furnace slag-based binary geopolymers. Materiales de Construcción, 66(321), 077.
39. Sukmak, P., Horpibulsuk, S., & Shen, S. L. (2013). Strength development in clay–fly ash geopolymer. Construction and building Materials, 40, 566-574.
40. Tashima, M. M., Soriano, L., Borrachero, M. V., Monzó, J., Cheeseman, C. R., & Payá, J. (2012). Alkali activation of vitreous calcium aluminosilicate derived from glass fiber waste. Journal of Sustainable Cement-Based Materials, 1(3), 83-93.
41. Hemmings, R. T. (2005). Process for Converting Waste Glass Fiber into Value Added Products, Final Report (No. DOE GO13015-1). Albacem LLC.
42. Chen, C. H., Huang, R., Wu, J. K., & Yang, C. C. (2006). Waste E-glass particles used in cementitious mixtures. Cement and Concrete Research, 36(3), 449-456.
43. Rangaraju, P. R., Rashidian-Dezfouli, H., Nameni, G., & Amekuedi, G. Q. Properties and Performance of Ground Glass Fiber as a Pozzolan in Portland Cement Concrete 2016 International Concrete Sustainability Conference.
44. Rashidian-Dezfouli, H., & Rangaraju, P. R. (in press). Role of Ground Glass Fiber as a Pozzolan

in Portland Cement Concrete (No. 17-04237).

45. Wang, H., Li, H., & Yan, F. (2005). Synthesis and mechanical properties of metakaolinite-based geopolymer. Colloids and Surfaces A: Physicochemical and Engineering Aspects, 268(1), 1-6.
46. Palomo, A., Grutzeck, M. W., & Blanco, M. T. (1999). Alkali-activated fly ashes: a cement for the future. Cement and concrete research, 29(8), 1323-1329.
47. Bakharev, T. (2005). Geopolymeric materials prepared using Class F fly ash and elevated temperature curing. Cement and concrete research, 35(6), 1224-1232.
48. Ismail, I., Bernal, S. A., Provis, J. L., Hamdan, S., & van Deventer, J. S. (2013). Microstructural changes in alkali activated fly ash/slag geopolymers with sulfate exposure. Materials and structures, 46(3), 361-373.
49. Muñiz-Villarreal, M. S., Manzano-Ramírez, A., Sampieri-Bulbarela, S., Gasca-Tirado, J. R., Reyes-Araiza, J. L., Rubio-Ávalos, J. C., ... & Amigó-Borrás, V. (2011). The effect of temperature on the geopolymerization process of a metakaolin-based geopolymer. Materials Letters, 65(6), 995-998.
50. Mo, Bing-hui., Zhu, H., Cui, X. M., He, Y., & Gong, S. Y. (2014). Effect of curing temperature on geopolymerization of metakaolin-based geopolymers. Applied Clay Science, 99, 144-148.
51. Nagral, M. R., Ostwal, T., & Chitawadagi, M. V. (2014). Effect Of Curing Temperature And Curing Hours On The Properties Of Geo-Polymer Concrete. International Journal of Computational Engineering Research, 4, 2250-3005.
52. Palomo, A., Alonso, S., Fernandez-Jiménez, A., Sobrados, I., & Sanz, J. (2004). Alkaline activation of fly ashes: NMR study of the reaction products. Journal of the American Ceramic Society, 87(6), 1141-1145.
53. Hardjito, D., & Fung, S. S. (2010). Parametric Study on the Properties of Geopolymer Mortar Incorporating Bottom Ash. Concrete Research Letters, 1(3), 115-124.

54. Somna, K., Jaturapitakkul, C., Kajitvichyanukul, P., & Chindaprasirt, P. (2011). NaOH-activated ground fly ash geopolymer cured at ambient temperature. Fuel, 90(6), 2118-2124.
55. Guo, X., Shi, H., & Dick, W. A. (2010). Compressive strength and microstructural characteristics of class C fly ash geopolymer. Cement and Concrete Composites, 32(2), 142-147.
56. Alonso, S., & Palomo, A. (2001). Alkaline activation of metakaolin and calcium hydroxide mixtures: influence of temperature, activator concentration and solids ratio. Materials Letters, 47(1), 55-62.
57. Komljenović, M., Baščarević, Z., & Bradić, V. (2010). Mechanical and microstructural properties of alkali-activated fly ash geopolymers. Journal of Hazardous Materials, 181(1), 35-42.
58. Chindaprasirt, P., Chareerat, T., & Sirivivatnanon, V. (2007). Workability and strength of coarse high calcium fly ash geopolymer. Cement and Concrete Composites, 29(3), 224-229.
59. Rattanasak, U., & Chindaprasirt, P. (2009). Influence of NaOH solution on the synthesis of fly ash geopolymer. Minerals Engineering, 22(12), 1073-1078.
60. Baščarević, Z., Komljenović, M., Miladinović, Z., Nikolić, V., Marjanović, N., & Petrović, R. (2015). Impact of sodium sulfate solution on mechanical properties and structure of fly ash based geopolymers. Materials and Structures, 48(3), 683-697.
61. Sata, V., Sathonsaowaphak, A., & Chindaprasirt, P. (2012). Resistance of lignite bottom ash geopolymer mortar to sulfate and sulfuric acid attack. Cement and Concrete Composites, 34(5), 700-708.
62. Nugteren, H. W., Butselaar-Orthlieb, V. C. L., & Izquierdo, M. (2009). High strength geopolymers produced from coal combustion fly ash. Global NEST Journal, 11(2), 155-161.
63. Davidovits, J. (1999, June). Chemistry of geopolymeric systems, terminology. In Geopolymer (Vol. 99, No. 292, pp. 9-39).
64. Duxson, P., Provis, J. L., Lukey, G. C., Mallicoat, S. W., Kriven, W. M., & Van Deventer, J. S.

(2005). Understanding the relationship between geopolymer composition, microstructure and mechanical properties. Colloids and Surfaces A: Physicochemical and Engineering Aspects, 269(1), 47-58.

65. De Silva, P., Sagoe-Crenstil, K., & Sirivivatnanon, V. (2007). Kinetics of geopolymerization: role of Al 2 O 3 and SiO 2. Cement and Concrete Research, 37(4), 512-518.
66. Kouamo, H. T., Elimbi, A., Mbey, J. A., Sabouang, C. N., & Njopwouo, D. (2012). The effect of adding alumina-oxide to metakaolin and volcanic ash on geopolymer products: A comparative study. Construction and Building Materials, 35, 960-969.
67. Fletcher, R. A., MacKenzie, K. J., Nicholson, C. L., & Shimada, S. (2005). The composition range of aluminosilicate geopolymers. Journal of the European
68. Zheng, L., Wang, W., & Shi, Y. (2010). The effects of alkaline dosage and Si/Al ratio on the immobilization of heavy metals in municipal solid waste incineration fly ash-based geopolymer. Chemosphere, 79(6), 665-671.
69. Asif, A., Man, Z., Azizli, M., Azizi, K., Nuruddin, M. F., & Ismail, L. (2014, July). The Effect of Si/Al Ratio and Sodium Silicate on the Mechanical Properties of Fly ash based Geopolymer for Coating. In Materials Science Forum (Vol. 803).
70. Xu, H., & Van Deventer, J. S. J. (2000). The geopolymerisation of alumino-silicate minerals. International Journal of Mineral Processing, 59(3), 247-266.
71. Lee, W. K. W., & Van Deventer, J. S. J. (2002). The effect of ionic contaminants on the early-age properties of alkali-activated fly ash-based cements. Cement and Concrete Research, 32(4), 577-584.
72. Van Jaarsveld, J. G. S., Van Deventer, J. S. J., & Lukey, G. C. (2002). The effect of composition and temperature on the properties of fly ash-and kaolinite-based geopolymers. Chemical Engineering Journal, 89(1), 63-73.

73. Duxson, P., & Provis, J. L. (2008). Designing precursors for geopolymer cements. Journal of the American Ceramic Society, 91(12), 3864-3869.
74. MINAØÍKOVÁ, M., & ŠKVÁRA, F. (2006). Fixation of heavy metals in geopolymeric materials based on brown coal fly ash. Ceramics− Silikáty, 50(4), 200-207.
75. Yip, C. K., Lukey, G. C., & Van Deventer, J. S. J. (2005). The coexistence of geopolymeric gel and calcium silicate hydrate at the early stage of alkaline activation. Cement and Concrete Research, 35(9), 1688-1697.
76. Buchwald, A., Dombrowski, K., & Weil, M. (2005). The influence of calcium content on the performance of geopolymeric binder especially the resistance against acids. Proceedings of the world geopolymer, 35-9.
77. Temuujin, J. V., Van Riessen, A., & Williams, R. (2009). Influence of calcium compounds on the mechanical properties of fly ash geopolymer pastes. Journal of hazardous materials, 167(1), 82-88.
78. Garcia-Lodeiro, I., Palomo, A., Fernández-Jiménez, A., & Macphee, D. E. (2011). Compatibility studies between NASH and CASH gels. Study in the ternary diagram Na 2 O–CaO–Al 2 O 3–SiO 2–H 2 O. Cement and Concrete Research, 41(9), 923-931.
79. Yip, C. K., Lukey, G. C., Provis, J. L., & van Deventer, J. S. (2008). Effect of calcium silicate sources on geopolymerisation. Cement and Concrete Research, 38(4), 554-564.
80. Buchwald, A., Hilbig, H., & Kaps, C. (2007). Alkali-activated metakaolin-slag blends—performance and structure in dependence of their composition. Journal of materials science, 42(9), 3024-3032.
81. Van Deventer, J. S. J., Provis, J. L., Duxson, P., & Lukey, G. C. (2007). Reaction mechanisms in the geopolymeric conversion of inorganic waste to useful products. Journal of Hazardous Materials, 139(3), 506-513.

82. Khater, H. M. (2012). Effect of cement kiln dust on Geopolymer composition and its resistance to sulphate attack. International Journal of Civil and Structural Engineering, 2(3), 740.
83. García-Lodeiro, I., Fernández-Jiménez, A., Palomo, A., & Macphee, D. E. (2010). Effect of calcium additions on N–A–S–H cementitious gels. Journal of the American Ceramic Society, 93(7), 1934-1940.
84. Li, C., Sun, H., & Li, L. (2010). A review: The comparison between alkali-activated slag (Si+ Ca) and metakaolin (Si+ Al) cements. Cement and Concrete Research, 40(9), 1341-1349.
85. Struble, L., Hicks, J. K. (2013). Geopolymer Binder Systems, ASTM International. New York, (2013).
86. Pouhet, R., & Cyr, M. (2015). Alkali–silica reaction in metakaolin-based geopolymer mortar. Materials and Structures, 48(3), 571-583.
87. Chen, H., Wu, X., & Hu, J. (2007, November). Adaptive K-means clustering algorithm. In International Symposium on Multispectral Image Processing and Pattern Recognition (pp. 67882A-67882A). International Society for Optics and Photonics.
88. Darken, C., & Moody, J. (1990, June). Fast adaptive k-means clustering: some empirical results. In Neural Networks, 1990., 1990 IJCNN International Joint Conference on (pp. 233-238). IEEE
89. Xu, H., & Van Deventer, J. S. (2002). Geopolymerisation of multiple minerals. Minerals Engineering, 15(12), 1131-1139.
90. Yao, Z., Ye, Y., & Xia, M. (2013). Synthesis and characterization of lithium zeolites with ABW type from coal fly ash. Environmental Progress & Sustainable Energy, 32(3), 790-796.
91. Fernández-Jimenez, A., De La Torre, A. G., Palomo, A., López-Olmo, G., Alonso, M. M., & Aranda, M. A. G. (2006). Quantitative determination of phases in the alkali activation of fly ash. Part I. Potential ash reactivity. Fuel, 85(5), 625-634.
92. Palomo, A., Krivenko, P., Garcia-Lodeiro, I., Kavalerova, E., Maltseva, O., & Fernández-

Jiménez, A. (2014). A review on alkaline activation: new analytical perspectives. Materiales de Construcción, 64(315), 022.

93. Turner, L. K., & Collins, F. G. (2013). Carbon dioxide equivalent (CO 2-e) emissions: a comparison between geopolymer and OPC cement concrete. Construction and Building Materials, 43, 125-130.
94. Granizo, M. L., Blanco-Varela, M. T., & Martínez-Ramírez, S. (2007). Alkali activation of metakaolins: parameters affecting mechanical, structural and microstructural properties. Journal of Materials Science, 42(9), 2934-2943.
95. Nuruddin, M. N., Kusbiantoro, A. K., Qazi, S. Q., Darmawan, M. D., & Husin, N. H. (2011). Development of geopolymer concrete with different curing conditions. IPTEK The Journal for Technology and Science, 22(1).

# CHAPTER 9

# A COMPARATIVE STUDY ON THE DURABILITY OF GEOPOLYMERS PRODUCED WITH GROUND GLASS FIBER, FLY ASH, AND GLASS-POWDER IN SODIUM SULFATE SOLUTION[1]

## 9.1 Introduction:

Sulfate attack is known as one of the major durability problems affecting the performance of portland cement concrete (1). This chemical attack is mainly associated with the formation of non-cohesive and expansive by-products such as gypsum and ettringite; which lead to cracking and softening of the paste matrix resulting in mass loss and reduction in the mechanical properties of the portland cement concrete (2). In order to mitigate durability issues associated with sulfate attack, use of adequate amounts of supplementary cementitious materials (SCMs) such as slag is practiced (3). According to Neville (4), the use of SCMs as cement replacement material can help the mitigation of sulfate attack by reducing the amount calcium aluminate ($C_3A$) and calcium Hydroxide (CH), which prevents the formation of deleterious compounds such as gypsum and ettringite. Considering the deterioration of concrete in the high sulfate environment, evaluation of the performance of any cementitious materials against a sulfate-rich environment is critical.

Geopolymer-based concretes have recently attracted attention as a potential replacement for portland-cement based concrete, particularly in applications where aggressive chemical environments are encountered. Typically, geopolymers are produced by the alkali activation of

---

1- Hassan Rashidian-Dezfouli, Prasada Rao Rangaraju (in press). A comparative study on the durability of geopolymers produced with ground glass fiber, fly ash, and glass-powder in sodium sulfate solution. Journal of Construction and Building material.

silica and alumina-rich materials using alkaline activators such as sodium hydroxide or sodium silicate solutions. This results in the production of an amorphous three-dimensional alumino-silicate network, known as the geopolymer (5). As it has been reviewed and summarized by Bascarevic (6), efforts to study the durability performance of geopolymer concrete and mortar against aggressive environments have been conducted by exposing test specimens to different sodium sulfate-rich solutions such as sodium sulfate and magnesium sulfate solutions. However, thus far most of the studies were conducted on fly ash or meta-kaolin based geopolymers (7-13); and no such durability studies have been conducted on geopolymers produced with glass-based precursor materials such as ground glass fibers (GGF) and ground soda-lime glass powder (GLP). The purpose of this investigation is to evaluate the performance of geopolymers produced using GGF and GLP precursors when exposed to sulfate rich environment. In this study a 5% sodium sulfate solution was used to simulate a sulfate-rich environment.

### *9.1.1 Background*

In recent years, large numbers of studies have been conducted to evaluate the potential of geopolymer-based concrete as an alternative to portland cement concrete (14-25). In these studies, the use of geopolymer concretes in specific applications such as precast concrete products, sewer pipes, culverts, railway sleepers, pre-fabricated units for housing market, etc. (14-19), repair or a retrofitting material for existing portland-cement-concrete elements or structures (20-22), and as a repair coating or a construction material in marine sites (23-25), has been reported in a laboratory (14, 17, 20-24) or a commercial scale (14-16, 18, 19).

Based on literature review, precursor materials such as fly-ash, slag, meta-kaolin and their combinations are the most widely used materials to manufacture geopolymer concrete (26-32). In addition, several other waste or industrial by-products such as: waste paper sludge ash (33), spent fluid catalytic cracking catalyst (34) waste glass-powder (35), palm oil fuel Ash (36),

kaolinitic clay (37), a combination of natural pozzolan and slag (38), blends of clay and fly ash (39), and vitreous calcium alumino-silicate (40) have been studied by other authors to produce geopolymer concrete. In addition to these materials, recent studies have shown that ground glass fiber (GGF) can be effectively activated by an alkali activator to produce a geopolymer mortar (41).

Each year, a large amount of glass fiber is produced around the world for use in various applications. The production process of high-quality glass-fiber is often associated with generation of hundreds of thousands of tons of waste glass fiber that is deemed off-specification, due to strict technical requirements. The waste glass fiber is typically disposed off in landfills. It has been reported that, in the United States alone around 250,000 tons to 500,000 tons of waste glass fiber ends-up in landfills each year (42). Considering the chemical composition of this material, which is rich in silica, alumina, and calcium, it could be potentially used as a supplementary cementitious material (SCM) or as a precursor for the production of geopolymer (43, 44). Recent studies have shown that activation of GGF using a sodium hydroxide solution, without the need for a sodium silicate solution, can produce a geopolymer mortar mixture with high early strength as high as 79 MPa after only 3 days (41).

Unlike portland cement paste in which calcium silicate hydrate (CSH) is the main constituent of the hydration product, geopolymers are made of an amorphous alumino-silicate matrix (45, 46). Therefore, the durability of geopolymers in aggressive environments can be expected to be different from that of portland cement-based materials. Several studies have reported findings on different durability aspects of geopolymer concrete. Studies on the durability properties such as resistance against alkali-silica reaction (ASR) of aggregates (47-49), resistance against acid attack (9, 50-53), sulfate-rich solutions (7-13), freeze and thaw (11, 54), etc. have shown superior performance of geopolymers produced from precursors such as fly ash, bottom

ash, meta-kaolin, slag etc., compared to portland cement concrete.

Considering the differences between the chemical nature of the matrix in portland cement and geopolymer concretes, particularly due to the lower amount of calcium in geopolymers, the behaviors of these materials (portland cement and geopolymers) are found to be different when exposed to a sulfate rich media (55). Monitoring the changes in material properties such as compressive strength (7, 12, 13, 36, 56, 57), length of specimens (i.e. expansion) (52, 576, 58), porosity and microstructure (58) have been used to study the behavior of geopolymers when exposed to a sulfate solution such as sodium sulfate or magnesium sulfate. In most of these studies, it was observed that geopolymers had a better performance when compared to portland cement concrete, i.e. lower expansion, lesser degree of loss in compressive strength, and minimal change in the microstructure of the matrix. The better performance of geopolymer samples has been attributed to factors such as: lower amount of calcium oxides in the structure of geopolymers (8, 36, 37, 56, 57), further geopolymerisation while exposed to the sulfate solution (7, 11), formation of new crystals in the structure of the exposed samples (9), and the cross-linked structure of the alumino-silicate gel of geopolymers (36, 55).

Despite its better performance in comparison to portland cement mixtures, in some cases, reduction (or fluctuation) in the mechanical properties has been reported for the geopolymer samples which were subjected to sulfate solutions (8, 9, 12, 13). In these studies, such behavior was mainly attributed to the leaching of alkalis from the geopolymer into the sulfate solution, which alters the structure of geopolymer and negatively affects the mechanical properties. Other observations have also reported the formation of ettringite and gypsum in the matrix of geopolymer exposed to sulfate solution, which leads to expansion and consequent mechanical degradation of the geopolymer (10, 13, 57, 58). However, the formation of these products was mostly observed when samples were exposed to the magnesium sulfate solution (10, 13, 55),

while it was not the case for the samples exposed to the sodium sulfate solution; as no or very small traces of gypsum and ettringite were seen in these samples (7, 10, 11, 36, 55).

Effect of sulfate solution on the geopolymers has been reported to depend on the cations accompanying the sulfate in the solution (i.e. Na or Mg) (10, 12). Some studies (10, 55, 57) reported magnesium sulfate solutions to be more aggressive towards geopolymer samples in comparison to sodium sulfate solution, while other studies (12), reported more damaging effect of sodium sulfate solution on geopolymer samples compared to magnesium sulfate solutions. Considering the dissimilar effects of these two different solutions and the associated mechanism of damages from these solutions, present study will focus only on the effect of a 5% sodium sulfate solution on a GGF and GLP-based geopolymer. In addition, results from glass-based geopolymers were compared with a fly ash-based geopolymer to investigate how different precursors affect the properties of geopolymers exposed to a sodium sulfate solution. Although, parallel studies on the effects of magnesium sulfate solutions on geopolymers were conducted, the findings from those studies are not presented here and will be presented in future.

### *9.1.2 Significance of the research*

Earlier studies have revealed the superior performance of geopolymers in comparison to portland cement concrete when exposed to sulfate-rich environment. However, most of these studies have been conducted on fly ash, meta-kaolin, or slag-based geopolymers; and very limited studies have been conducted on other alternative precursors. Two of such precursors are GGF and GLP, which can be activated by alkali solutions to form geopolymers. In order to evaluate the durability of these novel types of geopolymers when exposed to a sulfate-rich media, in this study the performance of GGF and GLP-based geopolymers exposed to sodium sulfate solution was evaluated and the results were compared to the performance of a geopolymer produced from fly ash. To study the deterioration mechanism, parameters such as the change in the pH of the sulfate

solution, change in the weight and compressive strength of geopolymer specimens, dissolution of geopolymer pastes in the sulfate solution were monitored during the test period. In addition, Scanning Electron Microscope (SEM) and Energy X-Ray Dispersive analysis (EDX), XRD and Thermogravimetric Analysis (TGA), were conducted to investigate the microstructure of the mortar samples.

## 9.2 Materials:

In this study, ground glass fiber (GGF) from a Type E glass fiber, a class F fly ash, and glass-powder (GLP) produced from crushing soda-lime glass bottles were used as the precursor source materials of alumino-silicate materials. GGF was obtained from a commercial source, where it is produced by grinding off-specification Type E glass fibers into particles with an average size of 4 microns. A class F fly ash with the average particle size of 28 microns was obtained from a local source. The GLP was obtained from a commercial source that produces the material by grinding waste glass container into a fine powder with an average particle size of 17 microns. The chemical composition and physical properties of the materials are presented in Table 9-1 and Table 9-2 respectively. Moreover, the XRD pattern of raw GGF, Fly ash, and GLP, are presented in Figure 9-1. In addition, a siliceous river sand with an absorption value of 0.30%, oven-dry specific gravity of 2.67, and the fineness modulus of 2.6 was used in all the mortar mixtures.

Table 9-1. Chemical composition of precursor source materials

| Cementitious material | $SiO_2$ | $Al_2O_3$ | $Fe_2O_3$ | $CaO$ | $MgO$ | $Na_2O$ | $K_2O$ |
|---|---|---|---|---|---|---|---|
| GGF (%) | 47.72 | 10.36 | 0.34 | 19.62 | 2.27 | 0.67 | 0.10 |
| Fly ash (%) | 50.70 | 25.10 | 12.50 | 3.30 | 1.10 | 0.51 | 2.27 |
| GLP (%) | 69.60 | 2.20 | 0.90 | 11.60 | 0.40 | 12.03 | 0.40 |

Two activators, including a combination of sodium-silicate and sodium hydroxide solution, and sodium-hydroxide solution were used in the present study. The sodium-silicate solution, with the solids-to-water ratio of 40% and $SiO_2$:$Na_2O$ ratio of 3 (by weight), and the

sodium hydroxide pellets, with 98% purity, were used to produce the activator solutions with different concentrations. For preparation of the sulfate exposure solution, ASC (American Society of Chemicals) grade anhydrous sodium sulfate ($Na_2SO_4$) powder was dissolved in deionized water to produce a 5% sodium sulfate solution (by weight).

Table 9-2. Physical properties of precursor source materials

| Material | Specific Gravity | Amount Passing #325 Sieve | Loss On Ignition | Blaine's fineness $(cm^2/g)$ |
|---|---|---|---|---|
| GGF | 2.60 | 96% | 1.0% | 10200 |
| Fly ash | 2.25 | 76% | 2.3% | 6040 |
| GLP | 2.40 | 83% | 1.5% | 5920 |

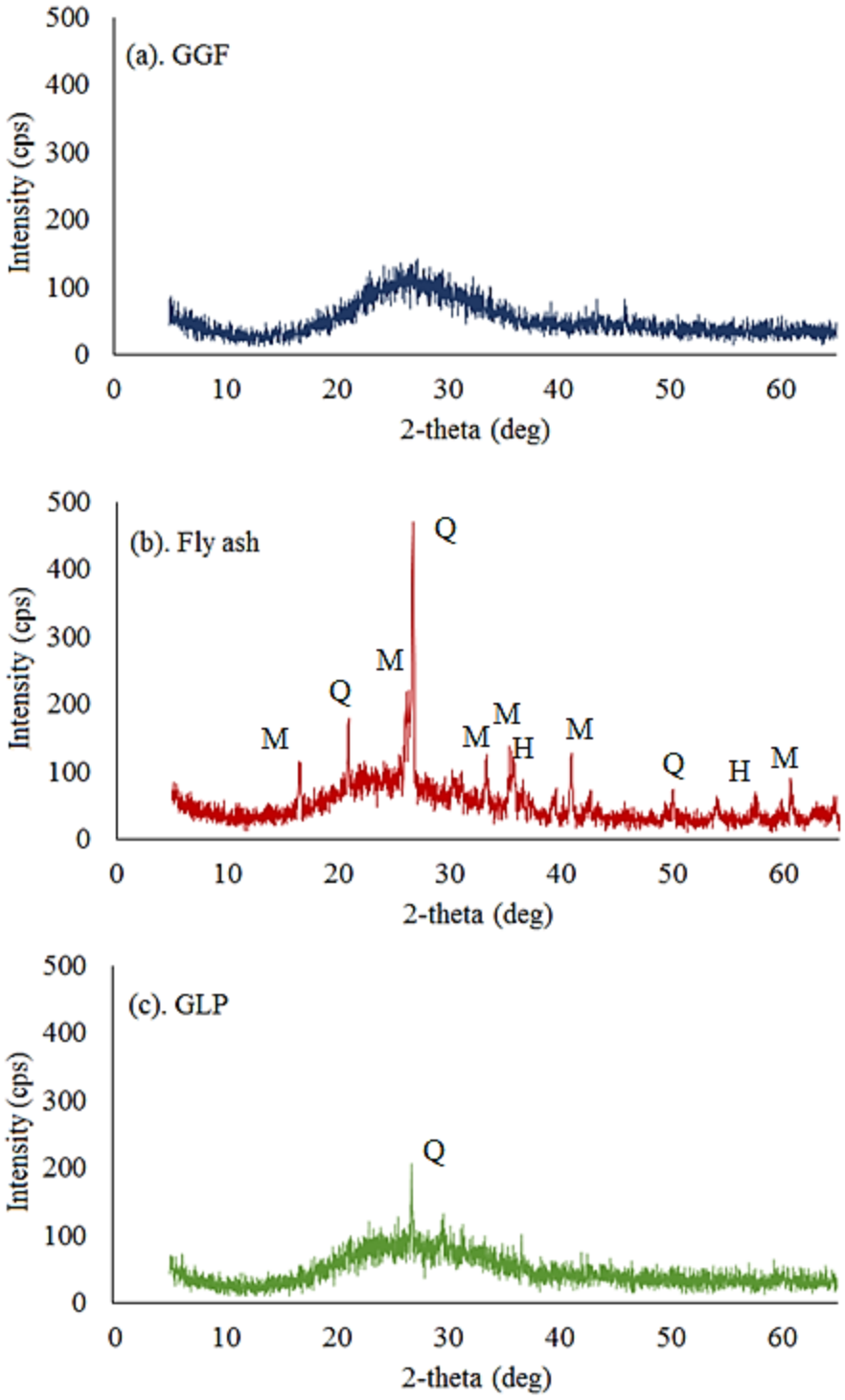


Figure 9-1. XRD pattern of the precursors. (a). GGF, (b). Fly ash, (c). GLP. (Q: Quartz, M: Mullite and H: Hematite)

### *9.2.1 Preparation and selection of mixture designs:*

To prepare the geopolymer mixtures, each of the precursors was activated with an alkali activator solution with the $Na_2O$-to-precursor mass ratio of 10% (based on the preliminary test results), while the $SiO_2$-to-$Na_2O$ ratio was studied at three levels, i.e. 0, 0.5 and 1.0. In all the mixtures, the sand content was selected to fill 55% of the total volume, and the water-to-binder ratio was maintained between 0.30 and 0.35. For this calculation, only water that is present in the solution was used. This range was chosen to get the highest possible strength while the mixtures were workable without the need for any water reducers.

Preliminary tests were conducted to select the mix design for each precursor. Compressive strength test was performed on at least three mortar cube samples at 3, 7 and 28 days age, and the mixture resulting in the highest compressive strength after 28 days was selected for the durability test. The mix designs of the geopolymer paste and results of compressive strength test are presented in Table 9-3. In addition, the mix proportion for per cubic meter of geopolymer mixtures are presented in Table 9-4. Based on the compressive strength tests results (Table 9-3), GGF-0-10, F-1-10, and GLP-1-10 mortar mixtures, which showed the highest compressive strengths were selected to be the mixtures to be exposed to the sodium sulfate solution.

To prepare the activator solutions, required amounts of sodium hydroxide pellets and sodium-silicate solution were dissolved in water to achieve the desired concentrations. After the dissolution of sodium hydroxide pellets, the precursor was added to the solution and mixed until a homogenous paste was achieved. Finally, the required amount of fine aggregate was added to the paste, and the mixture was further mixed for an additional 5 minutes. After completing the mixing process, the mixture was placed into 50 mm x 50 mm x 50 mm cube molds in two layers. Each layer was tamped and vibrated for 30 seconds using a vibration table. The molds were then placed

in sealed boxes and moved into a 60°C chamber for 24 h. After 24 hours, specimens were removed from their molds and kept in the ambient temperature for 48 h, before being introduced into the 5% sodium sulfate solution bath for exposure.

Table 9-3. Mix ID and the proportion of geopolymers

| Mix ID | Precursor | Water/Binder | $Na_2O$/Binder (%) | $SiO_2/Na_2O$ | Compressive strength (MPa) | | |
|---|---|---|---|---|---|---|---|
| | | | | | 3 days | 7 days | 28 days |
| GGF-0-10 | GGF | 0.33 | 10 | 0 | 79 | 78 | 82 |
| GGF-0.5-10 | GGF | 0.33 | 10 | 0.5 | 67 | 75 | 72 |
| GGF-1-10 | GGF | 0.33 | 10 | 1 | 69 | 72 | 67 |
| F-0-10 | Fly ash | 0.30 | 10 | 0 | 14 | 20 | 25 |
| F-0.5-10 | Fly ash | 0.30 | 10 | 0.5 | 35 | 36 | 46 |
| F-1-10 | Fly ash | 0.30 | 10 | 1 | 58 | 60 | 59 |
| GLP-0-10 | GLP | 0.35 | 10 | 0 | 7 | 11 | 14 |
| GLP-0.5-10 | GLP | 0.35 | 10 | 0.5 | 19 | 22 | 33 |
| GLP-1-10 | GLP | 0.35 | 10 | 1 | 37 | 40 | 43 |

Table 9-4. Mix proportion for per cubic meter of geopolymer mixtures.

| Mix ID | Precursor type | Precursor amount (kg) | NaOH pellets (kg) | 40% Sodium silicate solution [water content]* (kg) | Extra water (kg) | Sand (kg) | Total water** (kg) | Water/binder (ratio) |
|---|---|---|---|---|---|---|---|---|
| GGF-0-10 | GGF | 630 | 81 | 0 [0] | 208 | 1468 | 208 | 0.33 |
| GGF-0.5-10 | GGF | 630 | 69 | 103 [62] | 142 | 1468 | 208 | 0.33 |
| GGF-1-10 | GGF | 630 | 56 | 206 [124] | 84 | 1468 | 208 | 0.33 |
| F-0-10 | Fly ash | 604 | 78 | 0 [0] | 186 | 1468 | 181 | 0.30 |
| F-0.5-10 | Fly ash | 604 | 66 | 99 [60] | 121 | 1468 | 181 | 0.30 |
| F-1-10 | Fly ash | 604 | 54 | 197 [114] | 67 | 1468 | 181 | 0.30 |
| GLP-0-10 | GLP | 628 | 81 | 0 [0] | 220 | 1468 | 220 | 0.35 |
| GLP-0.5-10 | GLP | 628 | 69 | 103 [62] | 158 | 1468 | 220 | 0.35 |
| GLP-1-10 | GLP | 628 | 56 | 205 [123] | 97 | 1468 | 220 | 0.35 |

*- Numbers presented inside [] signs are representing the amount of water from the sodium silicate solution.
**- Total amount of water is the sum of water from sodium silicate solution (values presented in [] signs) and the extra water.

### *9.2.2 Test procedure:*

Three days after casting, mortar cube specimens were immersed in a 5% sodium-sulfate solution at ambient temperature. The weight change and the residual compressive strength of the specimens were measured at 7, 28, 56 and 120 days after submerging in the sulfate solution. The sulfate soak solutions were periodically replaced by a fresh sulfate solution at 7, 14, 21, 28 and 56 days. To measure the weight change, mortar cube specimens were weighed before exposing to the sodium-sulfate solution (initial weight), and then were weighed in the saturated surface dry condition at the above-mentioned time periods. After measuring their weights, the specimens were tested for their compressive strength.

To study the dissolution behavior of the geopolymers in the sodium sulfate solution, geopolymer paste samples from each source material (i.e. GGF, fly ash and GLP-based geopolymer) were used. In this test, representative paste samples prepared with each of the precursor materials were mechanically crushed using a hammer into a fine powder, and the portions passing #100 sieve (150 microns) and retained on #200 sieve (75 microns) were collected. Five grams of the sieved material was then introduced into 100 ml of the 5% sodium sulfate solution and stored in a sealed bottle. For each of the geopolymer specimens, six samples were prepared by the above-mentioned method. Each bottle was vigorously shaken for 1 minute and then left to rest at the ambient temperature until the test date (i.e. 3, 7, 14, 28 and 56 days).

On the test day, each solution was again vigorously shaken and then filtered using a micro-fiber filter (Whatman Grade 934-AH Micro Filter). The filtered solution was collected for pH measurement and elemental analysis using inductively coupled plasma mass spectrometry (ICP-MS) test to measure the amount of selected elements (i.e. Si, Al, Ca) that leached into the solution. Titration method was adopted to measure the pH of solutions. For this process, phenolphthalein was used as the indicator, while the solution was titrated with 0.01N HCl

solution. The filtrate part of each paste sample was also collected, washed with 100 ml of deionized water and was allowed to dry at 23°C and 50% relative humidity. After drying, the samples were sealed. Selected samples were then evaluated using XRD to examine any changes in mineralogy such as formation of gypsum and Ettringite.

To determine the amount of calcium hydroxide (CH) in the specimens, Thermogravimetric analysis (TGA) was performed on representative paste samples using TA Instrument (2950 model), employing a platinum pan with nitrogen purge gas was used for this purpose. The temperature was raised from ambient to 600 degrees Celsius at a temperature ramp of 10 degrees per minute. Representative crushed geopolymer paste samples passing #200 sieve were used for this test. The crushed geopolymer samples were gradually heated, and the change in their mass was recorded. Decomposition of CH occurs within the temperature range between 440 to 520°C and causes a mass loss in the sample (58). The mass loss in this range can be used to calculate the amount of calcium hydroxide in the sample.

Mercury Intrusion Porosimetry (MIP) was used to monitor the change in the porosity of samples exposed to the sodium sulfate solution. Three days after casting, geopolymer samples were cut into sections of 10 x 10 x 10 mm cubes and were placed in a 5% sodium-sulfate solution. On the test date (i.e. 7, 28, and 56 days), specimens were removed from the solution and were washed in deionized water. Specimens were then dried in an 110°C oven for 2 h and were tested using MIP to determine the porosity and pore characteristics. MIP test was conducted using a Quantachrome Poremaster 60 with mercury having a contact angle of 140°. Finally, to study the microstructure of the samples, scanning electron microscopy images was a Hitachi TM 3000 unit, equipped with a Swift EDX (energy-dispersive X-ray spectral analysis) was used in the back-scatter mode. The type of specimens (i.e. pate or mortar) and performed tests are summarized in Table 9-5.

Table 9-5. Specimen type used for each of the test.

| Specimen type | Experiment |
|---|---|
| Paste | Change in pH, leach of ions from the paste into the solution, XRD, TGA |
| Mortar | Compressive strength, Change in weight, SEM-EDX, MIP |

## 9.3 Results and Discussion

### *9.3.1 Change in the weight*

Weight change in the geopolymer mortar samples that were immersed in a 5% sodium-sulfate solution was monitored up to 120 days (Table 6). As it can be seen in Table 6, GGF and fly ash-based geopolymer samples showed 0.4% and 2.2% weight gain after 120 days of exposure to the sodium sulfate solution. On the other hand, GLP-based geopolymer showed a steady weight loss during the test period, and lost 2% of its initial weight after 120 days of exposure to the sodium sulfate solution. It should be noted that the change in the weight of specimens could happen because of two actions; 1) the dissolution of the paste into the solution (causing weight loss), and 2) the penetration of the solution into the geopolymer structure (causing weight gain).

Since all geopolymer specimens were cured at 60$^{o}$C temperature, it is thought that the voids and porosity in the specimens should have been almost free of water at the beginning of the test. Therefore, the weight gain of the fly ash and GGF-based geopolymer mortar samples can be related to the dominating effect of the saturation of the empty or partially filled voids and pores in comparison to the small amount weight loss due to the dissolution of the paste (Section 9.3.4). However, the smaller amount of weight gain in the GGF-0-10 specimens in comparison to the F-1-10 specimens can be related to the lower amount of porosity of the GGF-0-10 specimens (Section 9.3.5).

The visual appearance of F-1-10 and GGF-0-10 specimens after being soaked in the 5% sodium sulfate solution for 120 days are shown in Figure 9-2a, and 9-2b respectively. As it can be seen in these figures, neither F-1-10 nor GGF-0-10 sample showed any visible sign of cracking,

leaching, and deterioration. Therefore, in the absence of any visible damage the weight gain seen in the fly ash and GGF-based specimens can be related to the penetration of the solution into the voids and pores of these specimens.

Table 9-6. Change in the weight of geopolymer mortar specimens due to soaking in the 5% sodium sulfate solution (possitive values show weightn and negative values show weight loss)

| Submersion time (Day) | Weight change (%) | | |
|---|---|---|---|
| | GGF-0-10 | F-1-10 | GLP-1-10 |
| 0 | 0.0 | 0.0 | 0.0 |
| 7 | 0.2 | 1.4 | -0.4 |
| 28 | 0.3 | 2.2 | -0.9 |
| 56 | 0.3 | 2.1 | -1.6 |
| 120 | 0.4 | 2.2 | -2.0 |

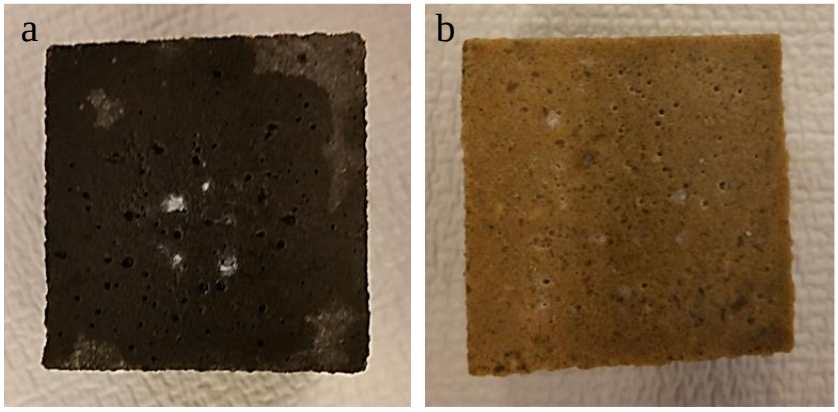


Figure 9-2. Visual appearance of geopolymer cubes after being soaked in the 5% sodium sulfate solution for 120 days, a) F-1-10 and, b) GGF-0-10.

The weight loss observed in the GLP-based specimens is likely to be due to the leaching and dissolution of the paste matrix into the soak solution, as presented in Figure 9-3. Figure 9-3a shows GLP-1-10 mortar cube after being removed from the sulfate solution and dried. Figure 9-3b shows the SEM and EDX analysis of the white deposit shown in Figure 9-3a. As it can be observed from the EDX results, there is a considerable amount of Si in the deposit; which has been released from the geopolymer sample. The high amounts of Na and S measured in the

deposit can be attributed the precipitation of these ions from the sodium sulfate solution on to the surface of the specimen.

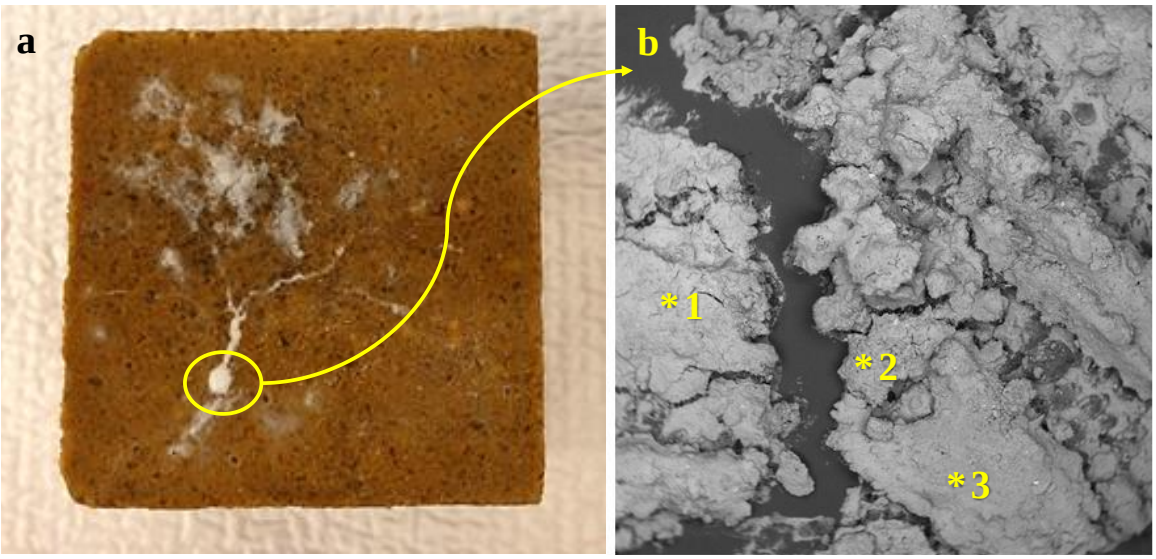


Average weight Percentage of Elements

| | Na | Mg | Al | Si | S | K | Ca |
|---|---|---|---|---|---|---|---|
| Average (W%) | 32.19 | 1.02 | 3.25 | 28.87 | 24.39 | 2.52 | 7.81 |

Figure 9-3. a) Formation of a white deposit on the surface of GLP-1-10 sample. b) EDX results of the white deposit

### *9.3.2 Change in the compressive strength*

The compressive strength of geopolymer mortar cubes that were immersed in the 5% sodium sulfate solution are presented in Table 9-7. It can be observed that the compressive strength of the fly ash and GGF-based specimens decreased in the early ages (7 to 28 days), and subsequently increased at the later ages (56 to 120 days). In the case of F-1-10 specimens, the lowest compressive strength (44 MPa) was seen after 7 days of exposure in the solution. Nevertheless, the specimens regained the compressive strength at later ages and reached 58 MPa after 120 days of exposure. In the case of GGF-0-10 specimens, the loss in compressive strength was not as rapid as observed in F-1-10 specimens, and the lowest compressive strength was seen after 28 days (61 MPa). However, similar to the F-1-10 mixture, the GGF-0-10 specimens regained their

compressive strength and reached 70 MPa after 120 days of the exposure.

On the other hand, in the case of GLP-1-10 specimens, a significant strength loss was seen up to 56 days. The strength gain of the GLP-1-10 specimens was not considerable at the later age (from 56 days to 120 days). These specimens lost more than 50% of their initial compressive strength after 120 days of immersion in the 5% sodium sulfate solution.

Table 9-7. Change in the compressive strength of geopolymer mortar samples due to the sulfate attack

| Submersion time (Day) | Compressive strength (MPa) | | |
|---|---|---|---|
| | GGF-0-10 | F-1-10 | GLP-1-10 |
| 0 | 79 | 58 | 37 |
| 7 | 67 | 44 | 22 |
| 28 | 61 | 51 | 16 |
| 56 | 76 | 61 | 15 |
| 120 | 70 | 58 | 18 |

From the previous studies that attempted to study the behavior of geopolymers exposed to sulfate-rich solutions, conflicting trends in compressive strength results were reported. While strength gain was reported in some studies (7, 36, 57, 60), strength loss was reported in other studies (7, 12, 13, 55, 61), and fluctuation in the mechanical properties has been reported by others (7-9, 12). In these studies, the principal reason for the strength gain was reported to be due to the further geopolymerisation process, formation of a new zeolite phase (faujasite), which reduces the porosity; while the main causes of the strength loss were attributed to the dissolution of alkali from the geopolymer matrix into the sulfate solution, leaching of Si in to the sulfate solution, and the formation of gypsum in geopolymer matrix.

In order to better understand the changes in the mechanical properties in geopolymer samples exposed to sodium sulfate solutions, a comprehensive experimental program was conducted to evaluate the effect of each of the above mentioned mechanisms on the compressive

strength of the geopolymer mixtures. Different parameters, including leaching of alkalis from the geopolymer paste, changes in the pH of the sodium sulfate solution and dissolution of geopolymer paste in the sodium sulfate solution were measured. In addition, other tests such as MIP, XRD, SEM-EDX and TGA analysis, were conducted on the geopolymer specimens to better understand changes in the porosity, mineralogy and microstructure. The results of these experiments are presented and discussed in the following sections.

### *9.3.3 Leaching of the alkalis from geopolymers into the soak solution*

The main mechanism for the deterioration of the geopolymer samples in a sulfate-rich media has been suggested to be due to dissolution of the alkalis from the geopolymer into the sodium-sulfate soak solution (9, 12) resulting in the increase in the porosity (9) or possibly causing the formation of micro-cracks (12), which decreases the mechanical properties. In the present study, dissolution of alkalis (Na and K cations) from the geopolymer samples was evaluated by measuring the changes in the alkali content of the paste portion of the geopolymers, as well as change in the pH of the filtered sodium sulfate solution. The procedure for obtaining the filtered solution is presented in section 2.2.

#### *9.3.3.1 Change in the alkali content of the geopolymers' paste*

Table 9-8 presents the alkali content of the paste portion of geopolymer samples before exposure to sodium sulfate solution, after 28 days, and after 120 days of immersion into the sodium sulfate solution. These values are based on the averaged EDX results from at-least three locations, at a distance of 1000 microns from the surface of specimens in the paste portion of the geopolymer samples. As this table shows, in all the geopolymer mixtures, the EDX results confirmed the dissolution of alkali into the sodium sulfate soak solution, as sodium content in the geopolymer matrix changed significantly before and after the exposure. In GGF-1-10 sample, a considerable reduction in the sodium content was seen at 28 days; however, after 28 days the sodium content

remained fairly stable between 28 and 120 days.

In the case of F-1-10, a rapid decrease in sodium and potassium contents was observed from the beginning of the test up to 28 days. Sodium content decreased from 11.70% to 8.26% and potassium content decreased from 3.21% to 2%. However, the alkali reduction mechanism seems to stop at later ages as the sodium and potassium content values at 120 days are close to the 28-day values. Similar trend was also seen in the case of GLP-1-10 sample. This material showed a rapid decrease in the both sodium and potassium content up to 28 days, and further reduction in the alkali content occurred at a much slower pace until 120 days. The significant reduction of alkali content in the GLP-1-10 mixture, suggests the weaker bonds of alkalis (or higher amount of un-fixed alkalis) in this material in comparison to other tested geopolymer mixtures (i.e. GGF and fly ash-based geopolymers). In addition, the dramatic strength loss of this material could be also related to the dissolution of the paste portion of GLP-1-10 geopolymer.

Table 9-8. Change in the sodium and potassium content of the geopolymer samples due to sulfate attack

| | Sodium | | | Potassium | | |
|---|---|---|---|---|---|---|
| Sample ID | GGF-0-1 | F-1-10 | GLP-1-10 | GGF-0-1 | F-1-10 | GLP-1-10 |
| Before immersion | 13.39 | 11.70 | 16.44 | 0.14 | 3.21 | 1.00 |
| After 28 days | 8.66 | 10.41 | 10.58 | 0.18 | 1.51 | 0.16 |
| After 120 days | 9.34 | 7.94 | 5.68 | 0.31 | 2.09 | 0.43 |

#### *9.3.3.2 Change in the pH of the sodium sulfate solution*

Considering that the pH of the 5% sodium sulfate solution is 7, change in the pH value of sodium sulfate solutions upon introduction of the geopolymer samples into the soak solution bath was tracked with age and these results are presented in Figure 9-4. With all the geopolymer samples, a significant change in the pH value of the sodium sulfate soak solution was observed within the first few days. This can be related to the dissolution of alkalis from the geopolymer matrix into the solution. However, the pH value of the soak solution remained almost constant after 7 days

and did not show a considerable change up to 56 days.

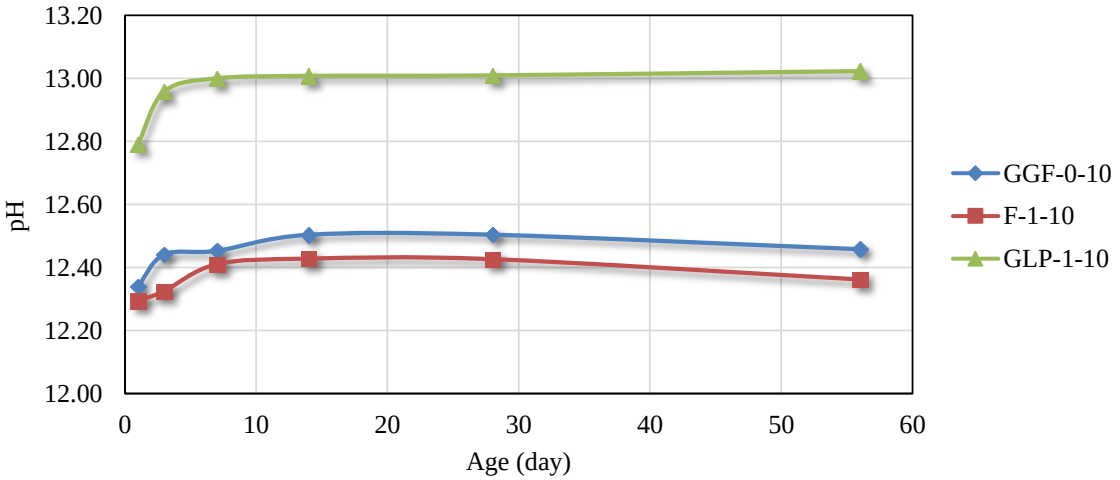


Figure 9-4. Change in pH of the solution versus time. (Five grams of crushed paste was introduced to 100 ml of 5% sodium sulfate solution)

Among the different samples tested, the largest change in the pH value of the sodium sulfate soak solution was seen with the GLP-1-10 sample, wherein the pH of the soak solution changed from 7 to almost 13 within the first seven days of exposure. On the other hand, solutions containing GGF-0-10 and F-1-10 samples showed an increase in pH from 7 to 12.45 and 12.41, respectively, within the first 7 days and thereafter showed almost the same pH. The higher initial pH in the case of GLP-1-10 samples is thought to be related to the large amount of available alkalis, as well as the low amount of Al in the GLP composition (Table 9-1). In the geopolymer systems, alkali ions are balanced with the negative charge of aluminum in a tetrahedral coordination (26, 62). Therefore, it is thought that the low amount of Al in the GLP structure results in a high amount of unfixed alkalis in the geopolymer matrix, which can freely leach into the sodium-sulfate solution and increase the pH value.

In the case of fly ash and GGF-based geopolymer samples, pH values increased up to 14 days of exposure, and reached 12.43 and 12.50 respectively. The values remained the same until 28 days, and then declined to 12.36 and 12.45 respectively after 56 days of exposure. While the

initial increase in the pH values has been related to the leaching of alkali ions from the pore solution and the dissolution of unfixed alkali ions (7, 9, 12), the later reduction in the pH contents thought to be related to the further geopolymerisation of the exposed samples. Further polymerisation of geopolymer samples in the sodium-sulfate solution was also suggested by Ismail et al. and Slaty et al. (10, 36). Moreover, a few studies have shown that sodium-sulfate solution can be used as an activator in activation of slag-based geopolymer systems (63, 64). It should be mentioned that the leaching of alkalis from the geopolymer samples in itself cannot be considered as the main deterioration mechanism of the geopolymer samples when exposed to a sulfate-rich solution such as sodium sulfate solution. Results from other studies have shown that leaching of alkalis (increase in the pH value of the exposed liquid) was observed for cases in which geopolymer samples had been kept in the deionized water or sea water (367, 50). Other studies have also shown a decrease or fluctuation in the mechanical properties of geopolymer samples kept in deionized water (8, 9, 37, 50, 65). Furthermore, results of our ongoing experiments showed an increase in the pH value of a deionized water sample that was in contact with geopolymer samples in comparison to a 5% sodium sulfate solution that had been kept in a same condition.

### *9.3.4 Dissolution of geopolymers in sodium sulfate-solution:*

Dissolution of key elements, including Ca, Si and Al from geopolymer samples into the sodium sulfate solution is presented in Table 9-9. These results can partially explain the reduction of mass and compressive strength of the GLP-1-10 samples, since a significant amount of Si was dissolved from this sample. Due to the high amount of already available Na (from the sodium-sulfate solution), it was not practical to trace the change in the concentration of this element; however, the measured high pH values in all the tested samples suggest the dissolution of Na from the paste into the solution.

Table 9-9. Concentration of ions leached from each geopolymer sample into the sodium sulfate solution (dissolution test)

| Age (day) | Ions leached from GGF-1-10 (ppm) | | | Ions leached from F-1-10 (ppm) | | | Ions leached from GLP-1-10 (ppm) | | |
|---|---|---|---|---|---|---|---|---|---|
| | Ca | Al | Si | Ca | Al | Si | Ca | Al | Si |
| 1 | 10 | 2 | 59 | 7 | 4 | 164 | 3 | 7 | 1481 |
| 7 | 12 | 2 | 113 | 6 | 5 | 231 | 4 | 8 | 1639 |
| 28 | 8 | 1 | 112 | 7 | 1 | 176 | 4 | 10 | 1467 |
| 56 | 14 | 1 | 113 | 6 | 1 | 204 | 3 | 12 | 1665 |

As it can be seen in Table 9-9, for the case GGF and fly ash-based geopolymers, low amounts of Si and negligible amount of Al and Ca was dissolved into the sodium-sulfate solution. The low amount of dissolution of Si and Al, which are known to form the main structural units of geopolymer paste, suggests that the main structure of geopolymers remains almost intact when GGF-0-10 and F-1-10 samples are immersed into the sodium-sulfate solution. It should be noted that due to the low amount of ions leachate from GGF and fly ash-based geopolymer samples into the sodium sulfate solution, the weight loss of these samples because of the dissolution is thought to be very small. One should note that, since five grams of the paste were dissolved into 100 ml of sodium sulfate solution, the initial concentration of the paste in the solution is ~50,000 ppm. Therefore, the total amount of leached Si+Al+Ca from GGF-0-10 and F-1-10 crushed paste samples after 56 days of soaking, would cause only 0.25% and 0.42% weight loss for these samples. Thus, the actual weight gain of GGF-0-10 and F-1-10 mortar samples could be related to the saturation of the empty voids and pores.

The high amount of Si dissolved into the sodium sulfate soak solution in the case of GLP-1-10 suggests that the Si in the GLP-based sample is not strongly bound. This is thought to be due to the formation of an ASR-like gel material in the GLP matrix, which was seen all over the paste matrix of GLP-1-10 sample. The chemical composition of the gel consisted of a low amount of

Ca along with the high amount of Si and Na (Figure 9-5). It has been proposed in earlier studies that in the absence of Ca, ASR gel has a low viscosity (66, 67), and would easily dissolve in the alkali solution. Therefore, the high amount of Si and Na in the exposed solution could be explained by the dissolution of the low-viscosity ASR gel into the sodium-sulfate solution.

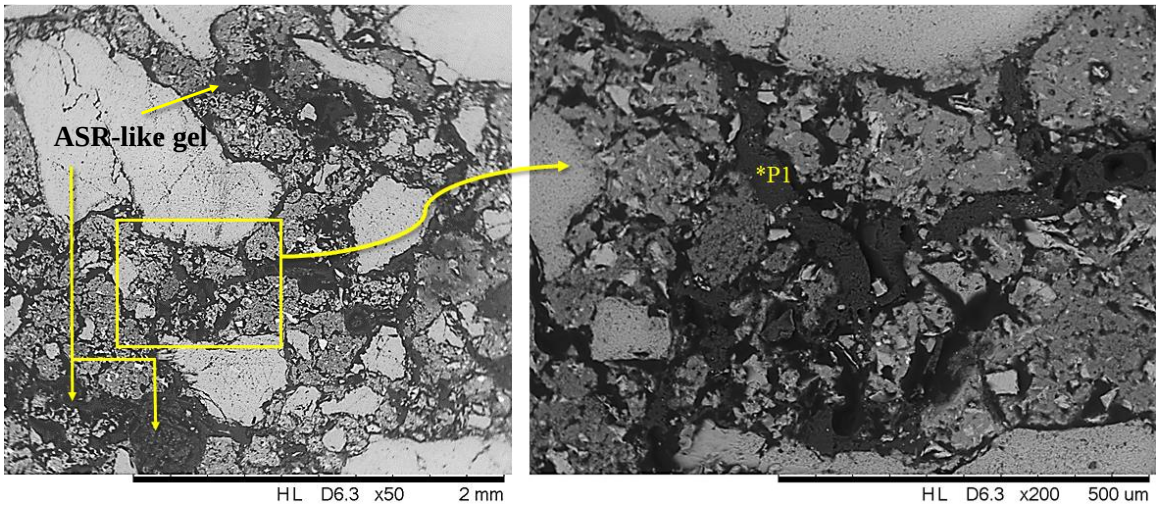


| Spectrum | Na | Mg | Al | Si | K | Ca | Fe |
|---|---|---|---|---|---|---|---|
| P1 | 26.55 | 0.44 | 1.22 | 64.13 | 0.44 | 6.36 | 0.85 |

Figure 9-5. Formation of an ASR-like gel in the structure of the GLP-1-10 sample

### *9.3.5 Mercury Intrusion Porosimetry (MIP)*

Pore size distribution of unexposed samples and change in the total porosity of exposed mortar samples are presented in Figure 9-6a and Figure 9-6b respectively. According to the results presented in Figure 9-6a, G-0-10 sample has the lowest total porosity (0.03 cc/g), which is followed by GLP-1-10 sample (0.07 cc/g), and F-1-10 sample (0.10 cc/g). In the case of GLP-1-10, GGF-0-10, and F-1-10 samples, most of the pore sizes were between the 1 to 100 $\mu$m, 1 to 20 $\mu$m, and 0.01 to 1 $\mu$m, respectively. In GGF and GLP-based samples, pores with the sizes larger than 1 $\mu$m accounted for 91% and 84% of the total intruded volume, respectively. On the other hand, in the case fly ash-based geopolymer sample most of the intruded volume occurred at smaller pore sizes. In this sample (F-1-10), 83% of the total intruded volume was shown to occur

at pore sizes smaller than 1 $\mu$m. However, considering the spherical shape of the fly ash particles and particularly the cenospheres (i.e. hollow fly ash particles) (Figure 9-7), the rapid rise in the intruded volume at the smaller pores size seems to result from the small size of pore entrances rather than the actual pore diameter itself. It should be pointed out that the MIP test identifies the size of the entrance paths to the pores not the actual pore diameters themselves. This phenomenon will cause a significant increase in the intruded volume to be registered at small pore sizes.

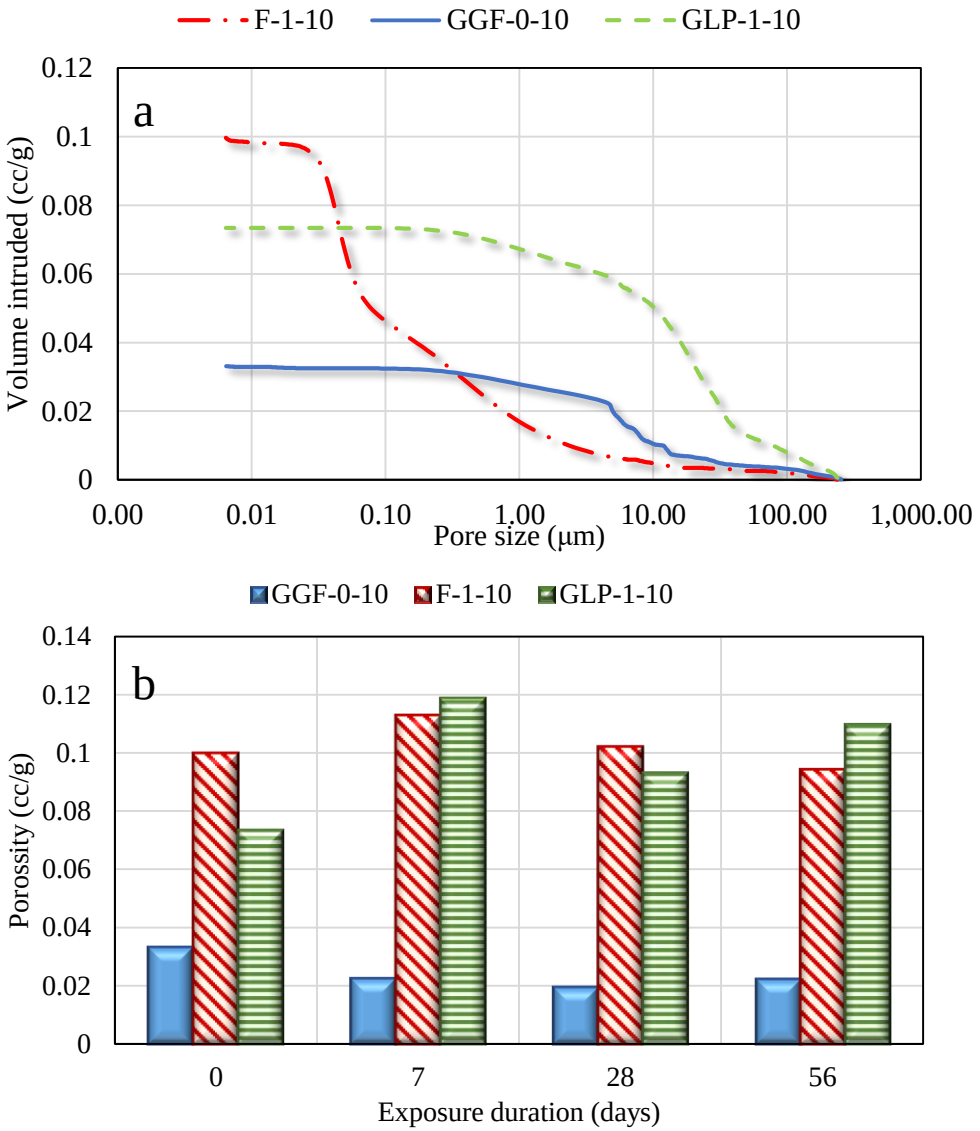


Figure 9-6. MIP test results. a) Pore size vs volume intruded for non-exposed samples, b) change in the

porosity of exposed samples by time.

Figure 9-6b shows the variation of the total porosity of geopolymer samples exposed in 5% sodium-sulfate solution with age. In this study, change in the total amount of intruded volume of the samples exposed to the sodium-sulfate solution is thought to occur because of the following reasons: 1) further geopolymerisation/hydration of the unreacted precursors, 2) dissolution of the paste components (Si, Al and Ca) in the solution, and 3) precipitation of the sodium sulfate into the voids.

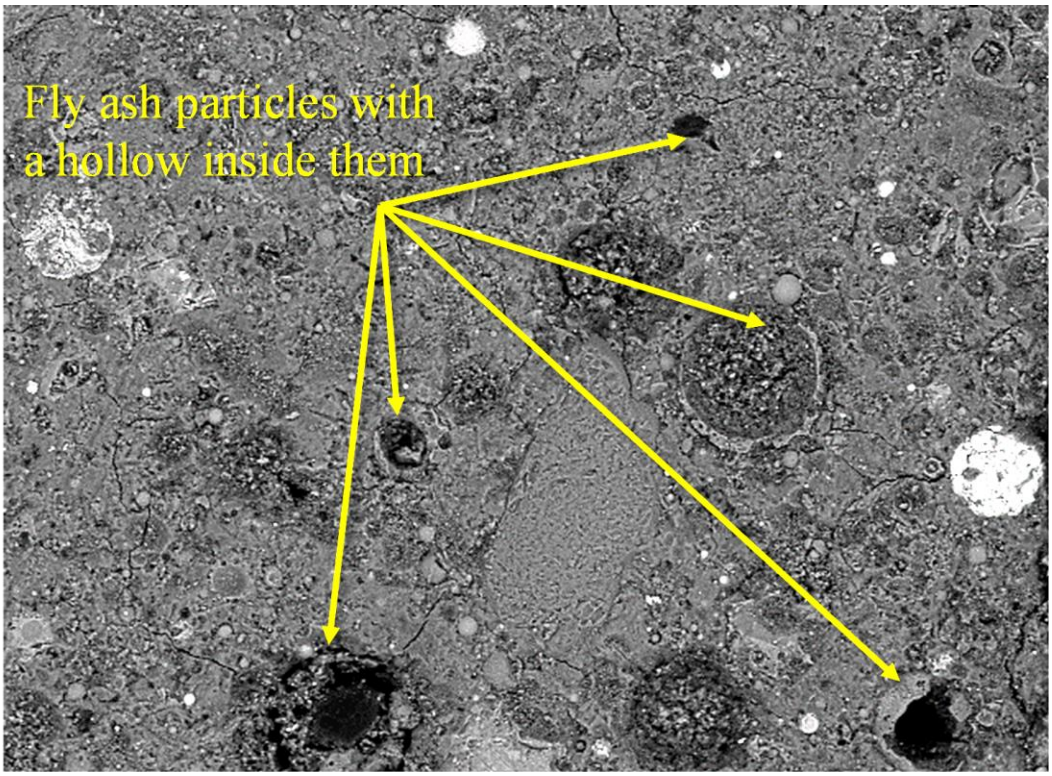


Figure 9-7. Hollow fly ash particles in F-1-10 sample

As it is obvious from the results, the total amount of porosity in the case GGF and fly ash-based geopolymer samples did not change significantly. The slight reduction in the porosity of the GGF and fly ash based samples is thought to be as a result of further geopolymerisation of the unreacted GGF and fly ash particles, which could refine the paste matrix of the samples and reduce the porosity. Preliminary results from an investigation on the alkali activation of GGF at

ambient temperature using the same activator as used in this study showed a gradual strength gain in the geopolymer mortar samples up to 28 days. In addition, SEM-EDX as well as XRD analysis that was performed on the exposed samples did not confirm the presence of any noticeable amount of sodium sulfate crystals. Therefore, considering the dissolution results (presented in section 9.3.4), in which no considerable amount of Si, Ca and Al, had leached from the GGF and fly ash-based geopolymer pastes (Table 9-9), it could be concluded that the dissolution of pastes into the sodium sulfate solution could not cause a possible increase in the pore volume. As a result the slight reduction seen in porosity of the exposed GGF and fly ash-based samples could be mainly attributed to the further geopolymerisation. The further geopolymerisation of fly ash-based geopolymer samples immersed in sodium sulfate solutions have been also suggested by other studies (7, 10).

In the case of GLP-1-10 specimens, an increase in the total porosity is thought to be as a result of significant dissolution of the paste, with an ASR gel-like composition, in the sodium sulfate solution. As it is presented in Table 9-9, high amount of Si and Ca had leached out from the GLP-based geopolymer paste. Considering the high amount of available alkalis in the GLP-1-10 geopolymer paste, both from the GLP precursors (Table 9-1) and the activator solution, the pH of the pore solution would be very high causing leaching of Si from the GLP-1-10 paste into the solution. As presented in Figure 9-6b, the total amount of porosity showed an almost 50% increase after 56 days of exposure to the sodium sulfate solution, which could significantly affect the mechanical properties of the GLP-based geopolymer.

### *9.3.6 X-Ray Diffraction (XRD)*

XRD patterns of 28-days exposed geopolymer pastes as well as unexposed ones are presented in Figure 9-8 through Figure 9-10. As it can be seen in Figure 9-8a, peaks in the unexposed F-1-10 sample are mostly associated with the presence of Quartz, Mullite and Hematite. These peaks

were also seen in the XRD pattern of the raw fly ash (Figure 9-1), indicating that the abovementioned crystalline phases do not readily contribute in the geopolymerisation reactions. The XRD results from the exposed sample showed the formation of a few new phases such as natrite ($Na_2CO_3$), as well as the small amount of calcite, and feldspar. Presence of the two later phases has been also reported in the previous works (7, 8).

Comparison between the XRD pattern of the raw fly ash and F-1-10 geopolymer paste showed a shift in the center of the hump for amorphous or vitreous phases of the original fly ash after the activation (see the hump between 18°-38° 2θ at Figure 9-1b and Figure 9-8a). Moreover, comparison of XRD pattern of the exposed and the unexposed F-1-10 samples (Figure 9-8a and Figure 9-8b) did not reveal any notable shift in the hump of the XRD pattern; however, peaks of some crystalline phases such as quartz, mullite, and hematite showed a lower intensity.

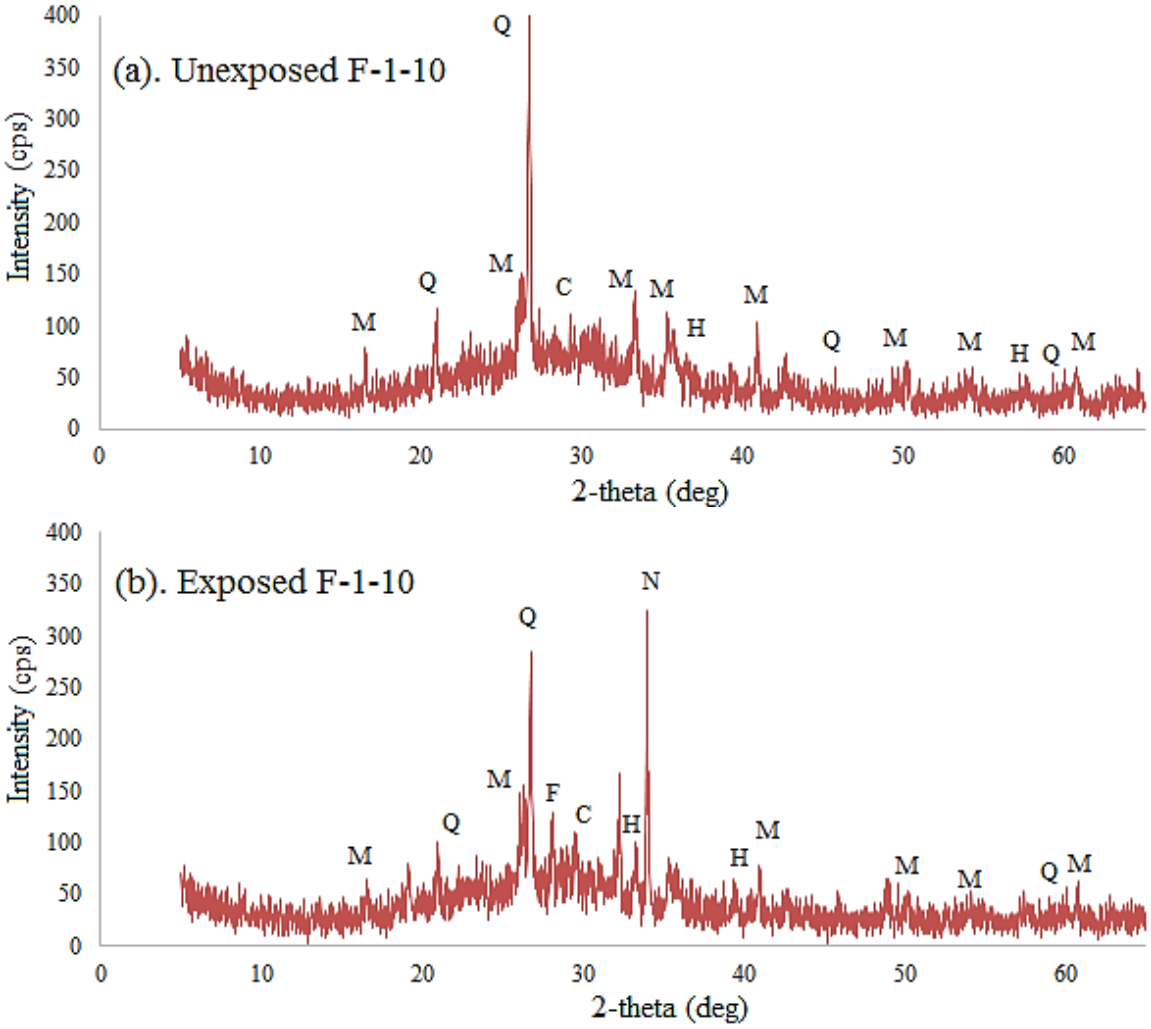


Figure 9-8. XRD pattern of the unexposed and exposed fly ash-based geopolymer samples. (Q: Quartz, M: Mullite, H: Hematite, C: Calcite, N: Natrite, F: Feldspar)

In the case of GGF-0-10 sample, crystalline phases such as quartz, calcite, and tobermorite were seen in the unexposed sample (Figure 9-9a). Formation of these phases has been also reported in an alkali activated VCAS by Tahsima et al. (40). The XRD pattern of the exposed GGF-0-10 sample (Figure 9-9b) indicated an amorphous phase with no major crystalline phases. In addition, no change was seen in the amorphous hump, suggesting that the major geopolymer phases did not go through any significant deterioration in the exposed solution. These results are in agreement with the results from the dissolution test (Table 9-9); in which no considerable

amount of Al was found in the filtered sodium sulfate solution that was in contact with the GGF-based geopolymer paste, even though there was an elevated level of Si in the solution. It should be mentioned that if geopolymer gel were to deteriorate in the sodium sulfate solution, Al ions should have been detected in the solution along with the Si ions. It is therefore suggested that the presence of the Si ions in the solution could be related to the dissolution of microcrystalline quartz grains (which are less stable than well-formed larger quartz grains) into the soak solution. Absence of the peaks associated with quartz in the exposed samples compared to the unexposed samples reinforces this hypothesis.

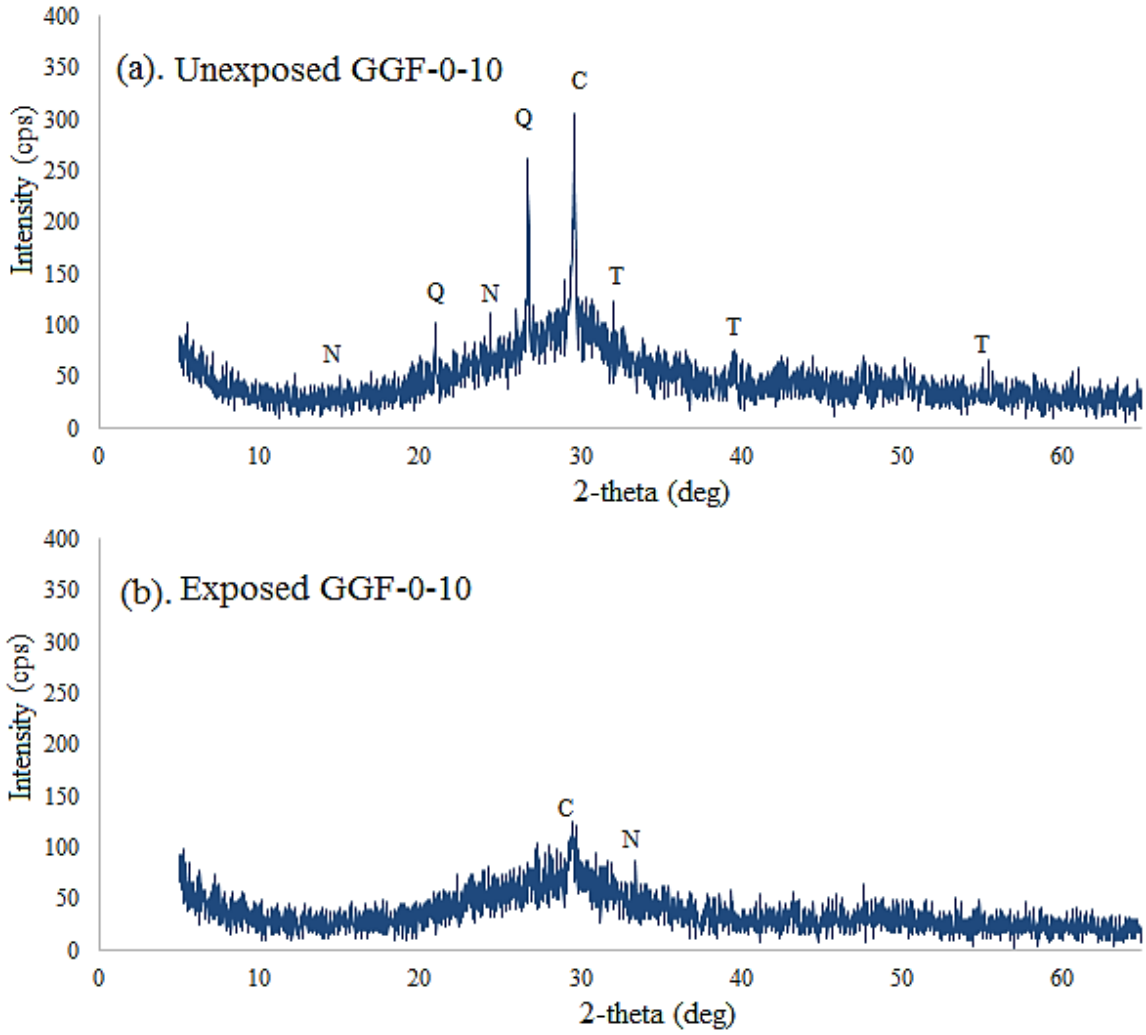

Figure 9-9. XRD pattern of the unexposed and exposed GGF-based geopolymer samples. (Q: Quartz, C: Calcite, T: Tobermorite, N: Natrite)

Figure 9-10a and 9-10b present the XRD pattern of unexposed and exposed GLP-1-10 geopolymers, respectively. As shown in these figures, both exposed and unexposed samples have an amorphous structure with a few recognizable peaks. In the case of the unexposed sample, quartz was the main crystalline phase; which was also seen in the raw GLP precursors. On the other hand, peaks associated with quartz (with a lower intensity), and calcite were observed in the exposed GLP1-10 sample. While the comparison between the XRD patterns of the unexposed GLP-base sample and the raw GLP precursor revealed a clear shift in the amorphous hump, comparison of the exposed and the unexposed XRD patterns of the GLP samples showed a reduction in the height of the amorphous hump. This suggests that the GLP-based geopolymer is not stable in contact with the sodium sulfate solution and would dissolve into the solution. The high amount of dissolved Si ions in the solubility test can therefore be explained by the dissolution of the reaction product of the GLP-based geopolymer in the exposure solution.

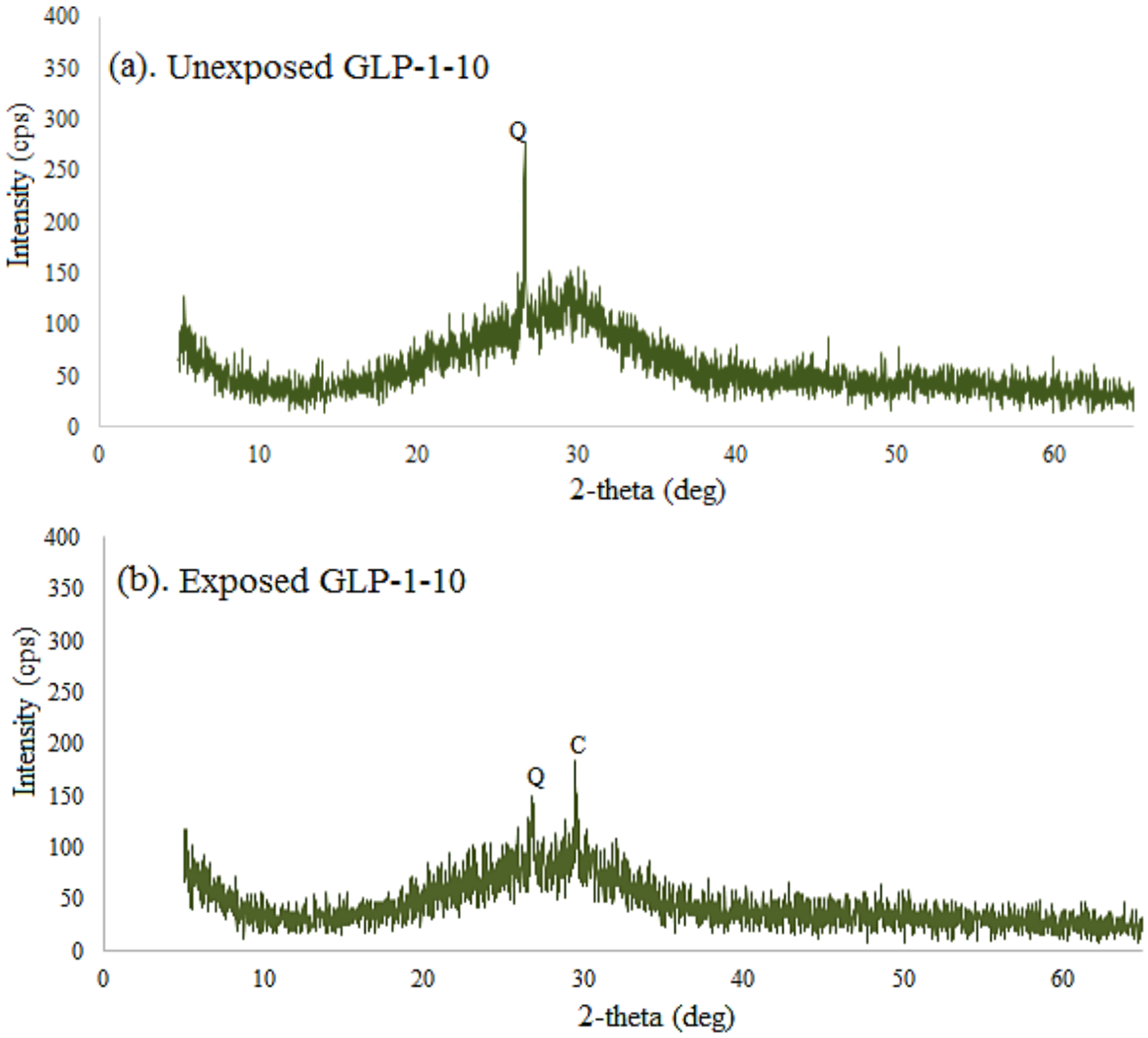


Figure 9-10. XRD pattern of the unexposed and exposed GLP-based geopolymer samples. (Q: Quartz, C: Calcite,)

While formations of gypsum and ettringite are known to be the main cause of deterioration in the portland cement based specimens that are exposed to a sodium sulfate solution, no clear sign of gypsum or ettringite was seen in XRD patterns of all the exposed samples. These results are in agreement with the previous studies (7, 10, 36, 55) in which formation of gypsum and ettringite was not confirmed in geopolymer samples exposed to sodium sulfate solutions. In GGF and Fly ash-based samples, the amorphous humps stayed unchanged

between the unexposed and the exposed samples; indicating that the geopolymer products stayed stable in the exposed solution. On the other hand, the amorphous hump of the GLP-based geopolymer sample exposed to the sodium sulfate solution showed a reduction in the height of the hump indicating the instability of the geopolymerized product when exposed to sodium sulfate solution. Finally, it should be added that the reduction in the intensity of the few crystalline phases of GLP-1-10 samples suggests the partial dissolution of the unreacted precursors' particles due to the high pH of the exposure solution (after being in contact with the geopolymer samples).

### *9.3.7 SEM analyses*

In this study, Scanning Electron Microscopy (SEM) and the Energy-Dispersive X-ray Spectral Analysis (EDX) were used to study the microstructure and the chemical compositions of the geopolymer mortars. The SEM images at a lower magnification showing the condition of the exposed samples after 28 and 120 days are presented in Figure 9-11. Figure 12 shows the microstructures of the 120-day exposed specimens at a greater magnification. SEM observation of GGF and fly ash-based mortar specimens did not show any significant signs of cracking or paste dissolution after 28 and 120-day exposure to the sodium sulfate solution. On the other hand, a clear sign of damage in the form of deep cracks was seen in the paste portion of the GLP-based specimens after 28 days. Further exposure of the GLP-based specimens, up to 120 days, led to the dissolution of the paste in the solution (Figure 9-12). As it can be observed in this figure, as a result of the paste dissolution, the paste has been dissolved away from the aggregate boundaries andin some cases, aggregate particles have been removed from their places. A magnified image of the geopolymer paste portion of each of the geopolymer mortar samples is presented in Figure 9-12. As it could be seen in the Figure 9-12a and 9-12b, the paste portion of the GGF and fly ash-based geopolymer remained intact after 120-day exposure to the sulfate attack. However, for the

case of GLP-based sample geopolymer, paste was readily dissolved in sodium sulfate solution (Figure 9-12c).

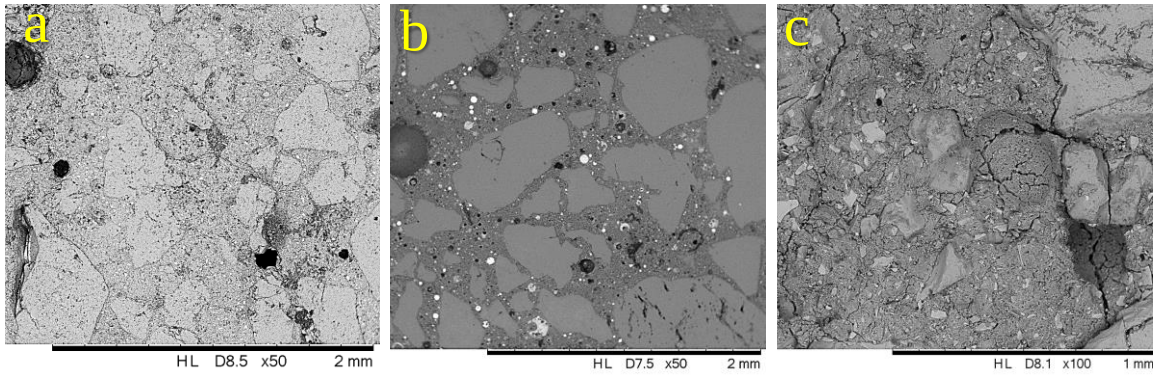


After 28 days of exposure: (a). GGF-0-10, (b). F-1-10, (c). GLP-1-10

After 120 days of exposure: (d). GGF-0-10, (e). F-1-10, (f). GLP-1-10

Figure 9-11. SEM images of the geopolymer specimen exposed to the 5% sodium sulfate solution

It should be noted that the SEM observations are in agreement with the findings from the dissolution test. Furthermore, the low amount of Si and Al leached from the GGF and fly ash-based samples, as well as the high amount of Si and Al leached from the GLP-based geopolymers in the dissolution tests, confirm the resistance of GGF and fly ash-based geopolymer and the susceptibility of the GLP-based geopolymer to sodium sulfate solution.

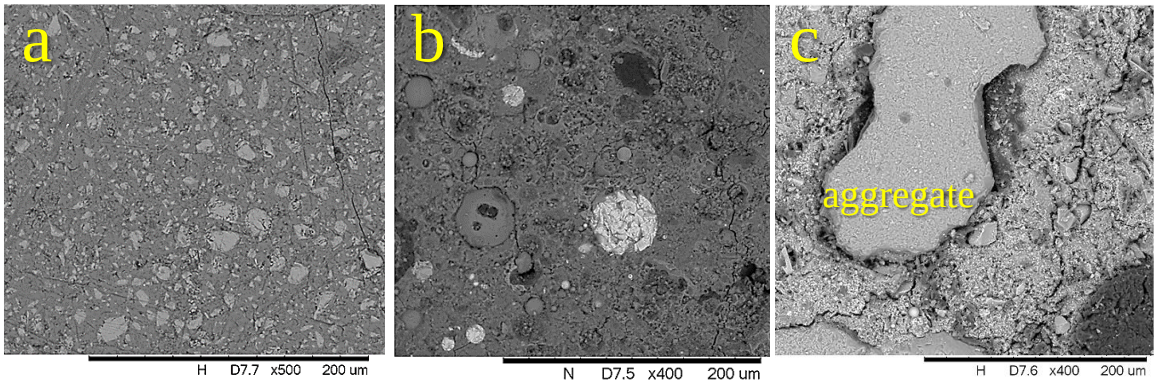


Figure 9-12. Paste portion of geopolymer samples after 120-day exposure to a 5% sodium sulfate solution. (a). GGF-0-10, (b). F-1-10, and (c). GLP-1-10.

### *9.3.8 EDX and TGA analysis:*

To investigate the penetration of sulfate ions into geopolymers, the EDX analysis was performed on the exposed and unexposed samples. This analysis was performed to evaluate the potential risk of formation of gypsum and ettringite in the exposed samples. As it is known, presence of sulfate ions is required for this process, and therefore, the penetration of sulfate ions could be harmful for the structure of geopolymers. Table 9-10 shows the weight percent of sulfur in the paste portion of all tested geopolymers before and after exposure to the sodium sulfate as determined in the EDX analysis. As it can be seen, the concentration of sulfur in the geopolymer samples slightly rises after being in contact with the sodium sulfate solution. However, the measured amounts are still very low and it is unlikely that this amount of sulfur could lead to the formation of compounds such as ettringite and gypsum.

Some of the earlier studies have attributed the good resistance of geopolymers against sulfate-rich solutions to their low amount of calcium oxides (8, 36, 37, 56, 57). These studies were mainly performed on fly ash, or meta-kaolin-based geopolymers in which the amount of available calcium in the precursors was limited. In the present study, however, a considerable amount of calcium was seen in the chemical compositions GGF and GLP (Table 9-1). Therefore,

one could consider the formation of gypsum, and ettringite could take place in the GGF and GLP-based geopolymers, once the sufficient amount of sulfur is available. According to the sulfate attack studies conducted on the portland cement systems, calcium hydroxide (CH) acts as the main source of calcium supply for the formation of gypsum (1, 68). Therefore, to measure the amount of CH in the geopolymers, TGA analysis was performed on the paste samples. The TGA and differential thermal gravimetric analysis (DTGA) results, presented in Figure 9-13, showed a very low level of CH in both GGF-based (1.1% of the total weight), and GLP based geopolymer (1.4% of the total weight) paste samples. This suggests that despite the relatively high amount of Ca in the composition of raw GGF and GLP, calcium is mainly fixed into the other reaction products and only a small portion of it has been consumed to form CH in the geopolymer systems.

Table 9-10. Sulfur content of geopolymers by EDX. (*The elements considered for the EDX analysis are: Si, Al, Ca, Na, K, Fe, and S)

| | Weight percent of sulfur in the paste portion * | |
|---|---|---|
| Sample ID | Before exposure | After 120 days exposure |
| GGF-0-10 | 0.01 | 0.34 |
| F-1-10 | 0.52 | 0.84 |
| GLP-1-10 | 0.06 | 1.29 |

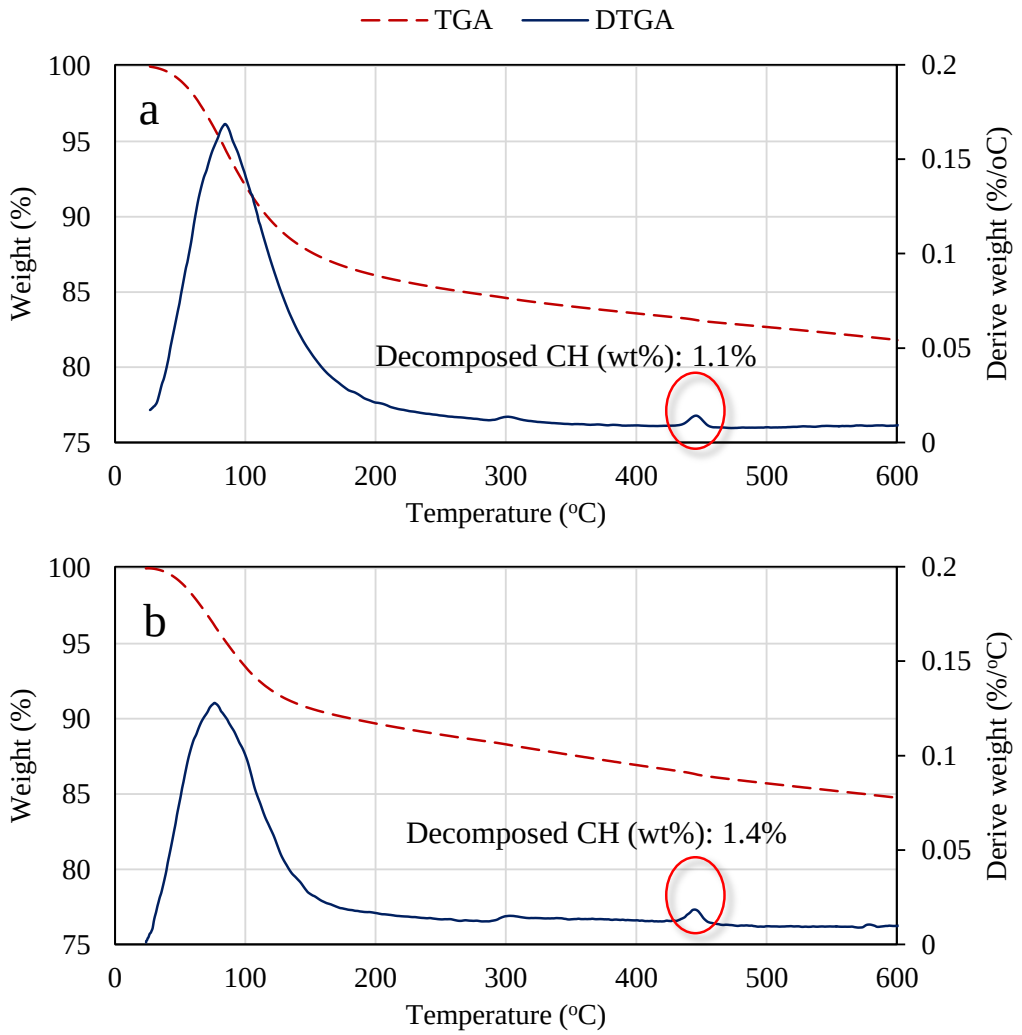


Figure 9-13. TGA and DTGA results of unexposed geopolymer pastes. (a). GGF-0-10, and (b). GLP-1-10.

## 9.4 Conclusion:

In this study the resistance of GGF, fly ash and GLP-based geopolymer mortar specimens exposed to a 5% sodium sulfate solutions were evaluated and compared with each other. For this purpose, parameters such as change in the visual appearance, weight and the compressive strength of geopolymer mortar samples were studied. In addition, techniques such as MIP, XRD, SEM-EDX and TGA were employed to investigate changes in porosity, mineralogy, microstructure and formation of any new phases in the samples. Based on the results obtained from this study the most notable findings could be summarized as follow:

1. GGF and fly ash-based geopolymer samples did not show any visual signs of deterioration when exposed to sodium sulfate solution, however, the GLP-based specimens showed signs of severe deterioration, which was revealed in the forms of cracking and leaching.
2. After 120 days of exposure to sodium sulfate solution, GGF and fly-ash based geopolymers showed a slight increase in the weight, while GLP samples showed weight loss indicating the instability of GLP based geopolymers in the sodium sulfate solution.
3. Monitoring the compressive strength of the geopolymer samples exposed to the 5% sodium sulfate solution showed a decrease in the compressive strength of the GGF and fly ash-based specimens during the early ages (i.e. 7 to 28 days), which was followed by strength gain at the later ages (i.e. 56 days to 120 days). The GLP-based specimens showed a rapid reduction in their compressive strength until 28 days of exposure. After this period, the compressive strength of these samples remained almost constant, and no considerable change was seen in recorded values.
4. Based on the MIP results, no significant changes were occurred in the porosity of the exposed GGF and fly ash-based geopolymer. These results showed a slight reduction in the porosity of the exposed GGF and fly ash-based geopolymer samples after 56 days of exposure; which was attributed to the further geopolymerisation of these specimens. On the other hand, as the result of dissolution of the geopolymer paste in the soak solution, a substantial increase (almost 50%) in the porosity was seen in the exposed GLP-based geopolymer mortar specimen.
5. Based on the XRD results, no notable changes were seen in the XRD pattern of the exposed and unexposed GGF and fly ash-based geopolymers. However, some changes were seen in the case of exposed GLP-based specimens. This suggests the instability of the GLP-based specimens in the sodium sulfate solution, in comparison to the GGF and fly ash-based

specimens,

6. In summary, based on the results obtained from this study, it can be concluded that the effect of sodium sulfate solution on the geopolymer samples is very much different than its effect on the portland cement-based material. As it is known, in the case sulfate attack on the portland cement-based specimens, sulfate plays its role by participating in deleterious chemical reactions leading to the formation of gypsum and ettringite. However, in this study, presence of sulfate seems to have no or a very limited effect on the mechanical properties of the GGF and fly-ash based geopolymer samples. It should be added that, in the case of GLP-based specimens, the main deterioration mechanism is thought to be because of the dissolution of the geopolymerised paste into the solution. Therefore, it is suggested that the term of “sulfate attack” might not be the best term, to describe the changes or fluctuations that might be seen in the mechanical properties of the geopolymer specimens produced from the tested precursors.

## References:


1. Marchand, J., Odler, I., & Skalny, J. P. (2003). Sulfate attack on concrete. CRC Press.
2. Committe, A. C. I. (2001). 201," Guide to Durable Concrete. ACI Manual of Concrete Practice.
3. Bhatty, J. I., & Taylor, P. C. (2006). Sulfate resistance of concrete using blended cements or supplementary cementitious materials (No. PCA R&D Serial No. 2916a). Portland Cement Association.
4. Neville, A.M. (1997). Properties of Concrete, 4th. ed. John Wiley & Sons, Inc., New York, New York, USA.
5. Li, Z., Ding, Z., & Zhang, Y. (2004, May). Development of sustainable cementitious materials. In Proceedings of international workshop on sustainable development and concrete technology, Beijing, China (pp. 55-76).
6. Baš˘carevic, Z. (2014). The resistance of alkali-activated cement-based binders to chemical attack. Handbook of Alkali-Activated Cements, Mortars and Concretes, 373-396 (Eds) Pacheco-Torgal, F.; Labrincha, J.; Palomo, A.; Leonelli, C.; Chindaprasirt, P., WoodHead Publishing-Elsevier, Cambridge.
7. Baščarević, Z., Komljenović, M., Miladinović, Z., Nikolić, V., Marjanović, N., & Petrović, R. (2015). Impact of sodium sulfate solution on mechanical properties and structure of fly ash based geopolymers. Materials and Structures, 48(3), 683-697.
8. Fernández-Jiménez, A., Garcia-Lodeiro, I., & Palomo, A. (2007). Durability of alkali-activated fly ash cementitious materials. Journal of Materials Science, 42(9), 3055-3065.
9. Palomo, A., Blanco-Varela, M. T., Granizo, M. L., Puertas, F., Vazquez, T., & Grutzeck, M. W. (1999). Chemical stability of cementitious materials based on metakaolin. Cement and Concrete Research, 29(7), 997-1004.

10. Ismail, I., Bernal, S. A., Provis, J. L., Hamdan, S., & van Deventer, J. S. (2013). Microstructural changes in alkali activated fly ash/slag geopolymers with sulfate exposure. Materials and structures, 46(3), 361-373.
11. Škvára, F., Jílek, T., & Kopecký, L. (2005). Geopolymer materials based on fly ash. Ceram.-Silik, 49(3), 195-204.
12. Bakharev, T. (2005). Durability of geopolymer materials in sodium and magnesium sulfate solutions. Cement and Concrete Research, 35(6), 1233-1246.
13. Thokchom, S., Ghosh, P., & Ghosh, S. (2011). Effect of Na2O content on durability of geopolymer pastes in magnesium sulfate solution. Canadian Journal of Civil Engineering, 39(1), 34-43.
14. Rangan, B. V. (2014). Geopolymer concrete for environmental protection. Indian Concr. J, 88(4), 41-59.
15. Gourley, J. T., & Johnson, G. B. (2005). Developments in geopolymer precast concrete. In World Congress Geopolymer (pp. 139-143).
16. Cheema, D., Lloyd, N., & Rangan, B. V. (2009). Durability of geopolymer concrete box culverts-A green alternative. In Proceedings of 34th Conference on Our World in Concrete and Structures (pp. 85-92). CI Premier Pty Ltd.
17. Hardjito, D., Wallah, S. E., Sumajouw, D. M., & Rangan, B. V. (2004). Factors influencing the compressive strength of fly ash-based geopolymer concrete. civil engineering dimension, 6(2), pp-88.
18. Aldred, J., & Day, J. (2012, August). Is geopolymer concrete a suitable alternative to traditional concrete. In 37th Conference on our world in concrete & structures, Singapore (pp. 29-31).
19. Royer, J. R., & Koo, D. D. Comparative Analysis of Geopolymer Technology for Sewer

System Rehabilitation. In Pipelines 2015 (pp. 1343-1354).

20. Balaguru, P., Kurtz, S., & Rudolph, J. (1997). Geopolymer for repair and rehabilitation of reinforced concrete beams. St Quentin, France, Geopolymer Institute, 5.
21. Pacheco-Torgal, F., Abdollahnejad, Z., Miraldo, S., Baklouti, S., & Ding, Y. (2012). An overview on the potential of geopolymers for concrete infrastructure rehabilitation. Construction and Building Materials, 36, 1053-1058.
22. Vasconcelos, E., Fernandes, S., de Aguiar, J. B., & Pacheco-Torgal, F. (2011). Concrete retrofitting using metakaolin geopolymer mortars and CFRP. Construction and Building Materials, 25(8), 3213-3221.
23. Zhang, Z., Yao, X., & Zhu, H. (2010). Potential application of geopolymers as protection coatings for marine concrete: II. Microstructure and anticorrosion mechanism. Applied clay science, 49(1), 7-12.
24. Reddy, D. V., Edouard, J. B., & Sobhan, K. (2012). Durability of fly ash–based geopolymer structural concrete in the marine environment. Journal of Materials in Civil Engineering, 25(6), 781-787.
25. Chindaprasirt, P., & Chalee, W. (2014). Effect of sodium hydroxide concentration on chloride penetration and steel corrosion of fly ash-based geopolymer concrete under marine site. Construction and Building Materials, 63, 303-310.
26. Duxson, P., Fernández-Jiménez, A., Provis, J. L., Lukey, G. C., Palomo, A., & Van Deventer, J. S. J. (2007). Geopolymer technology: the current state of the art. Journal of Materials Science, 42(9), 2917-2933.
27. Ganesan, N., Abraham, R., Raj, S. D., & Sasi, D. (2014). Stress–strain behaviour of confined Geopolymer concrete. Construction and Building materials, 73, 326-331.
28. Morsy, M. S., Alsayed, S. H., Al-Salloum, Y., & Almusallam, T. (2014). Effect of sodium

silicate to sodium hydroxide ratios on strength and microstructure of fly ash geopolymer binder. Arabian Journal for Science and Engineering, 39(6), 4333-4339.

29. Van Jaarsveld, J. G. S., Van Deventer, J. S. J., & Lukey, G. C. (2003). The characterisation of source materials in fly ash-based geopolymers. Materials Letters, 57(7), 1272-1280.
30. Ryu, G. S., Lee, Y. B., Koh, K. T., & Chung, Y. S. (2013). The mechanical properties of fly ash-based geopolymer concrete with alkaline activators. Construction and Building Materials, 47, 409-418.
31. Kumar, S., Kumar, R., & Mehrotra, S. P. (2010). Influence of granulated blast furnace slag on the reaction, structure and properties of fly ash based geopolymer. Journal of Materials Science, 45(3), 607-615.
32. Oh, J. E., Monteiro, P. J., Jun, S. S., Choi, S., & Clark, S. M. (2010). The evolution of strength and crystalline phases for alkali-activated ground blast furnace slag and fly ash-based geopolymers. Cement and Concrete Research, 40(2), 189-196.
33. Anuar, K. A., Ridzuan, A. R. M., & Ismail, S. (2011). Strength characteristics of geopolymer concrete containing recycled concrete aggregate. International Journal of Civil & Environmental Engineering, 11(1), 59-62.
34. Trochez, J. J., de Gutiérrez, R. M., Rivera, J., & Bernal, S. A. (2015). Synthesis of geopolymer from spent FCC: Effect of SiO2/Al2O<3 and Na2O/SiO2 molar ratios. Materiales de Construcción, 65(317), 046.
35. Pascual, A. B., Tognonvi, M. T., & Tagnit-Hamou, A. (2014). Waste glass powder-based alkali-activated mortar. Int. J. Res. Eng. Technol, 3(13), 32-36.
36. Bhutta, M. A. R., Hussin, W. M., Azreen, M., & Tahir, M. M. (2014). Sulphate resistance of geopolymer concrete prepared from blended waste fuel ash. Journal of Materials in Civil Engineering, 26(11), 04014080.

37. Slaty, F., Khoury, H., Rahier, H., & Wastiels, J. (2015). Durability of alkali activated cement produced from kaolinitic clay. Applied Clay Science, 104, 229-237.
38. Robayo, R. A., de Gutiérrez, R. M., & Gordillo, M. (2016). Natural pozzolan-and granulated blast furnace slag-based binary geopolymers. Materiales de Construcción, 66(321), 077.
39. Sukmak, P., Horpibulsuk, S., & Shen, S. L. (2013). Strength development in clay–fly ash geopolymer. Construction and Building Materials, 40, 566-574.
40. Tashima, M. M., Soriano, L., Borrachero, M. V., Monzó, J., Cheeseman, C. R., & Payá, J. (2012). Alkali activation of vitreous calcium aluminosilicate derived from glass fiber waste. Journal of Sustainable Cement-Based Materials, 1(3), 83-93.
41. Rashidian-Dezfouli, H., & Rangaraju, P. R. (in press). Comparison of Strength and Durability Characteristics of a Geopolymer produced from Fly ash, Ground Glass Fiber and Glass Powder. Materiales de Construcción.
42. Hemmings, R. T. (2005). Process for Converting Waste Glass Fiber into Value Added Products, Final Report (No. DOE GO13015-1). Albacem LLC.
43. Rangaraju, P. R., Rashidian-Dezfouli, H., Nameni, G., & Amekuedi, G. Q. Properties and Performance of Ground Glass Fiber as a Pozzolan in Portland Cement Concrete 2016 International Concrete Sustainability Conference.
44. Rashidian-Dezfouli, H., & Rangaraju, P. R. (in press). Role of Ground Glass Fiber as a Pozzolan in Portland Cement Concrete (No. 17-04237).
45. Van Jaarsveld, J. G. S., Van Deventer, J. S. J., & Lorenzen, L. (1997). The potential use of geopolymeric materials to immobilise toxic metals: Part I. Theory and applications. Minerals Engineering, 10(7), 659-669.
46. Lee, W. K. W., & Van Deventer, J. S. J. (2002). The effect of ionic contaminants on the early-age properties of alkali-activated fly ash-based cements. Cement and Concrete

Research, 32(4), 577-584.

47. Kupwade-Patil, K., & Allouche, E. N. (2012). Impact of alkali silica reaction on fly ash-based geopolymer concrete. Journal of materials in Civil Engineering, 25(1), 131-139.
48. Pouhet, R., & Cyr, M. (2015). Alkali–silica reaction in metakaolin-based geopolymer mortar. Materials and Structures, 48(3), 571-583.
49. Puertas, F., Palacios, M., Gil-Maroto, A., & Vázquez, T. (2009). Alkali-aggregate behaviour of alkali-activated slag mortars: Effect of aggregate type. Cement and Concrete Composites, 31(5), 277-284.
50. Zhang, M., Zhao, M., Zhang, G., Mann, D., Lumsden, K., & Tao, M. (2016). Durability of red mud-fly ash based geopolymer and leaching behavior of heavy metals in sulfuric acid solutions and deionized water. Construction and Building Materials, 124, 373-382.
51. Ariffin, M. A. M., Bhutta, M. A. R., Hussin, M. W., Tahir, M. M., & Aziah, N. (2013). Sulfuric acid resistance of blended ash geopolymer concrete. Construction and Building materials, 43, 80-86.
52. Sata, V., Sathonsaowaphak, A., & Chindaprasirt, P. (2012). Resistance of lignite bottom ash geopolymer mortar to sulfate and sulfuric acid attack. Cement and Concrete Composites, 34(5), 700-708.
53. Bakharev, T. (2005). Resistance of geopolymer materials to acid attack. Cement and Concrete Research, 35(4), 658-670.
54. Sun, P., & Wu, H. C. (2013). Chemical and freeze–thaw resistance of fly ash-based inorganic mortars. Fuel, 111, 740-745.
55. Bakharev, T., Sanjayan, J. G., & Cheng, Y. B. (2002). Sulfate attack on alkali-activated slag concrete. Cement and Concrete Research, 32(2), 211-216.
56. Rangan, B. V., Hardjito, D., Wallah, S. E., & Sumajouw, D. M. (2005). Studies on fly ash-

based geopolymer concrete. In Proceedings of the World Congress Geopolymer, Saint Quentin, France (Vol. 28, pp. 133-137).

57. Valencia Saavedra, W. G., Angulo, D. E., & Mejía de Gutiérrez, R. (2016). Fly Ash Slag Geopolymer Concrete: Resistance to Sodium and Magnesium Sulfate Attack. Journal of Materials in Civil Engineering, 28(12), 04016148.
58. Chotetanorm, C., Chindaprasirt, P., Sata, V., Rukzon, S., & Sathonsaowaphak, A. (2012). High-calcium bottom ash geopolymer: sorptivity, pore size, and resistance to sodium sulfate attack. Journal of Materials in Civil Engineering, 25(1), 105-111.
59. Pane, I., & Hansen, W. (2005). Investigation of blended cement hydration by isothermal calorimetry and thermal analysis. Cement and concrete research, 35(6), 1155-1164.
60. Wallah, S., & Rangan, B. V. (2006). Low-calcium fly ash-based geopolymer concrete: long-term properties.
61. Sanni, S. H., & Khadiranaikar, R. B. (2012). Performance of geopolymer concrete under severe environmental conditions. International journal of civil and structural engineering, 3(2), 396.
62. Barbosa, V. F., MacKenzie, K. J., & Thaumaturgo, C. (2000). Synthesis and characterisation of materials based on inorganic polymers of alumina and silica: sodium polysialate polymers. International Journal of Inorganic Materials, 2(4), 309-317.
63. Rashad, A. M., Bai, Y., Basheer, P. A. M., Collier, N. C., & Milestone, N. B. (2012). Chemical and mechanical stability of sodium sulfate activated slag after exposure to elevated temperature. Cement and Concrete Research, 42(2), 333-343.
64. Rashad, A. M., Bai, Y., Basheer, P. A. M., Milestone, N. B., & Collier, N. C. (2013). Hydration and properties of sodium sulfate activated slag. Cement and concrete composites, 37, 20-29.

65. Nikolić, I., Zejak, R., Janković-Častvan, I., Karanović, L., Radmilović, V., & Radmilović, V. (2013). Influence of alkali cation on the mechanical properties and durability of fly ash based geopolymers. Acta Chimica Slovenica, 60(3), 636-643.
66. Detwiler, R. (1997). The Role of Fly Ash Composition in Reducing Alkali-Silica Reaction. Portland Cement Association.
67. Lindgård, J., Andiç-Çakır, Ö., Fernandes, I., Rønning, T. F., & Thomas, M. D. (2012). Alkali–silica reactions (ASR): literature review on parameters influencing laboratory performance testing. Cement and Concrete Research, 42(2), 223-243.
68. Tian, B., & Cohen, M. D. (2000). Does gypsum formation during sulfate attack on concrete lead to expansion?. Cement and concrete research, 30(1), 117-123.

# CHAPTER 10

# STUDY ON THE EFFECT OF SELECTED PARAMETERS ON THE ALKALI SILICA REACTION OF AGGREGATE IN GROUND GLASS FIBER AND FLY ASH-BASED GEOPOLYMER MORTARS[1]

## 10.1 Introduction:

Geopolymer is a relatively new type of binders that is produced by the alkali activation of aluminosilicate rich materials. The main product of the activation reaction is a three-dimensional inorganic polymer known as alkaline aluminosilicate hydrate (N-A-S-H) (1). In such a structure, tetrahedral Si and Al atoms are connected by sharing oxygen atoms (2), while cations such as Na+, K+, Mg2+ and Ca2+ must be present to balance the negative charge of $Al^{3+}$ in its 4-fold condition (2-4).

A large number of earlier geopolymers' studies have utilized fly ash, meta-kaolin, slag, or their combinations as precursors (2, 5-11). In addition, several studies have investigated the potential of utilizing other waste or industrial by-products such as: spent fluid catalytic cracking catalyst (12) waste glass-powder (13, 14) waste paper sludge ash (15), kaolinitic clay (16), palm oil fuel Ash (17), combination of natural pozzolan and slag (18), combinations of sugarcane bagasse ash and blast furnace slag (19), blends of clay and fly ash (20), and glass produced from the DC plasma treatment of air pollution control residue (21), have been studied by other authors to produce geopolymer concrete. In addition to these materials, recent works have shown that

[1]- Hassan Rashidian-Dezfouli, Prasada Rao Rangaraju. Study on the effect of selected parameters on the alkali silica reaction of aggregate in ground glass fiber and fly ash-based geopolymer mortars. Submitted to Journal of Construction and Building material (under review).

ground glass fiber (GGF) can be effectively activated by an alkali solution to manufacture a geopolymer mortar (14, 21, 22).

According to a 2005 report by Hemmings (23), each year, around 250,000 to 500,000 tons of waste glass fiber end-up in U.S. landfills. The chemical composition of this material is rich in glassy silica, alumina, and calcium. Thus, it could be potentially used as a pozzolan, or a precursor to produce geopolymers, if milled to a fine powder. In recants works by Rangaraju et al and Rashidian-Dezfouli and Rangarju (14), mechanical and durability properties of portland cement concrete containing GGF as a pozzolan has been investigated. Moreover, in a recent work by authors, it has been shown that the alkali activation of GGF can produce a mortar mixture with the high early strength as high as 79 MPa in 3days (14).

Considering the high level of alkali present in the geopolymer mixtures, susceptibility of aggregates to alkali-silica reaction (ASR) in geopolymer matrix has been a big concern in assessing their durability (24-26).

Typically, alkali-silica reaction (ASR) has been a major cause of deterioration in portland cement concrete structures, when deleterious reactions between aggregates containing either amorphous and/or poorly crystalline silica bearing minerals occur in presence of highly alkaline pore solution present in concrete. This reaction leads to the formation of a reaction product known as ASR gel (27). Under certain conditions (i.e. presence of moisture, calcium, etc.), the ASR gel can absorb water and swell, leading to the expansion of concrete that eventually may causes cracking (27, 28). Use of supplementary cementitious materials (SCMs) is one of the methods known to mitigate the ASR-related expansion (29-31); and a large number of studies have been conducted on the performance of different SCMs in reducing the ASR expansion (14, 24, 25, 32-37.

Several studies have been conducted in order to evaluate the ASR behavior in

geopolymers produced from precursor materials such as fly ash (14, 25, 32-35) and meta-kaolin (24, 36, 37). According to these studies, geopolymers showed a better performance, in terms of less expansion, when compared to a portland cement mixture. In addition to the studies performed on geopolymers, as reviewed by Shi et al. large numbers of studies have been also conducted on the ASR resistance of alkali activated slag (AAS) mixtures (38).

The lower ASR-related expansion of geopolymer mixtures in comparison to the portland cement mixtures has been explained mainly by factors such as lower amount of Portlandite (CH) in the geopolymer matrix (25, 32, 33, 39). Furthermore, other factors such as further geopolymerisation of unreacted precursors, leading to the voids reduction and higher mechanical properties (25, 35), higher porosity of the geopolymer matrix in compare to the portland cement paste, which allows the fresh ASR gel to permeate into the pores easily, without causing a significant expansion (24), the interfacial voids between fly ash particles and the matrix, and autogenous shrinkage (25), have been suggested to address the lower expansion of geopolymer mixtures. On the other hand, the expansion (though much lower than portland cement mixtures) seen in geopolymer samples was related to both formations of ASR gel as well as new zeolite phases, which cause certain amount of stress in the geopolymer matrix that could lead to the expansion (33, 35, 40).

While most of the above mentioned studies have followed a procedure similar to the ATM C1260 procedure, other methods such as AFNOR. NF P18-454 (41) have been also used in evaluating the expansion behavior of geopolymers (24). Unlike the ASTM C1260, in which mortar bars are placed in an alkali solution, in the latter method, the specimens are placed on grids on top of water (no contact between specimens and water). Thus, effects of the alkali solution on the specimens, such as further geopolymerisation, might be reduced. Moreover, to investigate the effect of high alkali content of specimens on the expansion values, a steam curing

method (in 80°C) was considered by Shi et al. (42) to evaluate the ASR resistant of an alkali activated slag mixture.

The main objective of this work is to evaluate the ASR resistance of GGF-based geopolymers. For this purpose, the expansion of GGF-based geopolymer mortar bars were compared with the expansion of fly ash-based geopolymer and an ordinary portland cement mixture (OPC). Furthermore, the effect of curing condition and aggregate type, on the expansion and stiffness of geopolymer mortar bars was investigated. To study the effect of curing condition, GGF and fly ash-based specimens were cured under two different ASR accelerating conditions. In first curing condition, an ASR accelerating curing method as described in ASTM C1260 (1N NaOH solution and 80°C) was adopted. For the second test procedure, a steam curing condition providing more than 98% relative humidity and 80°C temperature was employed.

In this study, the variation in the length and the dynamic modulus of elasticity of the mortar bars were measured to assess the expansion and change mechanical behavior of each geopolymer mixture. To study the microstructure of the specimens, the scanning electron microscopy (SEM) and the energy-dispersive X-ray spectral analysis (EDX) were used. Moreover, to measure the amount of calcium hydroxide (CH) in the geopolymer pastes, the thermogravimetric analysis (TGA) was performed on the samples. Hence, this study provides an insight and new information on the ASR behavior GGF-based geopolymers.

## 10.2 Materials

### *10.2.1 Ground Glass Fiber (GGF):*

Ground Glass Fiber (GGF) is a fine powder material that is produced by milling the off-spec glass fiber using a mill machine (Figure 10-1). This material possesses the same chemical composition as the original glass fiber; but failed to achieve the required physical properties of the final product. The chemical composition and the physical properties of GGF are presented in Table 10-

1 and Table 10-2 respectively.

Figure 10-1. Appearance of GGF that used in this work

### *10.2.2 Fly ash:*

In this work, a class F fly ash (ASTM C618) was used. The chemical composition and the physical properties of the flay ash are presented in Table 10-1 and Table 10-2, respectively.

### *10.2.3 Cement*

For comparative pursues, a Type I/II portland cement, meeting ASTM C150 specifications was used. The chemical composition and the physical properties of the portland cement that used in this work, are presented in Table 10-1 and Table 10-2, respectively.

Table 10-1. Basic properties of the source materials

| | $SiO_2$ | $Al_2O_3$ | $Fe_2O_3$ | $CaO$ | $MgO$ | $Na_2O$ | $K_2O$ |
|---|---|---|---|---|---|---|---|
| GGF (%) | 47.72 | 10.36 | 0.34 | 19.62 | 2.27 | 0.67 | 0.10 |
| Fly Ash (%) | 50.70 | 25.1 | 12.50 | 3.30 | 1.10 | 0.51 | 2.27 |
| Cement (%) | 19.93 | 4.77 | 3.13 | 62.27 | 2.71 | 0.06 | 0.48 |

Table 10-2. Chemical composition of the source materials

| Material | Specific Gravity | Average particles size (μm) | Blaine's fineness ($cm^2/g$) |
|---|---|---|---|
| GGF | 2.6 | 4 | 10200 |
| Fly ash | 2.25 | 28 | 6040 |
| Cement | 3.15 | 16 | 4720 |

### *10.2.4 Activator solutions:*

Two alkali sources, including sodium hydroxide (NaOH) pellets, and sodium silicate solution, were used to prepare the alkali activator solutions. The NaOH pellets (with 98% purity) were obtained from AMERSCO Inc. The sodium silicate solution, with a 40% solids-to-liquid ratio and the $SiO_3$-to-$Na_2O$ weight ratio of 3.4, was obtained from the CQ concept company. To prepare the alkali activator, required amount of NaOH pellets and sodium silicate solution were introduced to water.

### *10.2.5 Fine aggregates (siliceous sand):*

A mineral non-reactive siliceous river sand with an absorption value of 0.30%, oven-dry specific gravity of 2.67 and the fineness modulus of 2.6 was used in this study.

### *10.2.6 Crushed aggregate for ASR studies*

In this study several crushed aggregates, including a las Placitas gravel from New-Mexico, USA (NM), a siliceous limestone from Spratt quarry in Ontario, Canada (SP), and a limestone from Adairsville Quarry in Adairsville, Georgia, USA (AD) were used to evaluate the ASR expansion of mortar mixtures. All the aggregates were mechanically crushed using a pulverizer to achieve the gradation specified by ASTM C 1260. The chemical compositions of the aggregates are presented in Table 10-3. The specific gravity of NM, SP, and AD aggregate is 2.60, 2.69, and 2.83 respectively.

Table-10-3.Chemical composition of crushed aggregates

| Oxide (weight %) | NM | SP | AD |
|---|---|---|---|

| | | | |
|---|---|---|---|
| $SiO_2$ | 75.14 | 10.47 | 7.01 |
| $Al_2O_3$ | 10.47 | 0.29 | 0.29 |
| $CaO$ | 4.20 | 85.17 | 58.90 |
| $Fe_2O_3$ | 3.40 | 0.63 | 0.68 |
| $MgO$ | 0.98 | 2.58 | 32.28 |
| $Na_2O$ | 2.82 | 0.93 | 0.52 |
| $K_2O$ | 2.42 | 0.13 | 0.62 |

The 14-day ASR-related expansion of the used aggregates, based on ASTM C1260, are presented in Table 10-4. As it can be seen the 14-day expansion of these aggregates covers a range between 0.08 to 0.81%. According to ASTM C1260, if the 14-day expansion is less than 0.10%, the aggregate can be recognized as innocuous; however, if the expansion is higher than 0.20%, its behavior is known to be deleterious in the field. Therefore, AD can be considered as innocuous, while NM and SP can be considered as deleterious aggregates. It should be added that if the 14-day expansion is between 0.10% and 0.20%, the aggregate is known to have a potentially deleterious behavior.

Table 10-4. Expansion (%) of NM, SP, and AD in portland cement mortar, based on ASTM C1260 test method

| Aggregates | NM | SP | AD |
|---|---|---|---|
| Expansion (%) | 0.81 | 0.40 | 0.08 |
| ASR-behavior | Deleterious | Deleterious | Innocuous |

## 10.3 Experimental program.

### *10.3.1 Preparation and selection of mixture designs:*

Before casting specimens for the ASR resistance tests, the mixture proportion of the paste portion of geopolymers has to be selected. To select the mixture proportion for each precursor, 50 × 50 × 50 mm geopolymer mortar cubes were fabricated. Based on the results of our past study (14), precursors were activated using an alkali activator solution which provides the fixed at $Na_2O$-to-precursor weight ratio of 10% for the mixtures. Further, the $SiO_2$-to-$Na_2O$ mass ratio of the

solution was varied from 0 to 0.5 and 1.0. The sand content of all mixtures were maintained at 55% of their volume, and the water-to-binder ratio was maintained between 0.30 and 0.35. This range was chosen to achieve the highest possible strength while mixtures were workable without the need for any water reducers.

To prepare the activator solutions, required amounts of NaOH pellets and sodium-silicate solution were introduced in a measured amount of water and were mixed using a Horbart-N50A mixer. After the dissolution of sodium hydroxide pellets, the precursor was added to the solution. The mixing was continued, until a homogenous paste was achieved. At the end, the required amount of sand was introduced to the mixture, and the mixing performed for an additional 5 minutes. After completing the mixing process, the mixture was cast into $50 \times 50 \times 50$ mm cube molds. The molds were then placed in sealed boxes and placed inside a 60°C chamber for 24 h. After this period, specimens were removed from their molds and kept in the ambient temperature until the test day. The mixture proportion, mix ID, and compressive strength of the geopolymer mixtures are presented in Table 10-5. As it can be seen in this table, GGF-0-10 and F-1-10 mixtures showed the highest compressive strength. Therefore, these mixtures were selected to study their behavior against the ASR.

### *10.3.2 Alkali-silica reactivity of aggregates in geopolymers*

To produce the geopolymer mortar selected aggregates, NM, SP, and AD were crushed to meet the gradation requirements of ASTM C1260 and were used as the fine aggregate for the ASR studies. The paste portion of the geopolymer samples were opted based on the proportioned that showed the highest compressive strength (i.e. GGF-0-10 and F-1-10 from Table 10-5). An identical mixing and curing method as defined in the section 3.1 was followed.

Table 10-5. Mix ID and the proportion of geopolymers.

| Mix ID | Precursor | Water/ | $SiO_2/Na_2O$ | $Na_2O$/Precursor | Compressive strength (MPa) |
|---|---|---|---|---|---|

| | Precursor | | | (%) | 3 days | 7 days | 28 days |
|---|---|---|---|---|---|---|---|
| GGF-0-10 | GGF | 0.33 | 0 | 10 | 79 | 78 | 82 |
| GGF-0.5-10 | GGF | 0.33 | 0.5 | 10 | 67 | 75 | 72 |
| GGF-1-10 | GGF | 0.33 | 1 | 10 | 69 | 72 | 67 |
| | | | | | | | |
| F-0-10 | Fly ash | 0.30 | 0 | 10 | 14 | 20 | 25 |
| F-0.5-10 | Fly ash | 0.30 | 0.5 | 10 | 35 | 36 | 46 |
| F-1-10 | Fly ash | 0.30 | 1 | 10 | 58 | 60 | 59 |

As no standard test procedure is available to evaluate the ASR behavior of aggregates in geopolymers, two testing methods were used in this study. For the first method, a procedure similar to the ASTM C1260 test method was followed, even though that it is realized that the test is being run on geopolymer mortars rather than portland cement mortars. After the curing period, specimens were demoulded and submerged in a water bath and kept at 80ºC for addition 24 h. The mortar bars were then removed from the water, and zero readings were taken. Finally, samples were immersed in a 1N Sodium hydroxide solution and kept in 80ºC temperature for the remaining duration of the experiment. The length change of the mortar bars was recorded up to 70 days after the zero reading. Henceforward, this method is called “solution method” in this study.

The second test method was chosen to eliminate the effect of alkali solution, which can promote the hardening procedure of geopolymer paste. In this method, the selected geopolymer specimens (i.e. GGF-0-10, F-1-10, and GLP-1-10) were tested in a 100% relative humidity (RH) and 80ºC. For this purpose, enough amount of water was poured in the bottom of sealed boxes, and specimens were placed on supports in a manner to not have any contact with the water (almost 0.5-inch clearance). The boxes were then closed and placed in an 80ºC. The length change of the mortar bars was recorded up to 70 days after the zero reading. Henceforward, this method is called “steam method” in this study.

For the comparison purposes, the performance of geopolymer samples that were tested under the "solution method", was compared with the expansion of portland cement mortar bars. To have an identical condition for the comparison, the cement mortar bars were produced using the same procedure as the "solution method". These mortar bars were produced with the water/cement ratio of 0.35, cured in a 60°C chamber, contained the same aggregate proportion as the geopolymer mixtures, and the same length change measurement as the "solution method" and "steam method" was performed on these specimens.

### *10.3.3 Dynamic modulus of elasticity*

To study the effect of ASR promoting conditions on the mechanical properties of geopolymers mortar bars, change in the dynamic modulus of elasticity of mortar bars was measured. It has been widely reported that ASR detrition, negatively affects the dynamic modulus of elasticity (DME) of concrete (43-46). In this study, to measure the change in the dynamic modulus of elasticity of the geopolymer mortar specimens, the transversal mode of vibration (in accordance to ASTM E1876) was conducted on the geopolymer mortar prisms. The resonant frequency and mass of the geopolymer mortar bars was measured by a GrindoSonic instrument (MK5 model) at the same time when the specimens were removed from the NaOH solution to determine their length for the expansion measurement.

### *10.3.4 Dissolution of paste in HCl acid solution*

In this study, HCl solution was used to determine the amount of unreacted fly ash particles of geopolymer mixtures. The HCl solution is reported to dissolve the geopolymer, leaving the unreacted fly ash particles behind (47, 48). Following Palomo et al. (48), in this work, dissolution of a fly ash-based paste in a 1:20 HCl solution (i.e. 50 ml of 1N HCl solution in 1000 ml water) were studied. To perform the test, the paste was mechanically crushed (using a hammer) to a fine powder and sieved. The portion passing sieve #50 and retaining #100 sieved was collected for the

test. Two grams of the dried paste powder was introduced to 500 ml of solution, and the solution was mixed for 3 h using a magnetic stirrer. The solution then was filtered using 1.5 µm filter. The residue was dried in 110ºC for 24 hours, then weighted and recorded.

### *10.3.5 Dissolution of geopolymer paste in the alkali solution:*

Solubility of geopolymer paste in the alkali solution (1N NaOH) was evaluated by measuring the concentration of ions that leached from geopolymer pastes into the solution. For this test, geopolymer $10 \times 10 \times 10\ mm$ paste cube were exposed to 100 ml of 1N NaOH solution, sealed, and stored in an 80ºC oven for seven days. After this time, each sample was removed from the soak solution, and solution was filtered using a micro-fiber filter (Whatman Grade 934-AH Glass Micro Fiber Filter), and ICP test was conducted on the solution.

### *10.3.6 Leachate of crushed aggregate in 1N NaOH solution:*

To evaluate the stability of aggregates in the "solution method" condition, the dissolution of Ca and Si ions in a high alkali solution was measured for each aggregate. For this purpose, aggregates were crushed to a fine powder, and twenty g of the material that remained between the sieves #50 and #100 was collected. The collected material, was added to 100 ml of 1N NaOH solution, sealed, and stored in an 80ºC oven for 24 h. The solution then filtered. Finally, the filtered solution was collected, and the ions concentration (Si, and Ca) was measured using the ICP test for each solution.

## 10.4 Results and discussion

In this section effect of different parameters namely, (i) the effect of the paste type (i.e. GGF, fly ash and GLP-based geopolymers versus a cement mixture), (ii) effect of curing condition (i.e. "solution method" versus 100% "steam method"), and (iii) effect of aggregate type (i.e. NM, SP, and AD) on the ASR expansion of the geopolymer and cement-based mortar samples will be investigated. This section is therefore divided into three subsections as follows:

### *10.4.1 Effect of the paste type*

The expansion results of the three types of aggregates in the geopolymer and cement mortar bars, which treated using the "solution method" are presented in Figure 10-2. As it can be seen for all the tested aggregates, using geopolymer pastes caused a reduction in the expansion of the mortar bars in comparison to the cement based specimens (labeled as OPC in the Figures). The reduction was seen to be more considerable in the case of the highly reactive aggregates, NM and SP; and less in the case of lower AD aggregate, which was less reactive (in comparison to the two other aggregates). Further, for all the tested aggregates, the GGF-based mortar bars showed a lesser expansion.

The superior performance of geopolymer samples can be related to their lower calcium content, and further geopolymerisation in the in comparison to the portland cement-based samples. In addition, the better performance of GGF-based mortars in comparison to the fly ash-based specimens could be explained by: the lower amount of porosity, as well as the higher degree of geopolymerisation of the GGF-based specimens in comparison to the fly ash-based ones.

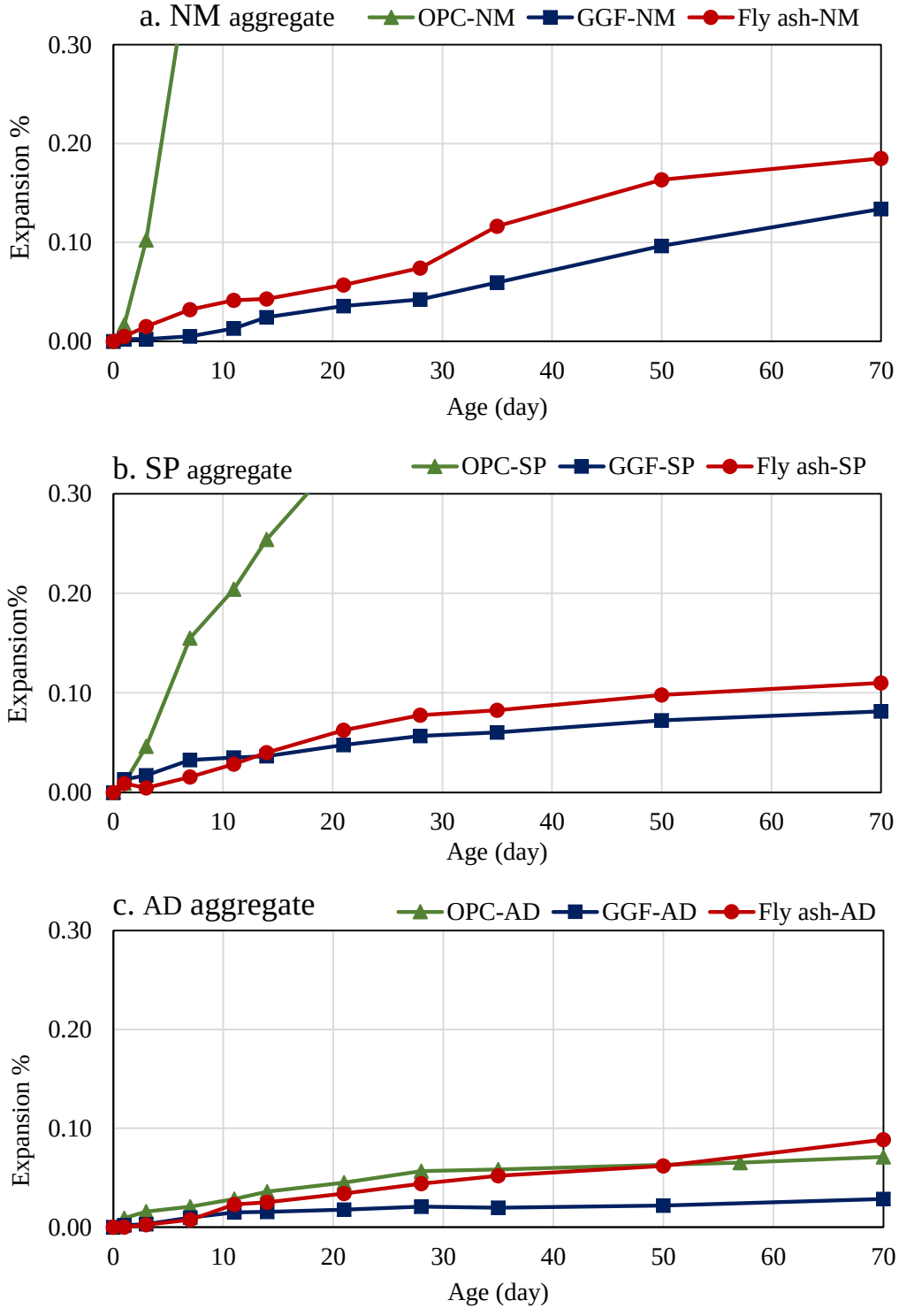


Figure 10-2. Expansion of mortar bars containing NM aggregate (a), SP aggregate (b), and AD aggregate

(c).

*Comparison of geopolymers to OPC specimens:* SEM images of OPC and geopolymer specimens containing NM aggregate are presented in Figure 10-3. It could be observed that due to ASR, aggregates in the OPC samples (Figure 10-3a) have gone through a severe damage and cracking, which eventually have led to the formation of a crack in the paste. On the other hand, no notable signs of damages were detected in the GGF and fly ash-based samples.

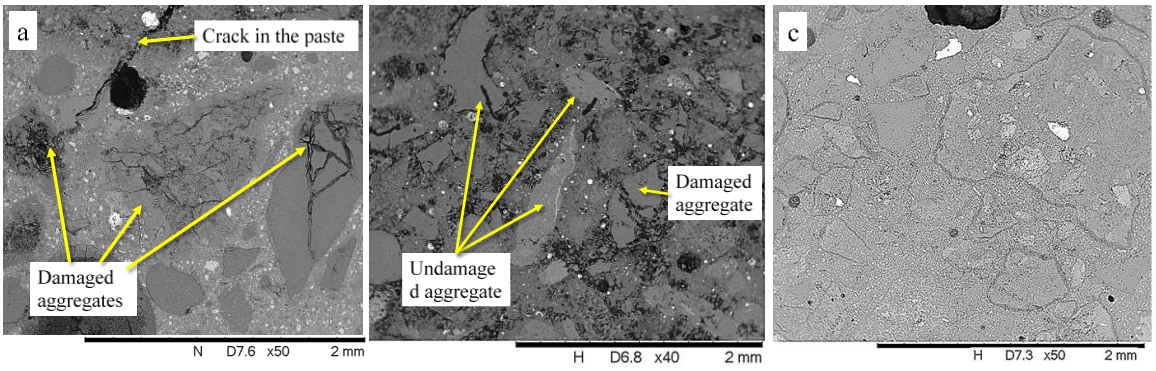


Figure 10-3. SEM image of exposed mortar bars containing NM aggregate. OPC mortar (a), F-1-10 mortar (b), and GGF-0-10 mortar (c)

While the presence of calcium is critical for the ASR-related expansion to occur; not all the available Ca content of the paste (i.e. the already fixed portion of Ca) will readily participate in the formation of the ASR gel. Therefore, analysis such as TGA could be beneficial in order to qualify the amount Ca that is present in the calcium hydroxide form (CH) and can promote the ASR-expansion by supplying the Ca, required for the hardening of the ASR gel.

To measure the CH content, TGA test was performed on the GGF and fly ash-based paste's samples. The results of TGA and DTGA are presented in Figure 10-4. As it can be seen a very small peak was observed in the DTGA graph; indicating the low amount of CH content of the paste. The low amount of CH in the fly ash-based paste can be related to the low amount of Ca in the raw fly ash (3.30% - Table 10-1). On the other hand, the low amount of CH in the GGF-based specimens suggests that the main portion of the released Ca, has been consumed in the

reactions other than those leading the CH production. In the earlier studies (14, 21), it has been proposed that Ca from GGF, is bounded in the geopolymer matrix, producing the (N, C)-A-S-H gel ((calcium-sodium)-aluminosilicate-hydrate). Thus, the very low expansion of geopolymer samples in comparison to the OPC samples can be explained by the lack of Ca in a reactive form (mainly in the form of CH), in these specimens.

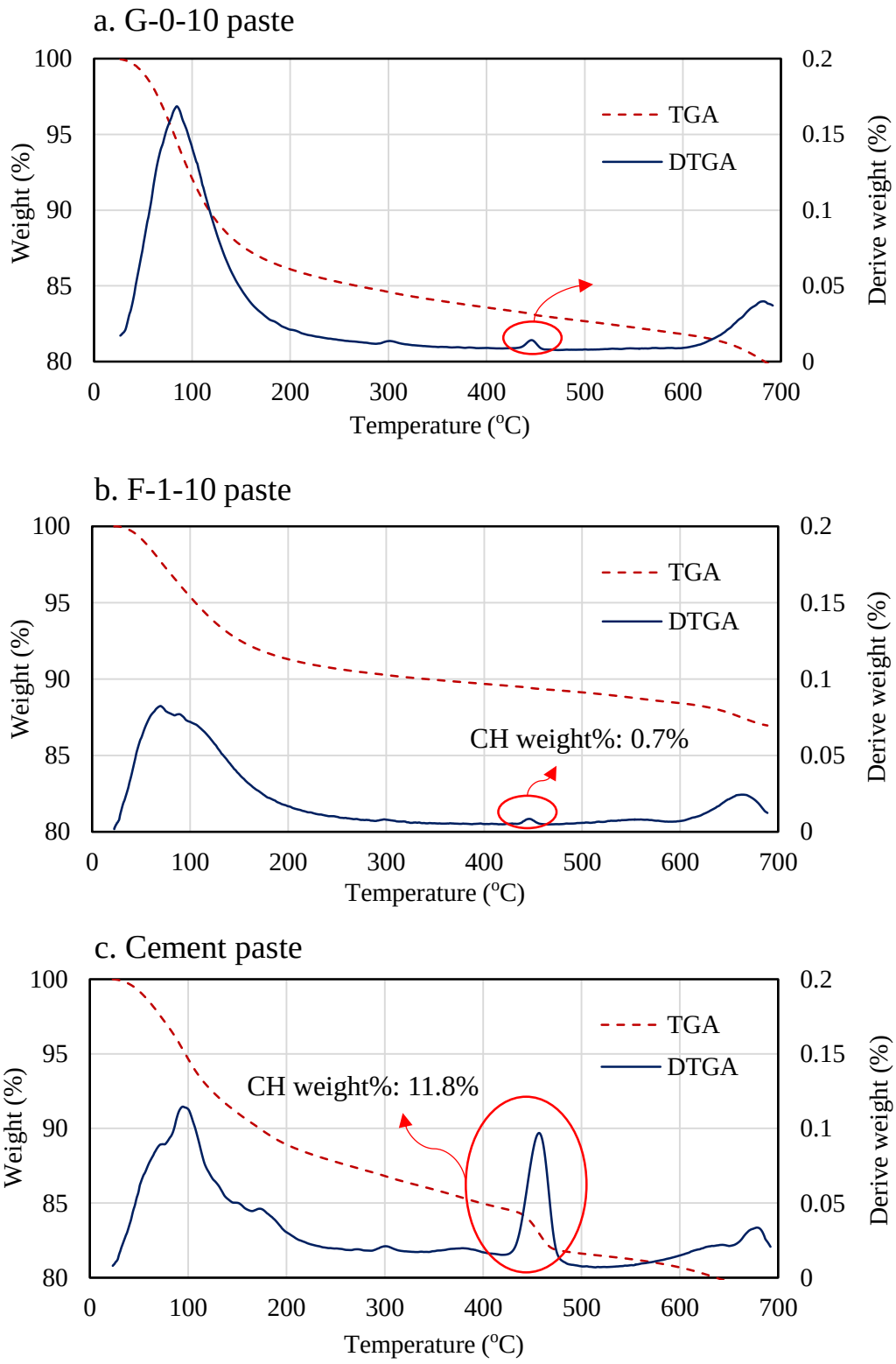


Figure 10-4. TGA and DTGA graphs of different paste samples. OPC (a), F-1-10 (b), GGF-0-10 (c)

*Comparison between GGF and fly ash-based specimens:* As it is obvious from Figure 10-2, for all the tested aggregates, GGF specimens showed lower expansion values when compared to fly ash. Since the amount of CH in both the specimens was in a same range (1.1% for GGF-based and 0.7% for the fly ash-based paste), the better performance of GGF shall be explained by other factors. In this study, the lower porosity of GGF-based geopolymers against the fly ash based samples.

Mercury intrusion porosimetry (MIP) test was performed on the GGF-0-10 and F-1-10 samples (prepared in accordance to the section 10.2.1) to find the amount of porosity of GGF and fly ash-based specimens. The results showed the total porosity was 6.8% (0.03 cc/g) and 19.0% volume (0.10 cc/g) for the case of GGF-0-10 and F-1-10 samples respectively. Thus, it was concluded that the alkali solution (used in the "solution method") would penetrate into the fly ash-based geopolymers easier than the GGF-based geopolymer.

To verify this, weight change of the 10x10x10 mm cubes of GGF and fly ash-based geopolymers paste (four cubes) that were immersed in 200 ml of 1N NaOH solution was monitored (Figure 10-5). As it can be observed in this figure, after one day of immersion in the "solution method" environment, fly ash-based samples showed a higher weight gain in comparison to the GGF-based samples. This can be explained by the penetration of the solution into the geopolymer paste specimens. The further curing of samples in the 1 N NaOH solution at 80$^{o}$C, showed a steady weight-gain and weight-loss for the case of GGF-based and fly ash-based samples, respectively. While the gradual weight-gain of GGF-based is due to the penetration of solution in the paste samples, the weight loss of fly ash-based specimen could be due to the dissolution of the geopolymer paste, or some of the unreacted particles, in the harsh environment of the "solution method" test (results are presented in section 10.4.2). Thus, it was concluded that the lower expansion in the case of GGF-based specimens versus fly ash-based specimens, can be

related to the lower porosity, causing less penetration of alkali-solution and hence leading to a lesser expansion of GGF-based specimens in comparison to the fly ash-based specimens.

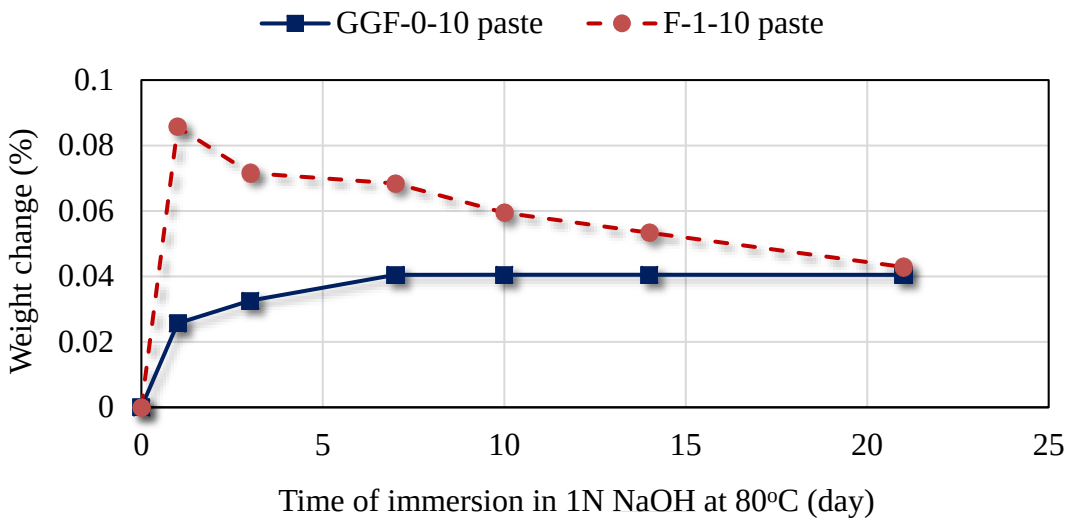


Figure 10-5. Weight change of F-1-10 and GGF-0-10 paste cubes immersed in 1N NaOH in 80°C

### *10.4.2 Effect of curing condition*

In order to evaluate the effect of high alkali solution (1N NaOH solution), on the expansion behavior of geopolymer samples, geopolymer mortar bars were tested in two separate test environments: 1) immersed in 1N NaOH solution in 80°C (solution method), and 2) placed in a ~100% RH and 80°C (steam method), as presented in section 10.3.2. The expansion of geopolymer mortar bars was evaluated with each of the ASR accelerated test methods are presented Figure 10-6.

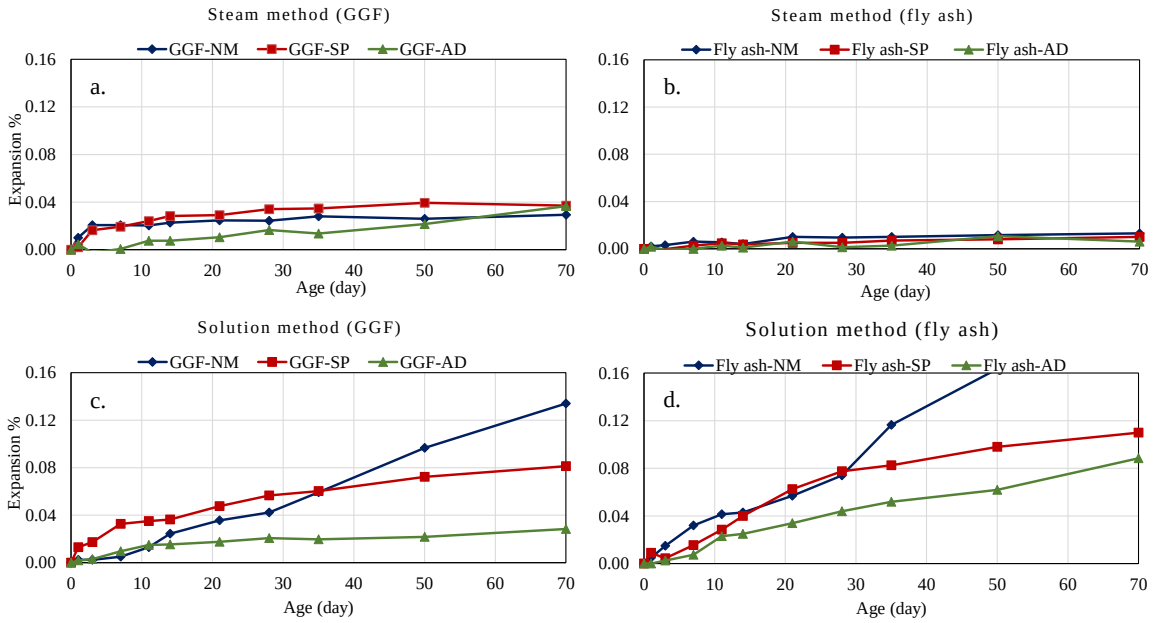


Figure 10-6. Expansion of geopolymer mortar bars cured in different testing condition. GGF-0-10 mortar cured by steam method (a), GGF-0-10 mortar cured by solution method (b), F-1-10 mortar cured by steam method (c), and F-0-10 mortar cured by solution method

As it is shown in this figure, regardless the aggregate type, all the GGF-based (Figure 10-6a) and fly ash-based specimens (Figure 10-6c) showed almost same expansion, when tested according to the "steam method". After ten weeks of exposure in the "steam method" condition, the expansion of GGF and fly ash-based specimens was about 0.04% and 0.01%, respectively (for all the aggregate). On the other hand, due to the presence of moisture and alkalis, the expansion of specimens that were cured in the "solution method" test environment was higher than the case of "steam method". Unlike the "steam method" in which the expansion behavior seems to be related to the paste type rather than the aggregate, for the samples used in "solution method", type of aggregate showed a clear effect on the expansion of geopolymer mortar bars. In the case of GGF-based specimens, the mixtures containing NM, SP and AD aggregate reached the expansion of 0.13%, 0.08% and 0.03%, respectively. Further, for the case of fly ash-based geopolymers, the mixtures containing NM, SP and AD showed the expansion of 0.19%, 0.11% and 0.09%, respectively. It should be noted that for all the tested mixtures, the 14-days expansion of the

specimens was far below the 0.10% limit specified by ASTM C1260.

It has been reported that one of the major parameters, which is affected by the ASR-related damage is the modulus of elasticity of the specimens (28, 49-52). Reduction in the modulus of elasticity (45, 49-52), and dynamic modulus of elasticity (43-46) of the concrete samples that damaged by ASR have been reported in several works. In this study, the change in the dynamic modulus of elasticity (DME) of geopolymer mortar bars was measured by following the ASTM E 1876-09 test procedure.

The results of DME of geopolymer specimens cured in accordance to "solution method" and "steam method" are presented in Figure 10-7. As it can be seen, in Figure 10-7a and Figure 10-7b, curing mortar bars in accordance to the "steam method", resulted in the rise in the DME of the specimens, regardless the aggregate type. The increase in the DME of the specimens is suggested to be due to the further geopolymerisation of specimens cured in the high temperature (80°C). The slight increase in the DME of geopolymer samples that steam cured in the 60°C temperature was also reported by Pouhet and Cyer (24). The increase in the DME values of mortar bars cured in the "steam method" condition, even for the mixtures containing reactive NM aggregate, suggests that the destress that could form due to the formation of ASR-gel was not enough to damage the geopolymer's matrix seriously. According to the results of works by Pouhet and Cyer (24) and Shi et al. (42), for steam cured geopolymer and alkali-activated slag specimens, the relatively low ASR-expansion of tested mixtures could be explained by the low pH of pore solution of the specimens cured in this condition (steam curing).

For the case of the GGF-based specimens cured in accordance to the "solution method", a slight reduction in the DME of the specimens containing NM aggregate, as well as the negligible rise in the DME values of SP and AD containing aggregate was observed. On the other hand, all the fly ash-based specimens showed some increase in DME values ate early ages (i.e. 3 to 7

days); which, was followed by a reduction at the later ages (after 7-10 days to 30 days). The initial increase in DME values could be related to the geopolymerisation of the geopolymerisation of the unreacted (or partially reacted) fly ash particles, as also reported by patil and allouche (42). Further, the later reduction in the DME values could be explained by the ASR-related damage of the aggregate as will be discussed in more details in the section 3.3.

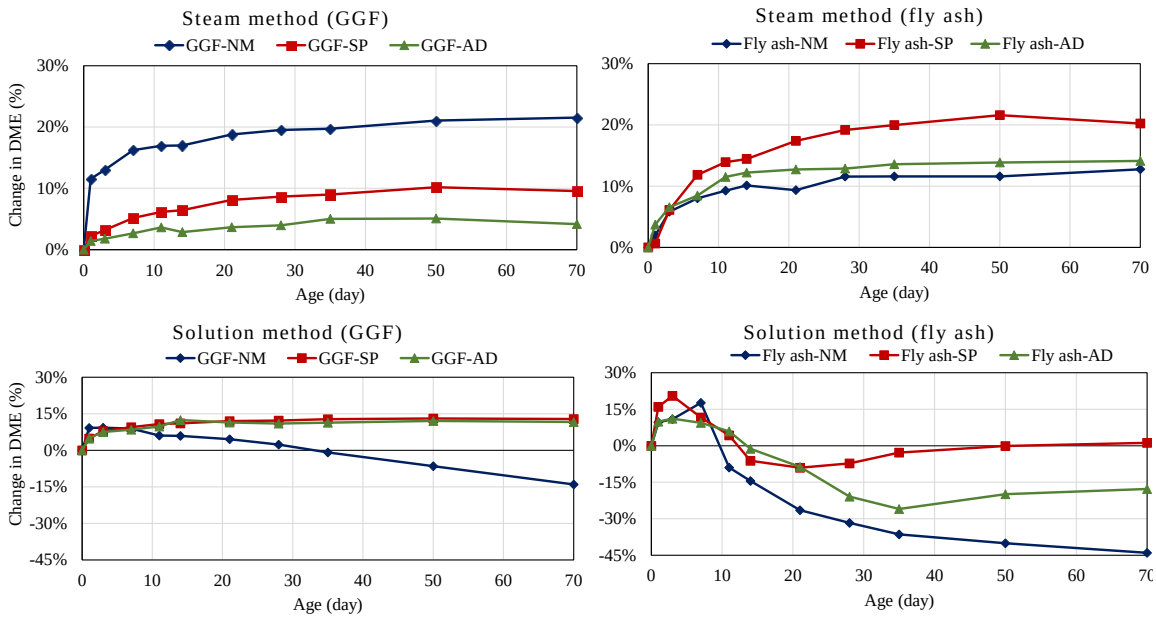


Figure 10-7. Change in DME of geopolymer mortar bars cured in different testing condition. GGF-0-10 mortar cured by steam method (a), GGF-0-10 mortar cured by solution method (b), F-1-10 mortar cured by steam method (c), and F-0-10 mortar cured by solution method

To examine the idea of further geopolymerisation of the unreacted, or partially reacted fly ash particles, the HCl dissolution test as described in section 10.3.4, was performed on the fly ash paste samples before, and after exposure to the "solution method" curing condition. For this purpose, $10 \times 10 \times 10$ mm of geopolymer pastes were prepared and were cured under the "solution method" curing condition for three days (this is the time that DME showed its highest value - Figure 10-7d). After three days, the cubes were removed from the solution, crushed, and dissolved into the HCl solution. The comparison between the dissolution results of unexposed fly

ash-based sample (0 day) and exposed samples are presented in Table 10-6. As it can be seen the amount of residue (unreacted particles) keeps decreasing with the rise in the immersion duration. This suggests that under the high temperature and in the presence of a highly alkaline solution, that is associated with the "solution method" test, the geopolymerisation can take place in the fly ash-based samples, leading to increase in the DME values at the early ages. It should be mentioned that, the curing of GGF-based geopolymer paste cubes under the "solution method" condition, did not seem to promote the geopolymerisation of the unreacted particles remarkably. After 21 days of exposure to 1N NaOH solution in the 80°C, the amount residue from the HCl test was measured to be 43.7%; which only showed a negligible reduction when compared to the 46.5% measured for the unexposed sample.

Table 10-6. Results of HCl dissolution test performed on F-1-10 paste immersed in 1N NaOH and 80°C

| Age of immersion | 0 days | 1 day | 7 days | 21 days |
|---|---|---|---|---|
| Residue (weight %) | 73.2% | 69.1% | 46.6% | 31.0% |

At the end, it should be added that the effect curing condition was seen to be curtail on the expansion of the tested specimens. While for the specimens cured in accordance to the "steam method", the aggregate type did not seem to cause any notable difference in the expansion values, the expansion results of the specimens that were tested in accordance to the "solution method" were seen to depend on the aggregate type. Therefore, the results of the "solution method" might be more reliable than the "steam method", for evaluating the ASR-potential of a certain aggregate type in a geopolymer system. However, it should be noted that despite the better discrimination of the "solution method" in comparison to the "steam method", this method suffers from following issues.

(1). Due to the very high alkali content of the soaking solution, the effect of internal alkali content of the system might be underestimated (35, 42).

(2) The hardening of the paste due to the further geopolymerisation in early ages can reduce the final expansion result. The results presented in Table 10-6 showed the further geopolymerisation of the fly ash-based specimens.

(3). Dissolution of geopolymer paste into the solution might occur. Considering the high amount of alkali in the solution that is surrounding the geopolymers paste, it is possible that Si and Al monomers released from the precursors, particularly those from the outer part of the specimens, leach into the alkali solution. Table 10-7 shows the ICP results of 1N NaOH solution samples that were in contact with the fly ash and GGF-based geopolymer paste in accordance to the "solution method" for seven days (see section 10.3.5 for the test detail). As it can be seen while the GGF-based paste was almost stable, a significant amount of leachate occurred for the case of fly ash-based geopolymer paste. Thus, It is thought that the reduction seen in the DME of the fly ash-based specimens containing none reactive AD aggregate could be related to the partial dissolution of the fly ash-based geopolymer paste, rather than the ASR damage of the aggregate (SEM images presented in the following section showed intact aggregates in the specimens containing AD aggregate).

Therefore, to obtain more reliable results, a method such as ASTM C1293, in which the expansion of specimens is monitored outside the high alkali environment and in a longer duration (i.e. 12 to 24 months) could be considered.

Table 10-7. Leachate of ions from geopolymer paste into alkali solution

| Paste ID | Leached ions concentration * | | | |
|---|---|---|---|---|
| | K (ppm) | Ca (ppm) | Al (ppm) | Si (ppm) |
| GGF-0-10 | 41.6 | 0.1 | 11.2 | 38.3 |
| F-1-10 | 192.2 | 0.1 | 32.9 | 343.7 |

### *10.4.3 Effect of aggregate type*

Expansion results of GGF and fly ash-based geopolymer mortars for the different types

of aggregates are presented in Figure 10-5. As it can be seen, the type of aggregates had no significant effect on the expansion of specimens that were cured using the "steam method". On the other hand, the type of aggregates had a clear effect on the expansion results of the specimens, which cured in according to the "solution method" procedure. Therefore, in this section, to investigate the effect of aggregate type on the expansion and the stiffness of exposed mortar bars, only results obtained from the "solution method" were considered.

In order to estimate the chemical stability of aggregate when exposed to a high alkali media and high temperature, leachate of Ca, Si, S, K and Al ions from the crushed aggregate was measured by using the test method presented in section 3.6, and are presented in Table 10-8. As it can be seen in the last column of this table, these ions are forming more than 99% of the total ions that leached from each aggregate. According to results of Table 10-8, NM aggregate was the most unstable aggregate and released a significant amount of Si in the solution. On the other hand, SP and AD aggregate was more stable and released lesser amount of ions into the solution.

Table 10-8.Concentration of K, Al, S, Ca and Si in the filtered solution*

| Aggregate ID | Si (ppm) | Ca (ppm) | K (ppm) | Al (ppm) | S (ppm) | (K+Al+S+Ca+Si)/(total leached ions**) (ppm/ppm) |
|---|---|---|---|---|---|---|
| NM | 2091 | 5 | 120 | 88 | 21 | 0.998 |
| SP | 80 | 10 | 104 | 11 | 32 | 0.990 |
| AD | 45 | 3 | 126 | 3 | 38 | 0.996 |

*- For each sample twenty grams of crushed aggregate was introduced to 100 ml of 1N NaOH solution
**- Measured ions in ICP test include: P, K, Ca, Mg, Zn, Cu, Mn, Fe, S, B, Al, and Si

As it was presented in Figure 10-5, the Adairsville and Spratt containing geopolymer specimens showed a very low expansions after 10 weeks of exposure to the "solution method" condition. The expansion for GGF-based specimens containing AD and SP aggregate was 0.03%and .0.08% respectively. On the other hand, the expansion of fly ash-based specimens containing AD and SP aggregate was 0.11% and 0.09% respectively. The SEM image taken from the GGF and fly ash-based geopolymer made from AD aggregate are presented in Figure 10-8.

Despite some partially damaged aggregates, in the SP aggregate containing specimens, the majority of aggregates and the geopolymer pastes were free of damage. The SEM-EDX results of fly ash-based geopolymer having AD and SP aggregate are presented in Figure 10-9a and Figure 10-9b respectively. The results showed that despite the high level Ca oxides in AD and SP aggregates (58.9% and 85.2% respectively), they seem to remain stable during the test condition, and did not leach into the surrounding geopolymer matrix (Compare Ca level in points 1-3 with 4-6 in Figure 10-9a and Figure 10-9b).

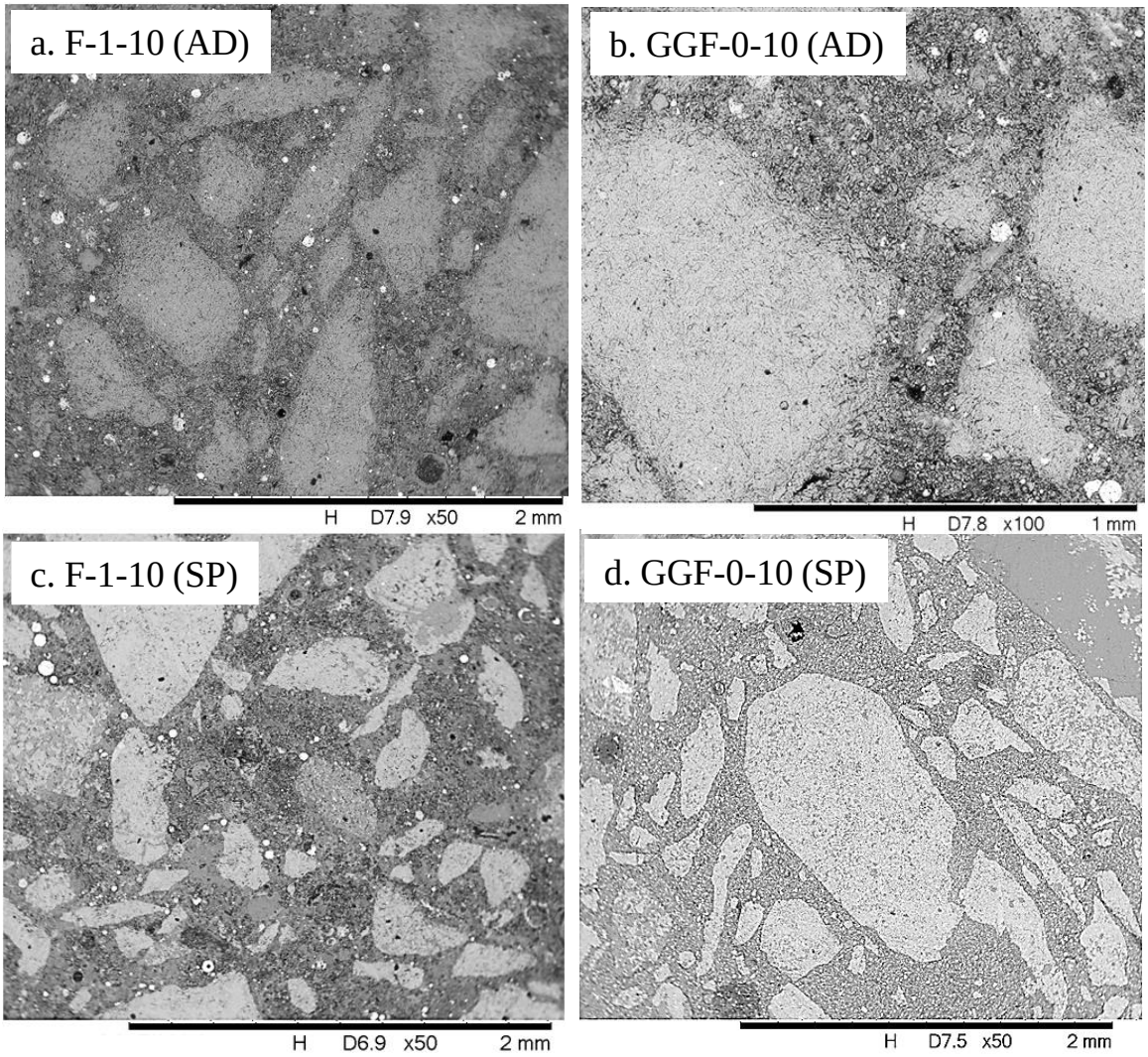


Figure 10-8. SEM image geopolymer mortars exposed to “solution method” test condition.

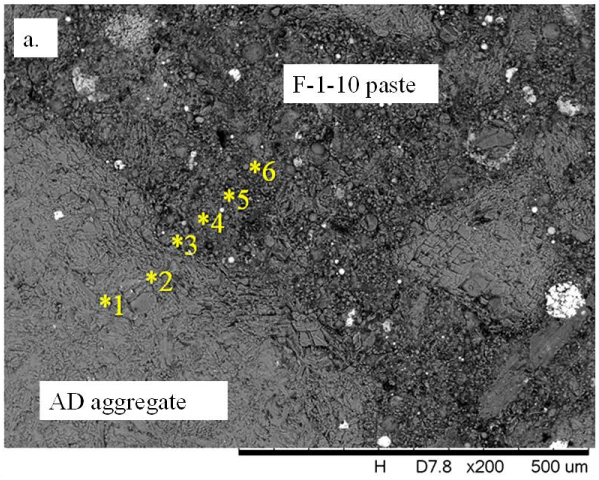


| Spectrum ID | Na | Mg | Al | Si | K | Ca | Fe |
|---|---|---|---|---|---|---|---|
| 1 | 1.6 | 12.8 | 1.8 | 3.3 | 0.3 | 79.1 | 1.1 |
| 2 | 1.5 | 37.9 | 0.9 | 2.4 | 0.0 | 57.2 | 0.1 |
| 3 | 2.1 | 35.5 | 1.9 | 7.4 | 0.2 | 51.6 | 1.3 |
| 4 | 10.5 | 3.5 | 19.1 | 41.2 | 1.2 | 20.2 | 4.2 |
| 5 | 9.3 | 8.5 | 9.7 | 45.9 | 1.5 | 13.0 | 12.1 |
| 6 | 9.7 | 1.9 | 28.9 | 43.6 | 2.2 | 10.7 | 3.0 |

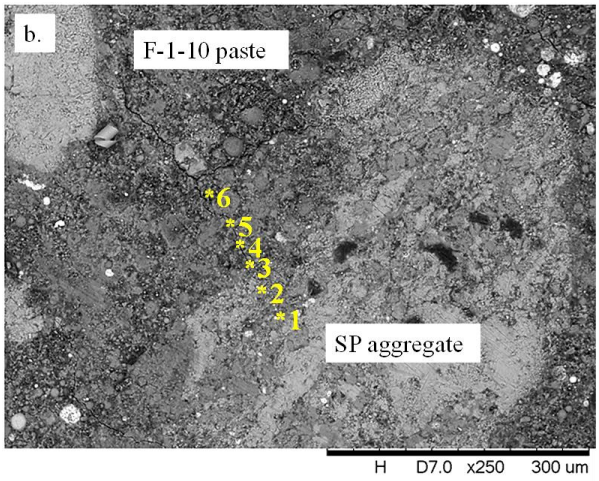


| Spectrum ID | Na | Mg | Al | Si | K | Ca | Fe |
|---|---|---|---|---|---|---|---|
| 1 | 4.2 | 2.9 | 3.4 | 17.9 | 1.4 | 65.0 | 4.9 |
| 2 | 3.4 | 11.8 | 3.7 | 22.4 | 1.9 | 53.3 | 3.5 |
| 3 | 7.9 | 1.4 | 5.8 | 43.9 | 1.2 | 33.5 | 6.3 |
| 4 | 3.4 | 1.2 | 44.5 | 37.0 | 0.7 | 8.6 | 4.5 |
| 5 | 9.8 | 1.1 | 27.1 | 47.9 | 1.6 | 8.2 | 4.3 |
| 6 | 8.7 | 0.6 | 29.7 | 50.2 | 1.1 | 6.2 | 3.4 |

Figure 10-9. SEM-EDX results of fly ash-based geopolymer with AD aggregate (a) and SP aggregate (b)

Among tested aggregate, the highest expansion level of geopolymer mortar bars was seen in the case of NM containing mixtures. When tested in accordance to the “solution method” for 10 weeks, the expansion value of GGF and fly ash-based specimens searched 0.13% and 0.19%, respectively. Despite the much lower expansion level in comparison to the NM containing OPC samples (1.31% after 10 weeks), expansions of these mixtures were about the twice of the SP containing geopolymer mixtures. As presented in Figure 10-4, although the overall appearance of the geopolymers mortar bars was in a much better form than the OPC mixture, however, some heavily damaged and partially damaged aggregates were seen in the case of fly ash and GGF-based samples respectively.

The SEM image of damaged aggregates in the NM containing fly ash-based geopolymer mixture is presented in Figure 10-11. It was observed that while the aggregate was heavily damaged, the damage in the aggregate does not seem to severely damage the surrounding paste. Unlike the case of ASR in the portland cement systems, in which the ASR-related expansion causes damage in the paste, in the damaged aggregates seems to be dissolving into the paste in the case of fly ash based geopolymer mixture. This could be explained by the high amount Si leachate from the NM aggregate in the high alkali media and the elevated temperature (Table 10-8). Due to the high porosity of the fly ash-based geopolymers (19.0%), and in the absence of the sufficient amount of available CH in the fly ash based paste, the fresh Si leached from the aggregate seems to penetrate the surrounding paste without causing measure damage to the paste. Although this mechanism did not seem to cause a significant expansion, however, due to the damage in aggregates, NM aggregate containing fly ash-based specimens lost almost 45% of their initial DME after 10 weeks of exposure to the "solution method" condition (Figure 10-7).

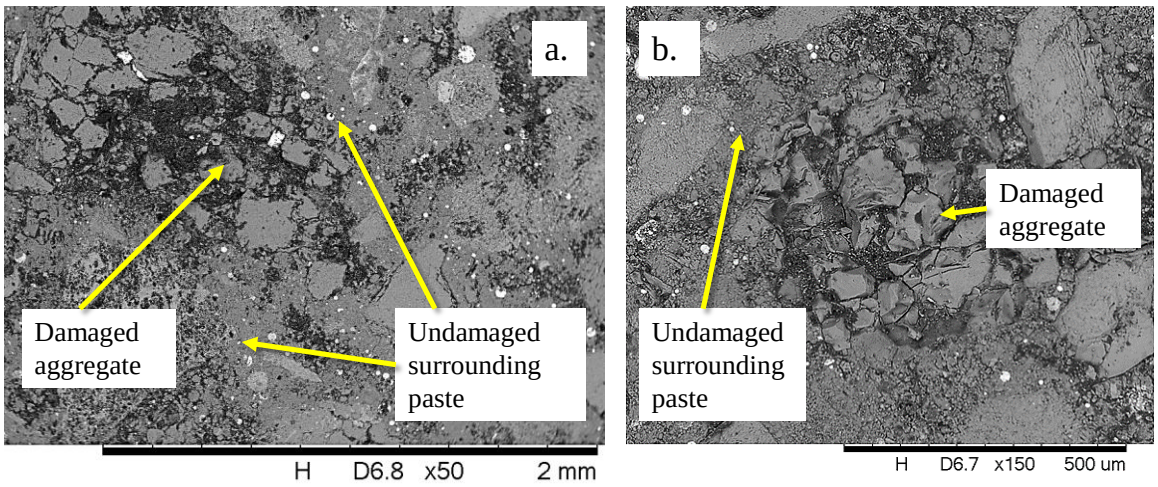


Figure 10-10. Dissolution of NM aggregate in the fly ash-based geopolymer

The damage mechanism in the NM containing GGF-based geopolymer was seen to be different from the fly ash-based mixtures. In this mixture, none of the aggregate particles were seen to suffer from a severe damage (presented Figure 10-4c). However, formation of a clear rim

was observed around NM aggregates (Figure 10-4c and Figure 10-11). Formation of this rim is thought to be due to the lower porosity of the GGF-based (6.8%) specimens in comparison to the fly ash-based (19.0%) ones. Because of the lower porosity, the reals ASR gel from the aggregate is not able to easily penetrate into the paste matrix; instead, formed a thin layer around the aggregate by penetrating into the geopolymer matrix. Although the presence of this gel did not lead to severe damages in the surrounding paste, presence of micro cracks was observed in the border between aggregates and the rim, or the aggregate and the surrounding paste (Figure 10-7).

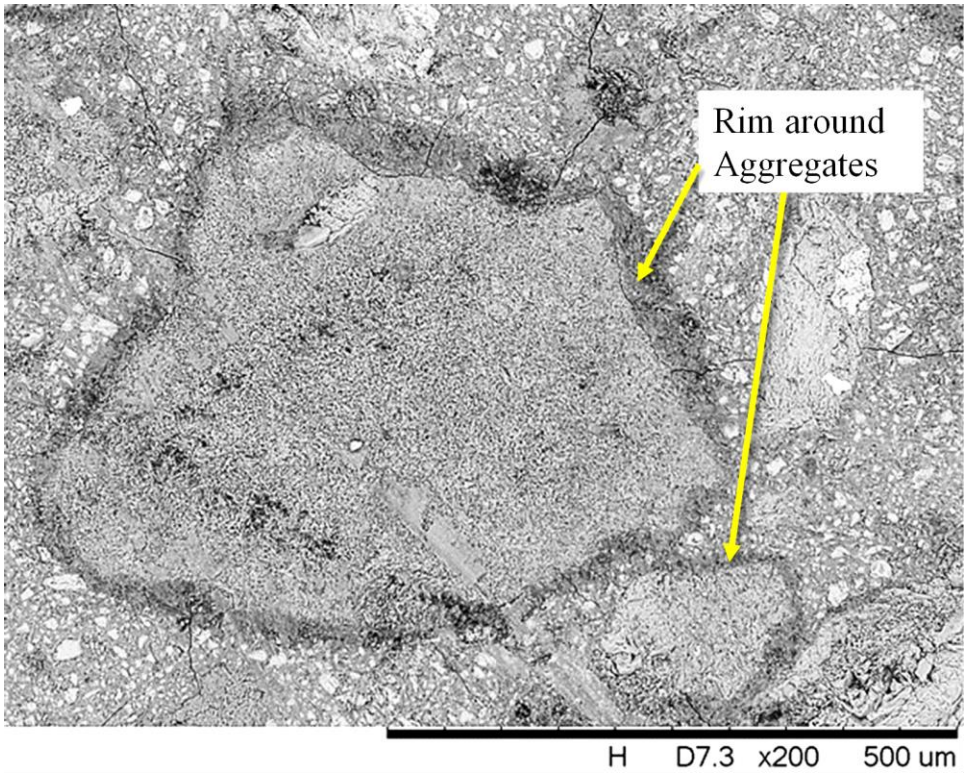


Figure 10-11. Formation of rim around aggregates in NM containing GGF-based geopolymer

In the absence of the high amount of CH, the silica rich gel liberated from the aggregate is not stiff enough to crack the cause a significant damage to the paste. However, the small amount expansion of mortar bars as well as the reduction in the DME of the NM containing GGF-based geopolymer could be related to the formation of this layer. The SEM-EDX analysis

performed on this sample showed that lower amount of Si/Ca ratio in this layer is higher in comparison to the Si/Ca ratio measured in the geopolymer paste (Figure 10-12); which suggest the penetration of a Si rich gel inside the paste around the aggregate.

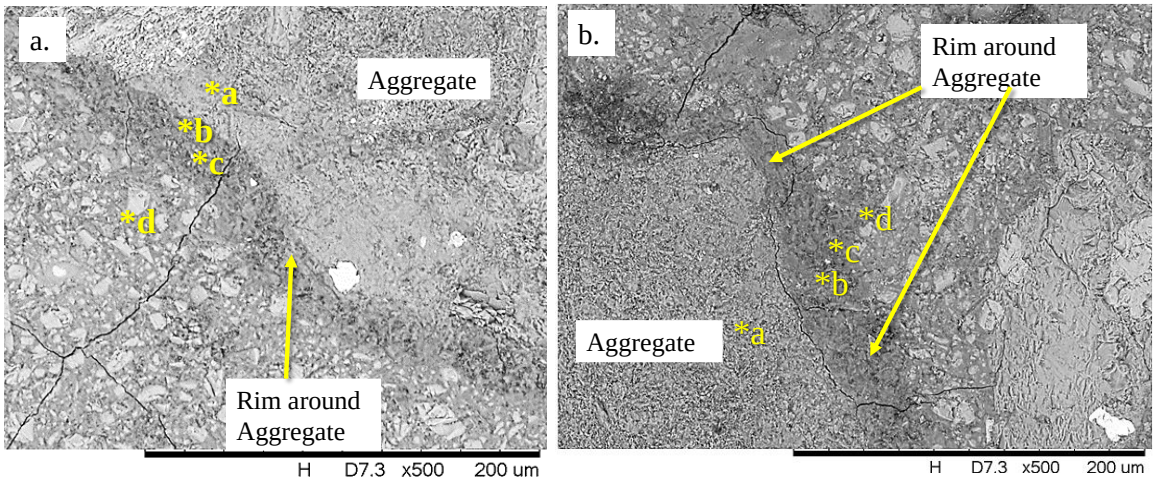


| Si/Ca weight ratio | In the aggregate | In the rim | | In the paste |
|---|---|---|---|---|
| Spectrum ID | a | b | c | d |
| Figure a | 10.3 | 5.0 | 3.5 | 2 |
| Figure b | 11.6 | 2.9 | 3.5 | 2.5 |

Figure 10-12. Leaching of Si in a NM aggregate into the GGF-based geopolymer paste

## 10.5 Conclusion

In this work, the resistance of GGF and fly ash-based geopolymer against alkali silica reaction of aggregate was evaluated. The ASR-induced expansion was measured, and results were compared with an OPC mixture. Two ASR accelerating conditions were provided by putting specimens in a 1N NaOH solution and 80ºC "solution method", and steam curing in 80ºC "steam method" to study the effect of curing condition on the ASR resistance of geopolymer mixtures. Change in the length and stiffness (DME) of the specimens was monitored for 10 weeks. Based on the results of this study the following conclusions could be drawn:

1. Both GGF and fly ash based geopolymer mixtures showed a better resistance against the ASR-related expansion in comparison to the OPC mixture. For the sample having NM aggregate,

the expansion of GGF-based geopolymer, fly ash-based geopolymer and the OPC mixture was 0.13%, 0.19%, and 1.31% respectively. The lower expansion of geopolymer samples could be mainly explained by the low amount of CH in the geopolymer paste in comparison to the OPC.

2. Presence of alkali solution seems to be curtail for the ASR-expansion of geopolymer mixtures. Comparison between the "solution method" and "steam method" showed the better ability of the first method in discriminating the ASR behavior of the used aggregate. An almost same level of expansion was seen for either GGF or fly ash-based geopolymer mixtures that were tested in accordance to the "steam method".

3. The high temperature and high alkali solution associated with the "solution method" curing condition caused the further geopolymerisation of the geopolymer pastes. However, this was more remarkable in the case of the fly ash-based geopolymer; and only small change was measured in the GGF-based geopolymer paste. It should be mentioned that despite the further geopolymerisation, a significant amount of ions were leached out of the fly ash-based geopolymer paste into the alkali solution.

4. Although geopolymer specimens showed lower expansions in comparison to the OPC specimens, a significant loss in the stiffness was measured for the NM containing geopolymer mixtures. In these mixtures, after 10 weeks of exposure, 15% and 45% reduction in the DME values was measured for GGF-based samples. So, it is thought that measuring the expansion might not be the best way to evaluate the ASR-related deterioration in geopolymer mixtures.

5. The main ASR deterioration mechanism seems to be different in the geopolymer mixtures and OPC mixture. While for the OPC mixtures, expansion in the ASR gel is known to cause cracking and damage in the surrounding paste; minimal damage in the paste was seen in case of geopolymer specimens. This could be due to the low amount of CH in the paste, so that the fresh ASR gel is not calcified and would penetrate into the geopolymer matrix causing no serious

damage. Nevertheless, due to the higher porosity of the fly ash-based geopolymer in comparison to GGF-based mixtures, more damages was seen in the aggregate.

## References:


1. Garcia-Lodeiro, I., Palomo, A., Fernández-Jiménez, A., Pacecho-Torgal, F., Labrincha, L. A., & Leonelli, C. (2015). An overview of the chemistry of alkali-activated cement-based binders. Handbook of alkali-activated cements, mortars and concretes, 19-47.
2. Davidovits, J. (1999, June). Chemistry of geopolymeric systems, terminology. In Geopolymer (Vol. 99, No. 292, pp. 9-39).
3. Duxson, P., & Provis, J. L. (2008). Designing precursors for geopolymer cements. Journal of the American Ceramic Society, 91(12), 3864-3869.
4. Komnitsas, K., & Zaharaki, D. (2007). Geopolymerisation: A review and prospects for the minerals industry. Minerals engineering, 20(14), 1261-1277.
5. Palomo, A., Grutzeck, M. W., & Blanco, M. T. (1999). Alkali-activated fly ashes: a cement for the future. Cement and concrete research, 29(8), 1323-1329.
6. Hardjito, D., Wallah, S. E., Sumajouw, D. M., & Rangan, B. V. (2004). Factors influencing the compressive strength of fly ash-based geopolymer concrete. civil engineering dimension, 6(2), pp-88.
7. Alonso, S., & Palomo, A. (2001). Alkaline activation of metakaolin and calcium hydroxide mixtures: influence of temperature, activator concentration and solids ratio. Materials Letters, 47(1), 55-62.
8. Van Jaarsveld, J. G. S., Van Deventer, J. S. J., & Lukey, G. C. (2003). The characterisation of source materials in fly ash-based geopolymers. Materials Letters, 57(7), 1272-1280.
9. Wang, H., Li, H., & Yan, F. (2005). Synthesis and mechanical properties of metakaolinite-based geopolymer. Colloids and Surfaces A: Physicochemical and Engineering Aspects, 268(1), 1-6.
10. Kumar, S., Kumar, R., & Mehrotra, S. P. (2010). Influence of granulated blast furnace slag on

the reaction, structure and properties of fly ash based geopolymer. Journal of Materials Science, 45(3), 607-615.

11. Oh, J. E., Monteiro, P. J., Jun, S. S., Choi, S., & Clark, S. M. (2010). The evolution of strength and crystalline phases for alkali-activated ground blast furnace slag and fly ash-based geopolymers. Cement and Concrete Research, 40(2), 189-196.
12. Trochez, J. J., de Gutiérrez, R. M., Rivera, J., & Bernal, S. A. (2015). Synthesis of geopolymer from spent FCC: Effect of SiO2/Al2O3 and Na2O/SiO2 molar ratios. Materiales de Construcción, 65(317), 046.
13. Pascual, A. B., Tognonvi, M. T., & Tagnit-Hamou, A. (2014). Waste glass powder-based alkali-activated mortar. Int. J. Res. Eng. Technol, 3(13), 32-36.
14. Rashidian-Dezfouli, H., & Rangaraju, P. R. (in press). Comparison of Strength and Durability Characteristics of a Geopolymer produced from Fly ash, Ground Glass Fiber and Glass Powder. Materiales de Construcción.
15. Anuar, K. A., Ridzuan, A. R. M., & Ismail, S. (2011). Strength characteristics of geopolymer concrete containing recycled concrete aggregate. International Journal of Civil & Environmental Engineering, 11(1), 59-62.
16. Slaty, F., Khoury, H., Rahier, H., & Wastiels, J. (2015). Durability of alkali activated cement produced from kaolinitic clay. Applied Clay Science, 104, 229-237.
17. Kupaei, R. H., Alengaram, U. J., & Jumaat, M. Z. (2014). The effect of different parameters on the development of compressive strength of oil palm shell geopolymer concrete. The Scientific World Journal, 2014.
18. Robayo, R. A., de Gutiérrez, R. M., & Gordillo, M. (2016). Natural pozzolan-and granulated blast furnace slag-based binary geopolymers. Materiales de Construcción, 66(321), 077.
19. Pereira, A., Akasaki, J.L., Melges, J.L., Tashima, M.M., Soriano, L., Borrachero, M.V.,

Monzó, J. and Payá, J. (2015). Mechanical and durability properties of alkali-activated mortar based on sugarcane bagasse ash and blast furnace slag. Ceramics International, 41(10), 13012-13024.

20. Sukmak, P., Horpibulsuk, S., & Shen, S. L. (2013). Strength development in clay–fly ash geopolymer. Construction and building Materials, 40, 566-574.
21. Rashidian-Dezfouli, H., & Rangaraju, P. R. (under review). Influence of Selected Parameters on Performance of Geopolymer Produced from Ground Glass Fiber. Construction and building materials.
22. Rashidian-Dezfouli, H., & Rangaraju, P. R. (under review). A comparative study on the durability of geopolymers produced with ground glass fiber, fly ash, and glass-powder in sodium sulfate solution. Construction and building materials.
23. Hemmings, R. T. (2005). Process for Converting Waste Glass Fiber into Value Added Products, Final Report (No. DOE GO13015-1). Albacem LLC.
24. Pouhet, R., & Cyr, M. (2015). Alkali–silica reaction in metakaolin-based geopolymer mortar. Materials and Structures, 48(3), 571-583.
25. Xie, Z., Xiang, W., & Xi, Y. (2003). ASR potentials of glass aggregates in water-glass activated fly ash and portland cement mortars. Journal of Materials in Civil Engineering, 15(1), 67-74.
26. Pacheco-Torgal, F. (2015). Introduction to handbook of alkali-activated cements, mortars and concretes. Handbook of alkali-activated cements, mortars and concretes, 1-16.
27. Stanton, T. E. (1940) Expansion of Concrete Through Reaction Between Cement and Aggregate. In Proceedings of the American Society of Civil Engineers(Vol. 66, No. 10, pp. 1781-1812). ASCE.
28. Thomas, M. D., Fournier, B., & Folliard, K. J. (2013). Alkali-aggregate reactivity (AAR)

facts book (No. FHWA-HIF-13-019).

29. Lindgård, J., Andiç-Çakır, Ö., Fernandes, I., Rønning, T. F., & Thomas, M. D. (2012). Alkali–silica reactions (ASR): literature review on parameters influencing laboratory performance testing. Cement and Concrete research, 42(2), 223-243.
30. Bhatty, M. S. (1985). Mechanism of pozzolanic reactions and control of alkali-aggregate expansion. Cement, concrete and aggregates, 7(2), 69-77.
31. Dyer, T. (2014). Concrete durability. Crc Press.
32. García-Lodeiro, I., Palomo, A., & Fernández-Jiménez, A. (2007). Alkali–aggregate reaction in activated fly ash systems. Cement and Concrete Research, 37(2), 175-183.
33. Fernández-Jiménez, A., Garcia-Lodeiro, I., & Palomo, A. (2007). Durability of alkali-activated fly ash cementitious materials. Journal of Materials Science, 42(9), 3055-3065.
34. Kupwade-Patil, K., & Allouche, E. (2011, May). Effect of alkali silica reaction (ASR) in geopolymer concrete. In World of Coal Ash (WOCA) conference(pp. 9-12).
35. Kupwade-Patil, K., & Allouche, E. N. (2012). Impact of alkali silica reaction on fly ash-based geopolymer concrete. Journal of materials in Civil Engineering, 25(1), 131-139.
36. Li, K. L., Huang, G. H., Jiang, L. H., Cai, Y. B., Chen, J., & Ding, J. T. (2006). Study on abilities of mineral admixtures and geopolymer to restrain ASR. In Key Engineering Materials (Vol. 302, pp. 248-254). Trans Tech Publications.
37. Davidovits, J. (1994, October). Properties of geopolymer cements. In First international conference on alkaline cements and concretes (Vol. 1, pp. 131-149).
38. Shi, C., Shi, Z., Hu, X., Zhao, R., & Chong, L. (2015). A review on alkali-aggregate reactions in alkali-activated mortars/concretes made with alkali-reactive aggregates. Materials and Structures, 48(3), 621-628.
39. Pacheco-Torgal, F., Abdollahnejad, Z., Miraldo, S., Baklouti, S., & Ding, Y. (2012). An

overview on the potential of geopolymers for concrete infrastructure rehabilitation. Construction and Building Materials, 36, 1053-1058.

40. Provis, J. L., & Van Deventer, J. S. J. (Eds.). (2009). Geopolymers: structures, processing, properties and industrial applications. Elsevier.
41. AFNOR. NF P18-454 (2004) Be´ton —Re´activite´ d'une formule de be´ton vis-a`-vis de l'alcali-re´action—Essai de performance
42. Shi, Z., Shi, C., Zhao, R., & Wan, S. (2015). Comparison of alkali–silica reactions in alkali-activated slag and Portland cement mortars. Materials and Structures, 48(3), 743-751.
43. Swamy, R. N., & Al-Asali, M. M. (1986). Influence of alkali-silica reaction on the engineering properties of concrete. In Alkalies in concrete. ASTM International.
44. Swamy, R. N., & Al-Asali, M. M. (1988). Engineering properties of concrete affected by alkali-silica reaction. ACI Materials Journal, 85(5), 367-374.
45. Sargolzahi, M., Kodjo, S. A., Rivard, P., & Rhazi, J. (2010). Effectiveness of nondestructive testing for the evaluation of alkali–silica reaction in concrete. Construction and Building Materials, 24(8), 1398-1403.
46. Rangaraju, P., Sompura, K., & Olek, J. (2006). Investigation into potential of alkali-acetate-based deicers to cause alkali-silica reaction in concrete. Transportation Research Record: Journal of the Transportation Research Board, (1979), 69-78.
47. Struble, L, Hicks, J. K. (2013) Geopolymer Binder Systems, ASTM International. New York, (2013).
48. Palomo, A., Alonso, S., Fernandez-Jiménez, A., Sobrados, I., & Sanz, J. (2004). Alkaline activation of fly ashes: NMR study of the reaction products. Journal of the American Ceramic Society, 87(6), 1141-1145.
49. Institution of Structural Engineers (ISE). 1992. "Structural Effects of Alkali-Silica Reaction –

Technical Guidance Appraisal of Existing Structures." Institution of Structural Engineers, London.

50. Hobbs, D. W. (1988). Alkali-silica reaction in concrete. Thomas Telford Publishing.
51. Smaoui, N., Bissonnette, B., Bérubé, M. A., Fournier, B., & Durand, B. (2005). Mechanical properties of ASR-affected concrete containing fine or coarse reactive aggregates. Journal of ASTM International, 3(3), 1-16.
52. Ahmed, T., Burley, E., Rigden, S., & Abu-Tair, A. I. (2003). The effect of alkali reactivity on the mechanical properties of concrete. Construction and Building Materials, 17(2), 123-144.

# CHAPTER 11

# OTHER DURABILITY STUDIES (RESISTANCE AGAINST MAGNESIUM SULFATE SOLUTION, DRYING SHRINKAGE, AND CORROSION OF REBAR):

In this chapter, preliminary results that were obtained from investigations on selected durability properties of the GGF-based geopolymer mixture will be presented. Selected durability properties include the resistance against magnesium sulfate solution, drying shrinkage, and corrosion of steel rebar. Although results from the preliminary experiments are presented here, additional data is needed to interpret the results. Thus, no conclusions were made on the performance of GGF-based geopolymers with reference to above-mentioned durability aspects.

## 11.1 Resistance against magnesium sulfate solution:

In this section, the resistance of GGF-based geopolymer mortars against a 5% $MgSO_4$ solution were studied. Change in the compressive strength and mass of geopolymer mortar specimens immersed in the solution was monitored up to 240 days. Based on the earlier literature review, the principle mechanisms of strength loss in the geopolymer samples produced from fly ash upon exposure to magnesium sulfate solution were attributed to: 1) the dissolution of alkalis from the geopolymer paste causing cracks in its microstructure; and 2) formation of a gypsum and ettringite in the geopolymer matrix, causing damage, and consequent strength loss. Thus, in the following sections the influence of each of the proposed mechanism on the compressive strength of the GGF-based geopolymer was investigated.

### *11.1.1 Change in mass and compressive strength*

To evaluate the resistance of geopolymer against the $MgSO_4$ solution, GGF-based geopolymer mortar specimens were immersed in a 5% $MgSO_4$ solution. The change in the mass and

compressive strength of the specimens were monitored and recorded up to 240 days (Table 11-1). In these specimens, a small weight gain was seen up to 28 days, which was then followed by a gradual weight loss. As the result of the heat curing (60°C for 24 h), the voids were assumed to be almost free of water. Therefore, the weight gain of specimens up to 28 days could be explained by the penetration of the solution into the voids of the specimens. On the other hand, beyond 28 days, the weight loss could be related to the dissolution of the paste in the solution as it is presented in the section 11.1.3.

Table 11-1. Effect of 5% $MgSO_4$ solution on the compressive strength and weight of GGF-0-10 specimens

| Age of immersion (day) | Compressive strength (MPa) | Chang in the weight (%) |
|---|---|---|
| 0 | 76 | 0.0 |
| 7 | 65 | 0.3 |
| 28 | 61 | 0.6 |
| 56 | 65 | 0.5 |
| 120 | 68 | 0.3 |
| 240 | 72 | 0.1 |

As presented in Table 11-1, the compressive strength of the GGF-based specimens showed a reduction in compressive strength of specimens at early ages (i.e. 7 and 28 days). However, at the later ages (i.e. after 56 days), specimens gained their strength back. To study the parameters that could influence the behavior of GGF-based geopolymer specimens immersed in the $MgSO_4$ solution, change in the pH of the soaking solution and the dissolution of the paste into the $MgSO_4$ solution was monitored. In addition, to examine the formation of any gypsum and ettringite in the soaked samples, XRD test was performed on the crushed pastes that have been soaked into the solution for 28 days. The procedure for the pH measurement, dissolution of the paste into the soak solution, and preparing the XRD samples, are presented in section 3.3.3.6.

### *11.1.2 Change in the pH of the soak solution:*

The results for the change in the pH of the filtered $MgSO_4$ solution is presented and compared to

the filtered $Na_2SO_4$ solution, which was studied in chapter 9 (Figure 11-1). As it can be seen the pH of the $MgSO_4$ solution is much lower than the case of $Na_2SO_4$ solution. While the pH for the case of $Na_2SO_4$ solution was in the range of 12.4 to 12.5, the pH of the $MgSO_4$ solution varied in the range of 10.6 to 11.1. However, this low increase in the pH (in comparison to the pH of the $Na_2SO_4$ solution) should not be interpreted as the lower dissolution of alkali from the geopolymer paste into the soak solution; as dissolution of $Na^+$ could be balanced by the penetration of Mg ions into the geopolymer matrix (see Table 11-2).

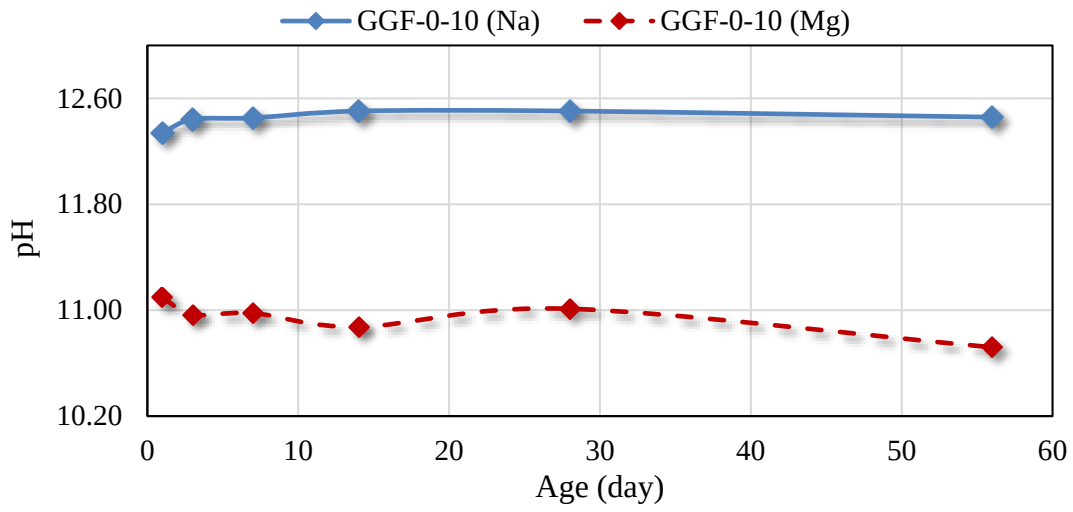


Figure 11-1. Change in pH of sulfate solution versus time. (Five grams of crushed GGF-0-10 paste was introduced to 100 ml of 5% of each sulfate solution)

### *11.1.3 Dissolution of the GGF-0-10 geopolymer paste in $MgSO_4$ solution*

Table 11-2 shows the dissolution of K, Ca, Si, Al and Na in the $MgSO_4$ solution. As it can be seen, a significantly high amount of Na have been leached into the solution. Since the original solution was free of Na ions, it is reasonable to think that all the Na have migrated from the geopolymer samples (either from un-reacted Na, or Na of the structure units) into the solution. In addition, unlike the test results of the $MgSO_4$ solution, a high amount of Ca, and a low amount of Si and Al were dissolved in this solution. Considering the negligible concentration of Si and Al in

the solution, it is reasonable to assume the main structure of the geopolymer remained stable when was in contact with the $MgSO_4$ solution; and did not leach into the solution.

Table 11-2. Ions concentration in $MgSO_4$ solution (ppm)

| Immersion age (day) | K | Ca | Si | Al | Na | Mg | S |
|---|---|---|---|---|---|---|---|
| 1 | 13 | 333 | 7 | 0.03 | Saturated signal | 5657 | 5104 |
| 7 | 22 | 448 | 10 | 0.03 | Saturated signal | 5060 | 4954 |
| 28 | 19 | 330 | 8 | 0.07 | 1121 | 4086 | 3993 |
| 56 | 19 | 327 | 11 | 0.06 | 1123 | 3883 | 4151 |

On the other hand, a considerable amount of Ca was leached into the solution. Further, it was seen that the concentrations of Mg and S were reduced with the time, implying that Mg and S are penetrating in the geopolymer structure. While more studies are needed before making any solid conclusion, it is assumed that a part of Mg might replace Ca, in any possible tobermorite structure. In addition, other parts might be replacing the Na ions in the gel structure, balancing the negative charge in the $Al(OH)_4^-$ units in the geopolymer gel. Finally, considering the reduction in the S ions level in the solution, it could be thought the rest part of the Mg might be deposited in the geopolymer paste, forming $MgSO_4$ salt, gypsum, ettringite, or other Mg rich compounds. Additional studies are needed to better understand the mechanism involved.

### *11.1.4 XRD pattern and expansion of GGF-0-10 geopolymer soaked in $MgSO_4$ solution*

The XRD pattern of the filtered GGF-0-10 paste, which was in contact with the $MgSO_4$ solution for 28 days, are presented in Figure 11-2. As it can be seen, main crystalline phases are calcite ($CaCO_3$), magnesite ($MgCO_3$), and quartz ($SiO_2$); and presence of peaks associated with gypsum or ettringite in their crystalline forms was not confirmed. In addition, in order to investigate the expansion behavior of GGF-based geopolymers in magnisum sulfate solution, GGF-0-10 mortar bars were placed in different aqueous media, including deionized water, a 5% $Na_2SO_4$ solution, a 10% $Na_2SO_4$ solution, a 5% $MgSO_4$, and a 10% $MgSO_4$ solution. The expansion of mortar bars

were monitored and recorded. As presented in Figure 11-3, it can be observed that regardless the exposing media, all the exposed mortar showed a similar expansion behavior.

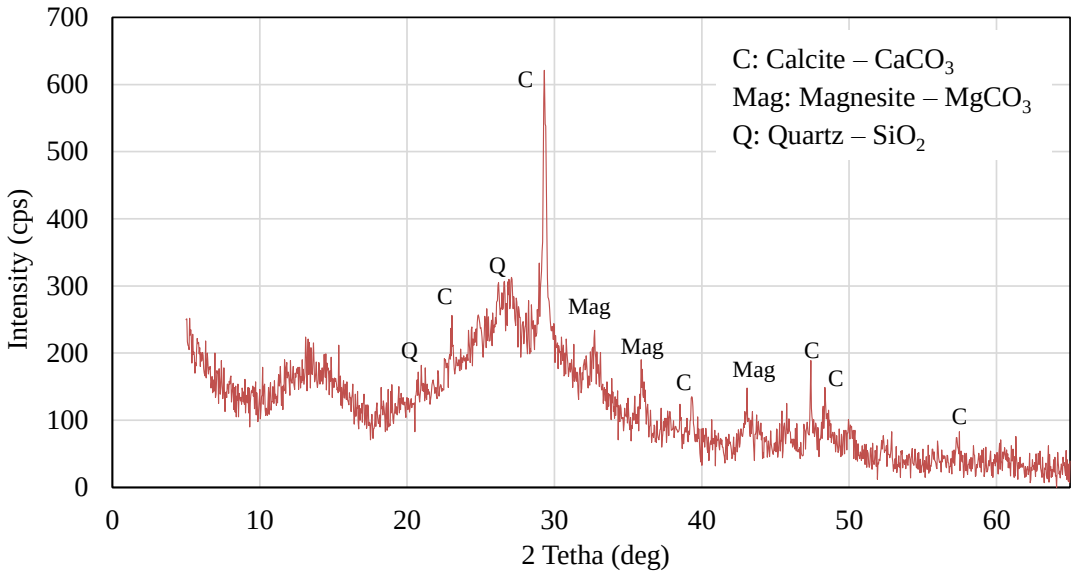


Figure 11-2. XRD pattern of GGF-0-10 paste after exposure to 5% $MgSO_4$ solution for 28 days

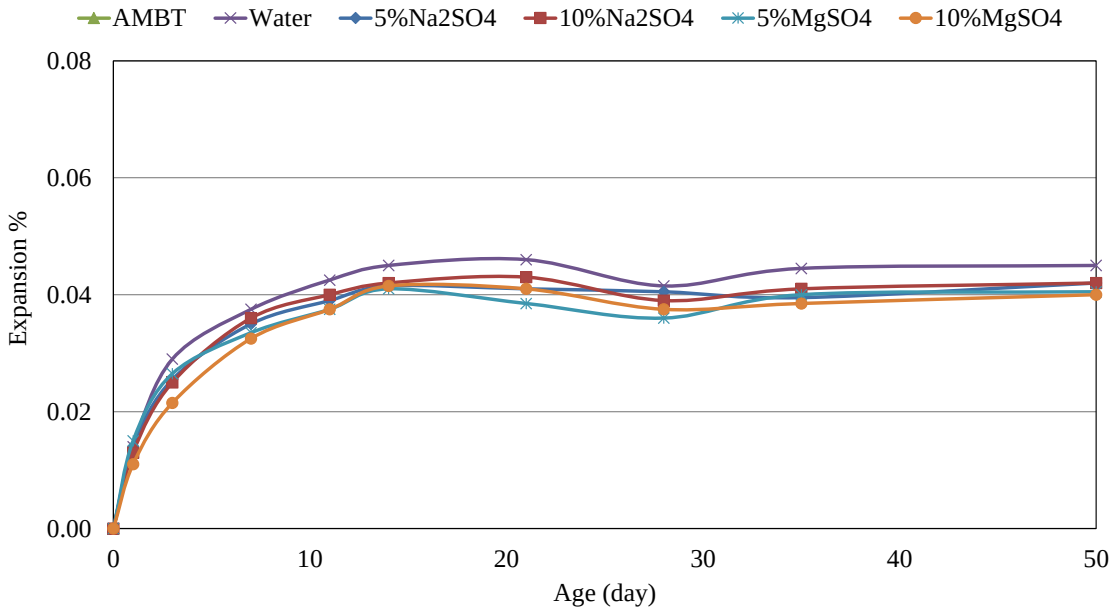


Figure 11-3. Expansion of GGF-0-10 mortar bars in different aqueous media

### *11.1.5 SEM images and EDX analyses:*

In order to investigate the effect of $MgSO_4$ solution on the structure of geopolymer specimens,

SEM images were taken from the GGF-0-10 mortar samples that were impressed in the solution for 240 days. As presented in Figure 11-4, despite high amount of Na and Ca that leached from the geopolymer sample into the solution (Table 11-2), the appearance of the GGF-0-10 mortar, did not revealed any significant sign of damages under the SEM.

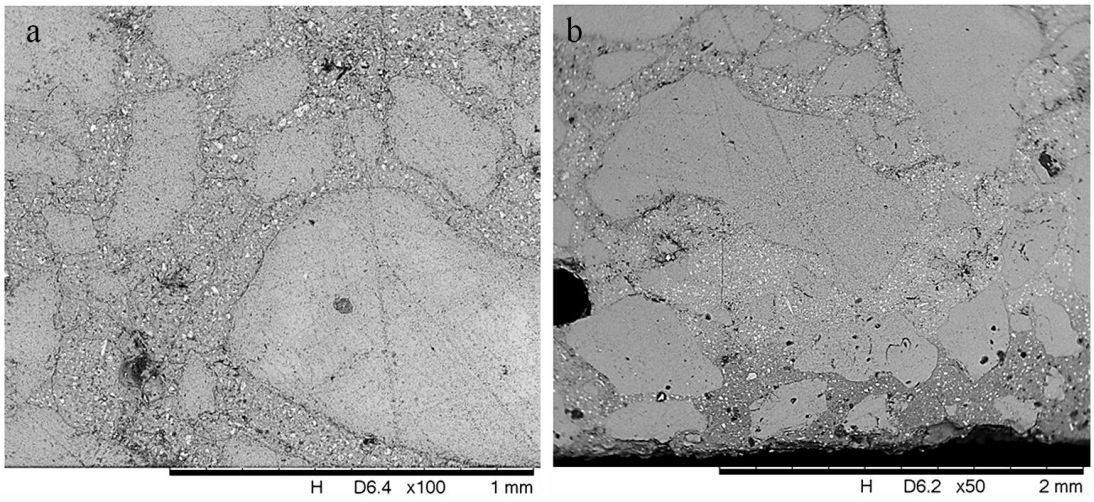


Figure 11-4. View of GGF-0-10 sample after 240 days of exposure to 5% $MgSO_4$ solution. A) Middle part of the crossed section, and b) edge of the crossed section.

As presented in Table 11-2, while concentration of Mg and S keeps decreasing with the time, high amounts of Ca and Na have leached from the geopolymer paste; even at the first day. This suggests that the Mg and S ions could have been penetrated into the geopolymer paste, forming new phase and also replacing Na and Ca ions in some cases. The SEM-EDX results presented in the Table 11-3, confirmed the penetration of Mg and S ions into the geopolymer mortar, as well as the leachate of Ca and Na from the geopolymer to the solution, for mortar samples that were exposed to the $MgSO_4$ solution. However, more studies are needed in order to make a more detailed conclusion on the mechanism of effect of $MgSO_4$ on the GGF-based geopolymer sample.

Table 11-3. Sulfur content of geopolymers by EDX. (*The elements considered for the EDX analysis are: Si, Al, Ca, Na, K, Fe, and S)

| Before exposure | | After 240days exposure | | | |
|---|---|---|---|---|---|
| Element ID | All depth | At the edge | 500 µm from the edge | 1000 µm from the edge | 2000 µm from the edge |
| Mg | 2.0% | 22.2% | 12.1% | 1.9% | 1.8% |
| S | 0.01 | 2.28% | 1.5% | 0.2% | 0.2% |
| Na | 11.2% | 0.9% | 1.6% | 3.9% | 5.7% |
| Ca | 23.1% | 7.8% | 21.9% | 35.7% | 28.3% |

## 11.2 Drying shrinkage

Results for the shrinkage behavior of the geopolymers and OPC samples are shown in Figure 11-5. As it can be seen after seven weeks, all the samples have reached a plateau state. As shown in this figure, the shrinkage of GGF-0-10 and F-1-10 mortar specimens are in the same range with heat cured OPC while it is much higher in the case of GLP-1-10. The higher shrinkage of this sample could be attributed to the higher content of Si/Al ratio. The higher alumina content in a geopolymer system fastens the reorganization (geopolymerisation) of the unstable gel in early ages of geopolymer specimens, hence reducing the shrinkage.

The lower shrinkage of GGF and fly ash based systems can be explained by the different role of water in the geopolymer system in compare to conventional OPC system. A hardened geopolymer system contains three types of water, 1) Physically bonded water 2) Chemical bonded water and 3) hydroxyl group of OH (1). Among these three types, almost 70% of the water is known to be physically bonded water. As a result, the majority of water used as the activator, forms physical water, which evaporates during the heat curing process and only small amount of water remains within the pore structure. In addition to this, presence of un-reacted GGF and Fly-ash particles which act as the micro aggregates reduces the shrinkage.

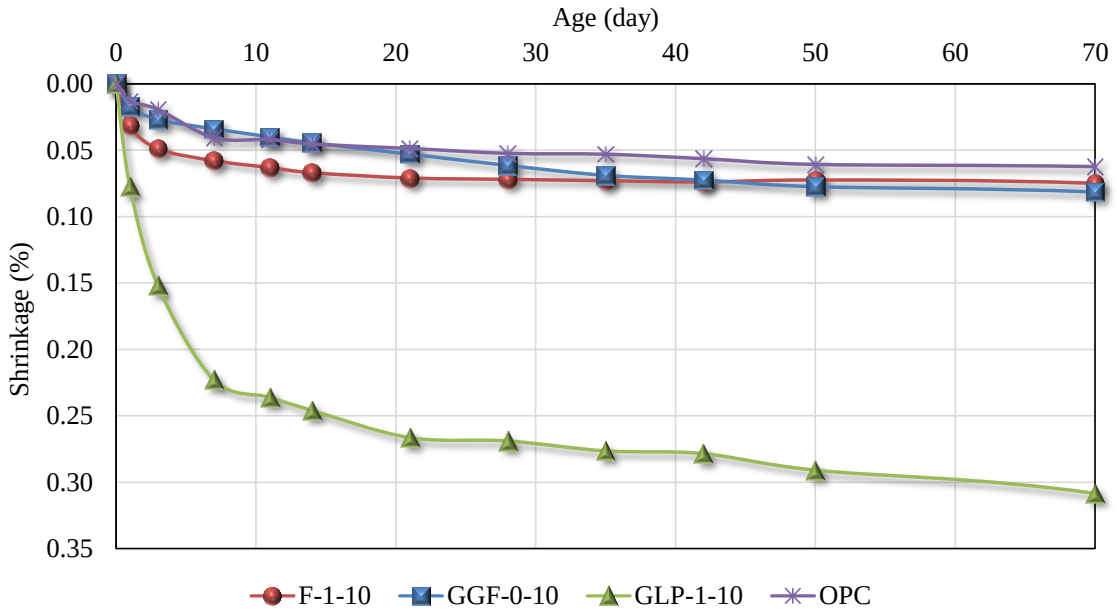


Figure 11-5. Shrinkage of mortar bars versus time

Finally, it should be noted that, although the shrinkage experiment set up in this study was similar to the test method that was used for the drying shrinkage test, it is thought that main cause of the shrinkage is as a result of the autogenous shrinkage. The fact that most of the shrinkage happens in the very early ages (3 days for F-1-10 and GGF-0-10, and 7 days for GLP-1-10) and also less availability of water in the heat cured geopolymer can be used to support this idea. However, more experiments are needed to evaluate the validity of this theory.

## 11.3 Corrosion studies:

In order to evaluate the resistance of GGF-based geopolymer against corrosion of embedded steel rears, series of tests, including RCPT, chloride ion penetration, and linear polarization resistivity were conducted on the specimens. For comparison purposes, the results were compared to two sets of a portland cement mixture and a fly ash-based geopolymer mixtures. While the specimens from the first set of the portland cement mixture (Ctrl-23°C) were cured in the curing room (23°C and ~100% RH), the specimens of the second set were cured in a 60°C oven for 24 h. All the samples that were cured in the 60°C, were removed from the 60°C chamber after the first 24 h,

and stored in the ambient condition until the test day. On the other hand, all the Ctrl-23ºC specimens were kept in the curing room until the test day. The mix proportion and the compressive strength of $50 \times 50 \times 50\ mm$ mortar cubes produced from each mixture are summarized in Table 11-4. It should be added that the sand content of all the mortar mixtures was selected to fill 55% of the volume of the mixture.

Table 11-4. Mixture design of the paste portion of mortar mixtures and their compressive strength (required amount of sand was used to fill 55% of the volume of each mixture)

| Mix ID | Precursor | Water/ Precursor | $SiO_2/Na_2O$ | $Na_2O$/Precursor (%) | Compressive strength (MPa) | |
|---|---|---|---|---|---|---|
| | | | | | 7 days | 28 days |
| GGF-0-10 | GGF | 0.4 | 0 | 10 | 63 | 81 |
| F-1-10 | Fly ash | 0.4 | 1 | 10 | 41 | 47 |
| Ctrl-23ºC | Cement | 0.4 | 0 | 0 | 37 | 48 |
| Ctrl-60ºC | Cement | 0.4 | 0 | 0 | 51 | 54 |

### *11.3.1 Rapid chloride permeability:*

The results of RCPT performed on portland cement-based and geopolymer mortar specimens are presented in Table 11-5. As it can be seen the GGF-based specimens showed a much lower charge passing value at both 7 and 28 days. While the charge passing value was seen to be not affected by the age and the values stayed almost in a same range, 28-day results showed a significant decrease in the amount of passing charge, for the cement based specimens. It should be added that the attempt to perform RCPT on fly ash-based specimens was not successful; and all the specimens showed a significantly high amount of charge passing rate, which was accompanied with a rapid increase in the temperature. Therefore, continuing the test procedure was not practical for the case of fly ash-base specimens. A same result, rise in temperature when testing fly ash-based specimens, has been also reported by other studies (2).

Table 11-5. RCPT test results at 7 and 28 days

| Mix ID | Ctrl-23°C | Ctrl-60°C | F-1-10 | GGF-0-10 |
|---|---|---|---|---|
| 7 days | 9785 | 10995 | NA | 835 |
| 28 days | 6275 | 2435 | NA | 745 |

### *11.3.2 Chloride penetration test*

The chloride penetration test was performed on geopolymer mortar samples, which were prepared in accordance to the test method presented in section 3.3.3.9. A 10% NaCl solution was used for this test, and the test was continued for eight months. Results of chloride penetration test are presented in Figure 11-6. As it can be seen in this figure, the Ctrl-60°C specimens showed the highest depth for the Chloride penetration. This could be attributed to its more porous structure, as well as presents of unsaturated voids in its matrix. The high porosity and unsaturated voids allow the easier penetration of the solution, increasing the chloride penetration depth. On the other hand, a lower depth of chloride penetration was seen in the case of Ctrl-23°C and GGF-1-10 samples. The lower depth of chloride penetration for the case of Ctrl-23°C in comparison to the Ctrl-60°C specimens, could be explained by the presence of more saturated voids in the specimens. On the other hand, the low chloride penetration could be related to its lower porosity and dense structure, as also was evidence from the RCPT results.

It was also seen that all the tested mixtures, the rate of penetration was much higher in the first 2-3 months and then gradually decreased after this time. This might be related to generation of cracks and damage accolated with the samples' preparation method, in which mortar cylinders were cut by a saw. It should be also noted, while the rate of penetration was considerably decreased for the case GGF-0-10 and Ctrl-230C specimens, the reduction in the rate of chloride penetration rate was less significant. The relatively high rate of chloride ions penetration in this case (Ctrl-60°C) could be due to the fact the not much refinement in the paste matrix is happening for in the later ages.

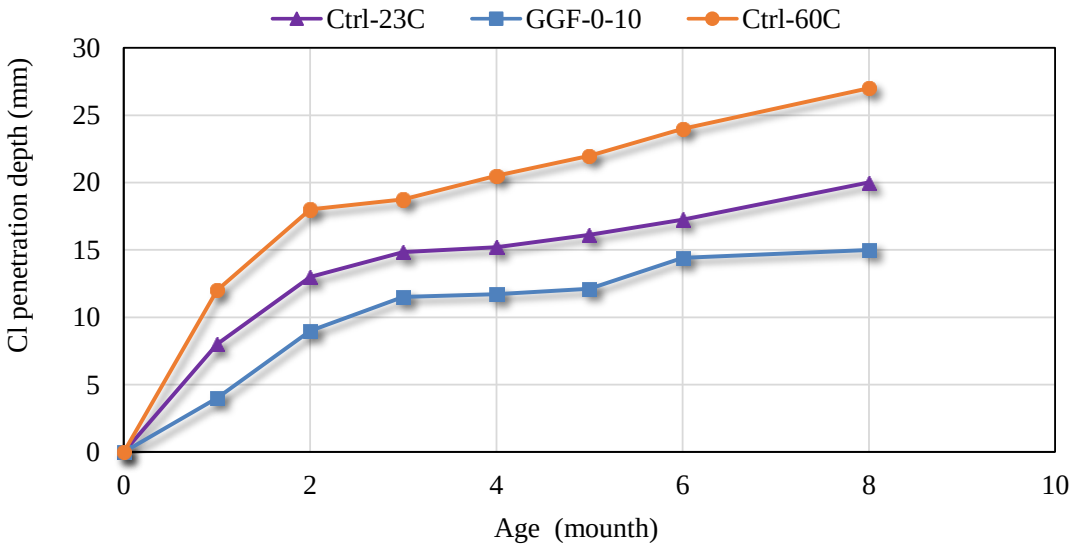


Figure 11-6. Depth of chloride penetration for each mixture versus time

### *11.3.3 Electrochemical test*

To evaluate the behavior of geopolymers and portland cement-based mixtures, series of electrochemical tests were performed on the geopolymers and portland cement-based mortar specimens. For all the electrochemical test, a 10% NaCl solution and a Saturated Calomel Electrode (SCE) were used. Considering the time taking nature of the corrosion tests, after nine months of exposure to the salt solution, chloride ions have not reached the rebar yet. The view of the specimens exposed to the NaCl solution and the broken specimens are presented in Figure 11-6 and Figure 11-7, respectively. Therefore, it was decided to give the test more time to proceed.

The name of the electrochemical test that was considered for this test is as below:

1. Linear polarization resistivity: To measure the change in the corrosion voltage and polarization resistivity ($R_P$)
2. Impedance: To separate the resistivity of the mortar and the resistivity of the embedded steel.
3. Polarization: To measure the Tafel slopes and calculate the corrosion current by following equation:

$$I_{cor.} = \frac{\beta_a \beta_c}{2.3 R_P (\beta_a + \beta_c)} = \frac{B}{R_P}$$

Where, $\beta_a$ and $\beta_c$ are the anodic and cathodic Tafel slopes respectively, and $R_P$ is the resistance measured by the linear polarization resistance test.

Figure 11-7. View of the exposure condition

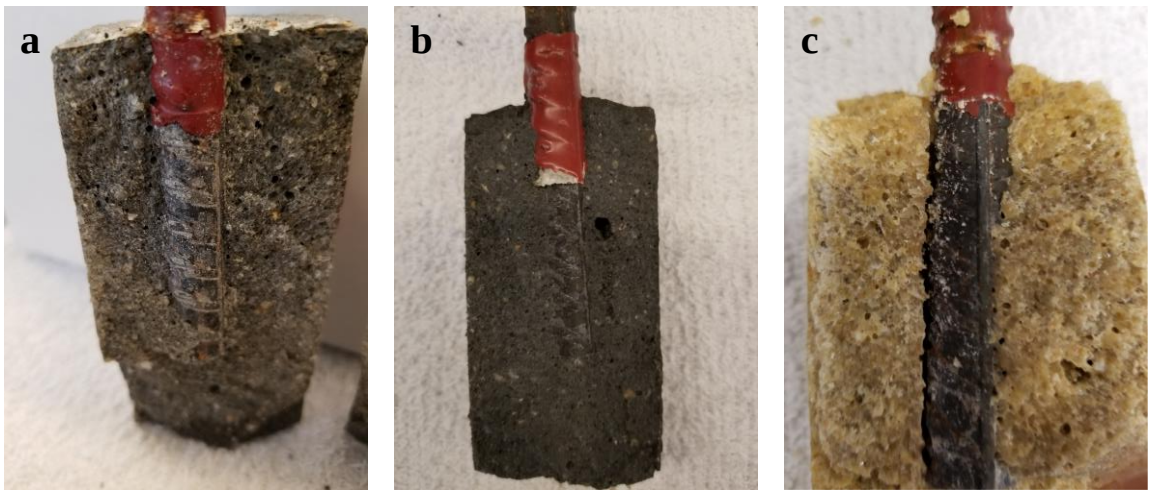


Figure 11-8. View of steel bars in the exposed specimens after nine month

## Reference:


1. Davidovits, j. 2008. Geopolymer Chemistry and Applications, Institute saint-quentin.
2. Law, D. W., Adam, A. A., Molyneaux, T. K., Patnaikuni, I., & Wardhono, A. (2015). Long term durability properties of class F fly ash geopolymer concrete. *Materials and Structures*, *48*(3), 721-731.

# CHAPTER 12

# CONCLUSION AND RECOMMENDATIONS

This work focused on evaluating the utilization of ground glass fiber as SCM in portland cement or as a source material (precursor) in geopolymer mixtures. The principal conclusions from the study can be summarized a follows:

## 12.1 Utilization of GGF as an SCM

Utilization of GGF as an SCM was studied at different replacement levels (i.e. 10, 20, and 30%) of portland cement in paste, mortar and concrete mixtures. It was observed that even though replacement of portland cement with GGF did not lead to any remarkable changes in the mechanical behavior of hardened concrete samples, significant improvements in durability properties were observed at replacement levels of 20% and above. Based on this study the following conclusions are drawn:

1. Increase in the level of replacement of cement with GGF from 0 to 30%, resulted in increase in the air content of the fresh mixtures, and improved their workability at the constant water-to-binder ratio. This can be attributed to the none absorptive nature of the GGF, as well as its smooth surface.
2. At all cement replacement levels (i.e. 10, 20 and 30% levels of substitution by mass of cement) GGF showed strength activity index values greater than 100% after 28 days. Note that in this standardized ASTM test a constant flow maintained across the mixtures and not the constant water-to-binder ratio. The reason for the improvement in the strength activity index appears to be more due to the refinement of the paste structure and to a lesser degree to the pozzolan reactivity.
3. The compressive strength results of concrete specimens showed that the addition of GGF as a cement replacement up to 30% did not lead to any significant reduction in the compressive

strength. Note that in this test the constant water-to-binder ratio was maintained.

4. The modulus of elasticity and the tensile splitting strength of GGF containing concrete mixtures was in the same range as observed with pure portland cement concrete specimens (CTRL-1).
5. At cement replacement levels of 20% and 30%, the use of GGF in mortar bars containing reactive NM aggregate was able to restrict 14-day expansion to less than 0.10%, in the accelerated mortar bar test (AMBT), indicating its ability to mitigate ASR. At these replacement levels, GGF containing mixtures showed better performance in ASR mitigation compared to the fly ash containing control mixture (CTRL-2 mixture). In addition, after 84 days of testing, negligible expansion was seen in concrete prisms containing GGF at all replacement levels investigated in the Miniature Concrete Prism Test (MCPT-AASHTO TP110). The improvement seen in the GGF containing mixtures is due to the higher Si/Ca and Al/Si ratio in the paste of these mixture in comparison to the CTRL-1 mixture.
6. At all cement replacement levels, GGF containing mixtures successfully mitigated ASR-related expansion of mortar bars containing crushed glass aggregate. On the other hand, when glass aggregate was used as a coarse reactive aggregate in the MCPT, only the mixture containing GGF at 30% level (GGF-30 mixture) was able to mitigate the concrete expansion.
7. Results from sulfate attack studies revealed that the use of GGF at all levels of cement replacement reduced the level of expansion in test specimens compared to control mixtures.
8. Use of GGF at all levels of cement replacement reduced chloride ion permeability values in concrete significantly (2768 coulombs for CTRL-1 versus 223 coulombs for GGF-30, after 56 days). The smaller particle size of GGF is likely to be responsible for refining the pore structure and improving its durability properties.

## 12.2 Utilization of GGF in geopolymer concrete

In this research, activation of GGF with different combination of alkali activator solutions was studied. The mechanical and durability properties of GGF-based geopolymer were investigated, and the results were compared to geopolymer mixtures made by the activation of fly ash and GLP in most of the cases. Results from this study showed the superior performance of GGF based geopolymers in comparison to fly ash and GLP-based geopolymers. Unlike the fly ash and GLP-based geopolymers, the strength gain of GGF based geopolymer did not depend on the presence of sodium silicate activator; and GGF was successfully activated with NaOH solution alone. Significant conclusions this study are summarized below:

1. Compressive strength of the GGF-based geopolymer was found to be related to the $Na_2O$ content of the activator solution used in the mixture. An increase in $Na_2O$ content up to 10% by the mass of the source materials showed an increase in the compressive strength of the mixture. However, beyond 10% (i.e. 15 and 20%) the compressive strength decreased.
2. Change in the curing temperature from 23ºC to 80ºC did not seem to affect the later age (i.e. 28-day and 56-day) strength of the GGF-based geopolymer specimens. However, specimens that were cured at 23ºC and 38ºC showed lower early-age strength compare to specimens that were cured at 60ºC and 80ºC (i.e. 3-day and 7-day results). No significant change was seen between the results of specimens cured at 60ºC and 80ºC. Curing GGF-based geopolymer at a high temperature on 110ºC caused a significant reduction in the compressive strength due to rapid evaporation of water from the mixture, leading to cracking in the geopolymer matrix.
3. Based on the optimal conditions identified in conclusion 1 and 2 a GGF-based geopolymer with a $Na_2O$-to-GGF mass ratio of 10% and cured at 60ºC for 24 h yielded a compressive strength of 79MPa at three days.
4. Prolonging the curing duration beyond 24 h led to a gradual rise in the strength of

geopolymer samples. For instance extending the heat curing (60ºC) period from 24 h to 168 h (7 days) for GGF-0-10 specimens, resulted in the increase in the 28-day compressive strength from 81 MPa to 95 MPa.

5. Geopolymer mixtures produced from GGF and fly ash precursors contained a negligible amount of CH in their structure. While CH is responsible for many durability issues in portland cement concrete, the lack of the this compound in the GGF and fly ash-based geopolymer is one the main reasons for its enhanced performance in durability tests.
6. GGF and fly ash-based samples showed an excellent performance against ASR when compared to a portland cement based mortar. However, GLP-based geopolymers showed a very poor performance against the ASR.
7. Exposure of GGF and fly ash-based geopolymer samples to a 5% sodium sulfate for 120 days did not result in any significant changes in the mass and the compressive strength. However, GLP-based specimens showed a large reduction in their mass and compressive strength due to significant leaching of Si from the matrix.
8. The structure of GGF and fly ash-based geopolymer samples appear to be stable when exposed to the sodium sulfate solution. However, GLP-based samples leached a significant amount of Si when exposed to sodium sulfate solution.
9. No notable amount of mass loss or reduction in the compressive strength was seen in the GGF-based geopolymer mortars when exposed to 5% magnesium sulfate solution for 240 days. However, the structure does not seem to be very stable, since a considerable amount of Ca and Na was leached from the geopolymer paste into the soaking solution.
10. Results from XRD test on the GGF-based geopolymer powder that was in contact with sodium sulfate or magnesium sulfate solution, did not confirm the formation of gypsum or ettringite. Formations of gypsum and ettringite are known to play an important role in the

damages associated with sulfate attack in conventional portland cement mixtures.

11. Drying shrinkage of the GGF and fly-ash samples was comparable that of a heat cured portland cement mortar mixture (550 to 700 micro-strain at 28 days).
12. GLP-based geopolymer samples showed significant expansion and cracking when tested for ASR-related expansion. They also showed an appreciable strength loss and a very high shrinkage, when tested for their resistance against sodium sulfate solution and drying shrinkage, respectively. Based on these results it can be concluded that GLP is not a suitable choice for use as a source material in geopolymers.
13. GGF-based geopolymer specimens showed better or equivalent mechanical and durability properties when compared to either portland cement mortar or fly ash-based geopolymer. Although more studies are needed before commercially using this material, the findings from this work showed an excellent potential of GGF to be considered as a precursor in producing geopolymer concrete.

## 12.3 Recommendations for future works

In this study, utilization of GGF as a SCM in portland cement mixtures, or as a source material for production of GGF-based geopolymer was studied. The results showed the good potential of GGF to be considered as a potential candidate in both applications. However, the followings additional studies would be helpful in characterizing the use of GGF either as an SCM or as a source material;

### *12.3.1 Using GGF as a SCM:*

1. Considering the remarkable durability properties of GGF containing mixtures, use of this material in combination with a class C flay ash could be considered for further studies (a ternary mixture).
2. Pore solution analysis studies could be helpful in better understanding the ASR-mitigation of

the mixtures containing GGF.

3. Effect of using different dosages of GGF on the pore structure (size and distribution of pores) of pastes should be studied.

### *12.3.2 Use in geopolymer mixtures:*

1. GGF releases a considerable amount of Si in an alkali media, therefore, the addition of this material to fly ash-based geopolymers could reduce the need for use of sodium silicate in the activator solution for fly ash-based geopolymers.
2. After 28 days, GGF-based geopolymer cured at the ambient temperature showed a compressive strength that was equivalent to the geopolymer that was cured at 60ºC. Therefore, the long-term durability properties of GGF-based geopolymer cured at ambient temperature should be studied.
3. Role of Ca in the structure of GGF-based geopolymer needs investigations. To better characterizing the mechanical and durability properties of GGF-based geopolymer.
4. The corrosion resistance of GGF-based geopolymer should be investigated.
5. Durability properties such as resistance against freeze-thaw and, shrinkage, thermal stability, and thermal resistivity of GGF-based geopolymer should be evaluated.
6. To establish the structural behavior of the GGF-based geopolymer the bound performance between geopolymer matrix and the reinforcing steel, the depth of embedment needed to achieve the development length should be investigated.
7. Effect of addition of an external Al source to GLP-based geopolymer should be investigated to improve its performance.